

DOTTORATO DI RICERCA IN SCIENZE CHIMICHE

CICLO XXXIII

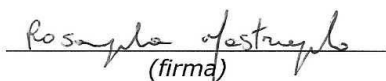
COORDINATORE Prof. PIERO BAGLIONI

A new class of hydrogels: PVA-based Twin-Chain Networks for the
cleaning of Modern and Contemporary Art

Settore Scientifico Disciplinare CHIM/12

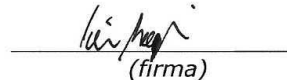
Dottorando

Dott. Rosangela Mastrangelo


(firma)

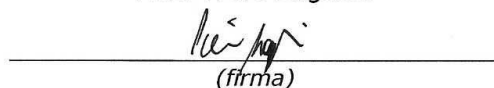
Tutore

Prof. Piero Baglioni


(firma)

Coordinatore

Prof. Piero Baglioni


(firma)

Anni 2017/2020

ABSTRACT

Untypical artistic techniques, fleeting materials and tridimensional surfaces make the artworks of the last century impermanent and delicate, if compared to traditional, flat easel paintings. As a result, the cleaning of Modern and Contemporary paintings is a very delicate process: the removal of dirt or grime deposited on their surface can be challenging. Traditional cleaning techniques were found to be unsuitable for this purpose: free solvents spread on the surface and swell the paint layers, water-based fluids can leach the paint components, while confining systems like traditional gels are too rigid, and/or leave residues on the surface.

Poly(vinyl alcohol) (PVA)-based cryogels can meet the demand for new, science-driven, materials for restoration. This class of hydrogels, obtained through a freeze-thawing (FT) process, exhibits unique properties, such as high water retentiveness, free water content and adaptability to rough surfaces, interconnected porosity, structural cohesion and ease of handling/removal. Cryogels can be loaded with cleaning fluids, or just be swollen in water, and then placed in contact with the surface to clean: the free water inside the network allows the detaching of dirt, that is eventually trapped in the polymer matrix.

The characteristics of PVA cryogels can be tailored by adding a second polymer that acts as a semi-interpenetrating agent, and/or varying the number of FT cycles. The chemical nature of polymer chains, and their molecular weight, also affect the final gel structure. As a result, the gel porosity, the rheological behavior and the dynamics of polymer chains embedded in the network are expected to change.

Twin-Chain Polymer Networks (TC-PNs) were obtained by mixing two PVAs with higher (H-PVA) and lower (L-PVA) molecular weight and hydrolysis degree. Despite the very similar structure of the two polymers, a liquid-liquid phase separation occurred in the pre-gel solution: L-PVA chains are expelled from the H-PVA continuous phase and form spherical blobs, which act as porogens during cryostructuration. Confocal and Scanning Electron Microscopies revealed the sponge-like structure of TC-PNs, with micron-sized and interconnected pores. Small Angle X-ray Scattering and Differential Scanning Calorimetry clarified details about the structure at the nanoscale,

while Fluorescence Correlation Spectroscopy (FCS) revealed the polymers dynamics. On the other hand, rheology data suggested that the semi-interpenetrating polymers can alter the gelation process, acting also as structuring agents.

The diffusion of cleaning nano-structured fluids (NSFs) through the gels matrix was investigated through FCS: polymer-surfactant interactions and gels porosity were proven to influence the diffusive components.

Overall, TC-PNs exhibited unprecedented cleaning performances, unconceivable with traditional methods. TC-PNs were successfully used to treat two Jackson Pollock's and one Pablo Picasso's masterpieces (Peggy Guggenheim collection, Venice), bringing back the paints original hue and brightness.

LIST OF ABBREVIATIONS

- PVA:** Poly(vinyl alcohol)
FT: freeze-thaw of PVA aqueous solutions, to obtain cryogels
NSFs: Nano-Structured Fluids
 μ Em: microemulsion
o/w μ Em: oil-in-water microemulsion
TC-PNs: Twin-Chain Polymer Networks
pHEMA: poly(2-hydroxyethyl methacrylate)
T_g: Glass transition temperature
M_n: number-average molecular weight of a polymer
M_w: weight-average molecular weight of a polymer, or generally, molecular weight of a polymer
M_z: Z-average molecular weight of a polymer
M_v: viscosity-average molecular weight of a polymer
UCST: Upper Critical Solution Temperature
LCST: Lower Critical Solution Temperature
JM theory: theory by Jones and Marques, describing rigid polymer gels
HD: Hydrolysis degree, the percentage of -OH groups on the PVA backbone
H-PVA: Polyvinyl alcohol with higher M_w and HD
L-PVA: Polyvinyl alcohol with lower M_w and HD
PVP: Polyvinylpyrrolidone
FITC: Fluorescein isothiocyanate
RBITC: Rhodamine B isothiocyanate
MPD: Methoxy pentadeca oxyethylene dodecanoate, a nonionic surfactant
PDE: Pentadeca oxyethylene dodecyl ether, a nonionic surfactant
SDS: Sodium Dodecyl Sulfate
PC: Propylene Carbonate
MEK: Methyl Ethyl Ketone
EA: Ethyl Acetate
Pe-OH: Pentanol
Bu-OH: Butanol
PVAc: Polyvinyl Acetate
PN: Pure Network, gels made on H-PVA only

i-PVA: gels containing H-PVA and L-PVA
i-PVP: gels containing H-PVA and PVP
DSC: Differential Scanning Calorimetry
SAXS: Small Angle X-Ray Scattering
FCS: Fluorescence Correlation Spectroscopy
FRAP: Fluorescence Recovery After Photobleaching
SEM: Scanning Electron Microscopy
LVE: linear viscoelastic range, identified in amplitude sweep measurements
RT: Room Temperature
G': Storage Modulus
G'': Loss Modulus

CONTENTS

Abstract	i
List of Abbreviations	iii
Introduction	1
Chapter 1. Cleaning of Paintings: from traditional to innovative methods	3
1.1 The ageing of painted surfaces	3
1.2 Cleaning paintings: a short history of the cleaning methods.....	4
1.3 Hydrogels to clean Modern and Contemporary paintings.....	8
Chapter 2. Polymer solutions	11
2.1 Polymers average Molecular Weights	11
2.2 Solvent quality and chain conformation in solution	12
2.3 Phase behavior of polymer-solvent systems	14
2.4 Polymer-polymer mixtures.....	15
Chapter 3. Polymer Gels.....	17
3.1 Chemical and physical gels.....	17
3.2 Gelation models	18
3.3 Poly(vinyl alcohol) cryogels	21
Materials and Methods	23
Chemicals	23
Hydrogels preparation	24
NSFs Preparation.....	25
Determination of commercial L-PVAs M_w	25
Labeling of polymers	26
Physico-chemical characterization of gels	26

Gels structure and morphology.....	28
Polymer chains dynamics - Diffusion of NSFs.....	31
Cleaning Tests.....	33
Results and Discussion.....	36
Chapter 4. PVA-based cryogels: the influence of the semi-interpenetrating polymer.....	37
4.1 Morphology and structure of PVA-based cryogels containing L-PVA and PVP.....	37
4.2 L-PVA and PVP as porogens: polymer-polymer interaction and segregation in aqueous solution	44
4.3 L-PVA and PVP as structuring agents.....	52
4.4 Gelation mechanism.....	55
Chapter 5. Twin-Chain Polymer Networks (TC-PNs): the influence of the freeze-thawing cycles	60
5.1. Cryogels morphology and structure	60
5.2 Physico-chemical and structural characteristics of PVA and TC-PN cryogels	64
5.3 TC-PNs structuration due to freezing and washing: the effects of H-PVA-L-PVA phase separation.....	67
5.4 The diffusion of PVA chains in the TC-PN network	69
5.5 Rheological behavior of PVA-based cryogels	71
Chapter 6. Twin-Chain Polymer Networks: the influence of L-PVA molecular weight.....	73
6.1. Determination of L-PVA molecular weight.....	73
6.2 How L-PVA chains length influences phase-separation and cryostructuration.....	75
6.3 The impact of L-PVA M_w on gels physico-chemical properties.....	76
6.4 SAXS characterization.....	78
Chapter 7. Nanostructured fluids: dewetting process and cleaning mechanism	81

7.1 NSF-induced dewetting of Paraloid B72 films: effects of the solvent and the surfactant	82
7.2 Dewetting mechanism	85
Chapter 8. The diffusion of cleaning Nanostructured Fluids into the gel matrix	90
8.1. How the porosity of hydrogels and the surfactant nature influence droplets diffusion in gels	90
8.2 Diffusion of a NSF in a FITC-labeled TC-PN FT1 for the selective cleaning of Picasso's <i>The Studio</i>	95
Chapter 9. Cleaning tests	97
9.1 How cryogels adapt to rough surfaces	97
9.2 Cryogels ability to clean soiled surfaces	99
9.3 Cleaning assessment through ATR-FTIR	102
Chapter 10. Cleaning Jackson Pollock's and Pablo Picasso's masterpieces with TC-PNs	106
Conclusions	110
References	112
Acknowledgements	126
Appendix: List of Publications	127
Paper I	
Paper II	
Paper IV	
Paper VI	

INTRODUCTION

“There really is no such thing as Art. There are only artists. Once these were men who took coloured earth and roughed out the forms of a bison on the wall of a cave; today some buy their paints, and design posters for the boardings [...]. There is no harm in calling all these activities art as long as we keep in mind that such a word may mean very different things in different times and places [...].”

E.H. Gombrich, *The Story of Art*

From the dawn of time, the creation of artworks has been an ancestral human need: whether they were used for propitiatory rites, as magic objects or to celebrate great battles, figures or events, they characterized the evolution of human history. In fact, the artists' work evolved, through the ages, with the way of thinking and behaving, shaping new ways of seeing the world.

While the artwork itself is a means of conveying a message, the artist's task is to shape the matter that will constitute the artwork, so that the dimension of thoughts and abstraction can be transferred to a material dimension, and then be recalled as ideas and feelings by the observers.

The preservation of the aesthetics of artworks and their constituent materials is, therefore, fundamental to ensure the accessibility of Cultural Heritage.¹

The readability of a work of art can be altered by the deposition of unwanted materials, due to environmental exposure, wrong handling, but also previous conservation treatments.²⁻⁴ In these cases, a cleaning action may be required.

As far as easel paintings are concerned, the action of cleaning may be referred either to a “surface cleaning”, i.e. the removal of surficial grime and soil, or to the removal of degraded layers⁵, such as yellowed varnishes or coatings².

Cleaning fluids⁶⁻⁹ (either aqueous solutions or nanostructured fluids/microemulsions, depending on the type of material to be removed) can be embedded in gel networks: in this way, a time- and space-controlled cleaning action can be performed¹⁰⁻¹³. The gels characteristics must be chosen depending on the type of surface to be cleaned: for example, Modern and Contemporary paintings are usually characterized by water-sensitive, textured surfaces^{14,15}. In this case, the ideal candidates would be gels with high adaptability and water retentiveness. Polymer gels and, more specifically,

Poly(vinyl alcohol) (PVA)-based cryogels, have shown the best cleaning performances in both laboratory trials and case studies.^{10,13,16,17}

PVA-cryogels constitute the main focus of this PhD thesis.

Their structural and physico-chemical properties were investigated by varying the formulation composition and the number of freeze-thaw (FT) cycles. The diffusion of Nano-Structured Fluids (NSFs), such as swollen micelles or o/w microemulsions (μEm), was tracked inside the gel matrix. Finally, cleaning abilities were assessed through cleaning tests on specific mockups.

In this context, a new class of hydrogels was formulated for the first time: Twin-Chain Polymer Networks (TC-PNs), obtained as a blended mixture of two PVAs with different hydrolysis degree and molecular weight.

TC-PNs are sponge-like networks with excellent water retentiveness and compliance, through which cleaning fluids diffuse in a controlled fashion. They showed unprecedented cleaning performances, surpassing the limitations of the traditional restoration approaches and classic detergency.

TC-PNs allowed a safe and controlled cleaning of Jackson Pollock's masterpieces *Two* and *Eyes in the Heat*, and Pablo Picasso's *The Studio*.^{13,17}

The introductory chapters (1 – 3) will describe in more detail the ageing of the paintings materials, the planning of the cleaning treatment and the new technologies for cleaning provided by scientific research. Finally, some theoretical background about polymer solutions, gels and PVA-based cryogels will be provided.

Chapter 1. Cleaning of Paintings: from traditional to innovative methods

Cleaning is a very delicate process: it involves the identification of the original materials constituting the artwork, the understanding of the dirt chemical nature, the study of the polarity, porosity and morphology of the surfaces, and the assessment of the general state of conservation.¹⁸ Such preliminary evaluation is necessary to predict the optimal cleaning treatment. However, this task is never easy: the paint composition changed over time and according to the artist's taste. In this sense, Modern and Contemporary paintings constitute a unique in the History of Art: the appearance, since 1940s, of hundreds of new synthetic pigments and binders¹⁹, and the experimentation of unconventional materials, led to the production of extremely complex painted surfaces. The ideal cleaning agent would act only on the layers to be removed, leaving the materials to be preserved unaffected.³ Hence, the need of science-driven, advanced cleaning tools is particularly felt, to ensure a safe and efficient treatment of vast collections.

1.1 The ageing of painted surfaces

The alterations occurring, over time, at the surface of a painting may be due to the ageing of the materials constituting the artwork or to the deposition of unwanted compounds. The chemical composition of the raw materials, their particles size, the manufacturing and purification processes are some of the intrinsic factors affecting the paint layers stability, while environmental factors such as light, moisture, heat or pollutants can facilitate the artwork surficial degradation.¹⁹ All these factors may lead to the fading of colors or the darkening of the paint, altering the contrasts and the color balance; physical and chemical changes can also occur, resulting in embrittlement or cracking of the paint layers, and in the alteration of the hydrophilic/hydrophobic characteristics of the exposed layers.

However, painted surfaces can also retain soil and grime. The surficial properties which facilitate soiling are: roughness, moisture resistance,

varnish/paint elasticity, relative hydrophobicity/hydrophilicity, tackiness and surface charge.²⁰

While the ageing of the original materials, the fading of the pigments and some alterations of the paint layers are often irreversible and, to some extent, inevitable, surficial soil or yellowed varnishes can be removed through cleaning treatments (fig. 1). To avoid any damage, an accurate assessment of the physico-chemical characteristics of the unwanted and original materials is required.

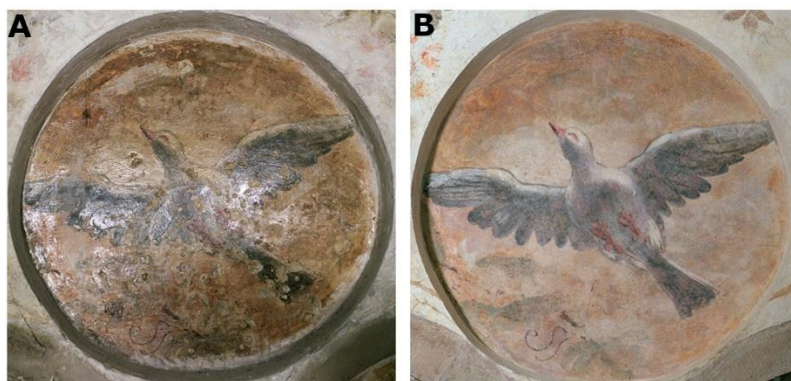


Figure 1. Removal of aged acrylic coatings from the wall paintings of the San Salvador church sacristy in Venice, Italy. Photographs taken (A) before the removal and (B) after the application of a high-viscosity polymeric dispersion loaded with an oil-in-water microemulsion. Reproduced from ref. [1].

1.2 Cleaning paintings: a short history of the cleaning methods

Aqueous media have been used, since the antiquity, to remove the particulate matter deposited on the surface of paintings; in fact, water is a highly polar solvent and can reduce or eliminate coulombic interaction, suspending small particles, or dissolving the hydrophilic compounds. Wine, ammoniated or potash solutions, soap preparations and especially saliva were often used as cleaning aids.²¹

Nowadays, restorers mainly use surfactant solutions, buffers and solutions of chelating agents, etc. to remove dust and hydrophilic dirt from painted surfaces. The removal of hydrophobic compounds (e.g. aged coatings or

varnishes), instead, is achieved by dissolving them in organic solvents, either neat or blended.² While the general rule of thumb is to choose solvents according to the law of “like dissolves like”, nowadays conservators can rely on tools such as the Teas diagrams.²² Teas charts are graphical representations of the reduced solubility parameters calculated by Hansen²³, based, in turn, on Hildebrand solubility parameters, δ . Such values can be calculated from the enthalpy of vaporization and the molar volume of a certain liquid²⁴. If the δ of two compounds matches, then solubilization occurs. Hansen refined the definition of δ , including in it three contributions: a term due to dispersion forces (δ_d), one due to polar interactions (δ_p) and the last to hydrogen bonding (δ_H). The quadratic sum of these three terms gives the square of the total solubility parameter, δ . Teas charts are triangle plots, reporting on their axes the reduced solubility parameters f_d , f_p and f_h , i.e. the Hansen parameters normalized by their sum and multiplied by 100 (so that $f_d + f_p + f_h = 100$).²⁵ The coordinates on Teas plot for a certain solvent, solvents blend or families of similar solvents can help to identify areas of solubility for a certain material, through testing⁷ (fig. 2 A). For example, the solubility diagram of Paraloid B72 is shown in fig. 2 B. Paraloid is a ethyl-methacrylate-methyl acrylate copolymer, commonly used as a waterproof and glossy coating to preserve the surface of painted artifacts; it is soluble in solvents like xylene, toluene, ethyl acetate, acetone and butanol,²⁶ the area of solubility delineated by such solvents is highlighted in fig. 2 B.

However, the spreading of free cleaning fluids (either organic solvents or aqueous media) on the surface of a painting can be risky, being uncontrolled and non-selective: leaching and deterioration of solvent-sensitive paints or pigments is likely to occur. Moreover, organic solvents are often volatile and toxic, therefore unsafe for the restorers.

The aggressiveness and the rate of evaporation of organic solvents can be limited by confining such solvents in μ Em.

μ Em are three- or four-components systems, containing two immiscible phases (water and oil), at least one surfactant and sometimes co-surfactants, as well. μ Em are thermodynamically stable systems, in which the interfacial tension between the water and oil phases must be extremely low.²⁷ To that end, the surfactant must saturate the oil-water interface, forming a layer between the two immiscible phases. Co-surfactants cooperate with the surfactant in reducing the interfacial tension, and fluidify the film; more

specifically, co-surfactants are able to reduce the bending rigidity of the interface, increasing its entropy and allowing the spontaneous formation of the μEm droplets.^{28–30}

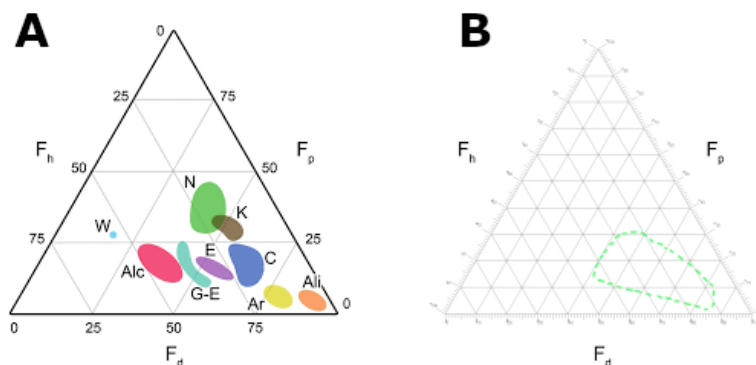


Figure 2. (A) Teas plot showing the solubility parameters for different families of solvents: water (W), solvents containing nitrogen (N), ketones (K), alcohols (Alc), glycol ethers and esters (G-E), esters (E), chlorinated solvents (C), aromatics (Ar), aliphatics (Ali). Reproduced from ref. [7]. (B) Teas plot for Paraloid B72.

When the water-surfactant interactions are more favored than the oil-surfactant interactions, and when the surfactant polar heads strongly interact with water, a positive curvature of the surfactant layer will be favored, resulting in an oil-in-water (o/w) μEm .³¹ If the organic solvent is partially miscible with water, the concept of two well-separated phases, therefore the concept of μEm , no longer applies. In that case, the continuous aqueous phase will contain a certain amount of solvent (depending on its solubility in water), and the solvent in excess will swell the micelles. Such systems have been defined as Nanostructured Fluids (NSFs).

Both μEm and NSFs have been largely investigated by our group as the optimal tool for the cleaning of polymer-coated painted surfaces (fig. 3 A, B)^{6–9,32}.

Namely, it has been observed that specific surfactants, included in good solvents/water mixtures, can enhance polymeric films dewetting^{33–36}.

Dewetting can be defined as the process in which the spontaneous withdrawal of a liquid from a non-wettable surface occurs.³⁷ The free energy of the liquid film depends on the interfacial energy, the gravitational energy and the long-range Wan der Waals forces. For thin films (thickness in the nm range) the

gravitational contribution is negligible with respect to the long-range forces; in this case the film is unstable and dewetting occurs through a spinodal decomposition. On the other hand, for thick films (thickness in the μm range, like those found on paintings), the long-range forces contribution is negligible with respect to the gravitational energy; these films are metastable and, when their thickness is lower than a critical value, dewetting occurs through nucleation and growth.^{37,38} In the case of a thick hydrophobic polymer film lying on a hydrophilic surface (glass), dewetting is thermodynamically favored but kinetically inhibited (see fig. 3 - 1).³⁹ For the dewetting process to occur, the polymer film must become liquid.⁴⁰⁻⁴²

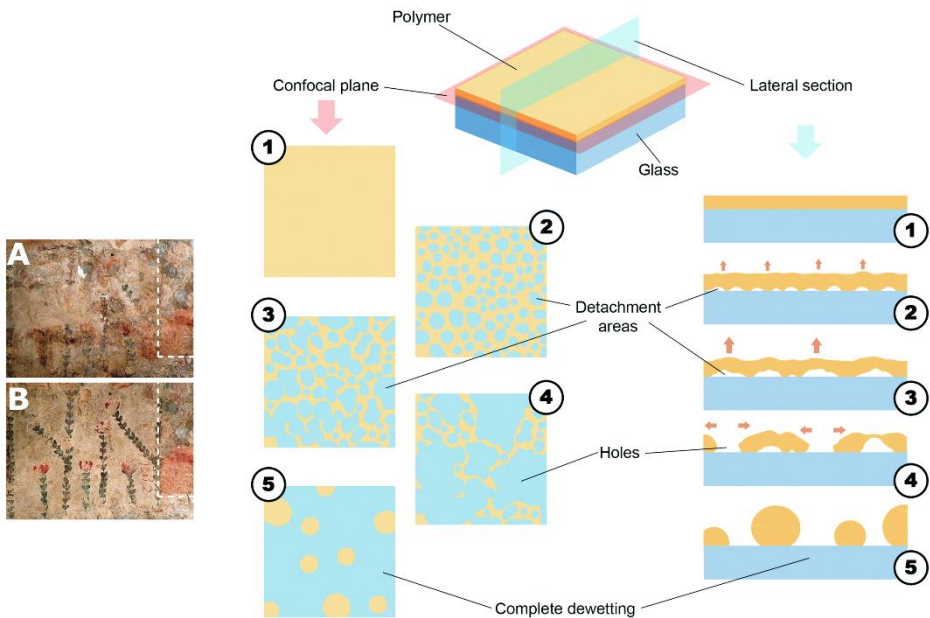


Figure 3. Left panel (A, B): Removal of an aged coating from a mural painting, in the Annunciation Basilica in Nazareth (Israel). (A) The surface before restoration: the aged coating caused a yellowing of the painted surface; (B) The painted surface after treatment with an o/w μEm . The highlighted rectangular area shows the untreated surface, as a reference. Reproduced from ref. [28]

Right panel (1 – 5): Dewetting process occurring when a model Paraloid B72 film, lying on a glass substrate, is treated with an o/w μEm . (1) Film before interaction; (2 – 3) Film destabilization and formation of cavities at the glass-film interface; (4 – 5) Polymer rearrangement in spherical blobs.

Reproduced from ref. [7].

More specifically, the temperature must be higher than the polymer glass transition temperature (T_g): this can be achieved either by heating the film, or by using a good solvent for the polymer, which lowers its T_g to room temperature, or below.⁴³ At that point, chains mobility increases and dewetting is no more inhibited: new polymer-fluid and substrate-fluid interfaces form, and the detached areas evolve through a nucleation and growth process (fig. 3 – 2, 3). Eventually, complete dewetting may occur (after a certain critical point), leading to polymer rearrangement in spherical blobs, completely detached from the substrate⁷ (see fig. 3 – 4, 5). Dewetting is of paramount importance in the removal of unwanted polymeric coatings from painted surfaces: the use of a o/w μ Em or a NSF grants the lowering of the polymer T_g , triggering the dewetting process.

1.3 Hydrogels to clean Modern and Contemporary paintings

In order to achieve a controlled cleaning action, capillary penetration and solvent evaporation must be reduced, while the solvent must be gradually released on the surface. In this regard, aqueous solutions, μ Em or NSFs can be mixed with thickeners to obtain the so-called “solvent gels”, or confined in rigid gels^{3,21,44}. Thickeners traditionally used in Conservation include cellulose ethers and poly acrylic acid polymers, while common examples of rigid gels are gellan and agar. While solvent gels leave residues that are difficult to remove, even after several rinsing steps, traditional rigid gels are not able to adapt to textured surfaces, limiting their application in the cleaning of clotted painted surfaces^{16,17}. Moreover, both systems are scarcely retentive and can damage solvent-sensitive artifacts.

Our research group, in the last decade, focused on the study of chemical pHEMA hydrogels and physical PVA-based cryogels for the treatment of water- and solvent-sensitive surfaces^{10,16,17,45} (see fig. 4). Both o/w μ Em and NSFs have been confined in these gels and used to clean hydrophobic dirt and polymer layers from both model substrates and paintings^{10,11,13}.

Hydrogels to clean Modern and Contemporary paintings should possess the following characteristics:

- a) High water retentiveness and free water content, to grant the diffusion of the cleaning fluids without excessive wetting of the substrate;

- b) An interconnected, micron-sized porosity;
- c) High adaptability on rough, clotted surfaces, to guarantee a uniform cleaning action;
- d) Ease of handling and a residue-free removal.³²

PVA-based cryogels, obtained through a FT process, satisfy all the aforementioned characteristics. In fact, PVA cryogels can be formulated to exhibit excellent strength and elasticity, with no need of toxic cross-linkers: PVA crystallites, formed during the polymer-water phase-separation occurring at low temperatures, are the only tie-points in the structure.⁴⁶

The FT process provides unique swelling and rheological properties to the gels: their structure is highly cohesive, which translates into easy handling and feasible removal from the treated artifacts, without leaving polymer residues¹⁶. Sponge-like networks can be obtained by exploiting semi-interpenetrating polymers as porogens. The interconnected porosity grants the diffusion of cleaning fluids, in a controlled fashion, at the gel-artifact interface: here dirt and grime are detached and included in the polymer matrix. The inclusion of cleaning fluids in cryogels also grants their controlled release on water- and solvent-sensitive artifacts, avoiding any leaching of paints or pigments.

Finally, adaptability of the gels to rough surfaces must be guaranteed, because homogeneous adhesion is essential to achieve optimal cleaning. Also in this case, the use of semi-interpenetrating polymers is crucial: they can change the gels rheological response and increase the systems compliance.

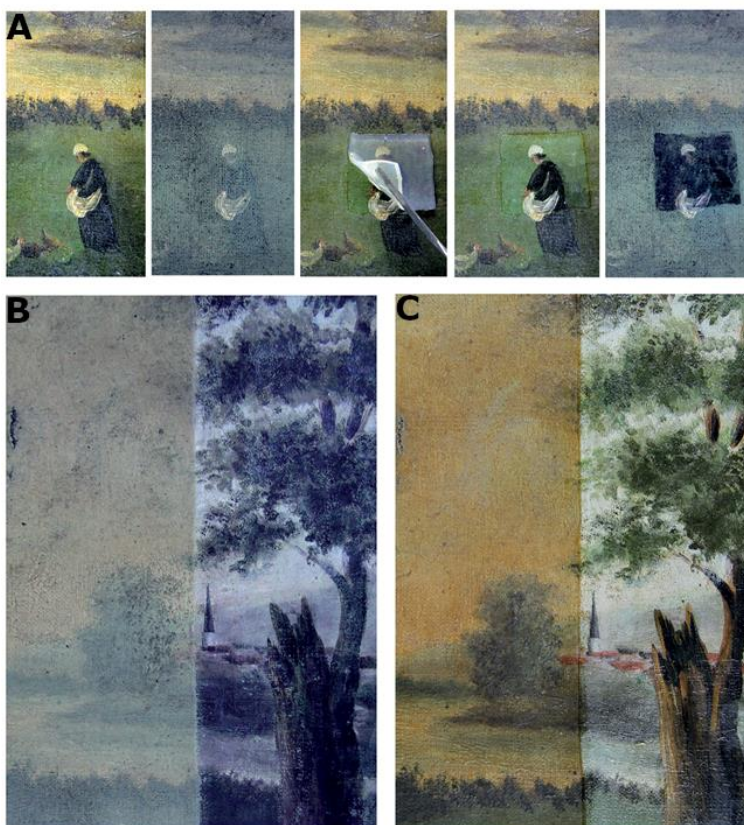


Figure 4. Chemical hydrogels, loaded with a o/w μEm , are used to remove an aged varnish from an eighteenth-century canvas painting. (a) From left to right: the appearance of the surface (detail) before cleaning, under visible light; the same surface under UV light; hydrogel application; cleaned area under visible light; cleaned area under UV light. (b) UV photographs of the painting showing the efficacy of the treatment: right-half is cleaned, while left-half is still uncleaned; (c) The painting under visible light: right-half is cleaned, while left-half is still uncleaned. Reproduced from ref. [1].

Chapter 2. Polymer solutions

Polymers are macromolecules, in which single repeating units, the monomers, are linked through covalent bonds to form long chains. The molecular weight of a single polymer chain can be calculated as:

$$M_{chain} = N m \quad (1)$$

where m is the monomer mass and N the degree of polymerization, i.e. the number of monomers constituting the polymer chain.

2.1 Polymers average Molecular Weights

For synthetic reasons, polymers are always characterized by a molecular weight distribution. Therefore, different average molecular weights can be obtained from different characterization techniques: the number average M_n from osmometry, the weight average M_w from light scattering, the Z-Average M_z from ultracentrifugation, and the viscosity average M_v from viscometry⁴⁷. M_n , M_w and M_z can be calculated from the following equation:

$$\bar{M} = \frac{\sum N_i M_i^a}{\sum N_i M_i^{a-1}} \quad (2)$$

where the parameter a is 1 for M_n , 2 for M_w and 3 for M_z , and N_i is the number of chains with weight M_i . On the other hand, M_v can be calculated from the intrinsic viscosity of the polymer solution, $[\eta]$, by applying the Mark-Houwink equation⁴⁷:

$$[\eta] = K M_v^\alpha \quad (3)$$

where K and α are known as Mark-Houwink parameters for the specific polymer-solvent system at a certain temperature.

Therefore, M_v can be defined as:

$$M_v = \left\{ \frac{\sum N_i M_i^{1+\alpha}}{\sum N_i M_i} \right\}^{1/\alpha} \quad (4)$$

From Eq. 2 and 4, it can be inferred that the polymer average molecular weights increase as follows:

$$M_n < M_v \leq M_w < M_z \quad (5)$$

and $M_v = M_w$ for $\alpha = 1$.

2.2 Solvent quality and chain conformation in solution

When a polymer is dissolved in a certain solvent, the conformation of polymer chains will depend on polymer-solvent interactions. Such interactions have been described by the Flory-Huggins theory^{48,49}: polymer chains are represented as random walks on a cubic lattice, each lattice site being occupied either by a monomer or by a solvent molecule (see fig. 5). If the volume fraction of sites occupied by the monomer is Φ and the number of monomers constituting the chain (i.e. the degree of polymerization) is N , the overall free energy per site is given by⁵⁰:

$$\frac{1}{k_B T} \Delta G_{mix} \Big|_{site} = \frac{\Phi}{N} \ln \Phi + (1 - \Phi) \ln(1 - \Phi) + \chi \Phi(1 - \Phi) \quad (6)$$

χ is the Flory interaction parameter, which takes into account monomer-monomer (MM), monomer-solvent (MS) and solvent-solvent (SS) interactions. More specifically:

$$\chi = \chi_{MS} - \frac{1}{2}(\chi_{MM} + \chi_{SS}) \quad (7)$$

χ is dimensionless and depends on temperature and pressure. If $\chi < 1/2$, the solvent is good for the polymer, while $\chi > 1/2$ is found for bad solvents. In good solvents, the polymer chain will be extended because solvent-polymer interactions are favored; in bad solvents, instead, polymer-polymer interactions will be favored and the chain will collapse.

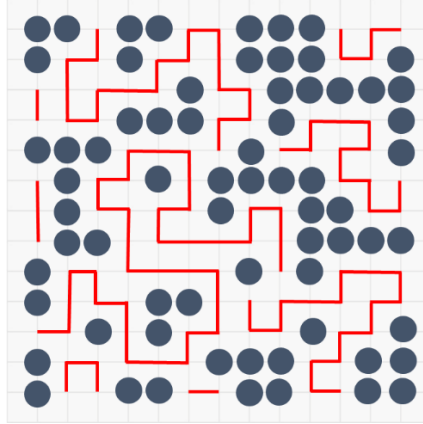


Figure 5. A bidimensional plane of the cubic lattice used to describe a polymer-solvent system in the Flory-Huggins theory. Each site on the lattice is occupied either by a solvent molecule or by a monomer: blue circles represent solvent molecules, while red lines represent polymer chains.

At $\chi = 1/2$ the solvent is called “theta” and the polymer chain assumes an ideal conformation (random walk), because polymer-solvent interactions are balanced as regards thermal energy.

Information about polymer conformation in solution and solvent quality can also be obtained from viscosity data of polymer solutions. For example, in the Mark-Houwink equation (Eq. 3), the α coefficient varies with chain conformation: $0 < \alpha < 0.5$ describes rigid spheres in ideal solvents, $\alpha = 0.5$ for theta solvent, $0.5 < \alpha < 0.8$ for polymers in good solvent (extended coil), while $0.8 < \alpha < 2$ is found for rigid/stiff chains.⁵¹ Also Huggins equation⁵² (Eq. 8) for dilute polymer solutions, and Martin equation⁵³ (Eq. 9) for semi-dilute polymer solutions, give some hints about chains conformation:

$$\eta_{sp} = [\eta]c + k_H[\eta]^2c^2 + k_2[\eta]^3c^3 + \dots \quad (8)$$

$$\ln \eta_{sp}/c = \ln[\eta] + k_M[\eta]c \quad (9)$$

η_{sp} is the specific viscosity, $[\eta]$ the intrinsic viscosity and c the polymer concentration.

The Huggins coefficient, k_H , describes polymer-solvent interactions: it has a lower value in good solvents (i.e., $k_H < 1/2$), while it increases in bad solvents

($k_H > 1/2$).⁵⁴ The Martin constant takes into account also polymer-polymer interactions, but varies like k_H .

Values of χ and k_H for aqueous solutions of PVA can be found in the literature⁵⁵⁻⁵⁹. For highly hydrolyzed PVAs, $\chi = 0.494$ at 30°C (it does not vary significantly with temperature) and $k_H = 0.51$; partially hydrolyzed PVAs, instead, are characterized by $\chi \approx 0.464$ (it increases with temperature to $\chi \approx 0.49$)⁶⁰ and $k_H = 0.39$ ⁵⁷.

These data suggested that, even if PVA is soluble in water, highly hydrolyzed PVA chains tend to self-associate in aqueous solutions ($k_H \approx 1/2$), while partially hydrolyzed chains are molecularly dispersed at room temperature. However, higher temperatures cause an increase in χ for partially hydrolyzed PVAs. In fact, at high temperatures, the hydrogen bonds formed among PVA chains and water become less effective: the polymer hydrophobicity, due to the presence of acetates, prevails. As a result, water becomes a poorer solvent and polymer chains collapse. Nonetheless, it should be noted that χ values are usually obtained in dilute conditions, i.e. for non-overlapping chains. Higher polymer concentrations and longer chains are expected to affect χ .⁶¹

2.3 Phase behavior of polymer-solvent systems

When χ exceeds $1/2$ polymer-solvent interactions could become so unfavorable that the solution may separate in two phases. More specifically, when χ is higher than a certain critical value χ_c (identified by a certain critical volume fraction) the system becomes unstable (see the critical point in fig. 6). The line between the stable and the unstable regions is the spinodal line (the dashed line in fig. 6).

χ for a polymer-solvent system can be changed by varying the temperature. In most of the cases, an increase in T causes χ to decrease: therefore, there will be a critical temperature, T_c , below which the system will separate in two phases. This temperature is called Upper Critical Solution Temperature (UCST). Conversely, when higher T causes an increase in the χ value, there will be a T_c above which two phases will form: in this case, the polymer-solvent system is characterized by a Lower Critical Solution Temperature (LCST). LCST behavior can occur more easily when hydrogen bonds are involved in the polymer-solvent interactions;⁶² in fact, hydrogen bonds are disrupted by high temperatures and an extended polymer chain conformation

is no longer favorable: polymer chains collapse and phase separation occurs. This is the case for aqueous solutions of partially hydrolyzed PVAs^{63,64}: they display a LCST behavior around 60°C.

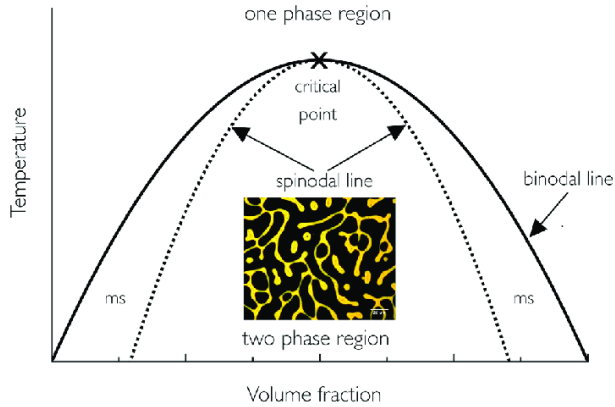


Figure 6. An example of phase diagram for a polymer-solvent system. The critical point indicates the critical temperature and volume fraction at which the system phase-separates. More specifically, the diagram describes a UCST behavior, as the separation occurs below a certain critical temperature. Between the binodal and the spinodal lines there is a metastable (ms) region: in this area the phase separation occurs as a nucleation and growth process. In the spinodal area, phase separation occurs through spinodal decomposition. Reproduced from *S. L. Burg and A. J. Parnell 2018 J. Phys.: Condens. Matter 30 413001*.

Phase-separation can occur through two distinct mechanisms: spinodal decomposition or nucleation and growth⁶⁵, depending on the position of the polymer-solvent mixture in the phase-diagram (fig. 6): unstable regions should give spinodal decomposition, while metastable regions result in nucleation and growth.

2.4 Polymer-polymer mixtures

Mixtures of two polymers can be described in term of Flory-Huggins theory: the polymers A and B, with degree of polymerization N_A and N_B , respectively, are positioned on a cubic lattice. The free energy per site can be written as⁵⁰:

$$\frac{1}{k_B T} \Delta G_{mix} \Big|_{site} = \frac{\Phi_A}{N_A} \ln \Phi_A + \frac{\Phi_B}{N_B} \ln \Phi_B + \chi \Phi_A \Phi_B \quad (10)$$

being Φ_A and Φ_B the volume fractions of the two polymers. For high molecular weight polymers the contribution of the entropic term to the free energy becomes negligible (the combinatorial entropy of mixing for the two polymers is much lower with respect to the polymer-solvent case).

Moreover, in most cases χ is positive. Therefore, A and B are usually not miscible. This description can be valid also when a concentrated solution of the two polymers is considered as, also in this case, the entropy of mixing is very low, and this prevails on the enthalpic term due to polymer-solvent interactions.^{50,66} As a matter of fact, segregation nearly always occurs in solutions containing two polymers.⁵⁰

While polymer-solvent mixtures (with a borderline miscibility) usually exhibit UCST behavior, polymer-polymer mixtures usually show a LCST.⁶⁷

Both UCST and LCST behaviors have been reported for mixtures of highly and partially hydrolyzed PVAs.⁶³

When the polymers composing the system are linear homopolymers, phase-separation results in macroscopic phase-separation (fig 7 A).

If linear homopolymers are mixed with the corresponding co-polymer, the co-polymer may act as a surfactant and stabilize phase-separation in micron-sized domains (fig. 7 B).⁶⁵

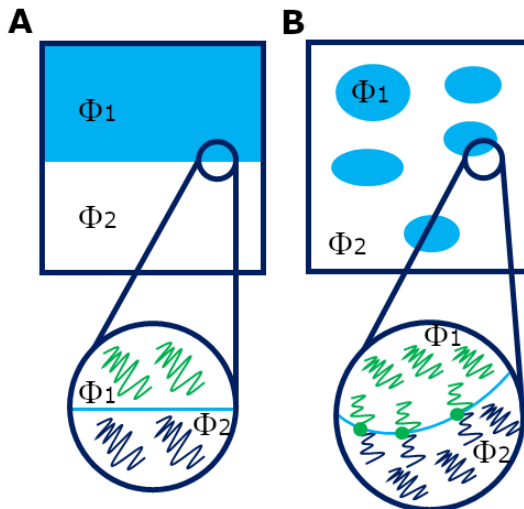


Figure 7. Two possible scenarios of phase-separation. (A) Two incompatible linear polymer are mixed: a macroscopic phase-separation results; (B) Linear homopolymers and the corresponding diblock copolymer are mixed: the latter stabilizes a phase-separation at the micron-scale, acting as a surfactant. Adapted from ref [59].

Chapter 3. Polymer Gels

A gel can be defined as a non-fluid network, expanded throughout its whole volume by a fluid.⁶⁸

Therefore, a polymer gel is expected to contain at least two components: a network, made of flexible polymer chains, and the liquid; systems of this type show both the cohesiveness of a solid and the diffusional properties of a liquid.⁶⁹ Depending on the nature of the fluid contained in the network, gels can be classified as hydrogels (containing water) or organogels (containing organic solvents).

3.1 Chemical and physical gels

Gels are obtained from chemical or physical processes. In the first case, the network forms by condensation of polyfunctional units, by additive polymerization or by covalent crosslinking of preexisting chains⁵⁰. Chemical gels are real macromolecules, with a nominally infinite molecular weight.

Physical crosslinks, instead, form because of physical interactions between polymer chains. Thus, in this case, the gelation is due to weak interactions, hydrogen bonds, or the formation of helix or crystallites⁵⁰. If the ordered regions containing such tie-point can be disrupted by a change in temperature, physical gels can also be defined “thermoreversible”.

It is convenient to distinguish between strong and weak gelation processes. In the first case, crosslinks are stable in the experimental conditions, and a sharp gelation threshold can be identified. In the second case, the gelation occurs due to a progressive decrease in the degrees of freedom in the system: the crosslinks can form and disrupt in the experimental condition, i.e. they are transient. Most gels obtained by chemical crosslinking are strong gels, while physical gels can be strong or weak. De Gennes defined the strong gelation regime as the case where polymer clusters, obtained at a certain polymer concentration p , at the beginning of the gelation process, could be isolated and subjected to different treatments (such as dilution, change of solvent, shear flow) without disrupting them.⁵⁰

From the rheological point of view, strong gels behave as solids at small and large deformations: the real and the imaginary part of their shear modulus G^* ,

i.e. the storage modulus, G' , and the loss modulus, G'' , are parallel and frequency-independent for a wide range of applied strain. In weak gels, instead, G' and G'' have more similar values and the G' - G'' crossover occurs at lower strains: the system starts to flow, behaving as a liquid⁷⁰ (fig. 8).

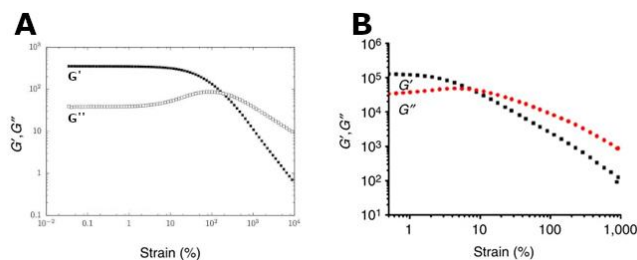


Figure 8. Rheological behavior of (A) a strong gel and (B) a weak gel. The crossover between G' and G'' occurs at higher strains in (A) and at lower strains in (B). Reproduced from: de Souza Mendes, P. R., *et al.* (2014). *Applied Rheology*, 24(5), 1-10; Lee, J. H., *et al.* (2015). *Nature communications*, 6(1), 1-9.

3.2 Gelation models

Gelation can be schematically described by considering a system containing monomers which are able to covalently link to each other, randomly. If the functionalities on each monomer are, at least, three, the system eventually evolves in an infinite, single macromolecule⁶⁹ (fig. 9).

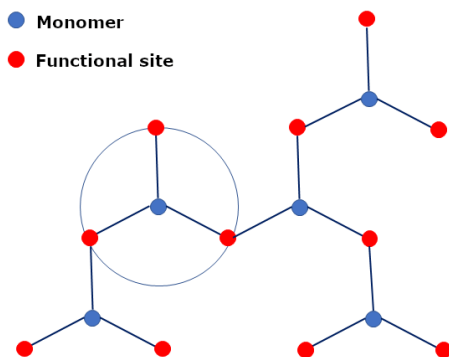


Figure 9. Tree-like branched molecule, obtained through the reaction of monomers with three functional sites. Flory-Stockmayer theory of gelation is based on this model.

This scenario constitutes the basis of the classical theory of gelation, developed by Flory and Stockmayer^{71,72}. The classical model is based on the following assumptions: monomers form tree-like clusters, the functionalities on each monomer having the same reactivity; intramolecular reactions cannot occur (closed cycles are never obtained); the reaction probability for each functional group depends on the mean monomer concentration (steric hindrance and excluded volumes are not considered). Due to these strong approximations, the classical model is able to describe the behavior at the gelation threshold only for vulcanization⁵⁰. In 1976, Stauffer⁷³ and De Gennes⁷⁴ applied percolation theory to describe the gelation mechanism. Percolation was first introduced to describe diffusion in disordered media.⁷⁵ However, it provides a model description for the gelation without considering diffusion processes, i.e. in absence of solvent. A two-dimensional lattice is considered, where each lattice site has z nearest-neighbors and z functionalities. Neighboring sites can react randomly, forming bonds (see fig. 10). If p is the number of reacted bonds at a certain time, a critical value p_c can be defined: when $p > p_c$, an infinite network is obtained. p_c is the gelation threshold.

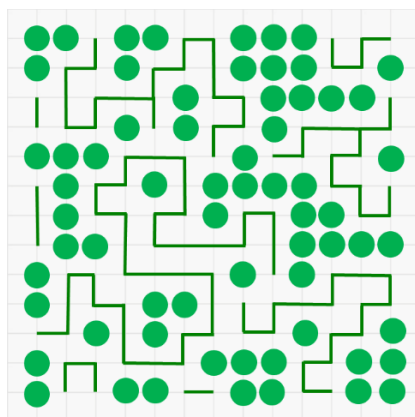


Figure 10. Percolation model: monomers (green circles) are represented in a tree-dimensional lattice (in the figure only one plane is shown). Neighboring units can react forming chains (green lines), until a single macromolecule forms.

De Gennes calculated different critical exponents, describing the characteristics of the system right below and above the gelation threshold.⁵⁰

Above the gelation point, the rheological characteristics of the system scale with polymer concentration and, more specifically, the following can be stated:

$$E \cong \Delta p^t \quad \text{for } p > p_c \quad (11)$$

where E is the elastic modulus, $\Delta p = p - p_c$ and $t \sim 1.7 - 1.9$ in three dimensions.

For gels swollen in good solvent, relationship (11) becomes:

$$E \propto c^{2.25} \quad (12)$$

where c is the polymer concentration⁵⁰.

The percolative approach fits particularly well with the gelation mechanism of chemical gels, but it has been widely used to describe the gelation of both chemical and physical networks, such as PVA cryogels⁷⁶⁻⁷⁸.

As far as physical gelation processes are concerned, Jones and Marques (JM) theory describing rigid polymer networks⁷⁹ has been readapted in an empirical model to describe the formation of fibrillar networks⁸⁰. According to the JM theory, the elastic modulus of rigid networks can be described as a function of the polymer volume fraction. More specifically, rigid networks are classified in *enthalpic networks*, containing frozen crosslinks, and *entropic networks*, whose crosslinks are defined as freely-hinged junctions. In enthalpic networks polymer chains are rigidly crosslinked and the network can deform only by bending the chains, while the freely hinged junctions of entropic networks can rotate freely about the tie-point, so that a certain entropy is associated to the crosslinks.⁷⁹

The following relationships have been established for enthalpic and entropic junctions, respectively:

$$E_{enthalpic} \propto C^{(3+D_F)/(3-D_F)} \quad (13)$$

$$E_{entropic} \propto C^{3/(3-D_F)} \quad (14)$$

C being the polymer concentration, and D_F the fractal dimension of the objects that connect at the tie-points.

According to JM theory, enthalpic and entropic behaviors can be simultaneously present in real systems, and a crossover concentration is

defined in passing from frozen to freely-hinged junctions in the final networks.

According to Guenet⁸⁰, JM model can be applied to physical gels with fibrillar morphology, where fibers have cross-sections in the nanometer range and mesh sizes of 0.1 – 1 μm . PVA cryogels have been already described as fibrillar networks: as will be evident by SEM micrographs, they are characterized by straight gel strands and a micron-sized porosity.

3.3 Poly(vinyl alcohol) cryogels

The term “cryogel” has been extensively used in the literature. The first publications describing such networks were about the chemical crosslinking of polymer chains or precursors in a moderately frozen organic solvent or in aqueous environment; in both cases, the solute was concentrated in restricted areas during the process, due to the partial freezing of solvent molecules.⁸¹ As a matter of fact, for FT gelation to occur, the low temperature of the freezing step must cause a phase-separation: water expels monomers or long chain molecules, which are concentrated in non-frozen areas, where they can react with crosslinking agents.

In the case of PVA cryogels, the crosslinking process has a physical nature. At low temperatures, the PVA chains in aqueous solution segregate in polymer-rich areas, while the water-rich phase is localized in pockets which eventually freeze. The ice exerts pressure on the polymer chains, until polymer crystallites form. PVA crystals are the physical tie-points, which hold together the hydrogel structure obtained after thawing (fig. 11). Ice crystals dissolve, but leave behind micron-sized pores: in other words, ice has served as a porogen during the process.

The literature concerning PVA physical cryogel is the widest: the applications range from medicine and biotechnology to environmental protection⁸¹, due to their high biocompatibility and non-toxicity.

PVA cryogels can have highly variable characteristics, which can be tuned and tailored to the desired application: gels rigidity, porosity, transparency, water content and retentiveness can be adjusted depending on the number of FT cycles, the type of polymers used in the formulation, their relative amounts or molecular weight.⁸²

More specifically, gels crystallinity and rigidity increase with the number of FT cycles^{46,83}, while pores enlarge by repeating FT steps⁸⁴.

A further increase in gels crystallinity is caused by curing/ageing of the networks in water.⁴⁶

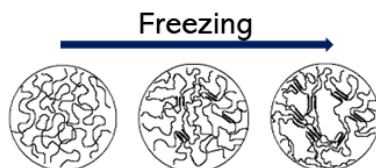


Figure 11. Effect of freezing on a PVA aqueous solution: a water polymer phase-separation occurs. Ice crystals form in polymer-poor areas, while concentrated polymer chains will interact with each other, forming crystallites. Ice will leave water pockets (pores) after thawing. Readapted from ref [53].

The addition of additives (co-solvents or oligomers) can also affect gels structure and rheological behavior.

For instance, low-molecular weight polyols interfere with PVA cryotropic gelation, while higher-molecular weight components can lead to a liquid-liquid phase separation at low temperatures⁸⁵; in this case PVA, as the most abundant component, concentrates in the continuous phase, and the resulting gels are stiffer. In fact, higher polymer concentrations in the pre-gels solution lead to more elastic and structured gels.

MATERIALS AND METHODS

Chemicals

PVAs coded as L-PVA, (HD = 88%, M_w 100 kDa) and H-PVA, (HD 98%, M_w 160kDa) were purchased from Sigma-Aldrich, while PVAs coded as K18_L-PVA, K32_L-PVA and K47_L-PVA (increasing M_w , HD = 88%) were purchased from Kuraray.

PVP (M_w 1300 kDa) was also purchased from Sigma-Aldrich.

For the polymer labeling reactions, Fluorescein isothiocyanate isomer I (purity \geq 90%, FITC), Rhodamine B isothiocyanate (mixed isomers, RBITC), triethylamine (purity > 99%) and DMSO (anhydrous, purity > 99.9%) were purchased from Sigma Aldrich; H-PVA was labeled with FITC, L-PVA and PVP with RBITC. When required, reaction steps were conducted under dry and inert atmosphere using standard Schlenk technique procedures. Rhodamine 110 chloride (purity \geq 99%) from Sigma-Aldrich was used to obtain confocal images of the four types of gel.

For the calibration procedure in Fluorescence Correlation Spectroscopy, the fluorescent probe Alexa Fluor 568 dye from Thermo Fisher Scientific was used. Ammonium citrate tribasic (TAC), 2,2-Bis(hydroxymethyl)-2,2,2-tris(hydroxymethyl)ethanol (Bis-Tris, purity \geq 98.0 %) and hydrochloric acid (37.0%), used for the cleaning tests, were all purchased from Sigma-Aldrich and used as received.

For the NSF's preparation, the following chemicals were used, without further purification: $C_{11}(C=O)EO_{15}-CH_3$, Methoxy pentadeca oxyethylene dodecanoate (MPD, Nikkol Chemicals, assay 99%), $C_{12}EO_{15}$, Pentadeca oxyethylene dodecyl ether (PDE, Nikkol Chemicals, assay 99%), sodium dodecyl sulfate (SDS, Sigma-Aldrich, assay 99%), propylene carbonate (PC, Sigma-Aldrich, assay 99%), 2-butanone (MEK, Sigma-Aldrich, purity 99%), 2-butanol (BuOH, Sigma-Aldrich, assay > 99%), ethyl acetate (EA, Sigma-Aldrich, ACS Reagents, assay \geq 99.5%), $C_{9-11}E_{5,5}$ alcohol ethoxylate (Berol 266®, AkzoNobel), $C_{9-11}E_6$ ethoxylated alcohol (Stepan, purity 95%), 1-pentanol (PeOH, Merck, purity \geq 98.5%), and p-xylene (Merck, purity > 99.5%). Bodipy® 558/568 C12 ((4,4-difluoro-5-(2-thienyl)-4-bora-3a,4a-

diaza-sindacene-3-dodecanoic acid), ThermoFisher) was used to label the surfactant shell of micelles/droplets in NSF.

Polymer films to mimic hydrophobic dirt were made of poly(ethyl methacrylate/methylacrylate) (p(EMA/MA) – Paraloid B72®). Paraloid was labeled with Coumarin 6 (Merk, Purity $\geq 97.5\%$).

Water used for the preparation of polymer solutions and NSF was purified by a Millipore system (resistivity $> 18\text{ M}\Omega\text{ cm}$).

Hydrogels preparation

PVA-based cryogels were prepared as follows: H-PVA was mixed with the semi-interpenetrating agent, according to the quantities reported below. The polymers were dissolved in pure water at 98°C , using a round flask equipped with a condenser. Once the solutions were homogeneously mixed, they were cooled to room temperature. The viscous liquids were poured in polystyrene molds ($14 \times 7 \times 0.2\text{ cm}^3$) and underwent the FT process. A FT cycle consists of one freezing step at $-18^\circ\text{C}/-23^\circ\text{C}$ for 16 hours, and one thawing step at RT, for 8 hours.

Chapter 4: H-PVA/L-PVA and H-PVA/PVP gels were prepared, varying H-PVA concentration (coded as X = 3-15 % w/v) and maintaining constant L-PVA and PVP concentrations (3 % w/v). Samples underwent 1 FT cycle. More specifically, three different series of cryogels were prepared:

- PN_X, with X = 3, 5, 7, 9, 12, 15 % w/v, are cryogels containing increasing concentrations of H-PVA (X);
- i-PVA_X, with X = 3, 5, 7, 9, 12, 15 % w/v, are cryogels containing 3% w/v of L-PVA and increasing concentrations of H-PVA (X);
- i-PVP_X, with X = 3, 5, 7, 9, 12, 15 % w/v, are cyogels containing 3% w/v of PVP and increasing concentrations of H-PVA (X);

Chapter 5: Gels were obtained either by H-PVA aqueous solutions (9 % w/w of polymer) or H-PVA/L-PVA solutions (12% w/w of polymers, in a ratio 3:1, respectively). The solutions underwent 1 or 3 FT cycles. Samples are denominated PVA FT1, PVA FT3, PVA/PVA FT1 (or TC-PN FT1), PVA/PVA FT3 (or TC-PN FT3).

Chapter 6: Gels were obtained by mixing H-PVA either with K18_L-PVA, K32_L-PVA, or K47_L-PVA. The ratio between the two polymer was 3:1, the total polymer concentration 12% w/v. The polymer solutions underwent

1 FT cycle. Samples obtained are denominated as TC-PN K18, TC-PN K32 and TC-PN K47.

In all cases, after the last thawing step, gel samples were washed in demineralized water for one week. Water was changed once per day during the storage time, to extract the unbound polymer.

NSFs Preparation

Chapter 7: Four different NSFs were prepared, containing the solvent PC or MEK, and the nonionic surfactant PDE ($C_{12}E_{15}$ -OH) or MPD (C_{11} -C=O- E_{15} -OCH₃). The quantities of each chemical are in w/w:

- H₂O/PC/PDE: H₂O (79.9 %), PC (15.1 %), PDE (5 %);
- H₂O/PC/MPD: H₂O (79.9 %), PC (15.1 %), MPD (5 %);
- H₂O/MEK/PDE: H₂O (83.8 %), MEK (11.2 %), PDE (5 %);
- H₂O/MEK/MPD: H₂O (83.8 %), MEK (11.2 %), MPD (5 %).

Chapter 8: XYL and BEMP NSFs were prepared as follows (concentrations are in w/w):

- XYL: H₂O (85.5 %), SDS (4 %), PeOH (8 %), xylene (2.5 %);
- BEMP: H₂O (60 %), C₉₋₁₁E₆ (5 %), BuOH (10%), PC (7 %), MEK (11 %), EA (7 %).

The NSF used to clean Picasso's painting (investigated in Chapter 8, paragraph 8.2) had, instead, the following composition (w/w): H₂O (65.9 %); C₉₋₁₁E_{5,5} (3.3 %), SDS (0.2 %), BuOH, (9.7 %), MEK (20.9 %).

Determination of commercial L-PVAs M_w

The viscometric molecular weight (M_v) of commercial L-PVAs (K18_L-PVA, K32_L-PVA and K47_L-PVA) was determined by calculating the value of the intrinsic viscosity, $[\eta]$, from the Martin equation (Eq. 9): solutions at increasing concentrations of each polymer were prepared, and their viscosity was measured through an Ubbelohde type viscometer, placed in a thermostatic bath (25.0 ± 0.1 °C). The values of $[\eta]$ obtained for each polymer were used to calculate M_v from the Mark-Houwink equation (Eq. 3). Values of K and α

parameters of the Mark-Houwink equation were obtained from Masuelli *et al.*⁵¹

The M_v of H-PVA and L-PVA from Sigma-Aldrich was calculated too, for comparison.

Labeling of polymers

See Paper II in Appendix¹⁷. PVP was labeled with RBITC (see the condition of L-PVA labeling), exploiting synthetic defects on the polymer backbone.

Physico-chemical characterization of gels

Gel fraction (G%). The gel fraction quantifies the percentage of polymer that is incorporated in the network. It was obtained gravimetrically, as the ratio between the weight of the residual dry matter of a gel sample after one week washing (W_{wa}) and the initial polymer content of the same gel (W_0):

$$G(\%) = W_{wa}/W_0 \times 100 \quad (15)$$

The residual dry matter was obtained by drying washed gel samples in an oven at 100 °C until constant weight is achieved. Values reported are averages of at least three measurements.

Equilibrium Water Content and Free Water Index (EWC % and FWI).

Water content of hydrogels, after washing, was calculated as follows:

$$EWC(\%) = W_w - W_d/W_d \times 100 \quad (16)$$

where W_w and W_d are the weights of the wet gel and the dry gel, respectively.

They were obtained through Thermogravimetric Analysis (TGA).

The Free Water Index (FWI) was calculated in order to determine the quantity of water in the samples that behaves as free water:

$$FWI = \frac{\Delta H_{exp}}{EWC \times \Delta H_{theo}} \quad (17)$$

where ΔH_{exp} (J /g) and ΔH_{theo} are the melting enthalpy of water in the gel sample and the theoretical value for pure water (334 J/g)⁸⁶, respectively. The experimental enthalpies of melting were obtained by Differential Scanning Calorimetry (DSC). DSC measurements were performed using a DSC Q1000 (TA Instruments) apparatus. Hydrogel samples (15–25 mg) were analyzed using “Tzero” aluminum hermetic pans with a temperature scan from -60 °C to 25 °C (heating rate: 0.5 °C/min). Water content was obtained on the same samples: hermetic pans were pierced to permit water to evaporate, and were subjected to a DTG run using a SDT Q600 (TA Instruments) apparatus. The temperature was increased from 25°C to 230°C with a heating rate of 10 °C/min, under nitrogen flow. The presented results are the average of at least three measurements.

Equilibrium Volume Swelling Ratio (q_v). The swelling degree was evaluated on washed gels sheets. The swelling capacity was calculated by measuring the variation of the width by means of a caliper rule (resolution 0.02 mm) according to⁸⁷:

$$q_v = \left(L/L_0 \right)^3 \quad (18)$$

where L_0 is the side's length after preparation (i.e. the mold's side), and L is the side's length after washing (at swelling equilibrium).

Crystallinity degree (X_c). The crystallinity degree of hydrogels was evaluated from the DSC melting peak of the freeze-dried samples. It was calculated as the ratio between the experimental specific enthalpy of fusion of the samples and the specific enthalpy of fusion of fully crystalline PVA (161 J/g)⁸⁸. The DSC experiments were carried out increasing the temperature from 25°C to 250 °C at a heating rate of 5 °C/min. The reported values are averages of 5 measurements.

Water release. Hydrogels surface was gently blotted, before a square sample was placed on Whatman filter paper, in a Petri dish covered with a lid to avoid evaporation. The amount of water released on the filter paper was recorded

by weighing the Petri dish before and after 30 minutes contact with the sample. Reported values are averages of 4-6 measurements.

Rheology. A Discovery HR-3 rheometer from TA Instruments (steel parallel plate geometry, diameter of 40 mm), equipped with a Peltier temperature control system, was used to investigate the hydrogels and pre-gel solutions rheological properties. Amplitude sweeps curves were collected in a range of oscillation strain between 0.01 and 50%, at a frequency of 1 Hz. The linear viscoelastic range, identified in the amplitude sweeps, lies between strains of 0.01-1 % for the FT1 gels, while it is located between 0.01 and 0.1% for the FT3 gels. Frequency sweeps curves were thus recorded within this range, at constant oscillation strain, by increasing the oscillation frequency (0.01-100 Hz). The measurements were conducted at constant temperature (25°C) on 40 mm diameter gel disks (thickness of 2 mm ca.). Data are averages of 3-6 measurements.

Gels structure and morphology

Confocal laser scanning microscopy (CLSM). Confocal images were acquired using a Leica TCS SP8 confocal microscope (Leica Microsystems GmbH, Wetzlar, Germany). The chosen laser lines were the Ar ion laser (488 nm laser line) for FITC and Rhodamine 110 and the DPSS 561 (561 nm) for RBITC and Bodipy. Fluorescence was detected using photomultiplier tubes (PMT) in the 498-540 nm and 571-630 nm ranges, respectively. The objective was a water immersion 63X/1.2 W (Zeiss). All samples were placed in the appropriate sample-holder (Lab-Tek® Chambered #1.0 Borosilicate Coverglass System, Nalge Nunc International, Rochester, NY, USA). 3D stacks were obtained for both pre-gel solutions, gels right after thawing and washed gels.

Image analysis. Chord distribution analysis was implemented on stacks of confocal images (obtained on washed gels, soaked in a Rhodamine 110 solution) containing about 100 2D images, corresponding to a thickness of ~50 μm . Each image of the stack was iteratively analyzed through the MATLAB® algorithm developed by M. Ryan MacIver⁸⁹, which we readapted to work on the Leica format (.lif) to obtain an average chord length

distribution representative of the whole stack of images. Briefly, in the chosen stack, each 2D image was converted to grayscale, contrast-enhanced and binarized. Then, a set of 10,000 lines, randomly oriented, were drawn on each image and the number of segments defining phase boundaries (changes from the pore- to the gel-phase) were binned according to chord dimension, R (μm) so as to extract a frequency, $f(R)$, histogram with a binning size of $1 \mu\text{m}$. The minimum chord length in pixels was set to 2, which corresponds to about $0.6 \mu\text{m}$. All histograms show an exponential decay if plotted in a semi-log plot (i.e. $\log f(R)$ vs R (μm)), that evolves according to:⁹⁰

$$f_{Pores}(R) \propto \exp\left(-\frac{R}{\lambda_{Pores}}\right) \quad (19)$$

$$f_{Gel-Phase}(R) \propto \exp\left(-\frac{R}{\lambda_{Gel-Phase}}\right) \quad (20)$$

where the persistence length λ describes the characteristic length scales of the of the two phases; λ was obtained for each gel by fitting the averaged exponential decays, considering only the most frequent chord lengths.

In the preliminary development of the code, the minimum chord length was varied from 2 to 6 pixels showing that the resulting extracted characteristic dimension was independent on the chosen length. The variation of the decay curves along the depth of the stack was reported in 3D graphs.

Scanning electron microscopy (SEM). SEM imaging was performed on freeze-dried gels samples, by using a Field Emission Gun Scanning Electron Microscope SIGMA (FEG-SEM, Carl Zeiss Microscopy GmbH, Germany). The acceleration potential was set to 5 kV and the working distance to 2.0–2.7 mm. Pure H-PVA (FT1 and FT3) and TC-PNs (FT1 and FT3) gels (chapter 5) were coated with an ultra-thin layer of gold, by using the Agar Scientific Auto Sputter Coater.

Small angle X-ray scattering (SAXS). SAXS measurements were performed using a HECUS S3-MICRO SWAXS-camera (Hecus XRS, Graz, Austria) equipped with a Hecus System 3 with a Kratky collimation system and a position-sensitive detector (PSD 50M), containing 1024 channels (width

= 54 μm). Cu $K\alpha$ radiation of wavelength, $\lambda = 0.1542 \text{ nm}$, was provided by a Cu anode from a 50W Microfocus source, with customized FOX-3D single-bounce multilayer point focusing optics (Xenocs, Grenoble, France). The voltage is generated by the GeniX system (Xenocs). The sample-to-detector distance was 281 mm. The volume between the sample and the detector was kept under vacuum during the measurements to minimize scattering from the air. Scattering curves were obtained in the Q-range between 0.009-0.54 \AA^{-1} . Temperature was kept at $25 \pm 0.1^\circ\text{C}$ by a Peltier element. A demountable sealed cell for solid was used as sample holder with Kapton as a window material (optical path = 1 mm). Gel samples were cut in thin slices, while precursor solutions were poured in the cell. Standard measurement conditions were 50 kV, 1 mA. The acquisition time was from 1 to 2 hours depending on the sample. Scattering curves were corrected for the empty cell/water contribution.

Scattering curves of both gels and pre-gel solutions were fitted, according to the literature^{91,92}, as a sum of two contributions to the scattered intensity, due respectively to fixed polymer junctions (i.e. the tie points of the network or polymer agglomerates in solution) and polymer chains in solution (i.e. chains in a liquid-like environment). Namely, SASView⁹³ was used to perform the fitting. The scattered intensity $I(q)$ is described as follows:

$$I(q) = I_L(0) \frac{1}{\left[1 + \frac{D+1}{3}(q^2\xi^2)\right]^{D/2}} + I_G(0)\exp(-q^2R^2/3) + B \quad (21)$$

where $I_L(0)$ and $I_G(0)$ are the Lorentzian and the Guinier parameters, D is the fractal exponent, ξ is the correlation length and R is the radius of gyration of larger objects. More specifically, the equation consists of two terms: the Lorentzian term, which describes the liquid-like fluctuations in the network, and is linked to ξ and D ; and the Guinier term, which describes solid-like fluctuations, and is related to R . Thus, ξ was assumed to describe the polymer chains conformation in liquid-like environments, while R describes the crystallites dimension in the gels, and to the radius of polymer aggregates in pre-gel solutions.

Nuclear Magnetic Resonance (NMR). NMR experiments were performed on i-PVA₉ and i-PVP₉ samples (Chapter 4), containing increasing amounts of L-PVA and PVP (2, 3, 4, 5 % w/v). A Bruker Avance Spectrometer was used, operating at the frequency of 400 MHz for ¹H in DMSO-d₆. The signal due to residual proton of the solvent was used as internal reference. The amount of semi-interpenetrated polymer after washing and storage in water (2 months) was calculated for i(2)-PVA, i(3)-PVA, i(4)-PVA and i(5)-PVA samples by comparing the signals due to residual esters moieties of L-PVA with alcohols' -CH- of L-PVA and H-PVA, according to the following equation:

$$\frac{L - PVA (wt)}{H - PVA (wt)} = \frac{\left(\frac{I_{1.9-2.1}}{3 \times (1 - HD_{L-PVA})} \times MW_{L-PVA} \right)}{\left[\left(\frac{I_{1-1.7}}{2} - \frac{I_{1.9-2.1}}{3 \times (1 - HD_{L-PVA})} \right) \times MW_{H-PVA} \right]} \quad (22)$$

where $I_{1.9-2.1}$ and $I_{1-1.7}$ indicate the peaks areas due to the 3 acetate's hydrogens (present in L-PVA only) and the 2 vinyl hydrogens (present in both H-PVA and L-PVA), respectively; HD is the hydrolysis degree of L-PVA; MW_{L-PVA} MW_{H-PVA} are the average molecular weights of H-PVA and L-PVA monomers, respectively. Assessment of residual PVP in the four i-PVP₉ gels was attempted following a similar procedure and, though a trend can be identified, exact quantification was not possible because of its very low amount (less than 6 wt% with respect to H-PVA).

Polymer chains dynamics - Diffusion of NSF's

Fluorescence correlation spectroscopy (FCS). FCS was used to determine: the diffusion free H-PVA, L-PVA and PVP chains (concentration of dye: 50 nM); the diffusion of L-PVA in TC-PNs pores; the diffusion of free NSF's droplets/micelles (concentration of dye: 10 nM); the diffusion of NSF's through the gel matrices.

FCS curves were obtained using a Leica TCS SP8 confocal microscope (Leica Microsystems GmbH, Wetzlar, Germany) equipped with a PicoQuant FCS modulus (PicoQuant, Berlin, Germany). Measurements were performed using a 63X/1.2 W water immersion objective (Zeiss). The RBITC labeled PVA and

PVP diffusion was monitored exciting the RBITC with the DPSS 561 laser (561 nm), while the fluorescence intensity was acquired using a Hybrid SMD detector in the 571–630 nm range. Bodipy is an amphiphilic dye, used to label the NSFs by forming mixed micelles. It was excited with the same laser line (561 nm). FITC-labeled H-PVA was tracked by exciting FITC with the 488 nm Ar laser line, and the fluorescence was collected with the Hybrid SMD detector in the 500–540 nm range. Analyzed samples were deposited in the appropriate sample-holder (Lab-Tek® Chambered #1.0 Borosilicate Coverglass System, Nalge Nunc International, Rochester, NY, USA). 10 nM aqueous solutions of Alexa Fluor 568 and Rhodamine 110 were used for FCS calibration⁹⁴.

The fitting model assumes that the three-dimensional Brownian diffusion of labeled molecules across a 3D-ellipsoidal Gaussian volume is the only contribution to the observed decay time. FCS curves were analyzed considering either a one-component decay⁹⁵:

$$G(\tau) = \frac{1}{N} \left[\left(1 + \frac{\tau}{\tau_D}\right)^{-1} \left(1 + \frac{\tau}{S^2\tau_D}\right)^{-1/2} \right] \quad (23)$$

or a two-components decay⁹⁶:

$$G(\tau) = \frac{1}{N} \left[f_1 \left(1 + \frac{\tau}{\tau_{D1}}\right)^{-1} \left(1 + \frac{\tau}{S^2\tau_{D1}}\right)^{-\frac{1}{2}} + (1 - f_1) \left(1 + \frac{\tau}{\tau_{D2}}\right)^{-1} \left(1 + \frac{\tau}{S^2\tau_{D2}}\right)^{-\frac{1}{2}} \right] \quad (24)$$

where N is the average number of fluorescent molecules detected inside the confocal volume ($N = CV$, with $V = \pi^{3/2}w_0^3S$ and C the concentration), f_1 is the percentage of the contribution of $\tau_{D,1}$ to the total decay time, $\tau_{D,i}$ are the decay times, and $S = z_0/w_0$ is the ratio between the axial and the lateral dimensions of the confocal volume, determined through the calibration procedure with Alexa 568. The diffusion coefficients D_i of the labeled species can be determined by:

$$\tau_{D,i} = \frac{w_0^2}{4D_i} \quad (25)$$

The hydrodynamic radii of the labeled species were calculated through the Stokes-Einstein equation.

Fluorescence recovery after photobleaching (FRAP). FRAP experiments were performed with the FRAP module of the Leica TCS SP8 confocal microscope (Leica Microsystems GmbH, Wetzlar, Germany). A 63X/1.2 W water immersion objective (Zeiss) was used. Gels containing RBITC-labeled L-PVA (after 1 week washing) were analyzed. The bleaching sequence lasted 7.74 s, while the recovery time was 155s for the TC-PN FT3 gel and 103s for the TC-PN FT1 gel (ROIs diameter: 2.5 μm). All measurements were performed at room temperature (25°C). FRAP curves were obtained through two subsequent normalizations: the first consisted in calculating the ratio between the signals of the bleached ROI and the reference ROI, and then the curves were normalized between their minimum and maximum values. The double-normalized curves were used to calculate an averaged final curve (7-10 repetitions per sample).

Cleaning Tests

Artificial soil preparation. An artificial soil mixture, containing both hydrophobic and hydrophilic compounds, and particulate matter, was prepared according to the literature⁹⁷.

Preparation of Paraloid coated glass slides. Paraloid films with a thickness of 2 μm ca. were obtained by spin-coating 200 μL of a 10% w/w Paraloid solution in EtAc on cover-glasses (2000 rpm, 120 s). Coumarin 6 was co-dissolved with the polymer solution, to obtain labeled films for confocal microscopy experiments.

Preparation of painting mockups. Painting mock-ups mimicking modern/contemporary painting techniques were prepared using a commercial primed canvas, oil (Winsor&Newton), and alkyd colors (Ferrario).

Cleaning of mockups with TC-PNs cryogels (loaded with aqueous solutions). After about one year from the preparation, an artificial dirt mixture in ligroin was applied on mockups, by means of a brush over the paint

layer. After one month, cleaning tests were performed using TC-PN FT1 gels. Prior to use, gels were immersed for 12 hours in the following cleaning solution: water, 98.88%; Bis-Tris, 1.09%; TAC, 0.03%. The solution was buffered to pH 7 using a mild HCl solution. This cleaning fluid was selected as it represents a standard choice by conservators for the removal of airborne dirt particles from paintings^{21,98}. Prior to the application, the gel sheets were gently squeezed with blotting paper to remove the water excess from their surface. During application, the contact time of the gel over the paint layer was one minute. Most of the soil was removed, and the left soil residues were softened and detached after contact with the gel. Gentle mechanical action with an “eraser-gum” shaped TC-PN was carried out to complete the cleaning. After soil removal, a water-loaded gel was applied for two minutes on the same spot to remove the possible residues of the cleaning solution.

Cleaning of mockups with TC-PNs cryogels (loaded with NSF). After 1 year ageing, some of the mockups were lined, using a wax-resin adhesive based on Watherston’s original recipe⁹⁹. Moreover, mockups were varnished by spraying with commercial PVAc (AYAC, Union Carbide, Dow Chemical, USA) dissolved (20% w/w) in toluene or methyl alcohol (Sigma-Aldrich). Then, the mock-ups were aged in a light box at 11,000 lux for 1 month. NSF-loaded TC-PNs were gently squeezed with blotting paper to remove the excess fluid from their surface. During application, the contact time of the gel with the paint layer varied from few seconds to 2 min. The varnish and wax layers were swollen and softened after the application; they were removed by gentle mechanical action with a dry cotton swab. Finally, a water-loaded gel was shortly applied on the same spot to remove possible residues of the NSF.

Fourier-transform infrared (FTIR) spectroscopy imaging. The 2D FTIR imaging of the painting mock-ups was carried out using a Cary 620-670 FTIR microscope, equipped with a Focal Plane Array (FPA) 128 x 128 detector (Agilent Technologies). This set-up was selected as it allows discriminating compounds with different chemical composition on a surface, down to a spatial resolution of few microns¹⁰⁰.

The spectra were recorded directly on the surface of the samples in reflectance mode, with open aperture and a spectral resolution of 8 cm⁻¹, acquiring 128 scans for each spectrum. A “single tile” map has dimensions of 700 x 700 μm²

(corresponding to 128 x 128 pixels), and a spatial resolution of 5.5 μm (i.e. each pixel has dimensions of 5.5 x 5.5 μm^2 , and is related to an independent spectrum). “Mosaic” maps were also recorded, composed of multiple single-tiles. In each 2D map, the intensity of characteristic bands of PVA or the artificial soil was imaged. The chromatic scale of the maps shows increasing absorbance of the bands as follows: blue < green < yellow < red.

RESULTS AND DISCUSSION

Gels for the cleaning of artworks require distinctive features to make them easy to use and effective in removing soil, aged coatings, and other unwanted materials from the artifacts' surface, preserving the original components and avoiding detrimental effects.

PVA-based cryogels here investigated were obtained by varying the formulation and the number of FT cycles.

More specifically, all cryogels were prepared by using a PVA with a high hydrolysis degree (HD), H-PVA, which constitutes the gel main structure.

The structural properties of cryogels, as well as pores shape and dimension, were investigated in the following cases:

- a) After the inclusion of a second polymer, acting as a semi-interpenetrating agent; polyvinylpyrrolidone (PVP) and a PVA with a lower HD (L-PVA) were used.
- b) Gels obtained by the combination of H-PVA and L-PVA performed better in the cleaning tests, therefore their structure was further investigated by varying the number of FT cycles applied to the formulation. These gels were called Twin-Chain Polymer Networks (TC-PNs), due to the similarity of the two polymers included in the network.
- c) After the inclusion of L-PVAs with three different molecular weights (M_v).

These investigations are described in chapters 4-6.

Later, the diffusion of NSFs through the gels matrix was tracked; the mechanism of removal of polymer coatings from model surfaces was also investigated (chapters 7-8).

Finally, cleaning abilities of TC-PNs were assessed, and compared to those of rigid gels, such as chemical gels or gels traditionally used in restoration (chapter 9).

TC-PNs were used to clean Jackson Pollock's *Two* and *Eyes in the Heat* (Peggy Guggenheim Collection, Venice) and Pablo Picasso's *The Studio* (Peggy Guggenheim Collection, Venice). More details on the restoration are reported in chapter 10.

Chapter 4. PVA-based cryogels: the influence of the semi-interpenetrating polymer

This chapter ¹ is aimed at deepening and analyzing physico-chemical properties of PVA-based cryogels, containing linear semi-interpenetrating polymers. Namely, the partially hydrolyzed L-PVA, and PVP, were dissolved with H-PVA in aqueous solutions, and the resulting mixtures underwent one FT cycle. L-PVA and PVP chains alter crystallinity, gel fraction and rheological properties of the networks, influencing the gelation mechanism; the nano- and micro-structure change: pores shape and dimension were proven to depend on the polymers phase-behavior in aqueous solution.

Rheological properties and porosity are deemed to be crucial for the cleaning action. However, this chapter explores the physical chemistry behind the gel formation at different polymer concentrations, trying to define the role of semi-interpenetrating polymers.

In the samples here investigated, H-PVA concentration (coded as X) was varied from 3 to 15 % w/v (X = 3, 5, 7, 9, 12 and 15 % w/v), while the semi-interpenetrating agent concentration was maintained constant ([L-PVA] = [PVP] = 3 % w/v).

Gels containing only H-PVA are coded as “Pure Networks” (PN_X), while gels containing also L-PVA or PVP are coded as “semi-interpenetrated” (i-PVA_X and i-PVP_X, respectively).

4.1 Morphology and structure of PVA-based cryogels containing L-PVA and PVP

Confocal images of PN_X, i-PVA_X and i-PVP_X gels (H-PVA concentration, X = 5-12 % w/v), washed for one week and swollen in a Rhodamine 110 solution are shown in fig. 12.

¹ Mainly based on Paper I, see Appendix.

Pores shape and dimension vary widely among the three series. As already explained in the Introduction, the low temperature of the freezing steps induces a water-polymer phase separation: ice crystals form in water-rich areas, while polymer crystallites are obtained in polymer-rich areas, due to the high local pressure induced by ice formation. Therefore, ice should play the role of porogen.¹⁷

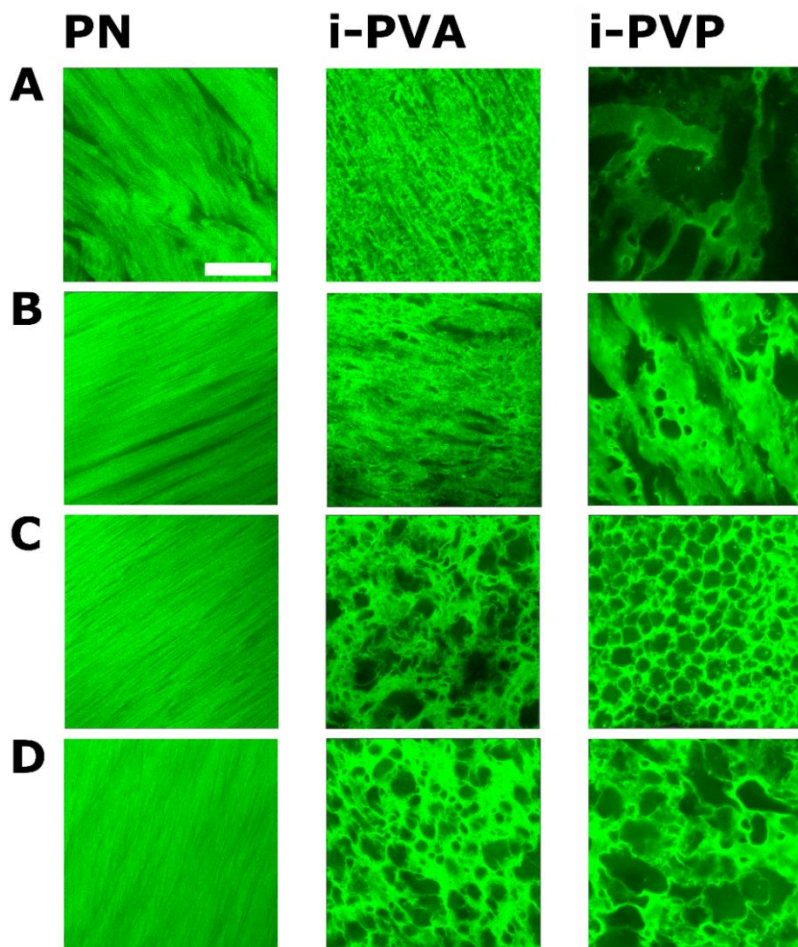


Figure 12. Confocal images of PN, i-PVA and i-PVP gels for different H-PVA concentrations: (A) X = 5; (B) X = 7; (C) X = 9; (D) X = 12. Gels are soaked in a Rhodamine 110 solution. Scale bar: 50 μm .

PN_X samples are strongly anisotropic: the elongated, needle-shaped porosity of the PN series can be ascribed to the crystallization of ice in aligned needles,

on surfaces perpendicular to the direction of freezing.^{101–103,17} This results in a linear ordering of the gel structure, where straight gels strands are interspersed with elongated pores. Directionality is stronger for higher values of X.

In both i-PVA and i-PVP series, porosity drastically changes in passing from X = 7 to X = 9: pores become almost spherical when X = 9, 12 and the networks become sponge-like.

In i-PVA_X series, gel walls still show a preferential orientation for X = 5 and X = 7, while in i-PVP_X gels, X = 5 and X = 7 samples do not show a high degree of local order: pores have random shapes and a wide size distribution. The variability of the cryogels structure may depend on the cryostructuration process, occurring during freezing: L-PVA or PVP concentrated aqueous solutions do not form gels if subjected to 1 FT cycle. Therefore, L-PVA and PVP are not expected to phase-separate from water, at low temperatures, with the same efficiency of H-PVA. In other words, H-PVA is expected to be the main structural polymer: the higher its concentration in the pre-gel solution, the better the chance of obtaining a stable gel (i.e. with numerous polymer crystals) during the freezing step.

As a results, L-PVA and PVP may affect H-PVA ability to crystallize and form a gel at low temperatures.

To verify this hypothesis, the effects of the semi-interpenetrating agents on gels crystallinity, swelling ability and gel fraction (i.e., the effective polymer content of the gels) were investigated.

Table 1 summarizes the principal physico-chemical properties of the PVA-based cryogels investigated in this chapter. Crystallinity of gels right after thawing, X_c AT, increases with X for all the series, as expected. X_c AT values decrease, under the same conditions, when L-PVA or PVP are added to the formulations. More in detail, X_c AT is lower for i-PVA_3-7 and for i-PVP_3-9, while it approximates PN series values for higher X.

X_c AT values indicate that the presence of a semi-interpenetrating polymer hinders H-PVA crystallization during the freezing step, especially when the initial concentration of H-PVA is lower than a threshold value. PVP has a stronger influence on crystallinity than L-PVA. So far, it can be ascribed to PVP higher molecular weight (see *Materials and Methods* Chapter).

When thawed gels are swollen and stored in water, a “second crystallization” (curing) may occur¹⁰⁴, enlarging the crystalline portions generated during the

FT process; at the same time polymer chains which are only weakly bonded in the network are extracted; the network fills with water, until the elastic forces due to the physical crosslinking are balanced by the osmotic pressure.

Table 1. Crystallinity degree after thawing (X_c AT) and after washing (X_c AW), Equilibrium Volume Swelling Ratio (q_v) and Gel Fraction (G%) of PN, i-PVA and i-PVP gels.

	PN_X				i-PVA_X				i-PVP_X			
X	X_c AT	X_c AW	q_v	G%	X_c AT	X_c AW	q_v	G%	X_c AT*	X_c AW	q_v	G%
3	21 ± 3 3	--	--	--	14 ± 1	--	--	18 ± 1	N.A.	--	--	--
5	26 ± 1	34 ± 1	--	27 ± 1	17 ± 2	35 ± 1	--	21 ± 1	9 \pm 3	19 ± 2	2.51	59 ± 1
7	32 ± 2	35 ± 2	1.40	29 ± 1	22 ± 1	36 ± 1	2.40	18 ± 7	11 \pm 3	26 ± 6	1.40	38 ± 1
9	30 ± 1	35 ± 1	1.77	29 ± 8	27 ± 1	38 ± 1	2.15	27 ± 1	15 \pm 2	26 ± 6	1.37	41 ± 2
1 2	33 ± 1	41 ± 5	1.90	30 ± 4	26 ± 1	39 ± 3	2.04	28 ± 1	30 \pm 1	33 ± 1	1.48	41 ± 1
1 5	36 ± 1	--	--	38 ± 3	30 ± 1	--	--	35 ± 1	31 \pm 1	--	--	--

*Data for i-PVP_X AT are indicative.

The effects of the second crystallization are stronger for i-PVA_X and i-PVP_X gels: due to the absence of cryostructuration for L-PVA and PVP, these polymers are expected to be preferentially extracted during washing. As a result, the structural H-PVA chains remaining in the network can interact more easily with each other, forming new crystallites.

Overall, the crystallinity of the gels after washing, X_c AW, shows the same trend of X_c AT: it is higher for PN_X and i-PVA_X with respect to i-PVP_X series.

The chains actively involved in the network formation can be quantified by calculating the gel fraction (G%). G% can be defined as the effective concentration of polymer constituting the network. It plays a major role in determining gel elasticity and the swelling ability (quantified through the swelling ratio, q_v). G% and q_v for the washed samples are reported in Table 1. G% increases with X in all the series. G% of i-PVP_X samples is the highest. In i-PVA_5 and i-PVA_7 gels, G% is lower than PN_5 and PN_7 samples:

in these cases L-PVA hindered polymer crystallization, causing a higher portion of H-PVA chains to be non-structural and, probably, a higher number of structural defects. G% values of i-PVA_X and PN_X samples for X = 9, 12, instead, do not differ significantly: as for crystallinity, L-PVA effects on cryostructure are less pronounced when H-PVA concentration is higher. The values of q_v show that L-PVA facilitates gels swelling for all X values. PVP does not alter the swelling ability when X = 5 or X = 7, while i-PVP_9 and i-PVP_12 are more elastic and, therefore, less swollen than their PN and i-PVA counterparts.

Overall, L-PVA has a strong impact on the crystallinity of thawed gels; in washed gels, elastic forces of the network are weaker and the swelling ability increases, with respect to PN_X gels. After washing, crystallinity values are not significantly different from those of PN_X gels.

PVP, on the other hand, strongly influences the crystallinity of both thawed and washed gels, lowering their values with respect to those of PN_X and i-PVA_X series. i-PVP_X gels have also a higher G% and a lower q_v , i.e. PVP causes more polymer chains to be structural components of the networks. Being i-PVP samples more rigid, it can be inferred that crystallization is not the only significant contribution to the structuration of these gels.

Further information on gels crystallinity and polymer chains organization were obtained through Small Angle X-ray Scattering (SAXS). SAXS curves of the thawed gels PN_5-12, i-PVA_5-12, i-PVP_5-12 (fig. 13) were fitted according to the model reported in the *Materials and Method* section (Eq. 21); fitting parameters are listed in Table 2.

The correlation length ξ describes chain conformation in the liquid-like portions of the networks; it usually decreases when the local polymer concentration increases.¹⁰⁵ Therefore, for gels with the same composition, submitted to one FT cycle, ξ should decrease by increasing H-PVA concentration, i.e. X. In fact, ξ values decrease along the PN_X series, suggesting that the gel walls become denser for higher X values. In i-PVA_X series ξ decreases with X, as well; however, ξ values are generally lower than those of PN_X gels. Moreover, an abrupt change in ξ (from 4.7 to 3.4 nm) occurs in passing from i-PVA_7 to i-PVA_9, as if chains crowding increased suddenly. ξ values in i-PVP_X series are close to those of i-PVA_9,12 gels and do not show significant variations with X: ξ is almost constant for i-PVP_5-9, while it increases for i-PVP_12. This suggest that, as for i-PVA_X

gels, H-PVA chains are crowded in the gel walls; such low values of ξ have been obtained for cryogels that underwent 3 FT cycles, i.e., for very high local polymer concentrations.¹⁷

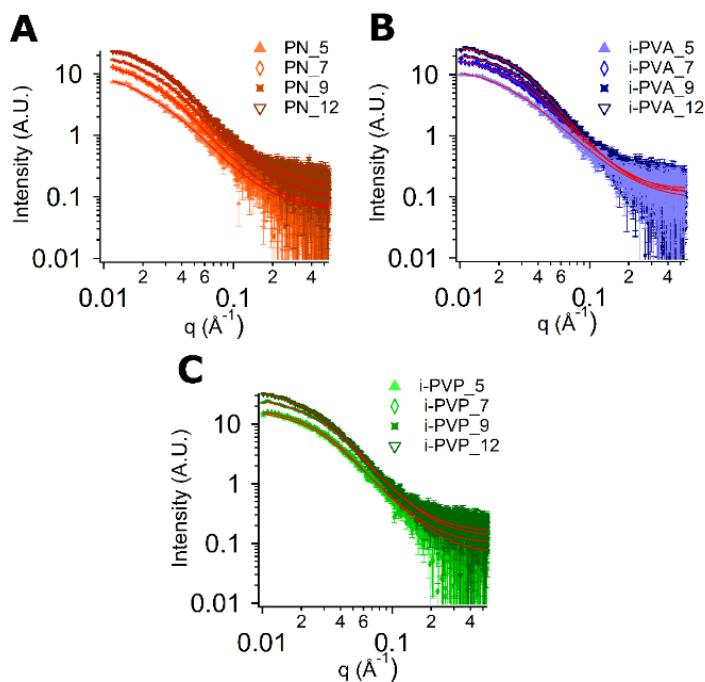


Figure 13. SAXS curves of (A) PN, (B) i-PVA and (C) i-PVP thawed gels.

The values of crystallites radius, R , are expected to follow an opposite trend with respect to ξ ; in fact, crystallites are more likely to form and grow when the local polymer concentration is higher. R increases with X for PN $_X$ and i-PVA $_X$ series. In i-PVA series, the abrupt change between i-PVA $_7$ and i-PVA $_9$ is again clearly visible: crystallites radius becomes almost 1 nm larger, confirming that polymer crowding increases abruptly from $X = 7$ to $X = 9$. As concerns i-PVP $_X$ series, R follows the opposite trend: it slightly decreases for increasing values of X : it passes from a value of ca. 6 nm (similar to i-PVA $_{12}$) to a value of 4.8 nm, close to those of PN $_7$ and i-PVA $_{5,7}$. $I_G(0)/I_L(0)$ ratio (Table 2) is an indication of the extension of crystalline portions in a sample. It confirms that the number of crystallites increases with H-PVA concentration in PN $_X$ and i-PVA $_X$ gels. For i-PVP, $I_G(0)/I_L(0)$

increases from i-PVP_5 to i-PVP_7, but then stabilizes to a limiting value for i-PVP_7-12.

The fractal dimension D of PN_5-12 and i-PVA_5,7 is similar to the fractal dimension of a polymer solution in semi-dilute regime. In fact, when D is about 2, the first term of the fitting equation takes the form of the Ornstein-Zernicke equation, describing a polymer system is in a semi-dilute regime. In other words, gels with $D \sim 2$ behave almost like concentrated polymer solutions.

Table 2. SAXS fitting parameters obtained for PN_5-12, i-PVA_5-12 and i-PVP_5-12 thawed cryogels.

Sample	Guinier Scale $I_G(0)$	Lorentz Scale $I_L(0)$	$I_G(0) / I_L(0)$	Correlation Length ξ (nm)	Fractal Dimension (D)	Crystallites Radius R (nm)	Background (B)
PN_5	0.3	5.5	0.05	5.7 ± 0.8	2.1 ± 0.1	3.9 ± 0.2	0.06
PN_7	0.9	6.9	0.13	5.4 ± 0.8	2.2 ± 0.1	5.0 ± 0.1	0.06
PN_9	2.6	11	0.24	5.2 ± 0.8	2.1 ± 0.1	5.1 ± 0.1	0.09
PN_12	4.1	14	0.29	4.9 ± 0.4	2.2 ± 0.1	5.2 ± 0.1	0.14
i-PVA_5	0.4	8.1	0.05	4.7 ± 0.1	2.1 ± 0.1	5.3 ± 0.4	0.09
i-PVA_7	2.2	14	0.16	4.6 ± 0.1	2.2 ± 0.1	5.1 ± 0.2	0.11
i-PVA_9	2.0	12	0.17	3.4 ± 0.1	2.6 ± 0.1	6.2 ± 0.2	0.13
i-PVA_12	4.8	15	0.32	3.3 ± 0.1	2.7 ± 0.1	5.9 ± 0.2	0.12
i-PVP_5	1.4	11	0.13	3.6 ± 0.1	2.5 ± 0.1	5.8 ± 0.2	0.10
i-PVP_7	3.1	13	0.24	3.7 ± 0.1	2.4 ± 0.1	5.4 ± 0.1	0.07
i-PVP_9	3.3	14	0.24	3.7 ± 0.1	2.5 ± 0.1	5.2 ± 0.1	0.13
i-PVP_12	3.2	18	0.18	4.3 ± 0.1	2.5 ± 0.1	4.8 ± 0.1	0.16

D values between 2.7 and 2.9, instead, were found for systems characterized by a significant number of H-bonds.¹⁰⁶ As these values describe i-PVA_9,12 samples it can be inferred that, in specific concentration ranges, the presence of a L-PVA enhances H-bonding in the cryogels, favoring network structuration. In i-PVP gels the H-bonding contribution is lower; in PN and i-PVA_5,7 gels, instead, the contribution of dangling or non-structuring chains is, probably, more significant.

Overall, also SAXS data suggest that PVP affects H-PVA crystallization. However, a comparison among $I_G(0)/I_L(0)$ and R values shows that H-PVA crystallization is enhanced by PVP almost for all X values ($X = 5, 7, 9$), but the crystallites size decreases with X . In other words, an increase of X in i-

PVP series causes more small crystallites to form, as for the presence of a high steric hindrance.

To sum up, confocal images suggest that semi-interpenetrating polymers play a key role in determining gel morphology and porosity at the microscale. Crystallinity, gel fraction and SAXS data showed that both L-PVA and PVP hinder H-PVA crystallization and gel cryo-structuration; however, the effect of PVP is different: while it causes the overall crystallinity to decrease, SAXS data showed that in *i*-PVP gels more small crystallites formed, and smaller crystallites are expected for increasing values of X. This could be caused by a higher steric hindrance at a local scale.

4.2 L-PVA and PVP as porogens: polymer-polymer interaction and segregation in aqueous solution

Fig. 12 showed that, in *i*-PVA_X and *i*-PVP_X gels, the pores formed during freezing are different with respect to PN gels. As a matter of fact, pore shape and dimension could also be a result of the morphology of the pre-gel solutions¹⁷. To explore the causes of such differences, morphologies of *i*-PVA_X and *i*-PVP_X pre-gel solutions and gels after thawing were investigated through confocal imaging. Pre-gel solutions of *i*-PVA and *i*-PVP series, for X = 5-12, were prepared using RBITC-labeled L-PVA and PVP: confocal images acquired at room temperature, for 2 days-aged solutions, are shown in fig. 14.

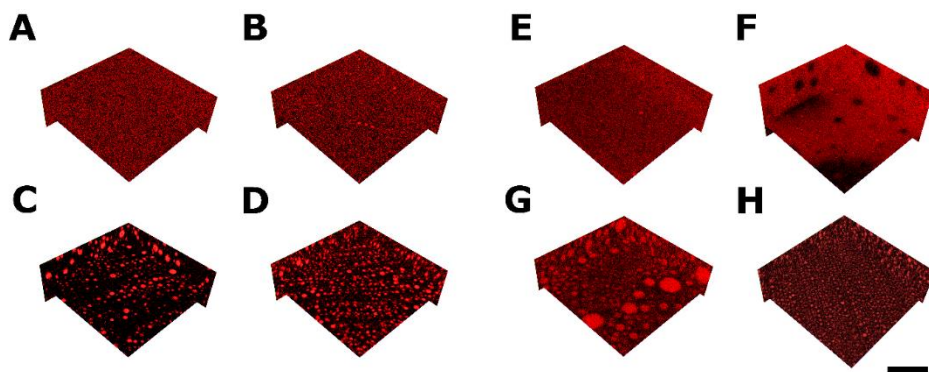


Figure 14. Confocal images of RBITC-labeled *i*-PVA₅₋₁₂ (A-D) and *i*-PVP₅₋₁₂ (E-H) pre-gel solutions. Scalebar: 50 μ m.

The RBITC-labeled polymers are shown in red. i-PVA_5 and i-PVA_7 solutions are homogenous, while phase separation occurs for $X = 9, 12$: spherical blobs where L-PVA concentrated are clearly visible in fig. 12 C-D. In i-PVP series, instead, phase-separation seems to occur at almost all X values: in i-PVP_7 solution H-PVA-rich areas and PVP-rich areas can be detected; in i-PVP_9 and i-PVP_12 solutions, PVP preferentially concentrates in blobs.

Confocal images of thawed gels containing red-labeled L-PVA and PVP are shown in fig. 15. The morphology of thawed gel confirms that phase-separation in the pre-gel solutions has an influence on the morphology of the gel structure and pores. In fact, in both i-PVA and i-PVP samples with $X = 5$ (fig. 15 A, E) and $X = 7$ (fig. 15 B, F) the semi-interpenetrated polymer occupies large areas of the samples. In i-PVA_7 the strong orientation given by cryostructuration is evident. In i-PVA_X and i-PVP_X samples with $X = 9$ (fig 15 C, G) and $X = 12$ (fig 15 D, H), L-PVA and PVP are confined in blobs, instead.

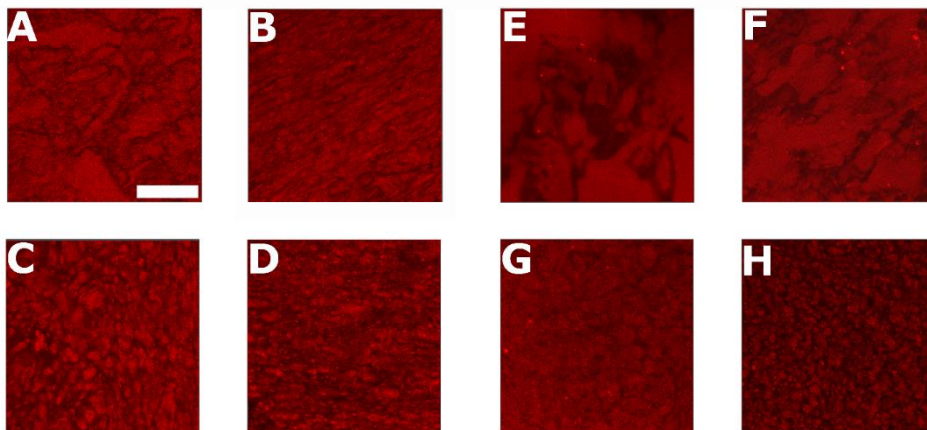


Figure 15. Confocal images of i-PVA and i-PVP gels containing RBITC-labeled L-PVA and PVP: i-PVA_5 (A), i-PVA_7 (B), i-PVA_9 (C), i-PVA_12 (D), i-PVP_5 (E), i-PVA_7 (F), i-PVA_9 (G), i-PVA_12 (H).

Fig. 14 and fig. 15 prove that, in both H-PVA-L-PVA and H-PVA-PVP aqueous solutions, phase segregation occurs and contributes to determine the final gel morphology during cryostructuration; therefore, some degree of incompatibility should exist among the two polymer pairs.

PVAs with $HD > 80\%$ are known to be water-soluble polymers^{107,108}. However, PVAs with very high HD (98-99%), as in the case of H-PVA, tend to self-associate in aqueous solution. Even if pre-existing crystals can be dissolved by heating the aqueous polymer solution at $T > 95\text{ }^{\circ}\text{C}$,^{109,110} concentrated solutions of H-PVA would be not stable at room temperature: a physical network forms, because H-PVA chains interact with each other through H-bonds, forming new crystallites.

On the other hand, aqueous solutions of partially hydrolyzed PVAs (as L-PVA) are stable, because chains have only a weak tendency to self-associate. The conformation of polymer chains in solution can play a role in determining polymer-polymer incompatibility.

The hydrodynamic radii of H-PVA and L-PVA chains, in dilute solutions, were calculated through the diffusion coefficients obtained from FCS experiments at RT (see Eq. 23-25), fig. 16 A-B and Table 3): they do not differ markedly, being 12 nm for H-PVA and 9 nm for L-PVA.

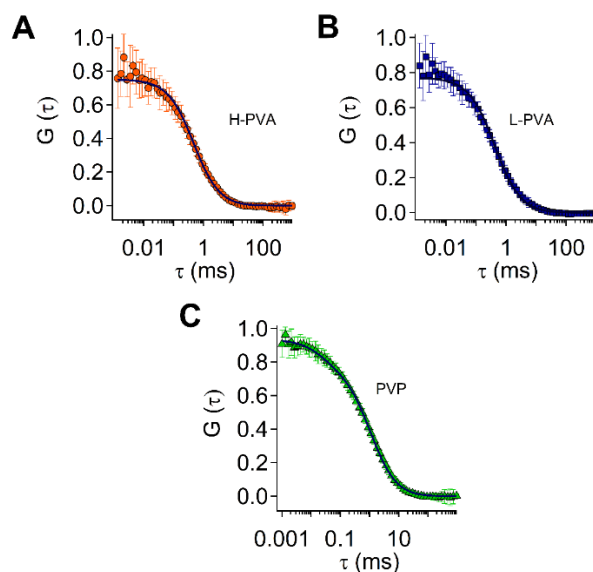


Figure 16. FCS curves of the three labeled polymers in diluted aqueous solution: (A) H-PVA, (B) L-PVA, (C) PVP. The diffusion coefficients obtained by curves fitting were used to calculate the hydrodynamic radius.

Partially hydrolyzed PVAs can adopt different conformations in solution, depending on the position and crowding of acetate groups along the polymer chain.¹¹¹ When acetate groups are not randomly distributed along the polymer

chain, the polymer arranges as a pseudo-micelle; this seems to be the case for L-PVA, as the calculated hydrodynamic radius, $R_H = 9$ nm, is in line with a collapsed conformation.¹¹¹

H-PVA conformation is supposed to be more extended and hydrophilic in character also at high temperature, while partially hydrolyzed PVAs undergo phase-separation in aqueous solution, for $T > 60$ °C ca.⁶⁴ This behavior is called Lower Critical Solution Temperature (LCST) and is due to the hydrophobic character of acetate groups: when temperature increases, H-bonds between PVA chains and water molecules are less effective, the solvent become poorer and the polymer chains tend to collapse, going through a phase-separation.

Table 3. Diffusion coefficients and hydrodynamic radii of H-PVA, L-PVA and PVP in dilute solution, obtained by fitting FCS curves. For PVP, also the diffusion of some free dye was detected.

Polymer in dilute solution	D ($\mu\text{m}^2/\text{s}$)	Hydrodynamic Radius (nm)
H-PVA	20 ± 1	12 ca.
L-PVA	26 ± 2	9 ca.
PVP	$D_1 = 10 \pm 1$ (80%) $D_2 = 420$ (for free RBITC)	25 ca.

The phase behavior of H-PVA and L-PVA in aqueous solution was investigated by varying polymer concentration (3 – 15% w/w) and temperature (5 – 100 °C) (see fig. 17 a-b).

No phase-separation was observed for H-PVA solutions¹⁷ (fig. 17 a), while sufficiently concentrated L-PVA solutions became hazy when heated at $T > 60$ °C; however, any micron-sized structures were observed through Confocal microscopy.

The phase behavior of H-PVA-L-PVA mixtures (ratio 3:1) in solution was also investigated (fig. 17 c). Incompatibility was found for concentrations equal or higher than 12% w/w: blobs of L-PVA formed in the continuous H-PVA phase. Blobs were detectable also for concentrations of 9 and 7 % w/w of polymer, but only above 60°C and 70°C.¹⁷

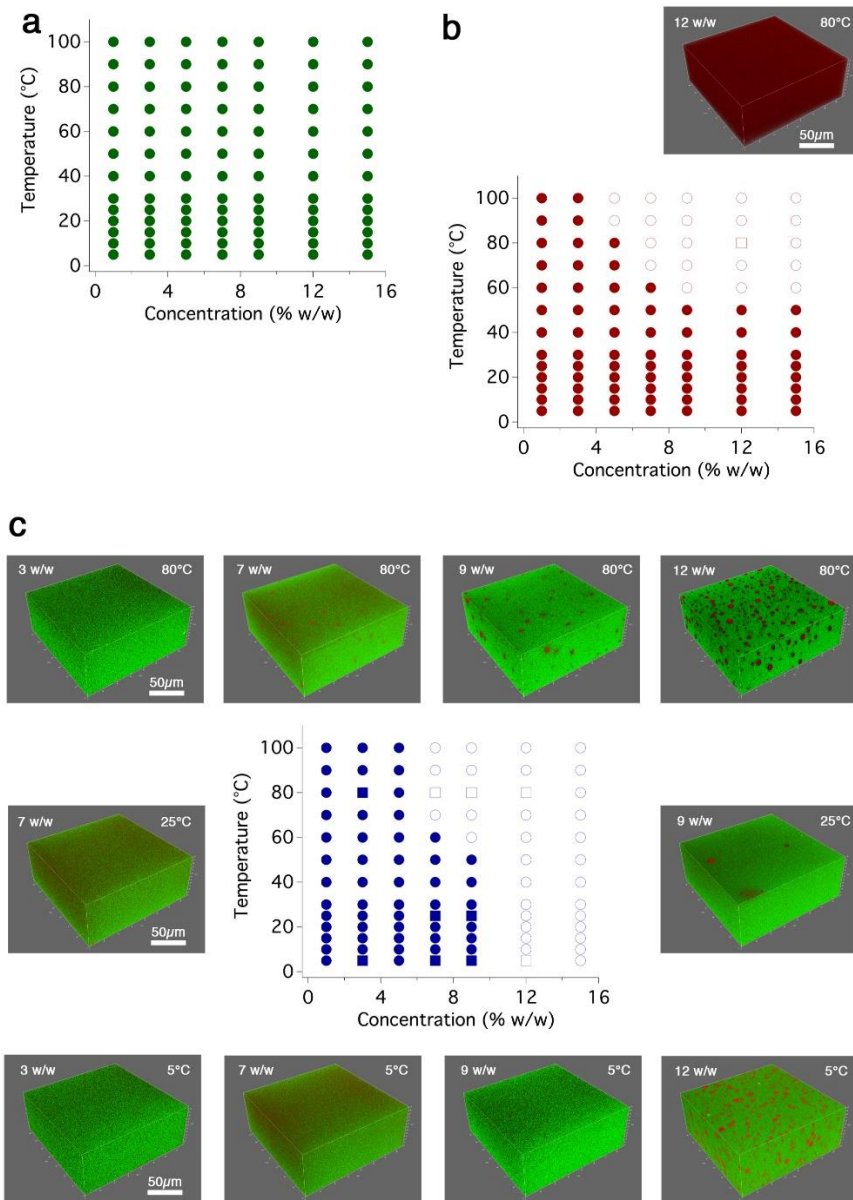


Figure 17. Phase behavior in aqueous solution of: (a) H-PVA; (b) L-PVA; (c) H-PVA-L-PVA mixtures (ratio 3:1). Reproduced from ref [17].

Such phase separation could be influenced by the different conformations of H-PVA and L-PVA chains in aqueous solution: H-PVA chains, with a more extended conformation, would preferentially interact with themselves;⁵⁷ on

the other hand, the coiled L-PVA chains would be expelled from the continuous H-PVA phase, concentrating in spherical droplets.

L-PVA blobs undergo a slow coarsening when the solutions are stored at RT, either because of Ostwald ripening, or for the further L-PVA expulsion from the H-PVA continuous phase. However, H-bonds probably form between L-PVA chains on the blobs surface and H-PVA chains in the continuous phase, so that a meniscus between H-PVA and L-PVA phases is never visible, even after several months.

PVP is a water-soluble polymer, as well. PVP interacts with PVA, especially if highly hydrolyzed, through H-bonds⁵⁸; negative values of $\chi_{PVP-PVA}$ are reported in the literature^{112,113}. However, the interaction occurs only when PVA chains are not included in polymer crystals; in fact, PVA-PVP miscibility is not optimal when PVA chains tend to self-association.⁵⁸

Nonetheless, PVA-PVP blends are usually described as homogeneous mixtures with a single glass transition temperature, and the two polymers are considered to be compatible.^{58,114–118}

As for i-PVA, i-PVP pre-gel solutions were obtained by mixing the two polymers in water at 98°C (see *Materials and Methods* section). H-PVA chains in solution probably behave in a similar fashion: they form inter- and intra-chain H-bonds and, especially in concentrated solution, they are also oriented by the shear of mixing. PVP chains, as opposed to those of L-PVA, are not collapsed in aqueous solution (the hydrodynamic radius obtained through FCS at room temperature is 25 nm, considering that some free dye, diffusing at 420 $\mu\text{m}^2/\text{s}$ ca.¹¹⁹, was also detected, see fig. 16 C and Table 3). The Flory parameter for the water-polymer interaction is reported to be 0.5 – 0.6 at room temperature, for low- and medium-molecular weight PVPs.^{120,121} The value slightly increases with temperature¹²⁰ while a LCST behavior occurs only at high temperatures (145 °C)¹²². Therefore, it is reasonable to assume that PVP chains are sufficiently extended, behaving as ideal chains, also at 98°C.

The phase behavior of H-PVA-PVP mixtures (H-PVA:PVP ratio 3:1) was investigated in a range of temperatures (80°C – 5°C). H-PVA-PVP do not segregate at high temperature, and phase separation is only incipient when the solution is cooled to RT (fig. 18).

Thus, it can be inferred that the principal cause of the formation of spherical pores in i-PVP_9 and i-PVP_12 gels (fig. 12, i-PVP) is the formation of blobs due to the temperature drop occurring during the freezing step.

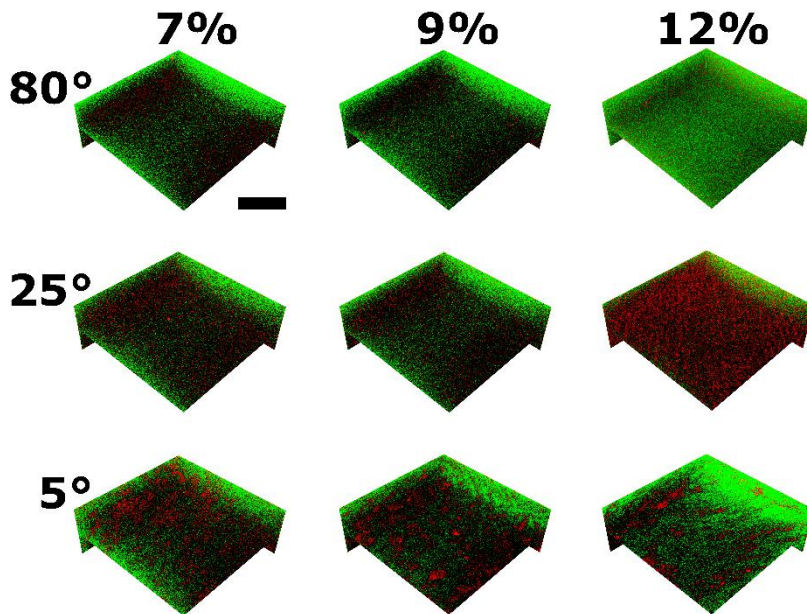


Figure 18. Phase behavior of i-PVP solution (H-PVA-PVP mixtures with ratio 3:1). Solutions are homogeneous, until they are cooled to 5°C. Scalebar: 50 μm .

The data on i-PVP gels crystallinity, G%, crystallites radius and on H-PVA – PVP phase behavior suggest that the structuration of i-PVP gels is only partially due to freezing. The enhanced phase separation occurring at low temperatures leads to two different polymer phases: a PVP phase, which contains a significant amount of water, due to the polymer hydrophilicity; and a H-PVA phase, which further expels water, as H-PVA self-interactions increase at low temperature. Consequently, H-PVA concentration in the continuous phase increases to the point that the physical gelation (i.e. formation of polymer crystals and glassy areas) starts before the effects of freezing become significant. When ice crystals finally form, they consolidate the preformed structure, causing the formation of small additional H-PVA crystallites. The crystallites dimension decreases as H-PVA concentration increases, because as H-PVA is more concentrated in the continuous phase, its physical gelation at low temperatures occurs more rapidly.

H-PVA self-interactions in concentrated solutions were demonstrated by investigating the shear thinning behavior of pre-gel solutions of PN, i-PVA and i-PVP samples ($X = 9, 12, 15$); the flow curves are shown in fig. 19.

Shear thinning is stronger for higher H-PVA concentrations, confirming that H-PVA self-interactions increase with X . Moreover, it is worth noting that i-PVA_15 solution is more viscous and displays stronger shear thinning than i-PVP_15 solution: this suggests that PVP is a better plasticizer than L-PVA.

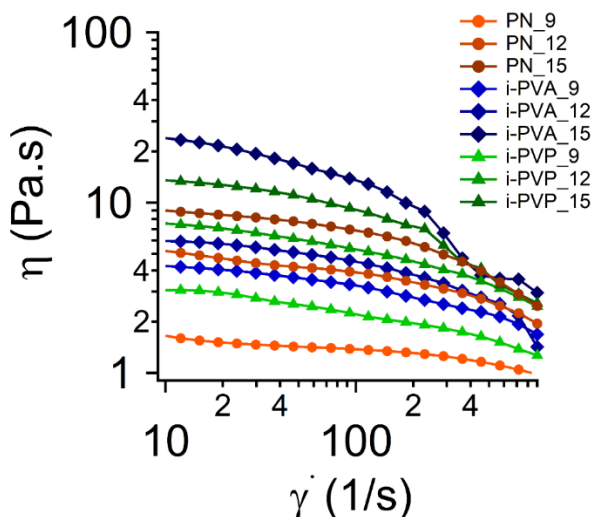


Figure 19. Shear thinning behavior of PN (orange markers), i-PVA (blue markers) and i-PVP (green markers) pre-gel solutions. At high H-PVA concentrations ($x = 15$) i-PVA solution is the most viscous and displays the stronger shear-thinning behavior, suggesting stronger H-PVA self-interactions.

To sum up, both H-PVA - L-PVA and H-PVA - PVP phase separations are probably driven by the tendency of H-PVA chains to interact with themselves. However, in i-PVA solutions, the contribution of the collapsed L-PVA chains conformation can also play a role in determining a polymer-polymer segregation. i-PVP gels, on the other hand, result from two different mechanisms occurring at low temperatures. In fact, PVP subtracts water from the H-PVA phase, forming water-rich PVP blobs; and the H-PVA phase expels water, in order to be able to phase-separate and crystallize. Physical gelation of H-PVA starts to occur before cryostructuring becomes effective,

probably forming small crystallites and glassy areas. The resulting networks are less crystalline than their i-PVA counterparts, but more rigid.

4.3 L-PVA and PVP as structuring agents

Confocal imaging, G%, SAXS and crystallinity measurement suggested that L-PVA and PVP act both as porogens and structuring agents in H-PVA cryogels, but in different ways.

To unravel the structuring effects induced by the semi-interpenetrating polymers, the rheological response of gels containing increasing amounts of L-PVA or PVP, and a constant concentration of H-PVA (9 % w/v), was investigated. Samples in these series were coded as i(Y)-PVA and i(Y)-PVP, Y having the following values: 0.5, 1, 2, 3, 4 and 5 % w/v.

The G' (1 Hz) data for i(Y)-PVA and i(Y)-PVP thawed gels are shown in fig. 20 A, B, in double logarithmic scale, versus the concentration of the semi-interpenetrating polymer added. The orange line represents the G' value in absence of L-PVA or PVP (i.e., PN_9 sample).

Fig. 20 A shows the effects of increasing concentrations of L-PVA on a H-PVA cryogel: the storage modulus steeply increases, and then stabilizes at a plateau value for i(1-3)-PVA samples. The addition of higher quantities of L-PVA (i(4-5)-PVA gels) causes a drop in G' values.

Fig. 20 B shows, instead, the trend of G' versus the concentration of PVP for i(Y)-PVP cryogels. In this case, G' increases with PVP concentrations up to 3% w/v (sample i(3)-PVP). For higher concentrations (i(4-5)-PVP), G' values drop.

Rheology data of fig. 20 A, B demonstrated that, up to the 3% w/v, semi-interpenetrating polymers contribute to the structuration of gels, while, at higher concentrations, L-PVA and PVP act as plasticizers.

The different trends observed in fig. 20 A and B confirm that L-PVA and PVP act as structuring agents, but in different ways: L-PVA has a lower structuring effect than PVP, and the maximum in G' is registered already for i(1)-PVA sample; conversely, PVP has a greater impact on G' : the storage modulus increases constantly between i(0.5)-PVP and i(3)-PVP samples, and $G'_{i(3)-PVP} > G'_{i(3)-PVA}$. It may be concluded that H-PVA maximized its structuring capacity after the inclusion of 1% w/v of L-PVA and 3% w/v of PVP.

The persistence of semi-interpenetrating polymers in in $i(Y)$ -PVA and in $i(Y)$ -PVP networks, after a 2-months washing, was tested through NMR (see fig. 20 C, D).

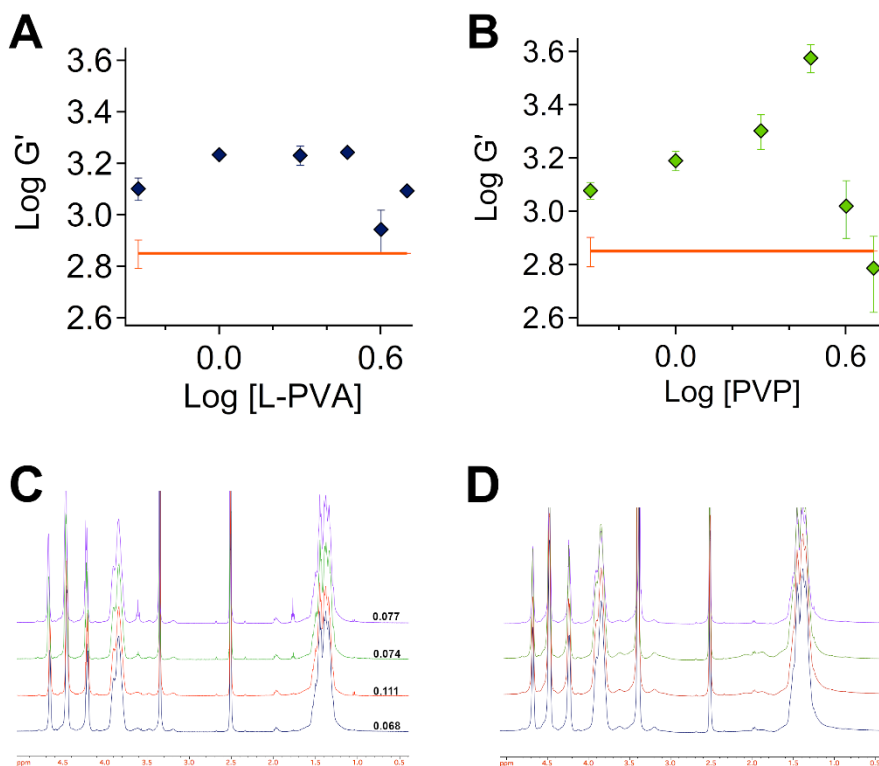


Figure 20. A – B: Log-log plots of the storage modulus, G' (1 Hz), versus the semi-interpenetrating polymer concentrations. (A) Effects of increasing concentration of L-PVA on a 9% w/v H-PVA network; (B) Effects of increasing concentration of PVP on a 9% w/v H-PVA network. The orange line in both graphs represents the correspondent H-PVA gel (PN_9). C – D: NMR spectra of $i(Y)$ -PVA and $i(Y)$ -PVP gels after washing and storage in water (2 months). (A) From top to bottom: NMR spectra recorded for $i(5)$ -PVA (violet), $i(4)$ -PVA (green), $i(3)$ -PVA (orange) and $i(2)$ -PVA (blue); the final L-PVA/H-PVA ratio, calculated according to Eq. 22, is indicated on the right. (B) From top to bottom: NMR spectra recorded for $i(5)$ -PVP (violet), $i(4)$ -PVP (green), $i(3)$ -PVP (orange) and $i(2)$ -PVP (blue); in this case only a minor trend is visible, but the amount of residual PVP is negligible.

The amount of L-PVA permanently embedded in $i(Y)$ -PVA networks was calculated through Eq. 22, and the values of the L-PVA/H-PVA ratio are shown in Fig. 20 C. They are almost independent on the concentration of L-PVA in the pre-gel solution: for a given and sufficiently high concentration of H-PVA, residual L-PVA tends to a constant quantity. Such quantity could be

related to H-PVA - L-PVA interactions in the pre-gel solutions. Conversely, NMR analysis of i(Y)-PVP samples (fig. 20 D) revealed that a negligible amount of PVP is retained during washing, and only a minor trend in its concentration can be identified, in good correlation with rheological data. These data support the hypothesis of PVP having only an “indirect” structuring effect, mainly due to its ability to concentrate H-PVA phase, before cryostructuration takes place.

Finally, the point of gelation of H-PVA in i-PVA and i-PVP mixtures, was evaluated. L-PVA and PVP concentrations were maintained at 3% w/v. The experiment (see fig. 21) showed that H-PVA alone forms a gel at 1.4 % w/v, i-PVP solutions become gels for a H-PVA concentration of 2% w/v and i-PVA solutions form a gel when H-PVA concentration is at least 1%. This confirms that not only L-PVA favors H-PVA self-interaction, but also that some L-PVA chains can take part to the cryostructuration process (H-PVA = 1% w/v, L-PVA = 3% w/v). PVP long chains, on the other hand, disrupt H-PVA chains ordering, and higher H-PVA concentrations are needed to achieve the gel state.

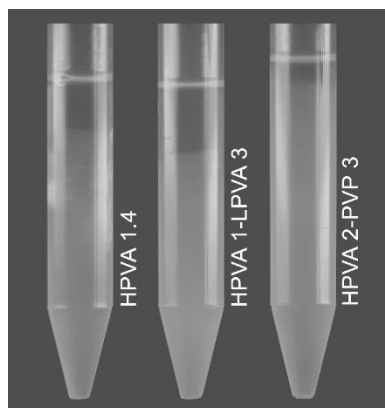


Figure 21. Gel points for PN, i-PVA and i-PVP series: H-PVA formed a gel at 1.4 % w/v; when mixed with 3% w/v L-PVA, H-PVA forms a gel at 1% w/v, while in presence of PVP at 3% w/v the gel point of H-PVA increases to 2 % w/v. Water on top is due to syneresis.

In conclusion, L-PVA and PVP were proven to play also the role of structuring agents in cryogels, even if in different ways: while L-PVA has both a direct and an indirect effect on the gel structuration, PVP structuration ability is only indirect, as it is completely extracted after washing. The next paragraph illustrates L-PVA and PVP impact on the gelation process.

4.4 Gelation mechanism

The impact of a semi-interpenetrating agent on the cryogel structuration can be investigated through rheology measurements, and specifically by observing the dependence of the storage modulus, G' , on the concentration of polymer constituting the network. G' represents the elastic response of the material to a certain stress applied and, according to the theory of rubber elasticity, it is proportional to the number of “active chains” in the network, i.e. the polymer chains whose ends are blocked in tie-points¹²³.

The gelation processes can often be described through the percolation model¹²⁴: according to this theory, G' is related to the fraction of reacted bonds, p , through: $G' \propto (p - p_c/p_c)^n$, where p_c is the critical value of p to obtain an infinite cluster (i.e., the gelation threshold). The exponent n , in three dimensions and just above the gelation threshold, should be 1.7-1.9.

For gels well beyond the gelation threshold and swollen in good solvents, the system can be considered a semi-dilute solution of polymer chains, and both G' and the osmotic pressure scale as: $G' \propto C^n$, where C is the polymer concentration and $n = 2.25$ ¹²⁴. However, the 2.25 exponent is generally more accurate to describe osmotic pressure, rather than rheology results, owing to the difficulties in preparing series of gels with negligible defects¹²⁵.

Experimental values of n usually range from 1.9 to 3.5^{126,127}. For PVA cryogels, $n = 2.4-3.8$ have been reported.^{76,77,128}

In cryogels, the network's tie-points are the polymer crystals formed during freezing, and crystallinity represents the main contribution to G' .¹²⁹ As already discussed, when such networks are swollen in water, a “second crystallization” (curing) occurs; moreover, a significant amount of polymer chains are extracted; therefore, elastic properties of the networks could change after washing. G' (1 Hz) data obtained for thawed and washed gels, reported as a function of $\frac{C_{H-PVA}}{C_g} - 1$ (being C_g the gel point) were compared (see fig. 22).

Values of the exponent n are reported in Table 4. Effective polymer concentrations in the washed gels were also calculated, considering the gel fraction, $G^0\%$, of each sample after washing.

Fig. 22 shows the trend of G' versus $\frac{C_{H-PVA}}{C_g} - 1$ for the PN_X (fig. 22 A), i-PVA_X (fig. 22 C) and i-PVP_X (fig. 22 E) series, right after thawing (full markers). The slope of the linear fitting is in agreement with a percolation

mechanism for PN_X and i-PVP_X, while, in i-PVA series, only the curve describing i-PVA_X with X < 7 points can be related to percolation.

Some samples of the three series were tested again after washing, and G' data are reported in the same figure (fig. 22 A, C, E), with empty markers, for comparison. Only gels containing very low concentration of polymer (i.e. PN_5 and i-PVA_3) changed significantly after washing. In fact, a low polymer concentration can cause the formation of instable polymer crystallites and a higher number of structural defects. G' (1 Hz) of the washed gels versus the effective polymer concentrations in the networks, calculated with G% values, are shown in the right side of fig. 22 (PN_X series in fig. 22 B, i-PVA_X series in fig. 22 D and i-PVP_X series in fig. 22 F).

The slope of curve in this case is higher, being around a value of 3 for PN_X series, 5.6 for the lower concentrations of i-PVA_X gels and 2.3 for i-PVP_X gels. The data of i-PVP_X series are the only ones in agreement with De Gennes theory of gels swollen in good solvents (i.e. slope of 2.25), probably because i-PVP_X networks are very stable and elastic, and contain less defects.

It is, in fact, well known¹²⁵ that the presence of dangling chains affects the exponents of the scaling laws, especially when the number of those chains is not constant at different gel's polymer fractions. Such defects could be more evident after washing because some structural compensation effects may fail when weakly- and non-bonded polymer chains are washed out.

It is worth noting that G' VS $\frac{C_{H-PVA}}{C_g} - 1$ trend is peculiar for i-PVA_X thawed and washed gels, as for this series two different regimes can be identified, one at lower, the other at higher H-PVA concentrations.

Gelation occurring in two different regimes was reported for agarose gels.¹³⁰ This was justified on the basis of the Jones-Marques (JM) theory. Guenet⁸⁰ adapted this model to the physical gelation processes characterizing fibrillar gels. PVA chains do not form fibrils in solution, that associate to build a network.

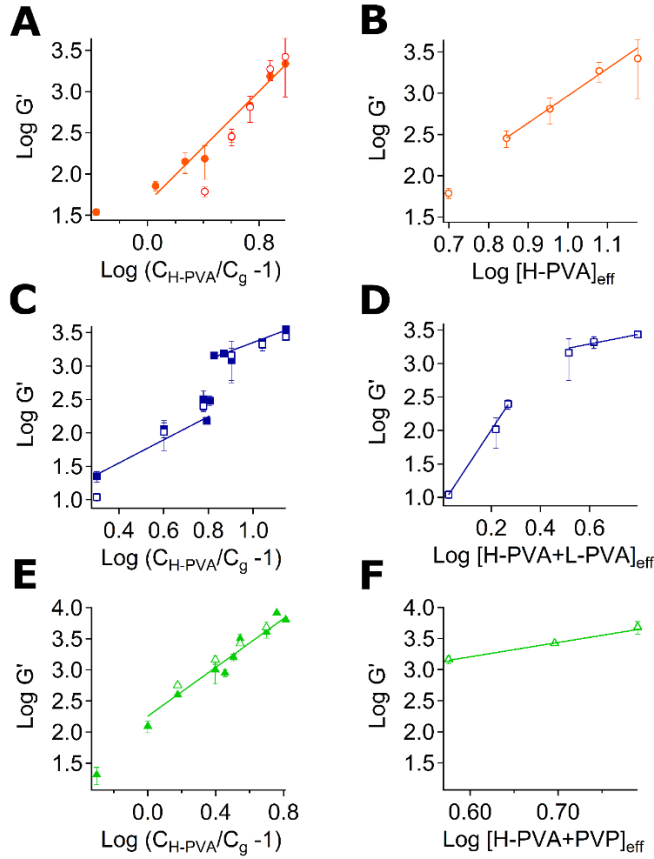


Figure 22. Log-log plots of the storage modulus (G' , 1 Hz) versus the effective concentration of polymer for the three series. A), C) and E) show the trend of G' for PN, i-PVA and i-PVP gels right after thawing (full markers) and after washing (empty markers), versus the effective H-PVA concentration, obtained by considering the gelation threshold (C_g). B), D) and F) show the trend of G' of some gel samples of each series after washing versus the effective polymer fraction constituting the networks, calculated using $G\%$ values.

Table 4. Values of the exponent n obtained for the gels after thawing, AT (see fig. 22 A, C, E), considering the gelation point, and the gels after washing, AW (see fig. 22 B, D, F), considering the effective concentration of polymer constituting the network.

Series	n (AT)	n (AW)	n (JM model)	D_F
PN	1.69 ± 0.06	3.3 ± 0.5	-	-
i-PVA	1.7 ± 0.1	5.6 ± 0.4	2.2 ± 0.2	1.1
	1.3 ± 0.1	0.7 ± 0.4	1.4 ± 0.1	0.9
i-PVP	1.96 ± 0.02	2.3 ± 0.5	-	-

However, a PVA cryogel can be described as an array of rigid objects connecting at junctions, due to the high directionality given by both the self-association of H-PVA chains in solution and the freezing step; in fact, cryogels have already been defined fibrillar networks.^{128,131,132} Clearly, the morphology of these gels is complex and the fibrillar description is not exhaustive, but it can be used as a starting point to shed light on the gels formation mechanism. In light of JM theory, the presence of two regimes in the G' VS [H-PVA] data for i-PVA series (see fig. 23 and Table 4) can be explained considering the presence of dangling polymer chains at lower H-PVA concentrations, which are gradually incorporated in the network when polymer concentration increases.

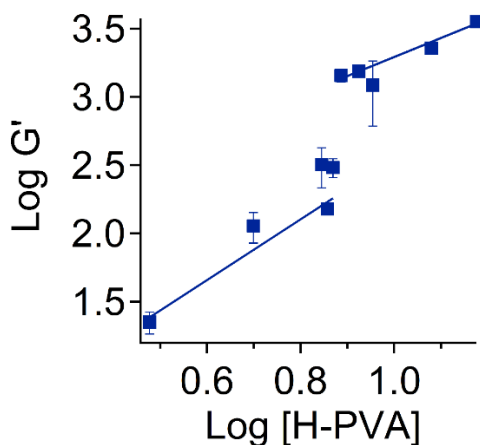


Figure 23. Log-log plots of the storage modulus (G' , 1 Hz) versus the concentration of H-PVA in i-PVA_X series. The slopes of the two curves were used to calculate the fractal dimensions according to Jones-Marques theory.

A fractal dimension, D_F , was calculated for i-PVA series by Eq. 12, 13 and reported in Table 3. Both values are ~ 1 , indicating the presence of straight elements. D_F decreases when H-PVA concentration increases, suggesting that gel strands contain more defects for $D_F = 1.1$ (low X values), which smooth as H-PVA concentration increases and dangling chains are included in the network.

Evidences to support this hypothesis can be obtained by observing the morphology and shape of gel strands in the gel series at two different H-PVA concentrations, through Scanning Electron Microscopy (SEM).

Fig 24 shows the SEM images obtained for two samples of each series ($X = 5$ and $X = 12$), after curing in water.

In PN (fig. 24 A, B) and i-PVP series (fig. 24 E, F) gel defects are almost absent, even if some structure refinement occurs when H-PVA concentration increases. For i-PVA series, instead, defined linear strands are clearly visible in i-PVA_12 (fig. 24 D) , while i-PVA_5 is characterized by more irregular objects (fig. 24 C): linear strands are still visible, but they show a high surface roughness.

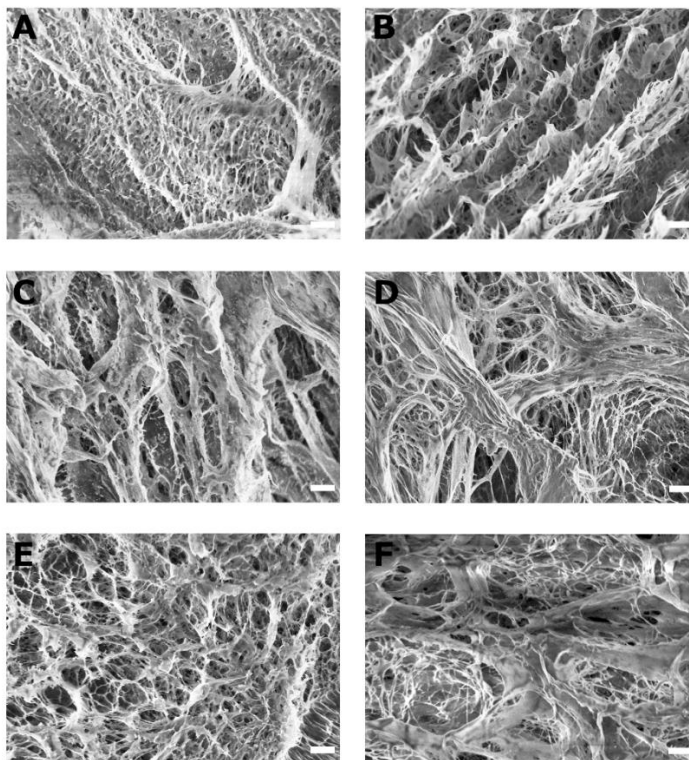


Figure 24. SEM images obtained for: (A) PN_5, (B) PN_12, (C) i-PVA_5, (D) i-PVA_12, (E) i-PVP_5, (F) i-PVP_12 samples. Scale bar: 1 μm .

Chapter 5. Twin-Chain Polymer Networks (TC-PNs): the influence of the freeze-thawing cycles

The number of FT cycles is known to be a critical aspect in determining physico-chemical properties of PVA cryogels.⁸² However, the effects of FT cycles on gels containing a semi-interpenetrating agent are not easily predictable. This chapter² explores the morphological, structural and rheological characteristics of cryogels obtained by mixing two different types of PVA: one with higher (H-PVA) and the other with lower (L-PVA) molecular weight and HD. Such networks, called TC-PNs because of the similar structure of the polymers composing them, showed unprecedented cleaning performances when tested on rough painted surfaces.

5.1. Cryogels morphology and structure

Four PVA-based cryogels were synthesized: two pure H-PVA hydrogels were prepared using only H-PVA (9% w/w, one and three FT cycles) and two TC-PNs were obtained by mixing H-PVA and L-PVA, in a 3:1 ratio (12% w/w, one and three FT cycles). The morphology of the four hydrogels, investigated by confocal imaging, is shown in Fig. 25.

The freezing of the sole H-PVA solution leads to a more homogeneous structure, with smaller pores than the TC-PNs (see Fig. 25 a).

As already explained in the previous chapter, the formation of the H-PVA gel walls takes place following the dendritic growth of ice during crystallization; as a consequence, pores have an elongated shape, and exhibit an elliptical section in the confocal images, as if ice grew in aligned needles along axes that are slightly tilted with respect to the plane of the gel surface (Fig. 25 a). Instead, in the TC-PNs, pores do not show any specific orientation: the networks become sponge-like, due to L-PVA phase separation in the pre-gel solution (Fig. 25 b).

² Mainly based on Paper II, see Appendix.

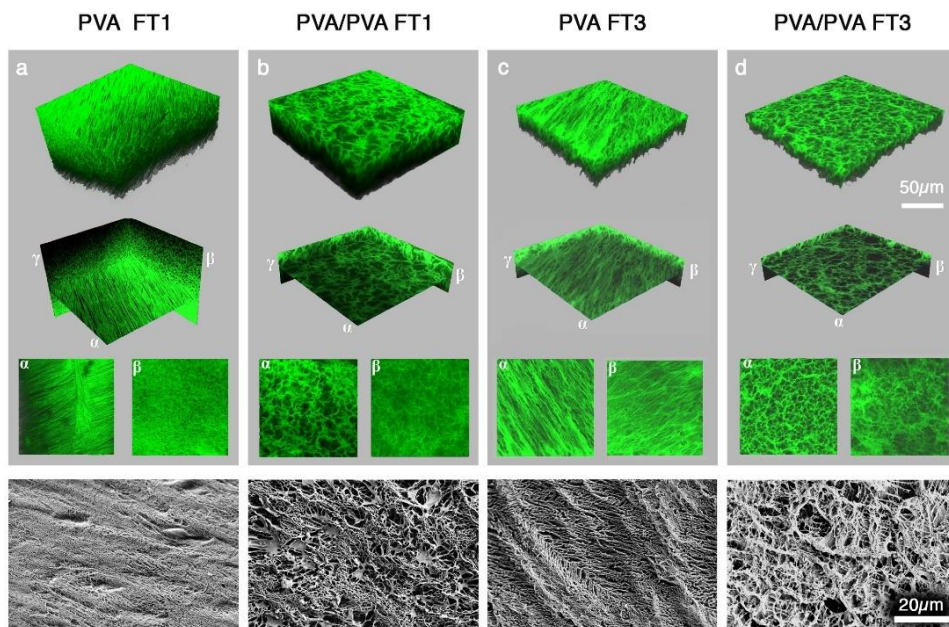


Figure 25. Confocal images and SEM micrographs of pure H-PVA and TC-PN gels. (a) Pure PVA FT1 gel; (b) PVA/PVA TC-PN FT1 gel; (c) Pure PVA FT3 gel; (d) PVA/PVA TC-PN FT3 gel. Reproduced from ref. [17].

The dimensions and distribution of the pores in the TC-PNs (3-30 μm) are such that the presence of an interconnected porosity across the gel network can be hypothesized. This feature can be attractive for applicative purposes: when the gel is applied on a soiled surface, the soil detached and dissolved by water can migrate inside the gel porosity, all through the gel volume; during the application, evaporation at the gel upper surface could recall water from the bulk through the interconnected porosity, favoring dirt pick up. Moreover, the larger pore dimensions in the TC-PNs result in a rougher gel surface, which could favor the capture and retaining of dirt, as opposed to the flat surface of pure H-PVA gels.

Gels obtained by three FT cycles do not differ significantly by FT1 networks; the main differences reside in a larger pores cross-section for PVA FT3 gels, and thicker gel walls for both PVA FT3 (fig. 25 c) and TC-PN FT3 (fig. 25 d) gels. In fact, the repeated FT cycles cause further phase separation between water and the polymer, and the latter is pressed against the walls as it separates¹³³. Overall, it can be inferred that the cryogel structure is already defined after the first FT cycle.

The bottom row of Fig. 25 shows the scanning electron microscopy (SEM) images of xerogels obtained from the H-PVA and TC-PN hydrogels. Because the freeze-drying of hydrogels causes some shrinkage, the SEM images cannot be directly compared to those obtained by confocal imaging; nonetheless, comparisons between the SEM images of different systems can be made, assuming that the process did not alter the pores shape and spatial arrangement. SEM analysis confirmed that the pure PVA gels display an ordered pores pattern. PVA FT3 exhibits larger channels, produced by the repeated FT cycles. The TC-PNs xerogels show the same disordered and sponge-like porosity observed for the hydrogels in confocal images; however, the SEM images highlighted the presence of smaller pores ($< 1 \mu\text{m}$) in the gel walls. The thickness of the walls increases with the number of FT cycles, and this trend is particularly evident for the TC-PN gels. Moreover, the larger pore dimensions in the TC-PNs result in a rougher gel surface, which could favor the capture and retaining of dirt, as opposed to the flat surface of pure H-PVA gels.

A thorough investigation of pores and walls average dimension was performed by implementing the chord-length distribution analysis on confocal stacks. Originally introduced by Tchoubar and Levitz^{90,134}, this method allows a quantitative description of biphasic media: a set of randomly oriented lines is drawn on a binary image (i.e. containing a continuous and a dispersed phase) and chords are defined as a line crosses phase boundaries. The frequency of chords with a certain length is then plotted against their length itself.

Fig. 26 shows the frequency $f(R)$ of chords for both the pores (fig. 26 a) and the walls (fig. 26 b) in confocal 3D images of the four systems (PVA and TC-PN, FT1 and FT3). All distributions show a peak and an exponential tail; the exponent describing the decay, λ , is a characteristic persistence length of the gel structure (see Table 5).

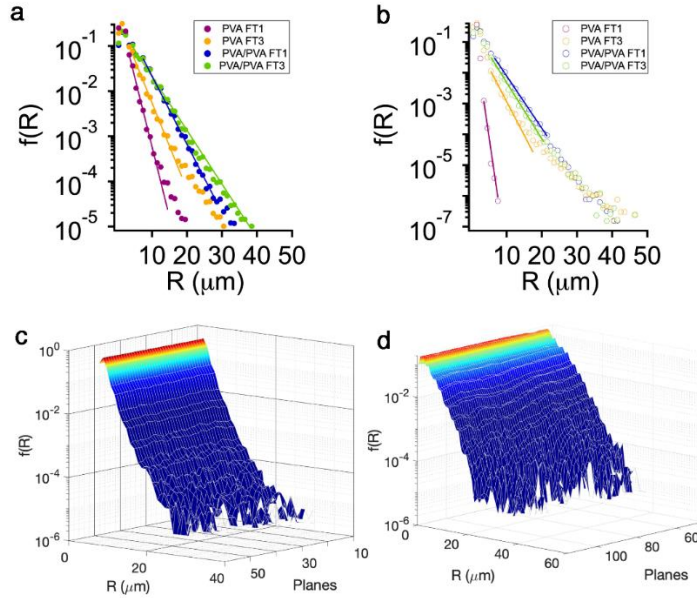


Figure 26. Averaged chord-length distributions for: (a) the pore phase and (b) the gel phase of PVA-based cryogels. The lines are the fitting of the data to exponential decays. The bottom panels show the variance of chord distributions of pores with the depth of confocal stacks for (a) PVA FT1 and (d) TC-PN FT1. Reproduced from ref. [17].

In the pores chord distribution (fig. 26 a) λ increases with the number of FT cycles and when L-PVA is added to the gel formulation: in TC-PNs the maximum pores size is higher than their pure PVA gel counterparts. This is due to the porogen action of L-PVA during cryostructuring.

Table 5. Parameters obtained by the exponential fitting of $f(R)$ VS R ($1/\lambda$), and persistence length (λ) for the pores and gel-phase chord distributions. Data were obtained by analyzing confocal stacks.

Gel	$1/\lambda$ Pores (μm^{-1})	λ Pores (μm)	$1/\lambda$ Gel phase (μm^{-1})	λ Gel phase (μm)
PVA FT1	0.702	1.4	1.805	0.6
PVA FT3	0.444	2.3	0.504	2.0
TC-PN FT1	0.349	2.9	0.391	2.6
TC-PN FT3	0.275	3.6	0.421	2.4

Gel walls (fig. 26 b) are thicker for PVA FT3 than PVA FT1, and their dimension further increases for the TC-PN gels. Any difference in wall thickness was detected among the FT1 and FT3 TC-PN gels (it was instead

clearly evident in SEM images), probably because it falls beyond the resolution of confocal images.

Pores dimension varies also along the single confocal stacks: in fig. 26 c - d, it is evident that $f(R)$ decays faster for confocal planes closer to the gel surface. This can be related to the temperature gradient formed across the gels thickness during freezing: the external surfaces are subjected to a sharp decrease in temperature and, therefore, to a higher directional stress, and the resulting pores are more elongated; in the inner confocal planes, instead, pores have larger cross-sections and higher polydispersity.

5.2 Physico-chemical and structural characteristics of PVA and TC-PN cryogels

As explained in chapter 4, the morphology of cryogels can be linked to some of their physico-chemical properties (Table 6). For example, the thickness of the gel walls is related to the effective polymer concentration in the network. After washing and storage in demineralized water, non-active polymer chains are washed out and the gel fraction (G%) can be determined. G% strongly depends on how far the compression of PVA chains went during the freezing steps, thus it increases with polymer concentration in solution and with the number of FT cycles. For the same number of FT cycles, the TC-PNs exhibit lower G% values than the pure PVA systems (Table 6).

Table 6. Some physico-chemical properties of PVA and TC-PNs FT1 and FT3 cryogels.

Sample Name	Gel fraction (G%)	Crystallinity (X_c %)	Equilibrium Water Content (EWC, %)	Free Water Index (FWI)	Water release (mg/cm ²)
PVA FT1	58 ± 2	39 ± 1	96.3 ± 0.4	98 ± 1	24 ± 3
PVA FT3	77 ± 1	50 ± 1	92.3 ± 0.6	94 ± 1	17 ± 2
TC-PN FT1	55 ± 1	46 ± 2	97.1 ± 0.2	98 ± 1	21 ± 1
TC-PN FT3	68 ± 5	41 ± 2	92.8 ± 0.3	96 ± 1	19 ± 1

By increasing the number of FT cycles, phase separation leads to water pools that are progressively poorer in polymer content, while more polymer chains

are pressed and stably accumulate on the gel walls; thus, less polymer chains are released during washing and storage in water, resulting in higher G% values.

As previously mentioned, an indication of the efficacy of cryostructuration can be provided also by the crystallinity of the systems. Crystallinity of gels should increase with the number of FT cycles¹³⁵⁻¹³⁷, and this is the case for pure PVA networks. For the TC-PN gels, crystallinity sharply rises above 45% after the first FT cycle, but its value slightly decreases after the third cycle (Table 6). This minor decrease is probably due to the equilibrium established between the crystallization of H-PVA occurring during freezing, and the crystals melting occurring during thawing: while in pure PVA gels the first process overruns the second, in TC-PNs the two processes are probably more balanced. In other words, in TC-PNs the highest level of structuration is obtained after the first FT cycle and, for the following FT cycles, the crystallization value varies slightly, due to the PVA crystallites formation/melting equilibria. All the washed/cured gels contain high percentages of water (> 90%), which behaves almost completely as free water (Table 6). High amount of free water ensures the effectiveness of the cleaning action. Both the EWC and FWI values decrease with increasing FT cycles. Water release data show a similar trend: the release decreases with the number of FT cycles. In general, the four gel types show a retentiveness that is 50% higher with respect to the traditional gels used in restoration¹⁶: the control of the water released during the cleaning action is fundamental when sensitive artifacts are treated. Systems previously reported showed similar performances¹⁶.

Further information on the polymer chains arrangements and crystallinity of the washed networks were obtained through Small Angle X-ray Scattering (SAXS).

SAXS curves of the four cryogels and the two pre-gel solutions are shown in Figure 27, while fitting parameters (obtained from Eq. 21) are listed in Table 7.

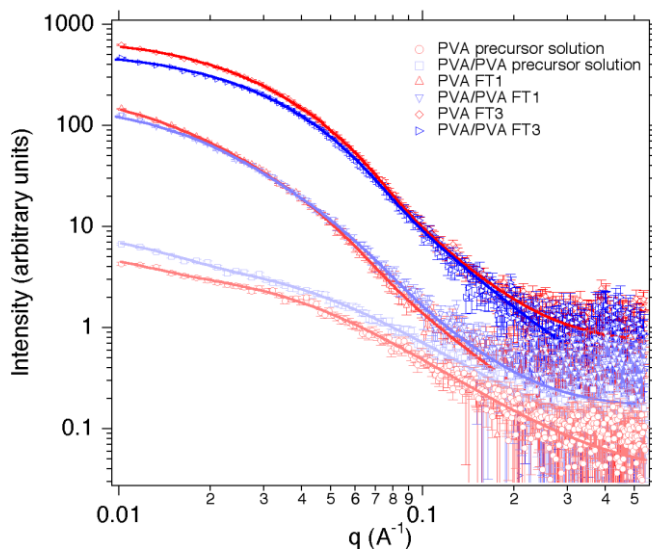


Figure 27. SAXS data (markers) and fitting (solid lines) of the PVA and TC-PN gels (FT1, FT3) and pre-gel solutions. The curves were shifted along the y-axis to improve the readability of the graph. Reproduced from ref. [17].

For the pre-gel solutions, the Lorentzian term reduces to the Ornstein-Zernicke equation for semi-dilute polymer solution, as the fractal dimension $D \approx 2$. ξ describes the conformation and extension of polymer chains in solution, being around a value of 2.5 for the pre-gel mixtures.

ξ strongly depends on the local concentration of polymer, thus it increases when the FT1 gels are stored in water: the polymer chains in the liquid-like portion of the hydrogels swell. The increase is less pronounced for the FT1 TC-PN network, probably due to the higher initial polymer concentration, which causes higher local crowding. The number of FT cycles is another key-factor affecting the value of ξ , due to the increased water-polymer phase separation as the freezing steps are repeated: as a consequence, the gel walls become denser also at the nanoscale. In both FT3 cryogels, ξ value decreases ($\xi = 3.5 - 3.6$ nm).

As regards the R parameter, in the case of pre-gel solutions it was associated with the formation of PVA aggregates before the FT gelation ($R = 13 - 20$ nm), while, in the cryogels, it was assumed to describe the polymer crystallites radius.

Table 7. Fitting parameters of the SAXS curves for the gel samples and pre-gel solutions.

Sample	Guiner Scale $I_G(0)$	Lorentz Scale $I_L(0)$	$I_G(0)/I_L(0)$	Correlation Length ξ (nm)	Fractal Dimension (D)	Crystallites Radius (R, nm)	Background (B)
PVA sol	4.8	4.5	-	2.4 ± 0.2	2.0 ± 0.1	13.9 ± 0.8	0.06
TC-PN sol	2.8	3.6	-	2.5 ± 0.2	2.1 ± 0.1	17.0 ± 2.2	0.03
PVA FT1	3.6	41	0.09	6.0 ± 0.3	2.7 ± 0.1	4.6 ± 0.1	0.01
PVA FT3	16	57	0.28	3.5 ± 0.1	2.9 ± 0.1	4.2 ± 0.1	0.07
TC-PN FT1	1.8	31	0.06	4.6 ± 0.2	2.8 ± 0.1	3.8 ± 0.2	0.03
TC-PN FT3	13	39	0.33	3.6 ± 0.1	2.7 ± 0.1	4.2 ± 0.1	0.02

R does not vary significantly among the four samples, being around a value of 4 nm. However, the Guiner Scale, $I_G(0)$, describes the magnitude of the contribution of the crystallites to the total scattering intensity, and the Lorentz Scale, $I_L(0)$, is the contribution of polymer chains in a liquid-like environment; therefore, the lower value of the $I_G(0)/I_L(0)$ ratio for the FT1 gels, as compared to FT3, indicates that after the first FT cycle polymer crystallites are less numerous in both the formulations.

These data, overall, confirm that, in both pure PVA and TC-PN gels, crystallites form in a similar fashion and reach the same final dimension, leading to the conclusion that they are made of H-PVA only.

The fractal exponent of the hydrogels obtained by fitting, D, ranges between 2.7 and 2.9, in agreement with previous observations on systems where strong hydrogen bond forms¹⁰⁶.

5.3 TC-PNs structuration due to freezing and washing: the effects of H-PVA-L-PVA phase separation

The sponge-like morphology of TC-PN hydrogels and the role of porogen played by L-PVA were further investigated by confocal imaging: H-PVA was green labeled with FITC, while L-PVA was red-labeled with RBITC. Confocal

images of the TC-PN pre-gel solution, fig. 28, at RT, show the presence of L-PVA blobs (2 – 20 μm) dispersed in the continuous H-PVA phase.

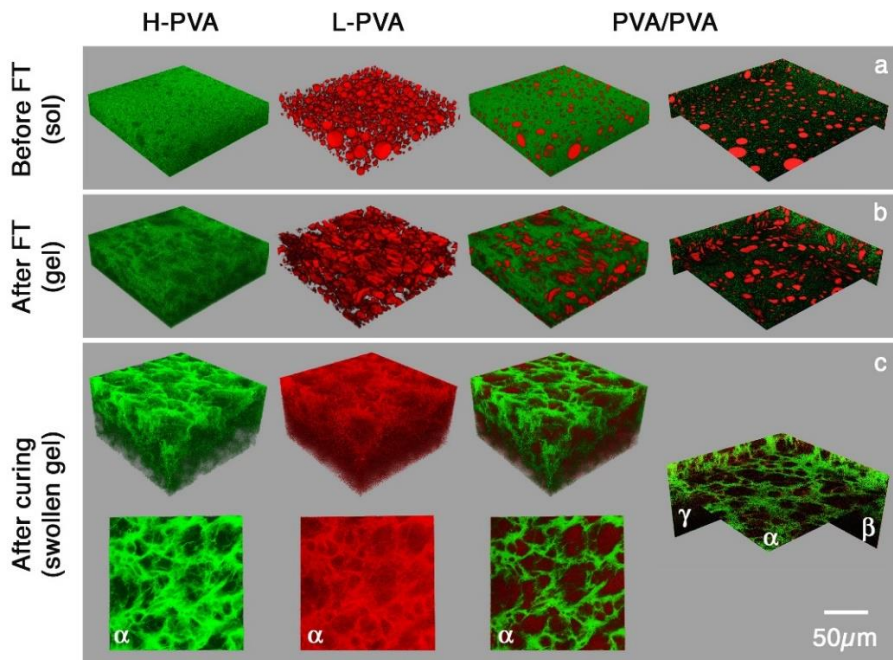


Figure 28. Confocal images of: (a) PVA/PVA pre-gel solution; (b) TC-PN gel obtained after 1 FT cycle; (c) TC-PN FT1 after 1 week of washing/curing in water. The 2D view of the top horizontal planes (α) highlights that L-PVA is preferentially localized on the gel walls, interacting with the H-PVA. Part of L-PVA is also present inside the pores, throughout the gel volume. Reproduced from ref. [17].

As a result, H-PVA accumulates in the continuous phase and its local concentration is higher than in the pure H-PVA pre-gel solution. As previously highlighted, this justifies the lower correlation length observed for TC-PN FT1 with respect to gels containing only H-PVA.

The spherical blobs act as templates during the cryo-formation of the TC-PN gel structure. Because water is a better solvent for L-PVA than H-PVA⁵⁷ at RT, L-PVA does not undergo further phase separation during the freezing step; L-PVA remains thus confined as blobs in water pockets during freezing, and after thawing. The formation of ice crystals along preferential axes leads to the deformation of the blobs, which are distorted from spherical to elongated shapes¹³⁸ (fig. 28 b).

After thawing and storage in water (1 week), most of the L-PVA is washed out of the network. However, confocal microscopy showed that the red-labeled L-PVA is still observable in the gel, either confined in the gel pores or stuck onto the gel walls (fig. 28 c). The FT3 TC-PN shows a more intense red fluorescence than the FT1 (fig. 29), suggesting that the amount of L-PVA that remains in the TC-PNs after washing increases with the number of FT cycles. This is in agreement with the higher G% observed for FT3 as compared to FT1 (Table 6).

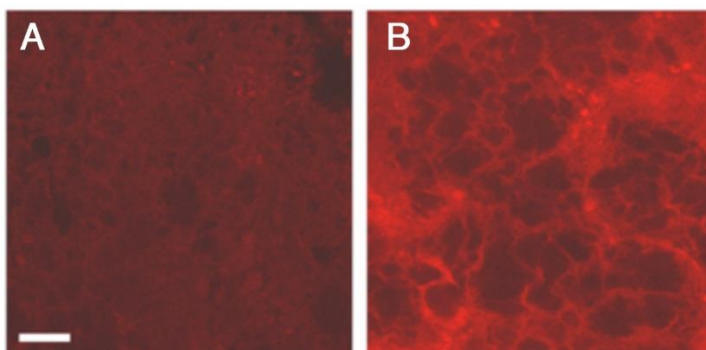


Figure 29. Confocal images (acquired at the same laser intensity and PMT voltage) of (A) TC-PN FT1 and (B) TC-PN FT3 gels, containing RBITC-L-PVA. The images were acquired after 7 days of washing/curing in water. Scale bar: 20 μm . Reproduced from ref. [17].

5.4 The diffusion of PVA chains in the TC-PN network

As mentioned in the previous sections, after the FT process, the cryogels are cured by one week washing in water. Confocal microscopy showed that L-PVA is still included in the TC-PNs structure, either as confined in the pores or stuck onto the gel walls. The dynamics of L-PVA chains were, then, investigated through FCS (gel pores) and FRAP (gel walls). The two techniques allow the measurement of diffusion coefficients, but on different ranges: ideally $D > 1 \mu\text{m}^2/\text{s}$ for FCS, and $0.01 \mu\text{m}^2/\text{s} < D < 50 \mu\text{m}^2/\text{s}$ for FRAP.¹³⁹

Fig. 30 shows the fitted FCS autocorrelation curves of RBITC-L-PVA chains in dilute aqueous solution (fig. 30 a), and in the pores of TC-PN FT1 and FT3 (fig. 30 b and 30 c respectively). In the first case, the curve is fitted by a single

decay function (Eq. 23). The calculated diffusion coefficient is reported in Table 8.

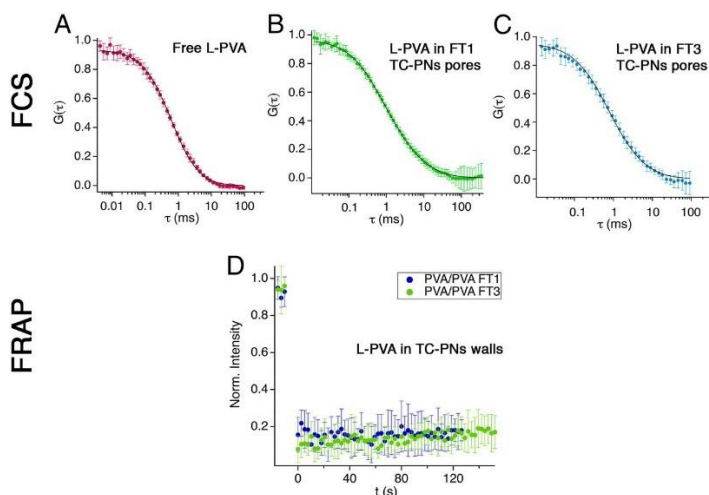


Figure 30. The diffusion of L-PVA in the TC-PN gels. (Top) FCS autocorrelation curves (marks) and fitting functions (solid lines) for (A) a diluted solution of L-PVA in water, L-(B) PVA in the pores of TC-PN FT1 gel, and (C) L-PVA in the pores of TC-PN FT3 gel. FRAP recovery profiles of L-PVA on the walls of TC-PN FT1 (blue markers) and FT3 (green markers) gels (D); the curves are flat, without recovery in the fluorescence intensity, which indicates that any diffusion of the polymer chains is detectable. Reproduced from ref. [17].

Instead, a double decay function (Eq. 24) was necessary to fit the autocorrelation curves for L-PVA chains in the gels pores. In this case, the fastest component of the decay (D_1) was assumed to correspond to that of free polymer chains (see Table 8), while the slow-diffusing elements were associated to L-PVA chains protruding from the gel walls or interacting with them through hydrogen bonds.

Table 8. Diffusion coefficient values (D) obtained from the fitting of FCS curves.

System	L-PVA D ($\mu\text{m}^2/\text{s}$)
PVA diluted solution (100 nM in RBITC)	24 ± 1
TC-PN FT1 pores	$D_1 = 24$ (65%) $D_2 = 4 \pm 1$ (35%)
TC-PN FT3 pores	$D_1 = 24$ (80%) $D_2 = 6 \pm 4$ (20%)

The FRAP data of L-PVA chains on TC-PNs walls are shown in fig. 30 d. No recovery was observed for both FT1 and FT3 gels within the first 140-160 s. For exposure times longer than 140-160 s, the gels are partially disrupted. FRAP measurements confirmed that, after curing in water, L-PVA chains are also partially blocked on the gels walls. Their diffusion coefficient is lower than $0.01 \mu\text{m}^2/\text{s}$, i.e., lower than the detection limit of FRAP.

5.5 Rheological behavior of PVA-based cryogels

The influence of the gel composition and the number of FT cycles on washed gels was investigated through rheology.

The amplitude sweep curves (fig. 31 a) show that the cross-over between the storage (G') and loss (G'') moduli can be found at lower oscillation strains for the FT3 hydrogels than for the FT1. Theoretically, the cross-over point is associated to a decrease in the cohesion of the structure: cohesive bonds should break, and systems should flow as liquids¹⁴⁰. In this case, no change to the liquid state is observed for the cryogels, and the cross-over point was interpreted as the partial rupture of weak bonds in the polymer network. The peak that appears in the G'' curves, the so-called "weak strain overshoot"¹⁴¹, can be reasonably attributed to weak interactions (i.e. hydrogen bonds not involved in the crystalline structure) that resist deformation until a certain strain value is reached (at the peak maximum, right before the cross-over). The peak position is shifted to lower strains when the number of FT cycles increases; this was explained considering that a higher number of FT cycles leads to stiffer and less mobile networks that are less capable of relaxing mechanical stresses. For the same number of FT cycles, the G'' peak moves to higher strain values for the TC-PNs. It can be argued that the chains of L-PVA act as plasticizers that make the final structure more compliant.

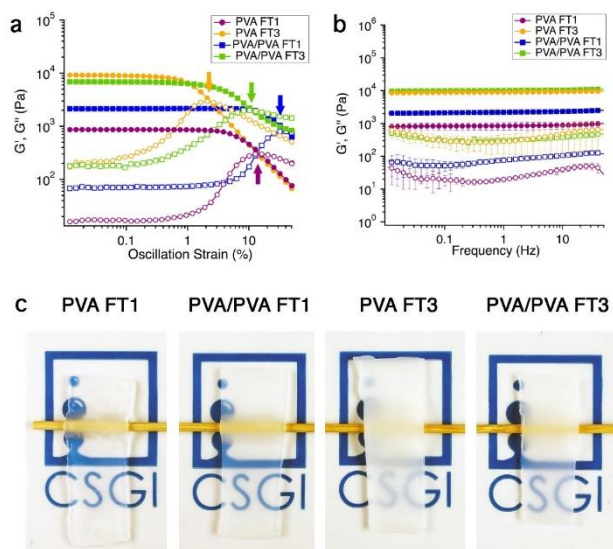


Figure 31. Rheological properties of PVA-based cryogels: (a) Amplitude sweep curves; arrows indicate the cross-over points; (b) Frequency sweep curves; (c) Visual aspect and adaptability on uneven surfaces. Reproduced from ref. [17].

Frequency sweeps (see fig. 31 b) were collected in the LVE range (linear viscoelastic range, identified in the amplitude sweeps), and show that for the FT1 gels G' is higher in the case of the TC-PN network. This is in apparent contrast to the lower G' observed for the TC-PNs, as G' is known to depend on the polymer concentration¹⁴². This further confirms the structural role of L-PVA in the gel structure.

No significant difference is observed among the FT3 gels; in any case, they have significantly higher G' than the FT1 systems, highlighting that structuration takes place during the freezing steps. It must be noticed that systems with excessively high elastic moduli are not able to adapt to surface irregularities in the typical range encountered in painted artifacts (i.e. ≥ 1 mm). In fact, the FT3 formulations were deemed too rigid for cleaning purposes, while the FT1 gels showed optimal adhesion to 3D textured surfaces (see fig. 31 c).

Chapter 6. Twin-Chain Polymer Networks: the influence of L-PVA molecular weight

Last chapters clarified L-PVA role as a porogen and structuring agent during the cryoformation of H-PVA-based hydrogels. The gel microstructure and porosity, observed through confocal imaging, were proven to be determined by a liquid-liquid phase-separation between the two polymers, occurring in the pre-gel solution. This influence structural and rheological properties of the final gels, deemed to be crucial for the cleaning action.

The polymers incompatibility is mainly determined by the different conformation of H-PVA and L-PVA in aqueous solution: while H-PVA chains are extended, L-PVA chains are partially collapsed, due to the presence of the hydrophobic acetate groups.

However, L-PVA molecular weight could also play a role in determining the physico-chemical properties of the resulting cryogels. In this chapter³, cryogels obtained by combining H-PVA with three different L-PVAs (K18_L-PVA, K32_L-PVA and K47_L-PVA, HD = 88 %, different molecular weights) are investigated.

6.1. Determination of L-PVA molecular weight

The M_v of the three commercial L-PVAs was determined by using viscometry. The viscosity of polymer solutions containing increasing concentrations of polymer was measured through a capillary viscometer (Ubbelohde). Data are shown in fig. 32. They were fitted according to Martin equation⁵³ for semi-dilute solutions (Eq. 9); the $[\eta]$ values were extrapolated and used in the Mark-Houwink equation (Eq. 3) to obtain M_v . The calculated $[\eta]$ and M_v values are reported in Table 9. For comparison, the viscometric M_v of L-PVA (from Sigma) was also determined with the same method.

³ Based on Paper III, see Appendix.

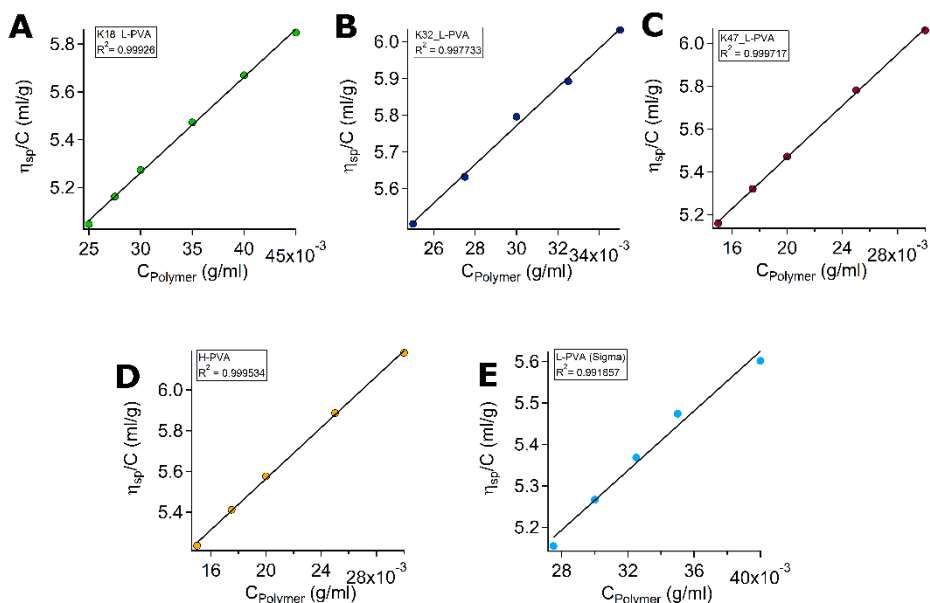


Figure 32. Data (full markers) of the reduced viscosity (η_{sp}/C) VS the polymer concentration (C_{Polymer}) for aqueous solutions of each polymer investigated. η_{sp} was obtained from viscosity measurements (with the Ubbelohde viscometer). Data were fitted with the Martin equation (solid black lines). (A) K18_L-PVA; (B) K32_L-PVA; (C) K47_L-PVA; (D) H-PVA (Sigma); (E) L-PVA (Sigma).

Table 9. Intercept ($[\eta]$) and slope ($K_M[\eta]$) obtained by fitting curves in fig. 32 with Martin equation. From $[\eta]$ values, M_V was calculated through the Mark-Houwink equation. The table shows also M_W for H-PVA and L-PVA (Sigma) and the calculated K_M values.

Polymer	$\ln [\eta]$	$K_M[\eta]$	Intrinsic Viscosity, $[\eta]$	Viscometric \bar{M}_v	Producer's M_w	Martin constant, K_M
K18_L-PVA	4.06 ± 0.03	40 \pm 1	58.12 \pm 0.03	73,050 (\pm 50)	-	0.69 \pm 0.01
L-PVA (Sigma)	4.19 ± 0.09	36 \pm 3	65.86 \pm 0.09	89,010 (\pm 190)	100,000	0.54 \pm 0.04
K32_L-PVA	4.19 ± 0.06	53 \pm 2	66.23 \pm 0.06	89,810 \pm (130)	-	0.79 \pm 0.03
K47_L-PVA	4.26 ± 0.02	60 \pm 1	71.27 \pm 0.02	100,860 \pm (40)	-	0.84 \pm 0.01
H-PVA (Sigma)	4.31 ± 0.02	63 \pm 1	74.42 \pm 0.02	--	160,000	0.84 \pm 0.02

$[\eta]$ values increase from K18 to K47 sample. The M_v of commercial L-PVAs ranges between 73,000 and 101,000 Da; the M_v of K47_L-PVA is probably higher than that of H-PVA (Sigma), given the similar $[\eta]$ values and the stronger inter- and intra-chain interactions in H-PVA solutions.

The fitting with Martin equation led also to the determination of the Martin constant (K_M); it is a measure of both the quality of the solvent and polymer-polymer interactions⁵³. K_M increases with the polymers M_v , with the exception of L-PVA (Sigma) sample. L-PVA (Sigma) and K32_L-PVA have very similar $[\eta]$ and M_v , but differ for the K_M value. Thus, we can suppose that, even if both polymers have a HD = 88 %, the positions of acetate groups on the chains backbone is not the same; as a result, chains conformation in aqueous solution will be different.

6.2 How L-PVA chains length influences phase-separation and cryostructuration

Three TC-PNs were prepared by mixing H-PVA with the three commercial L-PVAs, in a 3:1 ratio, respectively.

Fig. 33 shows the confocal images of pre-gel solution containing FITC-labeled H-PVA, and the resulting FT1 gels soaked in a Rhodamine 110 solution.

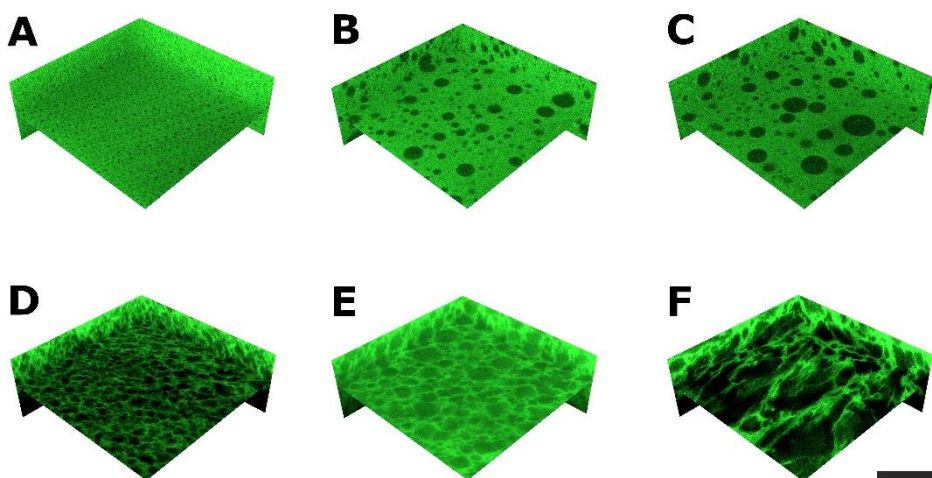


Figure 33. Confocal images of pre-gel solutions (A-C) and washed gels (D-E), containing respectively: K18_L-PVA (A, D); K32_L-PVA (B, E); K47_L-PVA (C, F). Scalebar: 50 μm .

L-PVA M_v affects the dimension of blobs formed during the liquid-liquid phase separation at RT; more in detail, blob dimensions increase with the length of L-PVA polymer chains: their diameter is less than 5 μm in TC-PN K18 pre gel solution, and it increases to tens of μm for TC-PN K32 and TC-PN K47 pre-gel solutions. As a consequence, also pore dimension changes, even if it does not reflect exactly the blob dimensions observed at RT; in fact, the low temperature of freezing enhances the phase-separation process (leading to larger and more numerous blobs), while the ice crystals formed during freezing compress the H-PVA chains contained in the continuous phase.

6.3 The impact of L-PVA M_w on gels physico-chemical properties

Physico-chemical properties of 1 week washed TC-PNs, such as gel fraction, crystallinity (by DSC, both thawed and washed gels), Equilibrium Volume Swelling Ratio and water release, were quantified (Table 10). The gel fraction is around a 30% of the initial polymer content; it did not vary even after 3 weeks of storage in water, suggesting that further loss of polymer is negligible.

Table 10. Gel fraction, Crystallinity (non-washed, NW, and washed, W, gels), Equilibrium Water Swelling Ratio and Water Release obtained for the three samples.

Sample Name	Gel fraction (G%)	Crystallinity NW (X_c %)	Crystallinity W (X_c %)	Equilibrium Volume Swelling Ratio (q_v)	Water release (mg/cm^2)
TC-PN K18	31 ± 8	24 ± 1	31 ± 1	1.73 ± 0.05	25 ± 2
TC-PN K32	29 ± 2	28 ± 1	32 ± 1	1.89 ± 0.05	27 ± 1
TC-PN K47	31 ± 4	24 ± 1	32 ± 1	2.12 ± 0.05	23 ± 2

Despite the very different structures of TC-PNs K18, K32 and K47, observed through confocal microscopy, the hydrogels properties here analyzed are, overall, not significantly different.

In general, the second crystallization occurring after washing is affecting the crystallinity values, and the swelling ability is higher for TC-PN K47, probably because of its larger pores.

TC-PN K32 seems to be more structured, before washing, than the other two samples: the value of the crystallinity of the non-washed gel is slightly higher. Otherwise, the three samples are almost identical.

Rheological properties of both pre-gel solutions and networks were also investigated. TC-PN K47 pre-gel solution has the highest viscosity: it is comparable to a 12 % w/v H-PVA aqueous solution at high shear rates (Fig. 34).

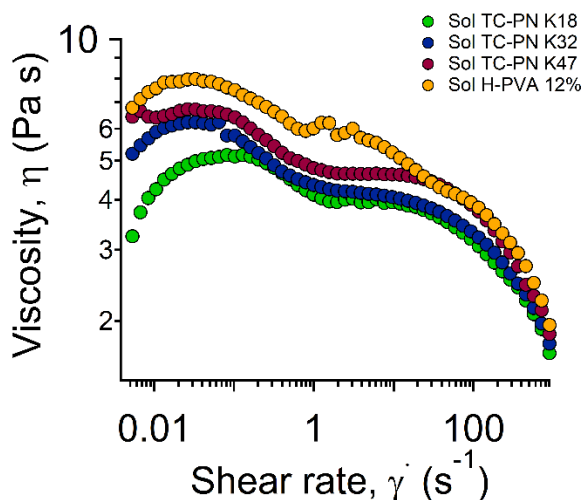


Figure 34. Flow curves of pre-gel solutions (Sol TC-PN K18, K32 and K47) compared to the flow curve of a H-PVA aqueous solution (12% w/v).

This could be an effect of the larger K47_L-PVA blobs: in fact, either the phase separation is more effective in concentrating H-PVA continuous phase, or the long K47_L-PVA chains remaining in the continuous phase are able to interact with H-PVA chains and increase the viscosity. All the TC-PN pre-gel solutions show a different shear thinning behavior (with a plateau region), around 1 s⁻¹, with respect to the concentrated H-PVA solution. This could be an effect of the presence of L-PVAs acetate groups, which act as plasticizers in the mixtures.

The rheological response of the non-washed TC-PN gels does not differ significantly (fig. 35).

However, after washing, TC-PN K32 appeared to be, like crystallinity data suggested, more structured than TC-PN K18 and TC-PN K47. TC-PN K47 showed the highest compliance after washing (G' is significantly lower with

respect to the other two samples), i.e., it is the most adaptable to rough and clotted surfaces; this could be an effect of its extended porosity.

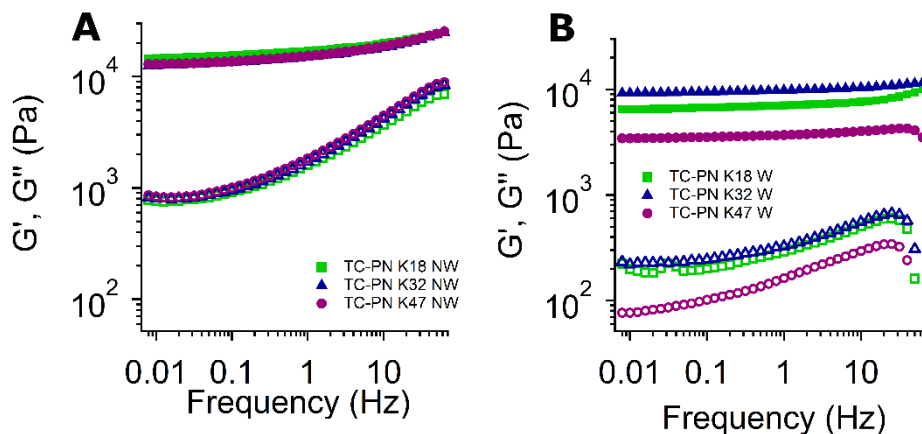


Figure 35. Frequency sweeps of TC-PNs containing K18, K32 and K47 L-PVAs. Measurements have been performed before and after washing.

6.4 SAXS characterization

Pre-gel solutions and TC-PNs nanostructure were investigated through SAXS. SAXS curves and fittings, obtained through Eq. 21, are shown in fig. 36. Fitting parameters are reported in Table 11.

The Guinier scale, $I_G(0)$, and the Lorentz scale, $I_L(0)$, have values that are almost comparable for the solutions. In that case, they quantify areas containing polymer aggregates and polymer chains in solution, respectively. For TC-PN gels, instead, $I_G(0)$ and $I_L(0)$ describe the solid-like portions of the networks, containing crystallites, and the liquid-like areas, containing swollen polymer chains. Therefore, the I_G/I_L ratio can be used to quantify the ordered regions in the networks: they are more extended in the non-washed gels with respect to the swollen networks, as the solvent causes the disruption of some polymer interactions established during freezing. Among the non-washed gels, ordered regions are less numerous in the TC-PN K47, probably because the long semi-interpenetrating chains prevent some of the H-PVA self-interactions.

TC-PN K18 is the sample that is more affected from the washing step: the ordered regions strongly decrease after washing. In this case, the short K18_L-

PVA chains have less interaction with the structural H-PVA: they are easily extracted by water, leaving structural defects in the networks.

The correlation length, ξ , increases from pre-gel solution to non-washed gels. This can be related to the swelling of polymer chains in the less dense areas of the gels, after the melting of ice crystals. A further increase in ξ is registered after gels swelling in water.

The fractal dimension, D , is around 2 for pre-gel solutions, as expected. D values increase for gels: networks where polymer chains interact through H-bonds have $2.7 < D < 2.9^{106}$; such values are reached, especially after swelling. The radius of aggregates in the pre-gel solutions, R , could be related to polymer complexes formed because of specific interactions.

Crystallites radius in the gels, R , has a value of 5.5 nm ca. It decreases for the washed TC-PN K18, confirming that the swelling in water causes a destabilization of the network structure.

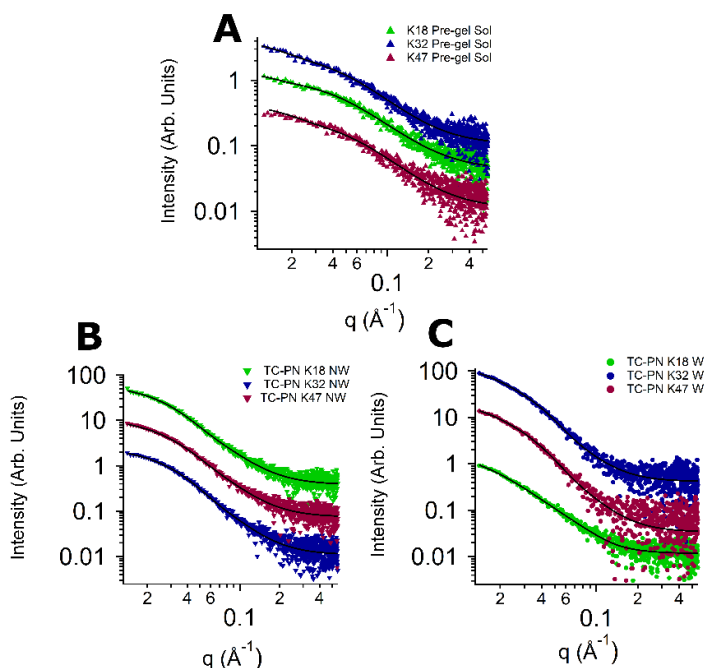


Figure 36. SAXS curves (full markers) and fittings (solid black lines) for pre-gel solutions, non-washed (NW) gels and washed (W) gels.

Table 11. SAXS fitting parameters for pre-gel solutions (Sol), non-washed (NW) gels and washed (W) gels.

Sample	Guiner Scale $I_G(0)$	Lorentz Scale $I_L(0)$	I_G/I_L	Correlation Length ξ (nm)	Fractal Dimension (D)	Radius of aggregates /Crystallites Radius (R, nm)	Background (B)
TC-PN K18 Sol	13	25	-	2.3 ± 0.1	2.0 ± 0.1	15.1 ± 0.6	0.14
TC-PN K32 Sol	26	34	-	2.1 ± 0.1	2.1 ± 0.1	11.6 ± 0.3	0.14
TC-PN K47 Sol	34	24	-	2.1 ± 0.1	2.2 ± 0.1	19.7 ± 0.6	0.10
TC-PN K18 NW	11	38	0.29	3.8 ± 0.1	2.5 ± 0.1	6.1 ± 2	0.21
TC-PN K32 NW	7	25	0.28	3.5 ± 0.1	2.6 ± 0.1	5.6 ± 0.1	0.10
TC-PN K47 NW	5	26	0.19	3.6 ± 0.1	2.6 ± 0.1	5.7 ± 0.2	0.16
TC-PN K18 W	0.5	42	0.02	5.5 ± 0.1	2.7 ± 0.1	2.4 ± 0.1	0.15
TC-PN K32 W	5	35	0.14	5.1 ± 0.1	2.8 ± 0.1	5.4 ± 0.1	0.08
TC-PN K47 W	4	29	0.14	5.2 ± 0.1	2.9 ± 0.1	5.6 ± 0.1	0.03

Chapter 7. Nanostructured fluids: dewetting process and cleaning mechanism

The dirt depositing on painted surfaces can be hydrophilic or hydrophobic in nature. Specific cleaning fluids can be embedded in gels to grant a selective and controlled removal of unwanted materials: the latter are solubilized at the gel-substrate interface, and kept inside the polymer matrix.

One of the most common hydrophobic grime found on painted surfaces is the resin Paraloid B72. It is usually applied on paintings because of its transparency and its ability to saturate the colors, giving a glossy appearance to the surface; moreover, it protects the paint from moisture. However, Paraloid becomes yellow over time, due to a crosslinking reaction induced by UV light, and its removal becomes necessary to grant the readability of the work of art.

o/w μ Em and NSF's were proven to be the most effective tools to clean Paraloid coated surfaces³³. The organic solvent contained in the droplets (for μ Em) or in both the micelles core and the continuous phase (for NSF's) contributes to lower the polymer T_g , inducing dewetting on thin films, while the surfactants act on the kinetics of the process^{35,36}.

In this chapter⁴, the dewetting mechanism of Paraloid B72 2 μ m thick-films, induced by four different NSF's, is investigated through Confocal imaging, DLS and FCS.

NSF's with a similar structure were loaded in TC-PN gels to clean Pablo Picasso's *The Studio* (see Chapter 8).

⁴ Based on Paper IV, see Appendix.

7.1 NSF-induced dewetting of Paraloid B72 films: effects of the solvent and the surfactant

The four NSFs here investigated contain two types of nonionic surfactants (MPD, $C_{12}E_{15} - OH$, methoxy-pentadeca(oxyethylene) dodecanoate, and PDE, $C_{11} - C=O - E_{15} - OCH_3$, pentadeca-(oxyethylene) dodecyl ether), which differ for the presence of a methyl group in the polar head of MPD, and two different solvents (propylene carbonate, PC, and Methyl Ethyl Ketone, MEK). The final NSFs result by the combination of each surfactant with each solvent, in an aqueous environment: H₂O/PC/PDE, H₂O/PC/MPD, H₂O/MEK/PDE, H₂O/MEK/MPD.

MPD and PDE have a very similar chemical structure; nonetheless, MPD cleaning performances are better, especially in steady condition, i.e., without any stirring or shaking. In fact, phase behavior in water, polar head hydration and CMC are different for the two surfactants.³⁶

As regards the organic phase, while both PC and MEK can induce the dewetting of thin Paraloid films, it was recently demonstrated that PC is more effective, leading to a complete dewetting of the polymer.^{33,34} As a matter of fact, both solvents should be ideal for Paraloid solubilization according to the relative Hansen parameters²², and MEK should even perform better (see Table 12). However, when combined with water in the NSFs, PC performances are superior: this could be due to a stronger interaction between MEK and water molecules.

Table 12. Hansen solubility parameters for PC, MEK and Paraloid B72. δ_d , δ_p and δ_h are the dispersion component, the polar component and the hydrogen bonding component, respectively.

	δ_d	δ_p	δ_h
PC	20.0	18.0	4.1
MEK	16.0	9.0	5.1
Paraloid B72	18.1	10.1	5.8

Fig. 37 shows the effects of the four NSFs on a Coumarin 6-labeled Paraloid B72 film, deposited on a microscope glass slide, over a time of 30 min. Confocal images were taken at the glass-film interface.

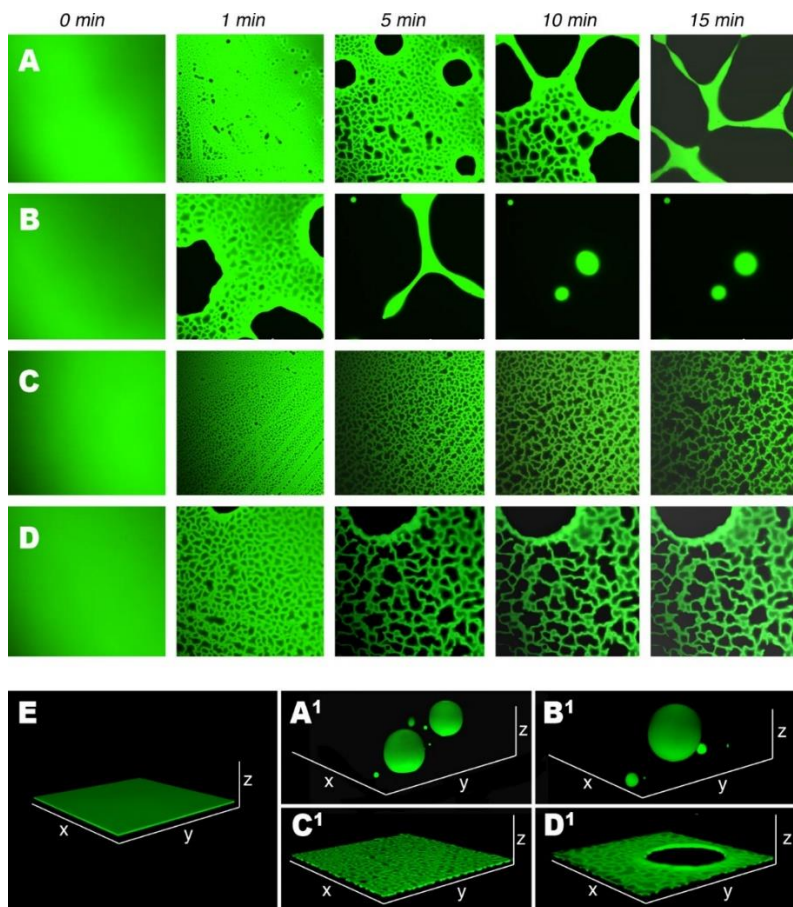


Figure 37. Confocal images of a 2 μm -thick, Coumarin 6-labeled Paraloid B72 film with: (A) H₂O/PC/PDE, (B) H₂O/PC/MPD, (C) H₂O/MEK/PDE, (D) H₂O/MEK/MPD. (E) 3D image of the polymer film before the interaction with the NSFs, and after a 30 min interaction with (A¹) H₂O/PC/PDE, (B¹) H₂O/PC/MPD, (C¹) H₂O/MEK/PDE, (D¹) H₂O/MEK/MPD. Each confocal image has a side of 150 μm . Reproduced from ref. [32].

The 2 μm -thick films here investigated are examples of metastable systems: the hydrophobic polymer covers an hydrophilic surface, therefore dewetting is thermodynamically, but not kinetically, favored.

In all cases, the polymer starts to detach from the surface forming liquid filled cavities, which expand as the liquid-polymer interaction goes on.

The stripes of polymer remaining in contact with the glass surface draw a typical pattern, called Voronoi pattern or tessellation¹⁴³. The evolution of the systems over time changes with both the surfactant and the solvent constituting the NSF; in fact, both NSFs containing PC lead to the complete

dewetting of the Paraloid film (fig. 37 A, B, A¹ B¹), i.e. the polymer detaches completely from the surface and eventually forms spherical blobs. However, it is evident that the kinetics of H₂O/PC/PDE (fig. 37 A) are slower than those of H₂O/PC/MPD (fig. 37 B).

As regards the MEK containing NSFs, the dewetting process is not complete after a 20 min interaction (fig. 37 C, D, C¹, D¹) and, even if the cavities at the polymer-glass interface become larger for longer interaction times, the Voronoi pattern eventually stabilizes.

Also in this case, the effect of the different surfactant is evident: PDE-based NSF is less effective in the dewetting process with respect to MPD NSF (see fig. 37 C, D, respectively).

The role of the surfactant can be explained considering the mechanism of the dewetting process: while the polymer locally detaches from the glass, new polymer-liquid and glass-liquid interfaces form, that is, the interfacial area of the system increases. Surfactants are able to reduce the energy cost of this transition, by reducing interfacial tension. The higher ability of MPD in “catalyzing” dewetting with respect to PDE can be explained also on the basis of their interfacial tensions: it was found that $\gamma_{\text{MPD}} \approx 34.5 \text{ N/m}$, while $\gamma_{\text{PDE}} \approx 37.5 \text{ N/m}$ (see fig. 38).

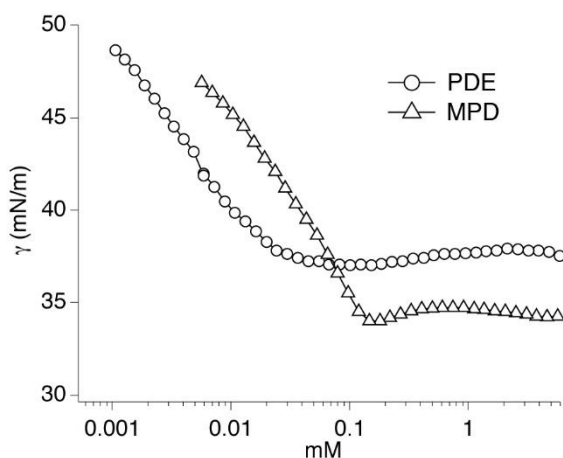


Figure 38. Surface tension of MPD and PDE aqueous solutions, as a function of surfactant concentration. Reproduced from ref. [32].

Moreover, MPD has a higher hydrophobicity than PDE, granted by the methoxy group at the end of the polyoxyethylene chain, and could be able to penetrate more easily into the hydrophobic polymer film.

7.2 Dewetting mechanism

The diffusion and evolution of the NSFs droplets during the interaction with the polymer film were investigated by combining DLS, Confocal imaging and FCS. Initially, micellar solution of PDE and MPD were labeled with the fluorescent, amphiphilic dye Bodipy and their diffusion was compared to that of neat micellar solutions through DLS. Then, the influence of the presence of Bodipy was investigated also on the four NSFs. The diffusion coefficients (see Table 13), obtained either from the cumulant analysis, or as a weighted average of the most recurrent D values obtained from the CONTIN analysis, show that both the labeling and the addition of the organic solvent do not drastically affect micelles dimension.

The average diffusion coefficient of $80 \mu\text{m}^2/\text{s}$ was used as a “guess value” for the FCS analysis. FCS probing was performed on the labeled NSFs before the interaction, in the liquid-filled cavities (during the interaction), and on top of the film, after a 20 min interaction. More in detail, FCS probing was performed in the cavities at the glass-polymer interface for the MEK-based NSFs only; for the PC-based NSFs, in fact, the evolution of the system was too fast, and measurements could be done only at the end of the polymer rearrangement, i.e., in liquid-filled cavities inside the spherical polymer blobs.

Table 13. Average Diffusion Coefficients, D ($\mu\text{m}^2/\text{s}$), obtained by DLS Analysis.

System	D ($\mu\text{m}^2/\text{s}$) for unlabeled sample	D ($\mu\text{m}^2/\text{s}$) for Bodipy-labeled sample
H2O/PDE	85 ± 3^a	81 ± 2^a
H2O/MPD	88 ± 6^a	86 ± 3^a
H2O/MEK/PDE	85 ± 11^b	87 ± 10^b
H2O/PC/PDE	72 ± 5^b	75 ± 15^b
H2O/MEK/MPD	73 ± 5^a	87 ± 6^b
H2O/PC/MPD	77 ± 2^a	78 ± 2^b

^aValues and standard deviations obtained by cumulant analysis.

^bWeighted averages of the most recurrent D values obtained by CONTIN algorithm, with standard deviation.

The probing is schematized in the cartoon of fig. 39, with the FCS curves obtained in each area of the samples.

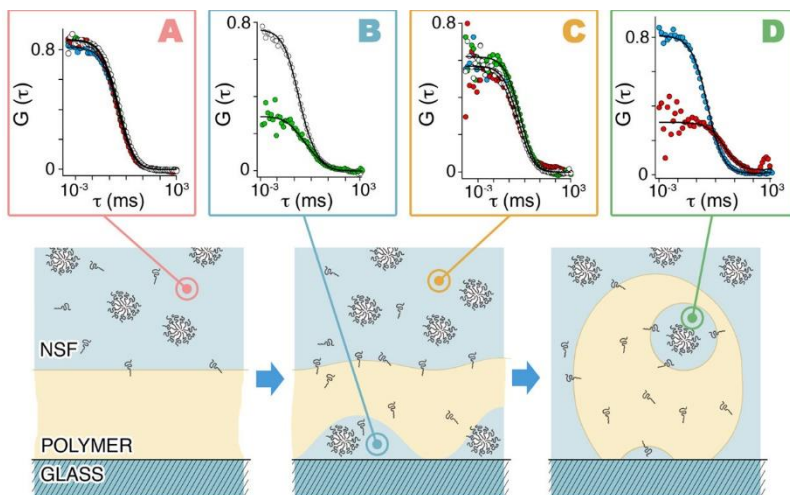


Figure 39. The cartoon illustrates the points of FCS probing during the film dewetting, while the panels A-D show the FCS curves acquired in each spot at $t = 0$ min (before interaction) (A), at time $t = 5-15$ min (only for MEK-based NSFs) (B), after 20 min of incubation of the polymer with the four NSFs (C), and in cavities inside polymer blobs after complete dewetting (only for PC-based NSFs) (D); H₂O/PC/PDE (blue circles), H₂O/PC/MPD (red circles), H₂O/MEK/PDE (white circles), and H₂O/MEK/MPD (green circles). Reproduced from ref. [32].

The real regions where measurements were performed are shown as confocal images in fig. 40, with the FCS curves fitting. All FCS decays were fitted accounting for the presence of two components (Eq. 24). The calculated diffusion coefficients are listed in Table 14 for MEK-based NSFs and Table 15 for PC-based NSFs.

Droplet sizes and polydispersity of the systems remain almost the same for the MEK-based NSFs before and after the interaction (see D_{bulk} at $t = 0$ and $t = 20$ min in Table 14), except for the lower $D_{2,\text{bulk}}$ of H₂O/MEK/MPD, probably due to MPD ability to solubilize low-molecular weight components of Paraloid.

However, the most remarkable feature of these systems lies in the surfactant ability, either as a monomer or as micellar aggregates, to penetrate the swollen polymer film and reach the cavities at the polymer-glass interface. In these cavities, the diffusion of micelles is detectable.

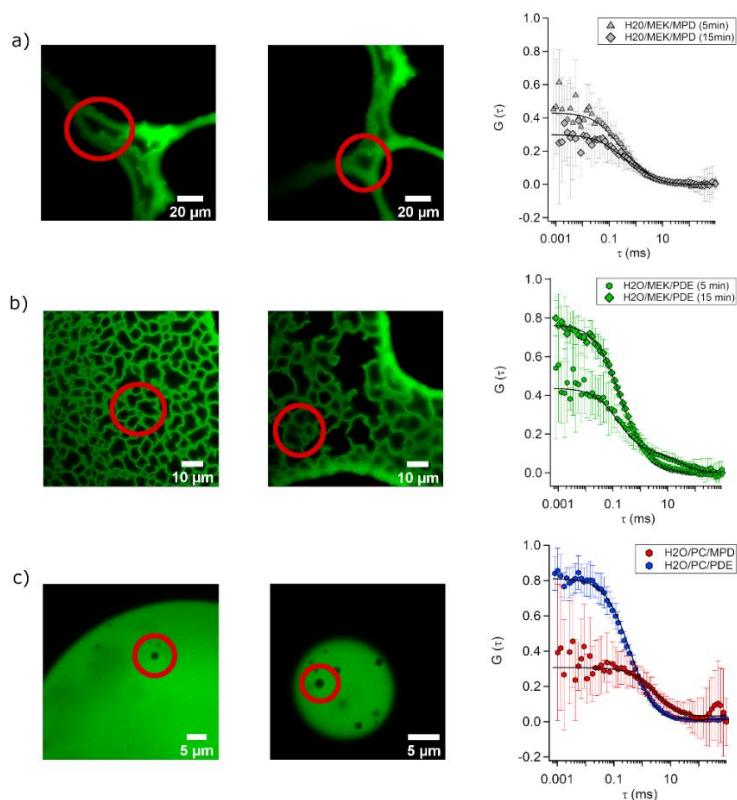


Figure 40. Confocal images show the areas where FCS probing was performed; FCS averaged curves and two-components decay fitting are shown for each panel. Panel (A): cavities formed at the glass-polymer interface after 5 and 15 min, respectively, of interaction, and FCS curves and fitting, for H₂O/MEK/MPD system. Panel (B): cavities formed at the glass-polymer interface after 5 and 15 min, respectively, of interaction, and FCS curves and fitting, for H₂O/MEK/PDE system; Panel (C): cavities formed in the dewetted polymer blobs for H₂O/PC/MPD (left) and H₂O/PC/PDE (right), and relative FCS decays and fitting. Reproduced from ref. [32].

More specifically, the micelles probably penetrates through polymer film defects¹⁴⁴ and reach the cavities, while some surfactant molecules are absorbed inside the polymer film and contribute to the T_g lowering induced by the solvents.

For H₂O/MEK/PDE NSF, the larger fraction of diffusing species in the cavities is represented by smaller micelles ($D = 80 \mu\text{m}^2/\text{s}$, 80% of the diffusing fluorescent molecules) and the system does not significantly change over the time of the interaction; H₂O/MEK/MPD NSF, instead, seems to penetrate

more trough the film as the contact time increases: the species detected in the cavities after a 12 min interaction are very similar to the bulk species (i.e. the species on top of the film, after a 20 min interaction), even if smaller species are still more numerous in the cavities.

As regards the PC-based NSF's, the diffusion of H₂O/PC/PDE micellar species, before and after the interaction with the Paraloid film, reflects the same situation observed for MEK-based systems: the systems did not evolve with time. However, H₂O/PC/MPD micelles grew bigger after the interaction, probably because MPD, in combination with the better solvent PC, was able to further extract soluble components of the film after a 20 min interaction (see Table 15).

The micelles entrapped in the liquid-filled cavities inside dewetted polymer blobs are either larger than the original micelles (especially for the MPD system) and/or their mobility is limited. The faster D_1 is, especially in PDE system, probably an average of faster and slower diffusing species, while the slow component D_2 , for both PC-based NSF's, indicates that the fluorescent species are strongly interacting with the polymer.

To sum up, the mechanism of polymer dewetting and removal strongly depends on the type of organic solvent and surfactant used in the NSF formulation: while a good solvent is necessary to grant a the polymer dewetting, different surfactants can be used to play with the kinetics of the process, granting a controllable but efficient treatment of several types of artifacts.

Table 14. Diffusion coefficients, in $\mu\text{m}^2/\text{s}$ obtained by FCS curves fitting for MEK-based NSF's in different areas of the samples, during a 20 min polymer-NSF's interaction (see the cartoon in fig. 39 and panels a, b in fig. 40).

NSF	D_{bulk} (t = 0 min)	D_{cav} (t = 5 min)	D_{cav} (t = 12 min)	D_{bulk} (t = 20 min)
H ₂ O/MEK/PDE	$D_1 = 80$ (40%) $D_2 = 17 \pm 2$	$D_1 = 80$ (80%) $D_2 = 0.4 \pm$ 0.2	$D_1 = 80$ (80%) $D_2 = 6 \pm 2$	$D_1 = 80$ (40%) $D_2 = 16 \pm 5$
H ₂ O/MEK/MPD	$D_1 = 80$ (50%) $D_2 = 17 \pm 3$	$D_1 = 80$ (70%) $D_2 = 7 \pm 3$	$D_1 = 80$ (60%) $D_2 = 6 \pm 3$	$D_1 = 80$ (50%) $D_2 = 6 \pm 2$

Table 15. Diffusion coefficients obtained by FCS curves fitting for PC-based NSF's in different areas of the samples, during a 20 min polymer-NSF's interaction (see the cartoon in fig. 39 and panel c in fig. 40).

NSF's with PC	D_{bulk} (t = 0 min)	D_{cav} (t = 10 min)	D_{bulk} (t = 20 min)
H ₂ O/PC/PDE	$D_1 = 80$ (50%) $D_2 = 19 \pm 4$	$D_1 = 33 \pm 2$ (99%) $D_2 = 0.01$	$D_1 = 80$ (50%) $D_2 = 13 \pm 4$
H ₂ O/PC/MPD	$D_1 = 80$ (60%) $D_2 = 18 \pm 4$	$D_1 = 5 \pm 2$ (90%) $D_2 = 0.1$	$D_1 = 64 \pm 40$ (40%) $D_2 = 4$

Chapter 8. The diffusion of cleaning Nanostructured Fluids into the gel matrix

The diffusion of micelles or solvent droplets contained in aqueous NSF_s and o/w μ Em can be controlled by embedding the cleaning liquids in a hydrogel network.

The species diffusion will depend on the specific micelles-polymer interaction and on the micro-porosity of the network.

This chapter⁵ explores the mobility of NSF_s, either containing nonionic or anionic surfactants, or both, in pure H-PVA and TC-PN cryogels, obtained by 1 or 3 FT cycles (see Chapter 5 for a description of the gels structure and properties).

The diffusion into the gels matrix was investigated through FCS.

8.1. How the porosity of hydrogels and the surfactant nature influence droplets diffusion in gels

Two aqueous NSF_s, coded as XYL and BEMP, were prepared according to the quantities reported in Table 16.

XYL contains the anionic surfactant SDS, Pe-OH as a co-surfactant and Xylene as “oil”. XYL is a proper o/w μ Em, i.e. the organic solvent is completely confined the core of the SDS micelles. BEMP, on the other hand, contains a nonionic surfactant (C₉₋₁₁E₆) and four organic solvents; one of them, Bu-OH, also acts as a co-surfactant. BEMP is defined a NSF: in this case, the organic solvents are partially soluble in water, so they will be found both in the micelles core (forming “swollen micelles”) and in the aqueous continuous phase.

Systems of this type were thoroughly characterized through SAXS and USAXS.

⁵ Based on Papers V and VI, see Appendix.

Table 16. XYL and BEMP NSF's composition.

Composition (% w/w)	XYL	BEMP
H2O	85.5	60
SDS	4	-
Pe-OH	8	-
Xylene	2.5	-
C ₉₋₁₁ E ₆	-	5
Bu-OH	-	10
PC	-	7
MEK	-	11
EA	-	7

The loading of XYL and BEMP in PVA-based cryogels does not affect significantly the gels structure; however, it is well known that hydrophobic polymer-surfactant interactions are likely to occur, especially in presence of anionic surfactants: the hydrophobic surfactant tail interacts with the backbone of the PVA chain, even for highly hydrolyzed PVAs¹⁴⁵. As a result, polymer chains behave as polyelectrolytes and the equilibrium swelling ratio can increase. Concurrently, network inhomogeneities in the hundreds of nanometers decrease, while polymer crystal size slightly increases (due to the local electrostatic repulsion of surfactant charged polar heads).

The diffusion of XYL and BEMP micelles in PVA-based cryogels was measured through FCS, after labeling both NSF's with the nonionic, amphiphilic dye Bodipy.

The comparison between the averaged autocorrelation curves of the free and confined NSF's are shown in fig. 41 A and B, for XYL and BEMP, respectively.

Curves fitting, obtained considering a single component decay (Eq. 23), are shown as dashed lines in figure 41 C and D, for XYL and BEMP, respectively. The diffusion coefficients are listed in Table 17.

XYL droplets are slightly smaller than BEMP “swollen micelles”: the diameters obtained by USAXS measurements are $d_{\text{XYL}} \approx 5$ nm and $d_{\text{BEMP}} \approx 6.3$ nm. However, the viscosity of XYL is far higher than that of BEMP; as a result, the diffusion coefficient of XYL droplet, D_{freeXYL} , is ca. 3 times smaller than D_{freeBEMP} . Such difference in viscosity can be ascribed both to the different composition of the continuous phase (in BEMP the organic solvents

mainly constitute the continuous phase, lowering its viscosity) and to the higher hydration of SDS head group, with respect to that of $C_{9-11}E_6$ contained in BEMP. In fact, it has been reported that sulfate groups of anionic surfactant are highly hydrated and strongly interact with water through hydrogen bonding.¹⁴⁶ This leads to a larger hydration shell for XYL droplets, and to a higher viscosity of the medium with respect to BEMP.

Fig. 41 A shows the effects of XYL inclusion in the four cryogels: the solid green line describing the free XYL diffusion is not significantly different from droplets diffusion in TC-PNs (i.e. PVA/PVA gels), while for both pure H-PVA gels FCS autocorrelation curves are significantly different, both displaying a faster decay, probably ascribable to the diffusion of free dye.

Fig. 41 B shows the comparison between free BEMP (solid light blue line) and BEMP included in the gels autocorrelation curves: in this case PVA FT1 and PVA/PVA FT3 are the systems that mostly differ from the others.

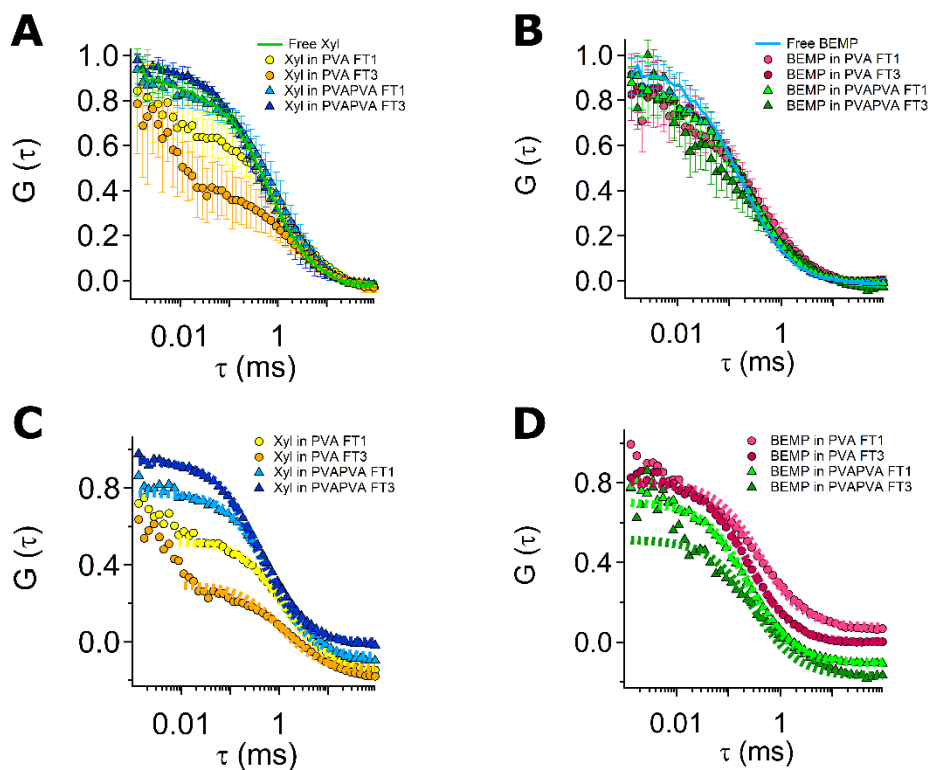


Figure 41. FCS autocorrelation curves describing the diffusion of NSF's in PVA-based cryogels. (A) Comparison between the curves describing the diffusion of free XYL and XYL embedded in the cryogels; (B) Comparison between the curves describing the diffusion of

free BEMP and BEMP embedded in the cryogels; (C) Autocorrelation curves (markers) and relative one-component fitting (dashed lines) of XYL diffusing in the networks; (D) Autocorrelation curves (markers) and relative one-component fitting (dashed lines) of BEMP diffusing in the networks. Curves are averages of 12 repetitions and error bars in (A) and (B) represent the standard deviations. Curves in (C) and (D) have been shifted along the Y axis for clarity.

A different diffusional behavior of micellar aggregates can be ascribed either to the different average viscosity of the medium, to a small average pore-size, or to surfactant-polymer interactions.

As regards XYL systems, it is known that anionic surfactants are likely to interact with polymers, such as PVA, through their hydrophobic tails, exposing polar heads and forming polyelectrolytes¹⁴⁷. As described in Chapter 5, PVA FT1 has long, needle-shaped pores whose diameter (0.5 μm ca.) slightly expands after the second and the third FT steps.¹⁷ Conversely, TC-PN gels have a sponge-like structure, with pores diameter ranging from 1 to 20 μm ca.¹⁷ Therefore, it is likely that SDS adsorbs on the gel walls in the four XYL systems. However, for needle-shaped pores, the bulky charged head-groups of SDS make the pores even narrower, due to their excluded volume. As a result, in PVA FT1 and PVA FT3 droplets diffusion is two times slower than in the free μEm (see Table 17).

Table 17. Diffusion coefficients, D ($\mu\text{m}^2/\text{s}$) obtained by FCS curves fitting, for XYL and BEMP loaded in PVA-based cryogels.

System	D ($\mu\text{m}^2/\text{s}$)
Free XYL	22 ± 1
XYL in PVA FT1	10 ± 1
XYL in PVA FT3	12 ± 2
XYL in TC-PN FT1	19 ± 2
XYL in TC-PN FT3	32 ± 3
Free BEMP	69 ± 3
BEMP in PVA FT1	32 ± 2
BEMP in PVA FT3	51 ± 3
BEMP in TC-PN FT1	50 ± 3
BEMP in TC-PN FT3	38 ± 4

Some droplets probably deform and disrupt in passing through the small channels, due to the strong electrostatic repulsion: that is why the diffusion of free Bodipy can be detected in these two systems (the fast decay visible for PVA FT1 and FT3 in fig. 41 A, C).

While XYL freely diffuse in TC-PN FT1 gel, a diffusion coefficient higher than that of the free μEm is detected in TC-PN FT3. To explain this effect, we need to consider the structure of TC-PN FT3: the gel was obtained after a phase-separated solution of L-PVA blobs in a H-PVA continuous phase underwent 3 FT cycles. The repeated FT process can contribute to produce a force-coating of the L-PVA chains on the H-PVA main structure¹⁷: in fact, TC-PN FT3 contained higher amounts of L-PVA with respect to TC-PN-FT1, after washing (see fig. 29). Consequently, TC-PN FT3 is the only gel under consideration which contains, in the pores and on its walls¹⁷, significant quantities of L-PVA, a partially hydrolyzed PVA with hydrophobic acetate groups, very likely to interact with surfactants tails. It can be inferred that, in this case, mixed micelles in which L-PVA chains interact with SDS form: an increase in the population of small surfactant aggregates occurs, and the measured diffusion coefficients are lower.

BEMP NSF contains only a nonionic surfactant. The slight decrease of D observed in PVA FT3 and TC-PN FT1 gels with respect to D_{freeBEMP} (see Table 17) can be due either to a different viscosity of the medium or to a change of equilibria between the micellar species, after loading. The micelles motion is significantly delayed in PVA FT1 gel, due to the narrow needle-shaped pores.

The low D value registered for BEMP in PVA/PVA FT3 gels can be linked, again, to the high amount of L-PVA contained in this network: free or dangling L-PVA chains probably interact with the micelles, lowering their mobility.

Overall, FCS measurements show that the gel-NSF interaction strongly depends on the functionalities lying on the polymer chain backbone or the surfactant tail, the type of polar head, the porosity of the network and the massive presence of dangling and/or free chains in the gel pores. All these characteristics can affect the mobility or even the nature of micellar aggregates in the system, and need to be considered in order to design an effective cleaning action.

8.2 Diffusion of a NSF in a FITC-labeled TC-PN FT1 for the selective cleaning of Picasso's *The Studio*

The diffusion, in TC-PN FT1 gel, of a NSF containing both a nonionic and an anionic surfactant, was investigated through FCS measurements. In this case, polymer-surfactant interactions were highlighted by confocal imaging: the TC-PN gel was prepared with FITC-labeled H-PVA (green fluorescence), while the NSF was labeled with Bodipy (red fluorescence, 10 nM).

NSF formulation components are listed in Table 18.

Table 18. NSF composition.

Composition (% w/w)	NSF
H2O	65.9
C₉₋₁₁E_{5,5}	3.3
SDS	0.2
Bu-OH	9.7
MEK	20.9

Labeled “swollen micelles” will be mixed micelles, containing two nonionic surfactants (C₉₋₁₁E_{5,5} and Bodipy) and an anionic one (SDS).

Their interaction with the cryogel walls is shown in fig. 42: fig. 42 A is the confocal image where only FITC is excited, and the structure of the loaded TC-PN gel is evident; in fig. 42 B only Bodipy is excited: the surfactant and the micelles trace the pattern of the gel pores, suggesting that some Bodipy (either as a monomer or included in the micelles) is interacting with the gel walls; fig. 42 C is the superposition of images A and B and confirms that the red fluorescence of Bodipy overlaps the green signal of FITC.

The diffusion of the free NSF was measured through FCS, and the resulting average autocorrelation curve was compared to the average decay detected in the gel pores (fig. 42 D). The related diffusion coefficients, obtained by Eq. 24, are listed in Table 19.

In this case, the decay of the fluid embedded in the network could be described only through two different diffusion coefficients (Eq. 24): one of them is the diffusion coefficient of the free NSF, accounting for the 60% ca. of the total decay; the other coefficient is far slower and accounts for a polymer-surfactant interaction: probably, also in this case the surfactants are

interacting with the gel walls; therefore, either because of the “surfactants-coated” gel walls, or due to the dangling L-PVA chains in the pores, the diffusion of micelles is slower.

The FITC-labeled H-PVA could also play a role in enhancing Bodipy-polymer interaction: the interaction between aromatic domains characterizing FITC and Bodipy could be facilitated in this system, leading to a higher amount of Bodipy and Bodipy-labeled micelles stuck on the gel walls.

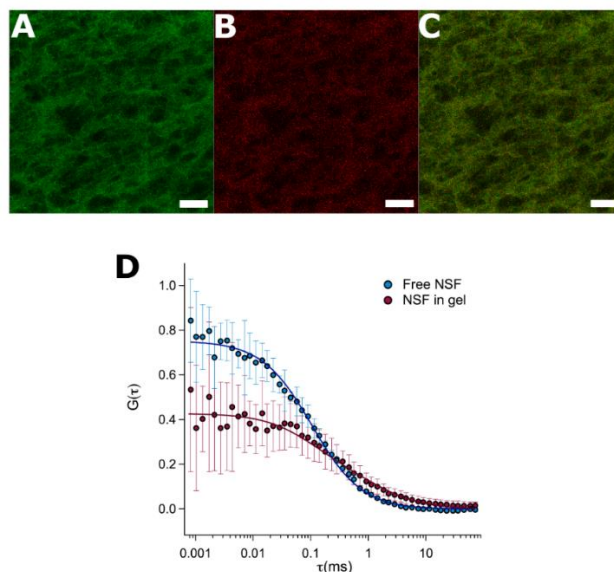


Figure 42. CLSM images of FITC-labeled TC-PN FT1 (green) loaded with Bodipy-labeled NSF (red): (A) only FITC is excited, showing the gels structure after loading; (B) only Bodipy is excited, and it draws the profile of the gel pores, suggesting that the surfactant sticks on the gel walls, either as a monomer or in micelles; (C) Overlay of (A) and (B). (D) FCS autocorrelation curves describing the diffusion of the free NSF (blue markers) and the NSF embedded in the gel (purple markers), with curves fitting. Error bars are the standard deviations of the averaged curves. Reproduced from ref. [13].

Table 19. Diffusion coefficients ($\mu\text{m}^2/\text{s}$) for the free NSF and NSF micelles embedded in TC-PN FT1 gel.

	Free NSF	NSF in TC-PN FT1
D_1 (μ^2/s)	100 ± 6	100
f_1 (%)	100	60 ± 16
D_2 (μ^2/s)	-	7 ± 4

Chapter 9. Cleaning tests

The cleaning of rough, clotted painted surfaces, as those characterizing Modern and Contemporary Art, requires particular care. On the one hand, knocks and crannies, formed by dripping paint or thick brushstrokes, are hard to reach with traditional tools used in restoration¹⁴⁸; on the other hand, the risk of leaving residues during cleaning must always be assessed: polymers, surfactants or solvents could react with the original materials constituting the work of art and accelerate a superficial degradation, altering the aesthetic aspect of the artwork.

In this chapter⁶, cryogels properties like adaptability to rough surfaces and cleaning abilities will be described. Cleaning tests, performed on mock-ups, will highlight how the best cleaning performances are obtained when compliant, sponge-like gels are used. Factors like the presence of a semi-interpenetrating polymer and the gel surface roughness could also play a key-role in enhancing PVA-based cryogels cleaning abilities. Overall, TC-PNs showed the best performances.

Also the problem of gel residues seem to be overcome when using TC-PNs: ATR-FTIR measurements showed that polymer and surfactant traces are not detectable on the treated surfaces.

9.1 How cryogels adapt to rough surfaces

As already discussed in Chapter 4 and 5, rheological characteristics of PVA-based cryogels depend on polymer concentration in the pre-gel solution and on the number of FT cycles. In fact, when polymer chains are more crowded in the final structure, i.e., when the FT process has a higher efficacy (either because the initial polymer concentration was higher, or the solution underwent more than one FT step), the final networks are stiffer.

As previously discussed, the surface of Modern and Contemporary paintings is often uneven and clotted. Therefore, ideal gels for cleaning should be highly adaptable to any surface roughness, and also able to stick on the surface.

For these reasons, FT1 hydrogels only were chosen to perform cleaning tests.

⁶ Based on Paper II and VI, see Appendix.

As regards polymer concentration in the pre-gel solution, TC-PN formulation was considered ideal. Its performance was compared to the pure H-PVA cryogel (9 % w/w).

Both gels are highly compliant and transparent. Pure PVA gel is slightly more transparent, but this is due to its small pores: micron-sized pores of TC-PNs cause multiple light-scattering.

PVA and TC-PN FT1 adaptability to a clotted painted surface, representative of modern/contemporary paintings and with surface irregularities ≥ 1 mm, was also evaluated (see fig. 43 a). Cryogels characteristics were compared to those of a traditional gels used in restoration, such as gellan¹⁶ and to a poly-hydroxyethyl methacrylate (pHEMA)/PVP gel previously formulated by our group⁴⁵. Gellan is a rigid, physical gel, obtained by dissolving Gellan gum in water and by evaporating the water in excess. Its structure is fragile and it usually leaves residues on the treated surfaces. Chemical gels, like pHEMA/PVP network, are usually rigid, due to the very nature of the chemical crosslinking process. They also contain low amount of free water and are used to treat water-sensitive artifacts. They do not leave residues on treated surfaces.

pHEMA/PVP gels storage modulus, G' , is roughly half the modulus of a typical gellan sheet.^{11,149} In turn, PVA and TC-PN FT1 gels have G' moduli 4 to 5 times lower than those of pHEMA/PVP, but being still resistant to handling and elongation.

Fig. 43 shows the behavior of these gels when in contact with surface harshness: while gellan and pHEMA/PVP sheets lay on the highest points of the paint (fig. 43 b and c, respectively), PVA and TC-PN FT1 completely cover the uneven surface, insinuating into the cavities (fig. 43 d, e).

The better adaptability on the surface is expected to facilitate the cleaning of difficult spots. Moreover, TC-PN has a high surface roughness and contains the partially hydrolyzed L-PVA: both these properties could result in a more efficient adsorption of hydrophobic particles, enhancing cleaning performances.

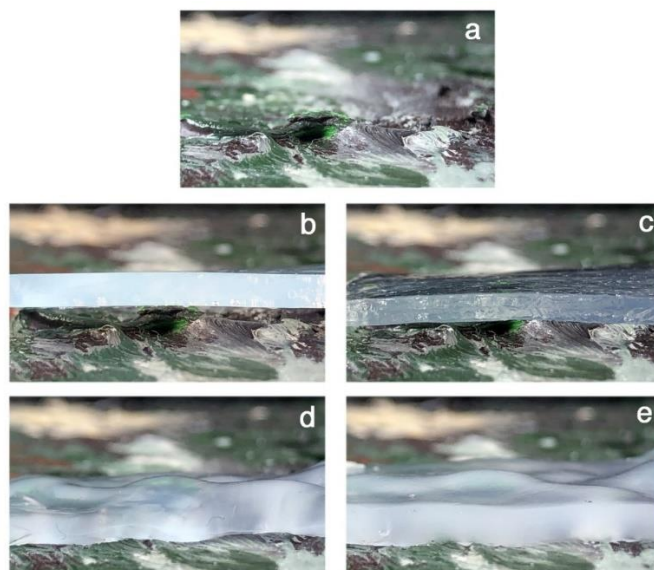


Figure 43. Adhesion of gels to rough painted surfaces. (a) A clotted painted surface, representative of modern/contemporary artifacts, with irregularities ≥ 1 mm. (b) A rigid gellan sheet, similar to those used in the traditional restoration practice for the cleaning of artworks. (c) A conventional pHEMA/PVP chemical gel, previously formulated for the cleaning of water-sensitive artistic surfaces ^{45,150}. (d) A FT1 PVA gel (H-PVA). (e) TC-PN FT1. Reproduced from ref. [17].

9.2 Cryogels ability to clean soiled surfaces

All PVA-based cryogels contain more than 90% of water at the swelling equilibrium (see Table 20); water behaves almost completely as “free water”, that is, its molecules are able to freely diffuse through the polymer matrix. Free water is a key-factor in granting an effective cleaning action. In fact, hydrophilic dirt and dust commonly found on the surface of artworks can be easily solubilized/suspended in water; moreover, water cleaning ability can be easily enhanced by dissolving chelants or surfactants in it.

Another crucial parameter that must be considered when choosing a cleaning system is its water release. In fact, especially when water-sensitive materials will be treated, the presence of free water on the surface can lead to the leaching of the paint or the swelling and successive cracking of the paint layers. Therefore, the gel should release just a thin film of fluid at the gel-surface interface, which will facilitate dirt detachment migration in the gel matrix. Water release of PVA-based cryogels is shown in Table 20. It ranges between

around 20 mg/cm² (over a 30 min application on Whatman paper) for FT1 gels and slightly decreases for FT3 gels. All formulations are more retentive than traditional gels, like agar or gellan (30 – 33 mg/cm²⁴⁵), which proved too risky to water-sensitive dyes.

Table 20. Equilibrium water content, Free Water Index and Water release for pure PVA and TC-PN cryogels.

Sample	Eq. Water Content (EWC %)	Free Water Index (FWI)	Water Release (mg/cm ²)
PVA FT1	96.3 ± 0.4	98 ± 1	24 ± 3
PVA FT3	92.3 ± 0.6	94 ± 1	17 ± 2
TC-PN FT1	97.1 ± 0.2	98.3 ± 0.4	21 ± 1
TC-PN FT3	92.8 ± 0.3	96.0 ± 0.2	19 ± 1

Even though water retention was higher for FT3 gels, they were excluded from the cleaning tests, due to their poor adaptability to rough surfaces.

Cleaning tests with PVA FT1 cryogels (just swollen in water) were initially performed on soiled glass slides. The artificial soil contained both hydrophobic and hydrophilic components. Fig. 44 shows the results obtained after 1-6 applications of 1 min: TC-PN was able to completely remove the grime after the sixth application, while, in the same conditions, the pure PVA gel left significant amounts of dirt on the glass (fig. 44 D).

PVA-based cryogels were further tested on mock-ups with the textured surface of a Modern-Contemporary art painting. Namely, the mock-up was prepared by mimicking Pollock's dripping technique and using alkyd paints; its surface was, then, covered with artificial soil.

Cryogels FT1 performance was compared to that of a gellan sheet (fig. 45), after a 8 min, single application.

Gellan performed worse than both cryogels, due to its poor adhesion, while PVA FT1 performed worse than TC-PN FT1, either because of lower stickiness (in absence of L-PVA, containing acetate groups which can facilitate hydrophobic dirt uptake), or for its reduced porosity.

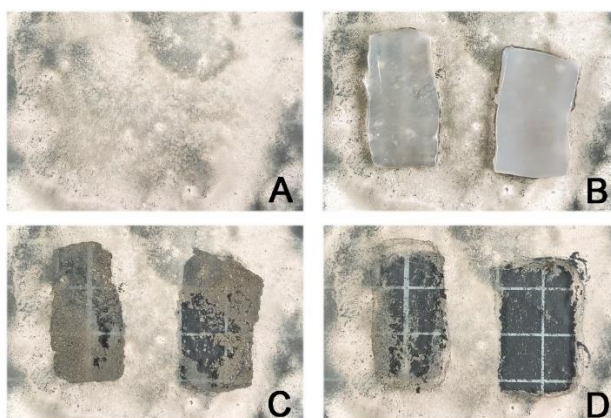


Figure 44. Cleaning tests on glass slides covered with artificial soil. (A) Soiled glass surface before cleaning. (B) Application of gels (left: pure PVA gel; right: PVA/PVA TC-PN). (C) Soil removal after one application (1 minute); no additional mechanical action was carried out after the removal of the gels. (D) Soil removal after six applications (1 minute each); the soil was removed using the TC-PN, while only partial removal was achieved using the pure PVA gel. Reproduced from ref. [17].

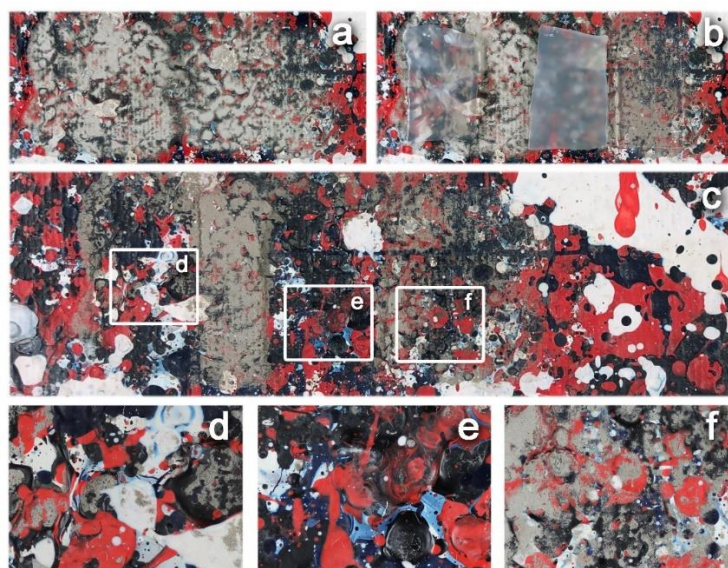


Figure 45. Cleaning tests on mockups. (A) Clotted painting mockup that mimics Pollock's alkyd paintings, artificially soiled. (B) Application of a pure PVA FT1 gel (Left), a TC-PN FT1 (Center), and a gellan gel sheet similar to those used in the traditional restoration practice (Right). (C) Soil removal after the application of the gels (8 min each); no additional mechanical action was carried out after the removal of the gels. D-F detail the removal efficacy of each type of gel. Reproduced from ref. [17].

The efficacy of traditional cleaning tools, such as cotton swabs, is shown in fig. 46. It is evident that the mechanical action, combined with a significant water release, causes paint leaching and pigment loss. The application of TC-PN cryogels, instead, favors dirt uptake or softening: any residues can be easily removed through the gentle mechanical action of an “eraser gum” shaped TC-PN, which avoids any damage of the treated surface.

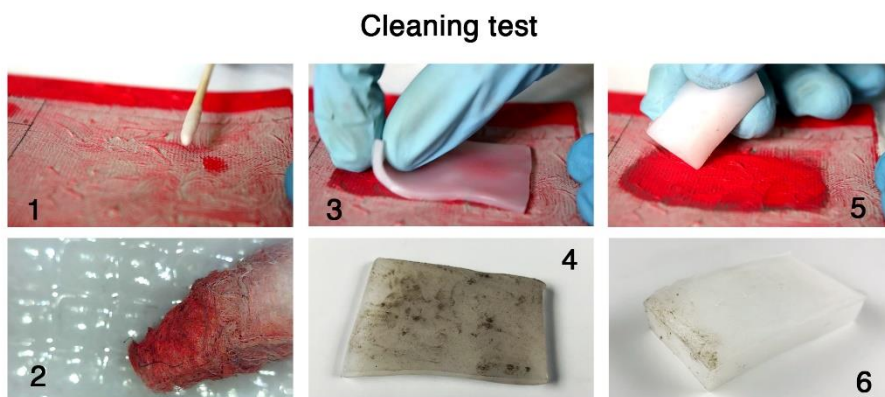


Figure 46. The cleaning of an artificially soiled mockup by applying mechanical action (cotton swab) causes paint loss (alkyd paint, 1-2). Conversely, the application of a TC-PN sheet favors only dirt uptake (3-4). Any residues can be removed by gently rubbing with a TC-PN gum (5-6). Reproduced from ref. [17].

9.3 Cleaning assessment through ATR-FTIR

The cleaning efficacy of TC-PN on artificially soiled mockups was assessed, up to the microscale, through two-dimensional (2D) Fourier-transform infrared spectroscopy (FTIR) imaging. Spectra of the soiled painted surface showed peaks due to kaolin in the $3,725$ to $3,592$ cm^{-1} region (Al–OH stretching at $3,665$ cm^{-1} ; OH stretching at $3,625$ cm^{-1} , due to crystalline hydroxyl groups).¹⁵¹ These peaks are not detected when TC-PN-treated or pristine surfaces are investigated, indicating the cleaning efficacy of PVA cryogels. Overall, the spectra acquired on the cleaned mockup are not significantly different from those of the pristine surface (fig. 47 A). In both cases, the peaks are mainly due to the components of the oil paint.¹⁵²

The presence of PVA residues on the cleaned surface was assessed through the same technique. The absorbance intensity due to OH- stretching of PVA

(region from $3,440$ to $3,180\text{ cm}^{-1}$) was mapped on both pristine and cleaned surfaces, and any signal ascribable to PVA was detected (fig. 47 B).

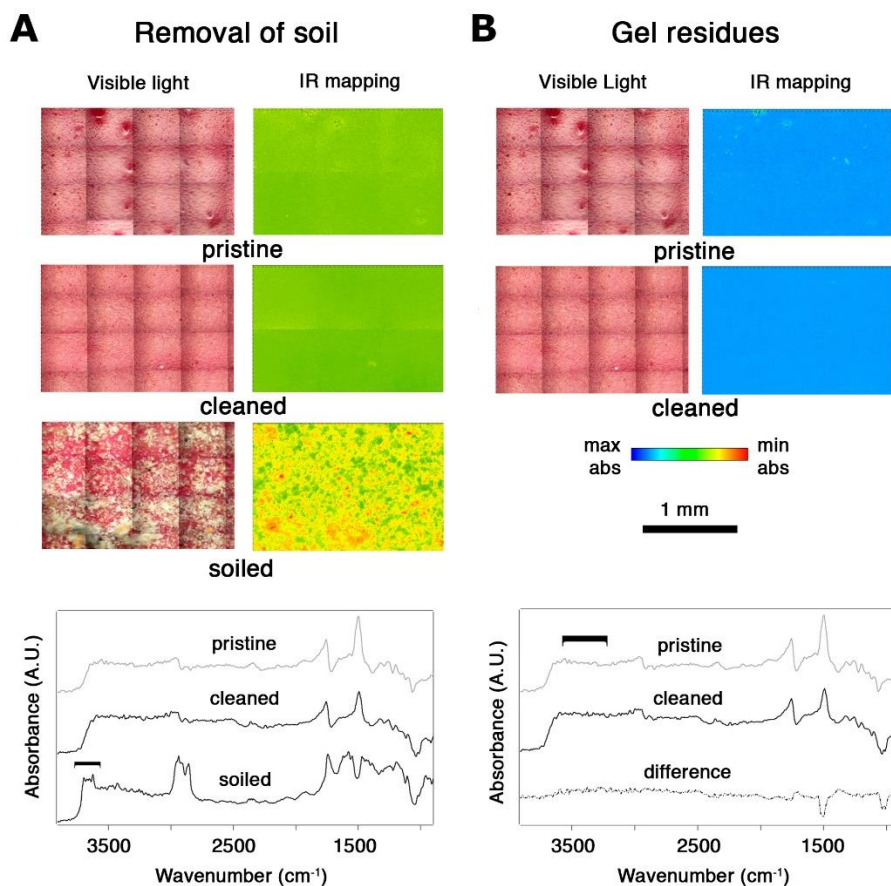


Figure 47. Assessment of the cleaning efficacy and gel residues through FTIR 2D imaging. (A) Cleaning efficacy. The IR maps show the presence of kaolin (contained in the artificial soil, bands in the $3,725$ to $3,592\text{ cm}^{-1}$ region). (Top) Pristine painted surface. (Center) Painted surface after soiling and subsequent cleaning with TC-PN gel. (Bottom) Soiled painted surface. Representative spectra of the pristine, cleaned, and soiled surfaces are shown below the maps. (B) Gel residues. The IR maps (acquired on the same areas as panel A) show the absorbance in the $3,440 - 3,180\text{ cm}^{-1}$ region, where characteristic bands of PVA fall. (Top) Pristine painted surface. (Bottom) Painted surface after soiling and subsequent cleaning with TC-PN gel. Representative spectra of the pristine and cleaned surface are shown below the maps, along with the difference between the two spectra; PVA absorption was not found. abs, absorbance; max, maximum; min, minimum. Reproduced from ref. [17].

Therefore, it can be inferred that any gel residue was left on the surface during cleaning (up to the detection limit of ca. $0.02 \text{ pg}/\mu\text{m}^2$), see fig. 48.

The FPA detector has, in fact, a lower detection limit than conventional mercury cadmium telluride (MCT) detectors, used to find materials in traces: heterogeneous distributions and small areas with high local concentration can be identified thanks to FPA detector spatial resolution.

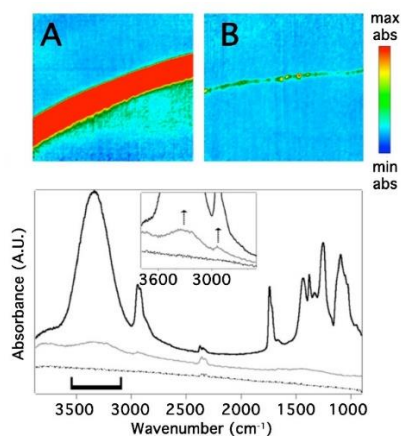


Figure 48. Determination of FTIR detection limit per unit area, for PVA. FTIR 2D Imaging of PVA rings on Al foils, obtained by depositing droplets of polymer solution. Images A (ca. $700 \times 700 \mu\text{m}^2$) and B (ca. $700 \times 700 \mu\text{m}^2$) show the mapping of the PVA band at 3330 cm^{-1} (OH stretching), in the $3660\text{--}3000 \text{ cm}^{-1}$ region. (A) $20 \mu\text{L}$ droplet, polymer concentration of $5 \times 10^{-2} \text{ g/L}$; (B) $20 \mu\text{L}$ droplet, polymer concentration of $5 \times 10^{-4} \text{ g/L}$. The bottom panel shows spectra from: (top) PVA rim, panel A; (center) PVA rim, panel B; (bottom) Al foil. Reproduced from ref. [17].

The cleaning performance of TC-PN gels loaded with a NSF (see paragraph 8.2) was also evaluated. Namely, wax-lining residues and polyvinyl acetate (PVAc) varnish (to mimic the dirt found on *The Studio*) were removed from mockups.

Superficial cleaning was obtained after a 10 - 40 s application (the PVAc layer was neatly softened). After 40-60 s of contact with the NSF-loaded gel, the PVAc film became streaky, but still separated easily from the paint layer. Final rinsing steps were performed with water loaded gels (applications of 1-2 s).

FTIR 2D imaging showed that the removal of the PVAc-based varnish and wax was completely achieved: characteristic bands (e.g. C = O stretching in the $1880\text{--}1705 \text{ cm}^{-1}$ region for PVAc, and CH_2 bending around 1475 cm^{-1} for wax) disappeared or were significantly reduced after the loaded gel

application (see fig. 49). Any residues was detected on the surface after the treatment, as any band was observable in the 3590–3380 cm^{-1} region (OH stretching of PVA), around 1120 cm^{-1} (C-O stretching of alcohol ethoxylates) or at 1220 cm^{-1} (asymmetric stretching of OSO₃ of SDS).

The absence of residues is a breakthrough in the cleaning of artworks: in fact, thickeners traditionally used as cleaning fluids-carriers (e.g. polyacrylic acid or cellulose ethers) require detrimental cleaning steps and cannot be removed completely from the surface after the cleaning treatment.^{3,153,154}

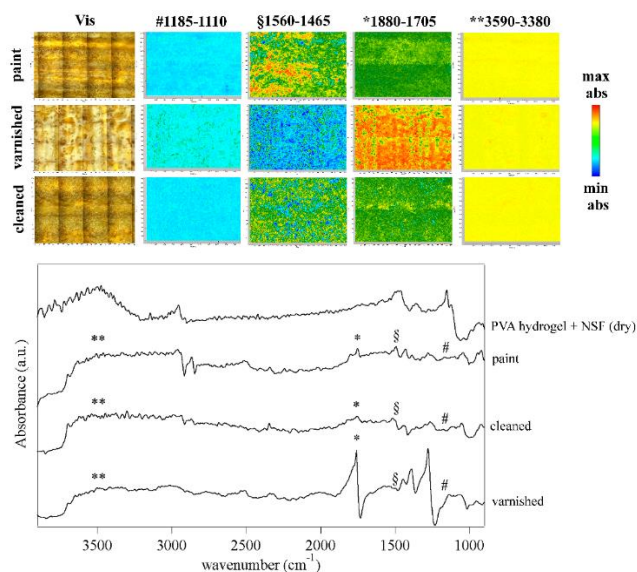


Figure 49. FTIR 2D imaging of mockups. Top panel: visible light and 2D FTIR maps of mockups that were unvarnished (“paint”, top row), varnished (center row), or varnished and then cleaned with TC-PN hydrogels loaded with the NSF (“cleaned”, bottom row). The tests were carried out in the wax-lined regions. For each sample, the images beside the visible map show the corresponding 2D FTIR maps, where the intensities of the following peaks were imaged: 1185–1110 cm^{-1} (C-O stretching band of the C₉₋₁₁ E_{5,5} surfactant), 1560–1465 cm^{-1} (CH₂ bending of wax), 1880–1705 cm^{-1} (C = O stretching of polyvinyl acetate) and 3590–3380 cm^{-1} (OH stretching band of PVA). All maps have dimensions of 2100 × 1400 μm^2 , each axis tick being 50 μm . The FTIR Reflectance spectra are shown in the bottom panel, each spectrum relating to a single pixel (5.5 × 5.5 μm^2) of the corresponding 2D imaging map. The maps show the removal of the varnish and surface removal of wax spots, while no absorptions ascribable to PVA or surfactants from the NSF could be detected. Reproduced from ref. [13].

Chapter 10. Cleaning Jackson Pollock's and Pablo Picasso's masterpieces with TC-PNs

The deposition of grime, due to ageing and exposure to ambient contaminants, is very common on the surface of artworks. Cleaning treatments are, therefore, required. This chapter ⁷ describes the cleaning procedures used to restore three masterpieces by Pollock and Picasso.

TC-PN FT1 hydrogels were used to clean the superficial layer of dust and airborne dirt particles that accumulated on two Jackson Pollock masterpieces (fig. 50): *Two* (1943 to 1945) and *Eyes in the Heat* (1946 to 1947). Both paintings belong to the Peggy Guggenheim Collection (Venice). *Two* is characterized by thick oil paint brushstrokes, which define two totemic figures, inspired to tribal painting and Cubist works by Picasso.

On the other hand, *Eyes in the Heat* represents a prelude to the revolutionary “drip” paintings: oil and alkyd paints were applied directly from the tube and then shaped in a thick and textured crust.

In both cases, traditional cleaning tools were proven to be too risky for such delicate and solvent-sensitive surfaces.

The cleaning with TC-PNs allowed to bring back the original paints hue in complete safety. Detrimental effects due to water release at the gel-paint interface or the mechanical action of cotton swabs were avoided, thanks to the gel controlled retention/release rate and its ability to detach and retain the hydrophilic dirt. The length of the cleaning process was also optimized: in fact, traditional methods sometimes require a meticulous work under the microscope, with unconfined solvents.

NSF-loaded FT1 TC-PNs (see paragraph 8.2) were used, instead, to remove a PVAc-based varnish and wax spots from the surface of Pablo Picasso's *The Studio* (1928; Peggy Guggenheim Collection, Venice). This painting is characterized by visible, thick brushstrokes and mixes the vivid palette of Synthetic Cubism with geometrized, planar figures. The painting was relined,

⁷ The cleaning treatments here described are reported in Paper II and VI, see Appendix.

using wax and resin, in the late 1960s. The intervention was aimed at laying down areas where the paint was lifted. Due to the ageing, efflorescence of wax were visible on the surface, while the PVAc-based resin yellowed; both the wax and the PVAc caused a darkening of the white. Moreover, dust particles deposited on the surface, interfering with the readability of the colors intensity and composition.

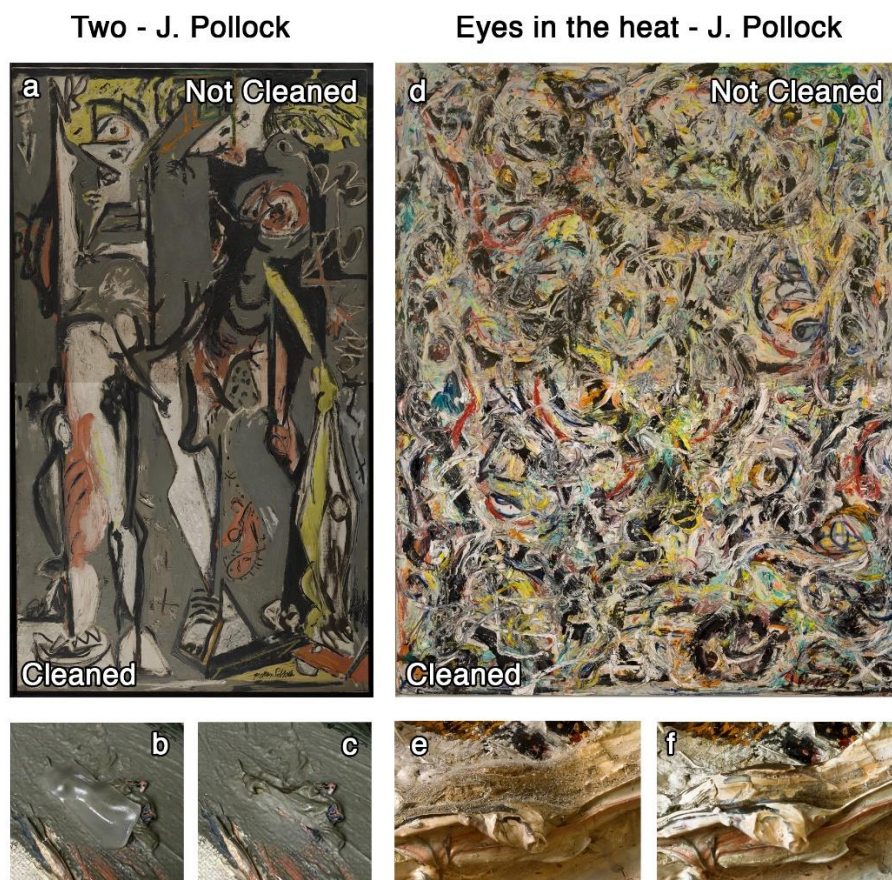


Figure 50. Cleaning of Pollock's (a) *Two* (1943-45, oil on canvas, 193 × 110 cm, Peggy Guggenheim Collection, Venice) and (b) *Eyes in the Heat* (1946, oil and enamel on canvas, 137.2 × 109.2 cm, Peggy Guggenheim Collection, Venice). (a) and (d) collages show the paintings before and after the cleaning intervention, where the soil was removed using the TC-PN FT1 hydrogels. (b and c) A detail showing the gel adhering to the painting and the same area after cleaning. (e and f) A detail of the painting before and after cleaning with the TC-PN gels. Reproduced from ref. [17].

The PVAc varnish was swollen after 5 s contact with the gel loaded with the NSF, and was easily “peeled-off” with a dry cotton swab. The paint layer remained unaltered after the treatment (fig. 51).

The black crayon lines, which defines a sculptured bust (on the left) and a full-length portrait (on the right) were hardly accessible during the cleaning: they lie at a lower level with respect to the white background, to simulate an incision in the canvas. Therefore, gels were cut and shaped to clean the varnish around those lines, without affecting them.

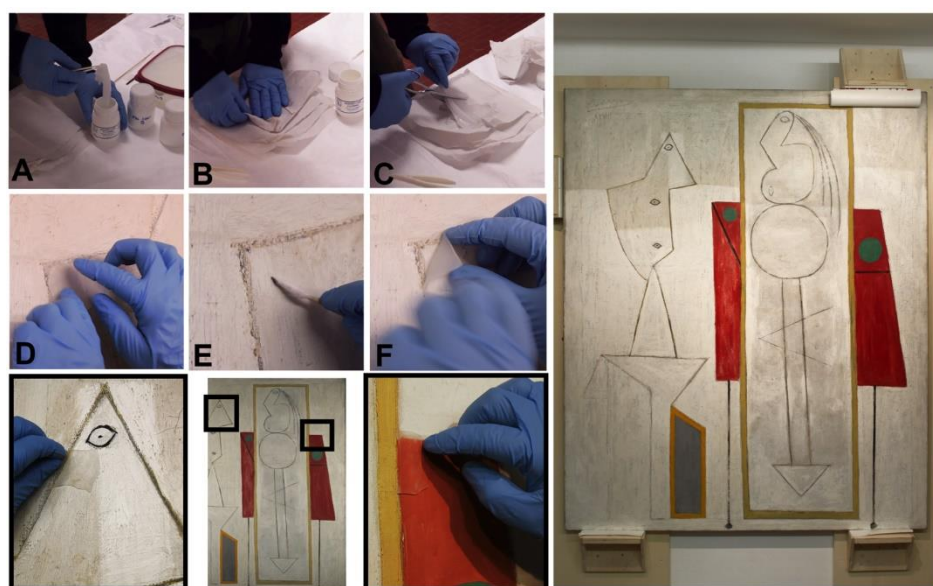


Figure 51. The cleaning of Pablo Picasso’s *The Studio* (A) TC-PN FT1 hydrogel is loaded with the o/w NSF (24 h immersion). (B) Gel sheets loaded with the NSF are gently squeezed with blotting paper to remove the fluid excess from their surface, and (C) cut to desired shape and size. (D) The gel is applied onto the painted surface. (E) Gentle mechanical action with a dry cotton swab allows the removal of the swollen/softened varnish and wax. (F) Rinsing step: a water-loaded gel is shortly applied on the same spot to remove possible residues of the NSF. Bottom: center panel and related black boxed details show the cleaning of white and red areas. On the right, the painting during the cleaning: the cleaned lighter areas can be easily distinguished from the darker uncleaned areas at the top. Reproduced from ref. [13].

Also in this case, the high retentivity of TC-PN gels ensured a controlled cleaning action, thanks to the thin liquid layer formed at the gel-painting

interface; the diffusive process at the interface allowed the transfer of small amounts of organic solvents and surfactants to the film, until it spontaneously detached from the painted surface.

Fig. 52 shows the painting before and after the cleaning treatment.

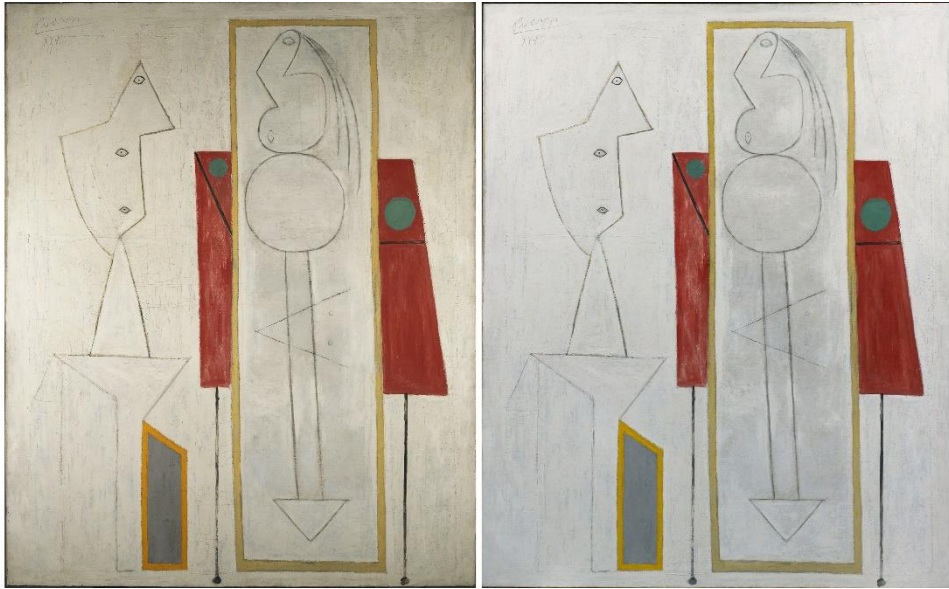


Figure 52. Pablo Picasso's *The Studio* (1928, oil and black crayon on canvas, 161.6 × 129.9 cm, Peggy Guggenheim Collection, Venice) (The Solomon R. Guggenheim Foundation, New York), before (left) and after (right) cleaning with NSFs loaded TC-PN gels. Reproduced from ref. [13].

CONCLUSIONS

In this thesis, the structure of PVA-based cryogels was investigated: the changes induced by varying the semi-interpenetrating agent, its molecular weight, and by increasing the number of FT cycles, were quantified.

The main cryogels structure was proven to be composed by a high molecular weight and HD PVA (H-PVA). Two different semi-interpenetrating polymers were added to the H-PVA network: a PVA with lower HD and M_w , L-PVA, and PVP. Gels made of H-PVA and L-PVA were called Twin-Chain Polymer Networks (TC-PNs), given the similarity of the chain backbone of the two polymers.

L-PVA and PVP, as semi-interpenetrating agents, changed the pores shape and dimension. In fact, a polymer-polymer phase separation occurred in the pre-gel solutions: L-PVA and PVP concentrated in spherical blobs, which acted as porogens during the cryostructuring. On the other hand, the H-PVA continuous phase formed the final gel walls. L-PVA and PVP affected the crystallinity, the rheology and the structure at the nanoscale of the cryogels. The gel point changed, as well as the mechanism of gelation. As a result, L-PVA and PVP were proven to behave as both porogens and structuring agents in the networks.

TC-PNs and pure H-PVA gels obtained after one or three FT cycles were, then, investigated. While the gels architecture and porosity are defined from the first freezing step, gels crystallinity, rigidity and chains crowding in the walls increase with the number of FT cycles. In TC-PNs, L-PVA is more tangled in the gel structure when the number of FT cycles is higher; after washing and storage in water, L-PVA chains diffuse in the pores and are stuck on the walls.

Pores dimension depends on L-PVA chains length: the blobs forming in the pre-gel solutions at RT grow larger as L-PVA M_w increases; as a consequence, gels pores are larger when L-PVA M_w is higher.

The diffusion of cleaning Nano-Structured Fluids (NSFs) through the gels matrix was proven to be influenced by the pores diameter and the specific polymer-surfactant interactions. Micelles and droplets diffusion was slower in FT1, pure H-PVA gels; as a matter of fact, these gels are characterized by needle-shaped pores, whose diameters are significantly smaller than 1 μm .

NSFs containing anionic surfactants, like SDS, interacted more easily with the polymeric network: in this case, the diffusive motion was significantly reduced, or the presence of a slower component, in addition to the free diffusion, was detected. Overall, the inclusion of NSFs in the gel networks granted a safer treatment of painted artifacts: the free-bound equilibrium of the micellar species embedded in the gels, or their slower diffusion, allowed a space- and time-controlled cleaning action.

TC-PNs loaded with aqueous cleaning solutions, or NSFs, were used to restore *Two and Eyes in the Heat* by Jackson Pollock, and *The Studio*, by Pablo Picasso. The surface of Pollock's masterpieces accumulated airborne dust particles, and was cleaned with TC-PNs loaded with buffered solutions. The surface of *The Studio*, instead, was covered with a PVAc layer; wax spots, due to a relining treatment, were also evident. In this case, the hydrophobic materials were removed with NSF-loaded TC-PNs.

In all these cases, due to the water-sensitivity of the paints, and the tridimensionality and the fragility of the brushstrokes, traditional cleaning treatments were not recommended.

The three paintings are on display at the Peggy Guggenheim Collection, in Venice. The cleaning treatment brought back the original hue and color brightness.

PVA-based cryogels properties can be tuned and tailored, adapting to specific cleaning tasks: adaptability to rough surfaces, porosity, water content and retentiveness vary when the semi-interpenetrating polymer, or its molecular weight, change. In the future, hydrogels with different features will be formulated, exploiting liquid-liquid phase separation in the pre-gel solutions. Moreover, the chains dynamics in the final structure will be further investigated (e.g. through Large Amplitude Oscillatory Strain or Quasi-Elastic Neutron Scattering measurements), and possibly linked to the gels cleaning ability.

REFERENCES

- (1) Baglioni, P.; Carretti, E.; Chelazzi, D. Nanomaterials in Art Conservation. *Nat. Nanotechnol.* **2015**, *10* (4), 287–290. <https://doi.org/10.1038/nnano.2015.38>.
- (2) Baglioni, P.; Chelazzi, D.; Giorgi, R. *Nanotechnologies in the Conservation of Cultural Heritage: A Compendium of Materials and Techniques*; Springer Netherlands, 2015. <https://doi.org/10.1007/978-94-017-9303-2>.
- (3) Stulik, D. *Solvent Gels for the Cleaning of Works of Art: The Residue Question*; Getty Publications, 2004.
- (4) Chelazzi, D.; Fratini, E.; Giorgi, R.; Mastrangelo, R.; Rossi, M.; Baglioni, P. Gels for the Cleaning of Works of Art. In *Gels and Other Soft Amorphous Solids*; ACS Symposium Series; American Chemical Society, 2018; Vol. 1296, pp 291–314. <https://doi.org/10.1021/bk-2018-1296.ch015>.
- (5) Cremonesi, P.; Signorini, E. *Un approccio alla pulitura dei dipinti mobili*; Il Prato: Saonara, 2013.
- (6) Giorgi, R.; Baglioni, M.; Berti, D.; Baglioni, P. New Methodologies for the Conservation of Cultural Heritage: Micellar Solutions, Microemulsions, and Hydroxide Nanoparticles. *Acc. Chem. Res.* **2010**, *43* (6), 695–704. <https://doi.org/10.1021/ar900193h>.
- (7) Chelazzi, D.; Giorgi, R.; Baglioni, P. Microemulsions, Micelles, and Functional Gels: How Colloids and Soft Matter Preserve Works of Art. *Angew. Chem. Int. Ed.* **2018**, *57* (25), 7296–7303. <https://doi.org/10.1002/anie.201710711>.
- (8) Carretti, E.; Salvadori, B.; Baglioni, P.; Dei, L. Microemulsions and Micellar Solutions for Cleaning Wall Painting Surfaces. *Stud. Conserv.* **2005**, *50* (2), 128–136. <https://doi.org/10.1179/sic.2005.50.2.128>.
- (9) Bordes, R.; Giorgi, R.; Holmberg, K.; Baglioni, P.; Chelazzi, D. The Use of Surfactants in the Cleaning of Works of Art. *Curr. Opin. Colloid Interface Sci.* **2020**, *45*, 108–123. <https://doi.org/10.1016/j.cocis.2019.12.007>.
- (10) Mastrangelo, R.; Montis, C.; Bonelli, N.; Tempesti, P.; Baglioni, P. Surface Cleaning of Artworks: Structure and Dynamics of Nanostructured Fluids Confined in Polymeric Hydrogel Networks. *Phys Chem Chem Phys* **2017**. <https://doi.org/10.1039/C7CP02662E>.
- (11) Baglioni, M.; Domingues, J. A. L.; Carretti, E.; Fratini, E.; Chelazzi, D.; Giorgi, R.; Baglioni, P. Complex Fluids Confined into Semi-Interpenetrated Chemical Hydrogels for the Cleaning of Classic Art: A

- Rheological and SAXS Study. *ACS Appl. Mater. Interfaces* **2018**, *10* (22), 19162–19172. <https://doi.org/10.1021/acsami.8b01841>.
- (12) Bonelli, N.; Montis, C.; Mirabile, A.; Berti, D.; Baglioni, P. Restoration of Paper Artworks with Microemulsions Confined in Hydrogels for Safe and Efficient Removal of Adhesive Tapes. *Proc. Natl. Acad. Sci.* **2018**, *115* (23), 5932–5937. <https://doi.org/10.1073/pnas.1801962115>.
- (13) Pensabene Buemi, L.; Petruzzellis, M. L.; Chelazzi, D.; Baglioni, M.; Mastrangelo, R.; Giorgi, R.; Baglioni, P. Twin-Chain Polymer Networks Loaded with Nanostructured Fluids for the Selective Removal of a Non-Original Varnish from Picasso’s “L’Atelier” at the Peggy Guggenheim Collection, Venice. *Herit. Sci.* **2020**, *8* (1), 77. <https://doi.org/10.1186/s40494-020-00420-0>.
- (14) *Conservation of Modern Oil Paintings*; Berg, K. J. van den, Bonaduce, I., Burnstock, A., Ormsby, B., Scharff, M., Carlyle, L., Heydenreich, G., Keune, K., Eds.; Springer International Publishing, 2019. <https://doi.org/10.1007/978-3-030-19254-9>.
- (15) Mills, L.; Burnstock, A.; Keulen, H.; Duarte, F.; Megens, L.; Van den Berg, K. J. Water Sensitivity of Modern Artists’ Oil Paints. *ICOM Comm. Conserv. 15th Trienn. Meet.* **2008**, *2*, 651–659.
- (16) Bonelli, N.; Poggi, G.; Chelazzi, D.; Giorgi, R.; Baglioni, P. Poly(Vinyl Alcohol)/Poly(Vinyl Pyrrolidone) Hydrogels for the Cleaning of Art. *J. Colloid Interface Sci.* **2019**, *536*, 339–348. <https://doi.org/10.1016/j.jcis.2018.10.025>.
- (17) Mastrangelo, R.; Chelazzi, D.; Poggi, G.; Fratini, E.; Buemi, L. P.; Petruzzellis, M. L.; Baglioni, P. Twin-Chain Polymer Hydrogels Based on Poly(Vinyl Alcohol) as New Advanced Tool for the Cleaning of Modern and Contemporary Art. *Proc. Natl. Acad. Sci.* **2020**. <https://doi.org/10.1073/pnas.1911811117>.
- (18) Dei, L. CHAPTER 3:Conservation Treatments: Cleaning, Consolidation and Protection. In *Nanoscience for the Conservation of Works of Art*; 2013; pp 77–92. <https://doi.org/10.1039/9781849737630-00077>.
- (19) Stoner, J. H.; Rushfield, R. *Conservation of Easel Paintings*; Routledge, 2013.
- (20) Zimon, A. D. *Adhesion of Dust and Powder*; Springer US, 1969. <https://doi.org/10.1007/978-1-4899-6600-1>.
- (21) Wolbers, R. *Cleaning Painted Surfaces: Aqueous Methods*; 2000.
- (22) Burke, J. Solubility Parameters: Theory and Application <https://cool.culturalheritage.org/coolaic/sg/bpg/annual/v03/bp03-04.html> (accessed Oct 27, 2020).

- (23) HANSEN, C. M. Three Dimensional Solubility Parameter and Solvent Diffusion Coefficient. Importance in Surface Coating Formulation. *Dr. Diss.* **1967**.
- (24) Mollet, H.; Grubenmann, A. *Formulation Technology: Emulsions, Suspensions, Solid Forms*; John Wiley & Sons, 2008.
- (25) Fardi, T.; Stefanis, E.; Panayiotou, C.; Abbott, S.; van Loon, S. Artwork Conservation Materials and Hansen Solubility Parameters: A Novel Methodology towards Critical Solvent Selection. *J. Cult. Herit.* **2014**, *15* (6), 583–594. <https://doi.org/10.1016/j.culher.2013.11.006>.
- (26) Carretti, E.; Dei, L. CHAPTER 5:Cleaning I: Application. In *Nanoscience for the Conservation of Works of Art*; 2013; pp 124–146. <https://doi.org/10.1039/9781849737630-00124>.
- (27) *Surfactants and Polymers in Aqueous Solution*, 1st ed.; John Wiley & Sons, Ltd, 2002. <https://doi.org/10.1002/0470856424>.
- (28) De Gennes, P. G.; Taupin, C. Microemulsions and the Flexibility of Oil/Water Interfaces. *J. Phys. Chem.* **1982**, *86* (13), 2294–2304. <https://doi.org/10.1021/j100210a011>.
- (29) Szleifer, I.; Kramer, D.; Ben-Shaul, A.; Roux, D.; Gelbart, W. M. Curvature Elasticity of Pure and Mixed Surfactant Films. *Phys. Rev. Lett.* **1988**, *60* (19), 1966–1969. <https://doi.org/10.1103/PhysRevLett.60.1966>.
- (30) Farago, B.; Richter, D.; Huang, J. S.; Safran, S. A.; Milner, S. T. Shape and Size Fluctuations of Microemulsion Droplets: The Role of Cosurfactant. *Phys. Rev. Lett.* **1990**, *65* (26), 3348–3351. <https://doi.org/10.1103/PhysRevLett.65.3348>.
- (31) Ruckenstein, E. Microemulsions, Macroemulsions, and the Bancroft Rule. *Langmuir* **1996**, *12* (26), 6351–6353. <https://doi.org/10.1021/la960849m>.
- (32) Baglioni, P.; Berti, D.; Bonini, M.; Carretti, E.; Dei, L.; Fratini, E.; Giorgi, R. Micelle, Microemulsions, and Gels for the Conservation of Cultural Heritage. *Adv. Colloid Interface Sci.* **2014**, *205*, 361–371. <https://doi.org/10.1016/j.cis.2013.09.008>.
- (33) Baglioni, M.; Montis, C.; Chelazzi, D.; Giorgi, R.; Berti, D.; Baglioni, P. Polymer Film Dewetting by Water/Surfactant/Good-Solvent Mixtures: A Mechanistic Insight and Its Implications for the Conservation of Cultural Heritage. *Angew. Chem.* **2018**, *130* (25), 7477–7481. <https://doi.org/10.1002/ange.201710930>.
- (34) Baglioni, M.; Montis, C.; Brandi, F.; Guaragnone, T.; Meazzini, I.; Baglioni, P.; Berti, D. Dewetting Acrylic Polymer Films with Water/Propylene Carbonate/Surfactant Mixtures – Implications for Cultural Heritage Conservation. *Phys. Chem. Chem. Phys.* **2017**, *19* (35), 23723–23732. <https://doi.org/10.1039/C7CP02608K>.

- (35) Montis, C.; Koynov, K.; Best, A.; Baglioni, M.; Butt, H.-J.; Berti, D.; Baglioni, P. Surfactants Mediate the Dewetting of Acrylic Polymer Films Commonly Applied to Works of Art. *ACS Appl. Mater. Interfaces* **2019**, *11* (30), 27288–27296. <https://doi.org/10.1021/acsami.9b04912>.
- (36) Baglioni, M.; Guaragnone, T.; Mastrangelo, R.; Sekine, F. H.; Ogura, T.; Baglioni, P. Nonionic Surfactants for the Cleaning of Works of Art: Insights on Acrylic Polymer Films Dewetting and Artificial Soil Removal. *ACS Appl. Mater. Interfaces* **2020**, *12* (23), 26704–26716. <https://doi.org/10.1021/acsami.0c06425>.
- (37) De Gennes, P.-G.; Brochard-Wyart, F.; Quere, D. *Capillarity and Wetting Phenomena: Drops, Bubbles, Pearls, Waves*; Springer Science & Business Media, 2003.
- (38) Redon, C.; Brochard-Wyart, F.; Rondelez, F. Dynamics of Dewetting. *Phys. Rev. Lett.* **1991**, *66* (6), 715–718. <https://doi.org/10.1103/PhysRevLett.66.715>.
- (39) Butt, H.-J.; Graf, K.; Kappl, M. *Physics and Chemistry of Interfaces*; John Wiley & Sons, 2013.
- (40) Reiter, G. Dewetting of Thin Polymer Films. *Phys. Rev. Lett.* **1992**, *68* (1), 75–78. <https://doi.org/10.1103/PhysRevLett.68.75>.
- (41) Lee, S. H.; Yoo, P. J.; Kwon, S. J.; Lee, H. H. Solvent-Driven Dewetting and Rim Instability. *J. Chem. Phys.* **2004**, *121* (9), 4346–4351. <https://doi.org/10.1063/1.1770475>.
- (42) Al-Khayat, O.; Hong, J. K.; Geraghty, K.; Neto, C. “The Good, the Bad, and the Slippery”: A Tale of Three Solvents in Polymer Film Dewetting. *Macromolecules* **2016**, *49* (17), 6590–6598. <https://doi.org/10.1021/acs.macromol.6b01579>.
- (43) Castro, L. B. R.; Almeida, A. T.; Petri, D. F. S. The Effect of Water or Salt Solution on Thin Hydrophobic Films. *Langmuir* **2004**, *20* (18), 7610–7615. <https://doi.org/10.1021/la049828f>.
- (44) Baglioni, P.; Dei, L.; Carretti, E.; Giorgi, R. Gels for the Conservation of Cultural Heritage. *Langmuir* **2009**, *25* (15), 8373–8374. <https://doi.org/10.1021/la900961k>.
- (45) Domingues, J. A. L.; Bonelli, N.; Giorgi, R.; Fratini, E.; Gorel, F.; Baglioni, P. Innovative Hydrogels Based on Semi-Interpenetrating p(HEMA)/PVP Networks for the Cleaning of Water-Sensitive Cultural Heritage Artifacts. *Langmuir* **2013**, *29* (8), 2746–2755. <https://doi.org/10.1021/la3048664>.
- (46) Hassan, C. M.; Peppas, N. A. Structure and Morphology of Freeze/Thawed PVA Hydrogels. *Macromolecules* **2000**, *33* (7), 2472–2479. <https://doi.org/10.1021/ma9907587>.
- (47) Hiemenz, P. C.; Lodge, T. P. *Polymer Chemistry*; CRC Press, 2007.

- (48) Flory, P. J. Thermodynamics of High Polymer Solutions. *J. Chem. Phys.* **1942**, *10* (1), 51–61. <https://doi.org/10.1063/1.1723621>.
- (49) Huggins, M. L. Solutions of Long Chain Compounds. *J. Chem. Phys.* **1941**, *9* (5), 440. <https://doi.org/10.1063/1.1750930>.
- (50) Gennes, P.-G. de; Gennes, P. P.-G. *Scaling Concepts in Polymer Physics*; Cornell University Press, 1979.
- (51) Masuelli, M. Mark-Houwink Parameters for Aqueous-Soluble Polymers and Biopolymers at Various Temperatures. *J Polym Biopolym Phys Chem* **2014**, *2*, 37–43.
- (52) Rao, M. V. S. Viscosity of Dilute to Moderately Concentrated Polymer Solutions. *Polymer* **1993**, *34* (3), 592–596. [https://doi.org/10.1016/0032-3861\(93\)90555-O](https://doi.org/10.1016/0032-3861(93)90555-O).
- (53) Kasaai, M. R.; Charlet, G.; Arul, J. Master Curve for Concentration Dependence of Semi-Dilute Solution Viscosity of Chitosan Homologues: The Martin Equation. *Food Res. Int.* **2000**, *33* (1), 63–67. [https://doi.org/10.1016/S0963-9969\(00\)00024-7](https://doi.org/10.1016/S0963-9969(00)00024-7).
- (54) Lămătic, I.-E.; Bercea, M.; Morariu, S. Intrinsic Viscosity of Aqueous Polyvinyl Alcohol Solutions. *Rev. Roum. Chim.* **2009**, *54*.
- (55) Sakurada, I.; Nakajima, A.; Fujiwara, H. Vapor Pressures of Polymer Solutions. II. Vapor Pressure of the Poly(Vinyl Alcohol)-Water System. *J. Polym. Sci.* **1959**, *35* (129), 497–505. <https://doi.org/10.1002/pol.1959.1203512916>.
- (56) Peppas, N. A.; Merrill, E. W. Crosslinked Poly(Vinyl Alcohol) Hydrogels as Swollen Elastic Networks. *J. Appl. Polym. Sci.* **1977**, *21* (7), 1763–1770. <https://doi.org/10.1002/app.1977.070210704>.
- (57) Lewandowska, K.; Staszewska, D. U.; Bohdanecký, M. The Huggins Viscosity Coefficient of Aqueous Solution of Poly(Vinyl Alcohol). *Eur. Polym. J.* **2001**, *37* (1), 25–32. [https://doi.org/10.1016/S0014-3057\(00\)00074-4](https://doi.org/10.1016/S0014-3057(00)00074-4).
- (58) Lewandowska, K. The Miscibility of Poly(Vinyl Alcohol)/Poly(N-Vinylpyrrolidone) Blends Investigated in Dilute Solutions and Solids. *Eur. Polym. J.* **2005**, *41* (1), 55–64. <https://doi.org/10.1016/j.eurpolymj.2004.08.016>.
- (59) Bercea, M.; Morariu, S.; Rusu, D. In Situ Gelation of Aqueous Solutions of Entangled Poly(Vinyl Alcohol). *Soft Matter* **2012**, *9* (4), 1244–1253. <https://doi.org/10.1039/C2SM26094H>.
- (60) van den Boomgaard, T.; King, T. A.; Tadros, Th. F.; Tang, H.; Vincent, B. The Influence of Temperature on the Adsorption and Adsorbed Layer Thickness of Various Molecular Weight Fractions of Poly(Vinyl Alcohol) on Polystyrene Latex Particles. *J. Colloid Interface Sci.* **1978**, *66* (1), 68–76. [https://doi.org/10.1016/0021-9797\(78\)90184-4](https://doi.org/10.1016/0021-9797(78)90184-4).

- (61) Flory, P. J.; Daoust, H. Osmotic Pressures of Moderately Concentrated Polymer Solutions. *J. Polym. Sci.* **1957**, *25* (111), 429–440. <https://doi.org/10.1002/pol.1957.1202511104>.
- (62) Teraoka, I. *Polymer Solutions*; John Wiley & Sons, Inc, 2002.
- (63) Bj, P.; Tj, M.; Ch, L.; Mb, K.; M, P.; S, L.; J, K.; Cr, C. Phase Behavior in PVA/Water Solution: The Coexistence of UCST and LCST. *Korea Polym. J.* **1997**, *5* (2), 126–130.
- (64) Elias, H.-G. Solution Thermodynamics. In *Macromolecules: Volume 1 · Structure and Properties*; Elias, H.-G., Ed.; Springer US: Boston, MA, 1977; pp 203–247. https://doi.org/10.1007/978-1-4615-7364-7_6.
- (65) Bates, F. S. Polymer-Polymer Phase Behavior. *Science* **1991**, *251* (4996), 898–905. <https://doi.org/10.1126/science.251.4996.898>.
- (66) Robeson, L. M. *Polymer Blends: A Comprehensive Review*; Hanser, 2007.
- (67) Paul, D. R. Polymer-Polymer Interactions. 8.
- (68) IUPAC. Compendium of Chemical Terminology, 2nd Ed. (the “Gold Book”). Compiled by A. D. McNaught and A. Wilkinson. Blackwell Scientific Publications, Oxford (1997). Online Version (2019-) Created by S. J. Chalk. ISBN 0-9678550-9-8. <https://doi.org/10.1351/Goldbook>.
- (69) Addad, J. P. C. *Physical Properties of Polymeric Gels*; John Wiley & Sons Inc: Chichester ; New York, 1995.
- (70) Ross-Murphy, S. B. Rheological Characterization of Polymer Gels and Networks. *Polym. Gels Netw.* **1994**, *2* (3), 229–237. [https://doi.org/10.1016/0966-7822\(94\)90007-8](https://doi.org/10.1016/0966-7822(94)90007-8).
- (71) Flory, P. J. Constitution of Three-Dimensional Polymers and the Theory of Gelation. 9.
- (72) Stockmayer, W. H.; Weil, L. L. The Sol–Gel Transition and Branched Polymers 50 Years Ago. *Polym. Int.* **1997**, *44* (3), 221–224. [https://doi.org/10.1002/\(SICI\)1097-0126\(199711\)44:3<221::AID-PI876>3.0.CO;2-Z](https://doi.org/10.1002/(SICI)1097-0126(199711)44:3<221::AID-PI876>3.0.CO;2-Z).
- (73) Stauffer, D. Scaling Theory of Percolation Clusters. *Phys. Rep.* **1979**, *54* (1), 1–74. [https://doi.org/10.1016/0370-1573\(79\)90060-7](https://doi.org/10.1016/0370-1573(79)90060-7).
- (74) De Gennes, P. G. On a Relation between Percolation Theory and the Elasticity of Gels. *J. Phys. Lett.* **1976**, *37* (1), 1–2. <https://doi.org/10.1051/jphyslet:019760037010100>.
- (75) Broadbent, S. R.; Hammersley, J. M. Percolation Processes: I. Crystals and Mazes. *Math. Proc. Camb. Philos. Soc.* **1957**, *53* (3), 629–641. <https://doi.org/10.1017/S0305004100032680>.
- (76) Takigawa, T.; Kasihara, H.; Urayama, K.; Masuda, T. Critical Behavior of Modulus of Poly(Vinylalcohol) Gels near the Gelation Point. *J. Phys.*

- Soc. Jpn.* **1990**, *59* (7), 2598–2599.
<https://doi.org/10.1143/JPSJ.59.2598>.
- (77) Takigawa, T.; Takahashi, M.; Urayama, K.; Masuda, T. Comparison of Model Prediction with Experiment for Concentration-Dependent Modulus of Poly(Vinyl Alcohol) (PVA) Gels near the Gelation Point. *Chem. Phys. Lett.* **1992**, *195* (5), 509–512.
[https://doi.org/10.1016/0009-2614\(92\)85553-M](https://doi.org/10.1016/0009-2614(92)85553-M).
- (78) Joshi, N.; Suman, K.; Joshi, Y. M. Rheological Behavior of Aqueous Poly(Vinyl Alcohol) Solution during a Freeze–Thaw Gelation Process. *Macromolecules* **2020**, *53* (9), 3452–3463.
<https://doi.org/10.1021/acs.macromol.0c00488>.
- (79) Jones, J. L.; Marques, C. M. Rigid Polymer Network Models. *J. Phys.* **1990**, *51* (11), 1113–1127.
<https://doi.org/10.1051/jphys:0199000510110111300>.
- (80) Guenet, J.-M. Structure versus Rheological Properties in Fibrillar Thermoreversible Gels from Polymers and Biopolymers. *J. Rheol.* **2000**, *44* (4), 947–960. <https://doi.org/10.1122/1.551121>.
- (81) Okay, O. *Polymeric Cryogels: Macroporous Gels with Remarkable Properties*; Springer, 2014.
- (82) Hassan, C. M.; Peppas, N. A. Structure and Applications of Poly(Vinyl Alcohol) Hydrogels Produced by Conventional Crosslinking or by Freezing/Thawing Methods. In *Biopolymers · PVA Hydrogels, Anionic Polymerisation Nanocomposites*; Advances in Polymer Science; Springer Berlin Heidelberg, 2000; pp 37–65.
- (83) Stauffer, S. R.; Peppast, N. A. Poly(Vinyl Alcohol) Hydrogels Prepared by Freezing–Thawing Cyclic Processing. *Polymer* **1992**, *33* (18), 3932–3936. [https://doi.org/10.1016/0032-3861\(92\)90385-A](https://doi.org/10.1016/0032-3861(92)90385-A).
- (84) Holloway, J. L.; Lowman, A. M.; Palmese, G. R. The Role of Crystallization and Phase Separation in the Formation of Physically Cross-Linked PVA Hydrogels. *Soft Matter* **2012**, *9* (3), 826–833.
<https://doi.org/10.1039/C2SM26763B>.
- (85) Lozinsky, V. I.; Solodova, E. V.; Zubov, A. L.; Simenel, I. A. Study of Cryostructuration of Polymer Systems. XI. The Formation of PVA Cryogels by Freezing–Thawing the Polymer Aqueous Solutions Containing Additives of Some Polyols. *J. Appl. Polym. Sci.* **1995**, *58* (1), 171–177. <https://doi.org/10.1002/app.1995.070580119>.
- (86) Nakamura, K.; Hatakeyama, T.; Hatakeyama, H. Relationship between Hydrogen Bonding and Bound Water in Polyhydroxystyrene Derivatives. *Polymer* **1983**, *24* (7), 871–876.
[https://doi.org/10.1016/0032-3861\(83\)90206-9](https://doi.org/10.1016/0032-3861(83)90206-9).

- (87) Yazici, I.; Okay, O. Spatial Inhomogeneity in Poly(Acrylic Acid) Hydrogels. *Polymer* **2005**, *46* (8), 2595–2602. <https://doi.org/10.1016/j.polymer.2005.01.079>.
- (88) Wunderlich, B. *Thermal Analysis of Polymeric Materials*; Springer Science & Business Media, 2005.
- (89) MacIver, M. R.; Pawlik, M. Analysis of In Situ Microscopy Images of Flocculated Sediment Volumes. *Chem. Eng. Technol.* **2017**, *40* (12), 2305–2313. <https://doi.org/10.1002/ceat.201600523>.
- (90) Levitz, P. Toolbox for 3D Imaging and Modeling of Porous Media: Relationship with Transport Properties. *Cem. Concr. Res.* **2007**, *37* (3), 351–359. <https://doi.org/10.1016/j.cemconres.2006.08.004>.
- (91) Mallam, S.; Horkay, F.; Hecht, A. M.; Rennie, A. R.; Geissler, E. Microscopic and macroscopic thermodynamic observations in swollen poly(dimethylsiloxane) networks <https://pubs.acs.org/doi/pdf/10.1021/ma00002a031> (accessed Apr 29, 2020). <https://doi.org/10.1021/ma00002a031>.
- (92) Shibayama, M.; Tanaka, T.; Han, C. C. Small Angle Neutron Scattering Study on Poly(N-isopropyl Acrylamide) Gels near Their Volume-phase Transition Temperature. *J. Chem. Phys.* **1992**, *97* (9), 6829–6841. <https://doi.org/10.1063/1.463636>.
- (93) Doucet, M.; Cho, J. H.; Alina, G.; Bakker, J.; Bouwman, W.; Butler, P.; Campbell, K.; Gonzales, M.; Heenan, R.; Jackson, A.; Juhas, P.; King, S.; Kienzle, P.; Krzywon, J.; Markvardsen, A.; Nielsen, T.; O’Driscoll, L.; Potrzebowski, W.; Ferraz Leal, R.; Richter, T.; Rozycko, P.; Snow, T.; Washington, A. *SasView Version 4.1.2*; Zenodo, 2017. <https://doi.org/10.5281/zenodo.825675>.
- (94) Montis, C.; Maiolo, D.; Alessandri, I.; Bergese, P.; Berti, D. Interaction of Nanoparticles with Lipid Membranes: A Multiscale Perspective. *Nanoscale* **2014**, *6* (12), 6452–6457. <https://doi.org/10.1039/C4NR00838C>.
- (95) Ries, J.; Schwille, P. Fluorescence Correlation Spectroscopy. *BioEssays* **2012**, *34* (5), 361–368. <https://doi.org/10.1002/bies.201100111>.
- (96) Milani, S.; Baldelli Bombelli, F.; Pitek, A. S.; Dawson, K. A.; Rädler, J. Reversible versus Irreversible Binding of Transferrin to Polystyrene Nanoparticles: Soft and Hard Corona. *ACS Nano* **2012**, *6* (3), 2532–2541. <https://doi.org/10.1021/nn204951s>.
- (97) Ormsby, B.; Keefe, M.; Phenix, A.; Learner, T. A Summary of Recent Developments in Wet Surface Cleaning Systems: Unvarnished Modern and Contemporary Painted Surfaces; 2015.
- (98) Cremonesi, P. *L’ambiente acquoso per la pulitura di opere policrome*; Il Prato, 2011.

- (99) The Winterthur Library
http://findingaid.winterthur.org/html/HTML_finding_Aids/col0935.htm (accessed Oct 24, 2020).
- (100) Cincinelli, A.; Scopetani, C.; Chelazzi, D.; Lombardini, E.; Martellini, T.; Katsoyiannis, A.; Fossi, M. C.; Corsolini, S. Microplastic in the Surface Waters of the Ross Sea (Antarctica): Occurrence, Distribution and Characterization by FTIR. *Chemosphere* **2017**, *175*, 391–400. <https://doi.org/10.1016/j.chemosphere.2017.02.024>.
- (101) Gutiérrez, M. C.; García-Carvajal, Z. Y.; Jobbágy, M.; Rubio, F.; Yuste, L.; Rojo, F.; Ferrer, M. L.; del Monte, F. Poly(Vinyl Alcohol) Scaffolds with Tailored Morphologies for Drug Delivery and Controlled Release. *Adv. Funct. Mater.* **2007**, *17* (17), 3505–3513. <https://doi.org/10.1002/adfm.200700093>.
- (102) Mattiasson, B.; Kumar, A.; Galeaev, I. Y. *Macroporous Polymers: Production Properties and Biotechnological/Biomedical Applications*; CRC Press, 2009.
- (103) Zhang, L.; Zhao, J.; Zhu, J.; He, C.; Wang, H. Anisotropic Tough Poly(Vinyl Alcohol) Hydrogels. *Soft Matter* **2012**, *8* (40), 10439–10447. <https://doi.org/10.1039/C2SM26102B>.
- (104) *Biopolymers · PVA Hydrogels Anionic Polymerisation Nanocomposites*; Springer, 2003.
- (105) Yukioka, S.; Higo, Y.; Noda, I.; Nagasawa, M. Correlation Lengths of Linear and Branched Polymers in a Good Solvent. *Polym. J.* **1986**, *18* (12), 941–946. <https://doi.org/10.1295/polymj.18.941>.
- (106) Shibayama, M.; Kurokawa, H.; Nomura, S.; Muthukumar, M.; Stein, R. S.; Roy, S. Small-Angle Neutron Scattering from Poly(Vinyl Alcohol)-Borate Gels. *Polymer* **1992**, *33* (14), 2883–2890. [https://doi.org/10.1016/0032-3861\(92\)90072-5](https://doi.org/10.1016/0032-3861(92)90072-5).
- (107) Briscoe, B.; Luckham, P.; Zhu, S. The Effects of Hydrogen Bonding upon the Viscosity of Aqueous Poly(Vinyl Alcohol) Solutions. *Polymer* **2000**, *41* (10), 3851–3860. [https://doi.org/10.1016/S0032-3861\(99\)00550-9](https://doi.org/10.1016/S0032-3861(99)00550-9).
- (108) Marin, E.; Rojas, J.; Ciro, Y. A Review of Polyvinyl Alcohol Derivatives: Promising Materials for Pharmaceutical and Biomedical Applications. *Afr. J. Pharm. Pharmacol.* **2014**. <https://doi.org/10.5897/AJPP2013.3906>.
- (109) Hassan, C. M.; Stewart, J. E.; Peppas, N. A. Diffusional Characteristics of Freeze/Thawed Poly(Vinyl Alcohol) Hydrogels: Applications to Protein Controlled Release from Multilaminar Devices. *Eur. J. Pharm. Biopharm.* **2000**, *49* (2), 161–165. [https://doi.org/10.1016/S0939-6411\(99\)00056-9](https://doi.org/10.1016/S0939-6411(99)00056-9).

- (110) Lozinsky, V. I.; Damshkaln, L. G. Study of Cryostructuration of Polymer Systems. XVII. Poly(Vinyl Alcohol) Cryogels: Dynamics of the Cryotropic Gel Formation. *J. Appl. Polym. Sci.* **2000**, *77* (9), 2017–2023. [https://doi.org/10.1002/1097-4628\(20000829\)77:9<2017::AID-APP18>3.0.CO;2-6](https://doi.org/10.1002/1097-4628(20000829)77:9<2017::AID-APP18>3.0.CO;2-6).
- (111) Budhlall, B. M.; Landfester, K.; Sudol, E. D.; Dimonie, V. L.; Klein, A.; El-Aasser, M. S. Characterization of Partially Hydrolyzed Poly(Vinyl Alcohol). Effect of Poly(Vinyl Alcohol) Molecular Architecture on Aqueous Phase Conformation. *Macromolecules* **2003**, *36* (25), 9477–9484. <https://doi.org/10.1021/ma030027d>.
- (112) Nishio, Y.; Haratani, T.; Takahashi, T. Miscibility and Orientation Behavior of Poly(Vinyl Alcohol) / Poly(Vinyl Pyrrolidone) Blends. *J. Polym. Sci. Part B Polym. Phys.* **1990**, *28* (3), 355–376. <https://doi.org/10.1002/polb.1990.090280308>.
- (113) Ping, Z.-H.; Nguyen, Q. T.; Néel, J. Investigations of Poly(Vinyl Alcohol)/Poly(N-Vinyl-2-Pyrrolidone) Blends, 2. Influence of the Molecular Weights of the Polymer Components on Crystallization. *Makromol. Chem.* **1990**, *191* (1), 185–198. <https://doi.org/10.1002/macp.1990.021910115>.
- (114) Abou_Taleb, M. H. Thermal and Spectroscopic Studies of Poly(N-Vinyl Pyrrolidone)/Poly(Vinyl Alcohol) Blend Films. *J. Appl. Polym. Sci.* **2009**, *114* (2), 1202–1207. <https://doi.org/10.1002/app.30082>.
- (115) Bernal, A.; Kuritka, I.; Saha, P. Preparation and Characterization of Poly(Vinyl Alcohol)-Poly(Vinyl Pyrrolidone) Blend: A Biomaterial with Latent Medical Applications. *J. Appl. Polym. Sci.* **2013**, *127* (5), 3560–3568. <https://doi.org/10.1002/app.37723>.
- (116) Bercea, M.; Morariu, S.; Teodorescu, M. Rheological Investigation of Poly(Vinyl Alcohol)/Poly(N-Vinyl Pyrrolidone) Mixtures in Aqueous Solution and Hydrogel State. *J. Polym. Res.* **2016**, *23* (7), 142. <https://doi.org/10.1007/s10965-016-1040-3>.
- (117) Teodorescu, M.; Bercea, M.; Morariu, S. Miscibility Study on Polymer Mixtures in Dilute Solution. *Colloids Surf. Physicochem. Eng. Asp.* **2018**, *559*, 325–333. <https://doi.org/10.1016/j.colsurfa.2018.09.062>.
- (118) Boonsuk, P.; Kaewtatip, K.; Chantarak, S.; Kelarakis, A.; Chaibundit, C. Super-Tough Biodegradable Poly(Vinyl Alcohol)/Poly(Vinyl Pyrrolidone) Blends Plasticized by Glycerol and Sorbitol. *J. Appl. Polym. Sci.* **2018**, *135* (26), 46406. <https://doi.org/10.1002/app.46406>.
- (119) Guldbbrand, S.; Kirejev, V.; Simonsson, C.; Goksör, M.; Smedh, M.; Ericson, M. B. Two-Photon Fluorescence Correlation Spectroscopy as a Tool for Measuring Molecular Diffusion within Human Skin. *Eur. J. Pharm. Biopharm.* **2013**, *84* (2), 430–436. <https://doi.org/10.1016/j.ejpb.2012.10.001>.

- (120) Zaslavsky, B. Y. *Aqueous Two-Phase Partitioning: Physical Chemistry and Bioanalytical Applications*; CRC Press, 1994.
- (121) Guettari, M.; Belaidi, A.; Abel, S.; Tajouri, T. Polyvinylpyrrolidone Behavior in Water/Ethanol Mixed Solvents: Comparison of Modeling Predictions with Experimental Results. *J. Solut. Chem.* **2017**, *46* (7), 1404–1417. <https://doi.org/10.1007/s10953-017-0649-0>.
- (122) Sakellariou, P. Theta Temperature of Poly(N-Vinyl Pyrrolidone) in Water. *Polymer* **1992**, *33* (6), 1339–1342. [https://doi.org/10.1016/0032-3861\(92\)90788-X](https://doi.org/10.1016/0032-3861(92)90788-X).
- (123) Larson, R. G.; Larson, R. G. *The Structure and Rheology of Complex Fluids*; OUP USA, 1999.
- (124) Gennes, P.-G. *Scaling Concepts in Polymer Physics*; Cornell University Press: Ithaca, NY, 1979.
- (125) Candau, S.; Bastide, J.; Delsanti, M. Structural, Elastic, and Dynamic Properties of Swollen Polymer Networks. In *Polymer Networks*; Dušek, K., Ed.; Advances in Polymer Science; Springer: Berlin, Heidelberg, 1982; pp 27–71. https://doi.org/10.1007/3-540-11471-8_2.
- (126) Li, L.; Aoki, Y. Rheological Images of Poly(Vinyl Chloride) Gels. 3. Elasticity Evolution and the Scaling Law beyond the Sol–Gel Transition. *Macromolecules* **1998**, *31* (3), 740–745. <https://doi.org/10.1021/ma971449o>.
- (127) Sakai, T. Sol-Gel Transition. In *Physics of Polymer Gels*; John Wiley & Sons, Ltd, 2020; pp 161–171. <https://doi.org/10.1002/9783527346547.ch8>.
- (128) Hernández, R.; Sarafian, A.; López, D.; Mijangos, C. Viscoelastic Properties of Poly(Vinyl Alcohol) Hydrogels and Ferrogels Obtained through Freezing–Thawing Cycles. *Polymer* **2004**, *45* (16), 5543–5549. <https://doi.org/10.1016/j.polymer.2004.05.061>.
- (129) Ricciardi, R.; Gaillet, C.; Ducouret, G.; Lafuma, F.; Lauprêtre, F. Investigation of the Relationships between the Chain Organization and Rheological Properties of Atactic Poly(Vinyl Alcohol) Hydrogels. *Polymer* **2003**, *44* (11), 3375–3380. [https://doi.org/10.1016/S0032-3861\(03\)00246-5](https://doi.org/10.1016/S0032-3861(03)00246-5).
- (130) Ramzi, M.; Rochas, C.; Guenet, J.-M. Structure–Properties Relation for Agarose Thermoreversible Gels in Binary Solvents. *Macromolecules* **1998**, *31* (18), 6106–6111. <https://doi.org/10.1021/ma9801220>.
- (131) Artyukhov, A. A.; Shtilman, M. I.; Kuskov, A. N.; Pashkova, L. I.; Tsatsakis, A. M.; Rizos, A. K. Polyvinyl Alcohol Cross-Linked Macroporous Polymeric Hydrogels: Structure Formation and Regularity Investigation. *J. Non-Cryst. Solids* **2011**, *357* (2), 700–706. <https://doi.org/10.1016/j.jnoncrysol.2010.06.038>.

- (132) Hernandez, R.; Lopez, D.; Mijangos, C.; Guenet, J.-M. A Reappraisal of the ‘Thermoreversible’ Gelation of Aqueous Poly(Vinyl Alcohol) Solutions through Freezing–Thawing Cycles. *Polymer* **2002**, *43* (21), 5661–5663. [https://doi.org/10.1016/S0032-3861\(02\)00470-6](https://doi.org/10.1016/S0032-3861(02)00470-6).
- (133) Peppas, N. A.; Stauffer, S. R. Reinforced Uncrosslinked Poly (Vinyl Alcohol) Gels Produced by Cyclic Freezing–Thawing Processes: A Short Review. *J. Controlled Release* **1991**, *16* (3), 305–310. [https://doi.org/10.1016/0168-3659\(91\)90007-Z](https://doi.org/10.1016/0168-3659(91)90007-Z).
- (134) Levitz, P.; Tchoubar, D. Disordered Porous Solids : From Chord Distributions to Small Angle Scattering. *J. Phys. I* **1992**, *2* (6), 771–790. <https://doi.org/10.1051/jp1:1992174>.
- (135) Yokoyama, F.; Masada, I.; Shimamura, K.; Ikawa, T.; Monobe, K. Morphology and Structure of Highly Elastic Poly(Vinyl Alcohol) Hydrogel Prepared by Repeated Freezing-and-Melting. *Colloid Polym. Sci.* **1986**, *264* (7), 595–601. <https://doi.org/10.1007/BF01412597>.
- (136) Ricciardi, R.; Gaillet, C.; Ducouret, G.; Lafuma, F.; Lauprêtre, F. Investigation of the Relationships between the Chain Organization and Rheological Properties of Atactic Poly(Vinyl Alcohol) Hydrogels. *Polymer* **2003**, *44* (11), 3375–3380. [https://doi.org/10.1016/S0032-3861\(03\)00246-5](https://doi.org/10.1016/S0032-3861(03)00246-5).
- (137) Lozinsky, V. I.; Damshkaln, L. G.; Kurochkin, I. N.; Kurochkin, I. I. Study of Cryostructuring of Polymer Systems: 28. Physicochemical Properties and Morphology of Poly(Vinyl Alcohol) Cryogels Formed by Multiple Freezing–Thawing. *Colloid J.* **2008**, *70* (2), 189–198. <https://doi.org/10.1134/S1061933X08020117>.
- (138) Lozinsky, V. I.; Vainerman, E. S.; Domotenko, L. V.; Mamtsis, A. M.; Titova, E. F.; Belavtseva, E. M.; Rogozhin, S. V. Study of Cryostructurization of Polymer Systems VII. Structure Formation under Freezing of Poly(Vinyl Alcohol) Aqueous Solutions. *Colloid Polym. Sci.* **1986**, *264* (1), 19–24. <https://doi.org/10.1007/BF01410304>.
- (139) Lorén, N.; Hagman, J.; Jonasson, J. K.; Deschout, H.; Bernin, D.; Cella-Zanacchi, F.; Diaspro, A.; McNally, J. G.; Ameloot, M.; Smisdom, N.; Nydén, M.; Hermansson, A.-M.; Rudemo, M.; Braeckmans, K. Fluorescence Recovery after Photobleaching in Material and Life Sciences: Putting Theory into Practice. *Q. Rev. Biophys.* **2015**, *48* (03), 323–387. <https://doi.org/10.1017/S0033583515000013>.
- (140) Song, G.; Zhao, Z.; Peng, X.; He, C.; Weiss, R. A.; Wang, H. Rheological Behavior of Tough PVP- in Situ -PAAm Hydrogels Physically Cross-Linked by Cooperative Hydrogen Bonding. *Macromolecules* **2016**, *49* (21), 8265–8273. <https://doi.org/10.1021/acs.macromol.6b01448>.

- (141) Hyun, K.; Wilhelm, M.; Klein, C. O.; Cho, K. S.; Nam, J. G.; Ahn, K. H.; Lee, S. J.; Ewoldt, R. H.; McKinley, G. H. A Review of Nonlinear Oscillatory Shear Tests: Analysis and Application of Large Amplitude Oscillatory Shear (LAOS). *Prog. Polym. Sci.* **2011**, *36* (12), 1697–1753. <https://doi.org/10.1016/j.progpolymsci.2011.02.002>.
- (142) Kjøniksen, A.-L.; Nyström, B. Effects of Polymer Concentration and Cross-Linking Density on Rheology of Chemically Cross-Linked Poly(Vinyl Alcohol) near the Gelation Threshold. *Macromolecules* **1996**, *29* (15), 5215–5222. <https://doi.org/10.1021/ma960094q>.
- (143) Gentili, D.; Foschi, G.; Valle, F.; Cavallini, M.; Biscarini, F. Applications of Dewetting in Micro and Nanotechnology. *Chem. Soc. Rev.* **2012**, *41* (12), 4430–4443. <https://doi.org/10.1039/C2CS35040H>.
- (144) Reiter, G.; Hamieh, M.; Damman, P.; Slavov, S.; Gabriele, S.; Vilmin, T.; Raphaël, E. Residual Stresses in Thin Polymer Films Cause Rupture and Dominate Early Stages of Dewetting. *Nat. Mater.* **2005**, *4* (10), 754–758. <https://doi.org/10.1038/nmat1484>.
- (145) Lozinsky, V. I.; Damshkaln, L. G.; Kurochkin, I. N.; Kurochkin, I. I. Study of Cryostructuring of Polymer Systems: 25. The Influence of Surfactants on the Properties and Structure of Gas-Filled (Foamed) Poly(Vinyl Alcohol) Cryogels. *Colloid J.* **2005**, *67* (5), 589–601. <https://doi.org/10.1007/s10595-005-0137-x>.
- (146) Gradzielski, M.; Hoffmann, H. Influence of Charges on Structure and Dynamics of an O/W Microemulsion. Effect of Admixing Ionic Surfactants. *J. Phys. Chem.* **1994**, *98* (10), 2613–2623. <https://doi.org/10.1021/j100061a019>.
- (147) Ionut Atanase, L.; Bistac, S.; Riess, G. Effect of Poly(Vinyl Alcohol-Co-Vinyl Acetate) Copolymer Blockiness on the Dynamic Interfacial Tension and Dilational Viscoelasticity of Polymer–Anionic Surfactant Complex at the Water–1-Chlorobutane Interface. *Soft Matter* **2015**, *11* (13), 2665–2672. <https://doi.org/10.1039/C4SM02766C>.
- (148) Aut, L. M. J. author. *Spongy Hydrogels Clean Rough Paintings.* **2020**. <https://doi.org/10.1063/PT.6.1.20200326a>.
- (149) Mazzuca, C.; Micheli, L.; Cervelli, E.; Basoli, F.; Cencetti, C.; Coviello, T.; Iannuccelli, S.; Sotgiu, S.; Palleschi, A. Cleaning of Paper Artworks: Development of an Efficient Gel-Based Material Able to Remove Starch Paste. *ACS Appl. Mater. Interfaces* **2014**, *6* (19), 16519–16528. <https://doi.org/10.1021/am504295n>.
- (150) Bonelli, N.; Montis, C.; Mirabile, A.; Berti, D.; Baglioni, P. Restoration of Paper Artworks with Microemulsions Confined in Hydrogels for Safe and Efficient Removal of Adhesive Tapes. *Proc. Natl. Acad. Sci.* **2018**, *115* (23), 5932–5937. <https://doi.org/10.1073/pnas.1801962115>.

- (151) Saikia, B.; Parthasarathy, G. Fourier Transform Infrared Spectroscopic Characterization of Kaolinite from Assam and Meghalaya, Northeastern India. *J. Mod. Phys.* **2010**, *1*, 206–210.
- (152) Duce, C.; Della Porta, V.; Tiné, M. R.; Spepi, A.; Ghezzi, L.; Colombini, M. P.; Bramanti, E. FTIR Study of Ageing of Fast Drying Oil Colour (FDOC) Alkyd Paint Replicas. *Spectrochim. Acta. A. Mol. Biomol. Spectrosc.* **2014**, *130*, 214–221. <https://doi.org/10.1016/j.saa.2014.03.123>.
- (153) Burnstock, A.; White, R. A preliminary assessment of the aging/degradation of Ethomeen C-12 residues from solvent gel formulations and their potential for inducing changes in resinous paint media.
- (154) Casoli, A.; Di Diego, Z.; Isca, C. Cleaning Painted Surfaces: Evaluation of Leaching Phenomenon Induced by Solvents Applied for the Removal of Gel Residues. *Environ. Sci. Pollut. Res.* **2014**, *21* (23), 13252–13263. <https://doi.org/10.1007/s11356-014-2658-5>.

ACKNOWLEDGEMENTS

This thesis work is the result of the guidance and the collaboration of several people, who have allowed me to grow, personally and scientifically, during these years.

First, I would like to express my deepest gratitude to my scientific supervisor and PhD tutor, Prof. Piero Baglioni. His intuitions and ideas guided my research, his passion for science motivated me, while his persistence led me to investigate thoroughly the phenomena observed during the experiments and the theory behind them. During these years, my passion for science grew stronger, and I owe him for that. Secondly, I would like to sincerely thank Prof. Emiliano Fratini, for his guidance, patience and advice. His help about SAXS fitting and MATLAB programming was precious. My gratitude further extends to Dr. David Chelazzi and Dr. Giovanna Poggi. David taught me how to effectively organize ideas and write them down; our scientific discussions greatly improved my way of working. Giovanna provided suggestions and valuable help, always keeping things under control. I would also like to thank Prof. Emiliano Carretti and Michele Baglioni for their collaboration. A special thanks goes to Dr. Claudio Resta, for always planting the “seed of doubt” over my scientific theories; our discussions made me eager to learn more about several topics, and improved my critical thought. I would like to thank my friends and colleagues Teresa, Andrea, Vanessa, Marco, Lucrezia and Raffaello for sharing the PhD path with enthusiasm and sense of humor.

I wish also to thank Dr. Taku Ogura and Mr. Felipe Hidetomo Sekine (NIKKOL Group – Japan) for providing the chemicals for NSF's formulation; Luciano Pensabene, Marialaura Petruzzellis and the Peggy Guggenheim Foundation for the research work, the tests and the pictures of the cleaning performed on Pollock's and Picasso's paintings.

CSGI and the European Projects NANORESTART and APACHE (Horizon 2020, agreements 646063 and 814496, respectively) are acknowledged for financial support.

I would finally like to thank my family, and Matteo, for their endless support, and for helping me to pursue my dreams.

APPENDIX: LIST OF PUBLICATIONS

Publications related to this PhD thesis

Paper I: R. Mastrangelo, C. Resta, E. Carretti, E. Fratini, & P. Baglioni. PVA-based cryogels for the Cleaning of Modern Art: delving into the role of semi-interpenetrating polymers. Submitted to ACS Applied Materials & Interfaces.

Paper II: R. Mastrangelo, D. Chelazzi, G. Poggi, E. Fratini, & P. Baglioni (2020). Twin-chain polymer hydrogels based on poly(vinyl alcohol) as new advanced tool for the cleaning of modern and contemporary art. Proceedings of the National Academy of Science, 117(13), 7011-7020.
DOI: 10.1073/pnas.1911811117.

Paper III: R. Mastrangelo, E. Mascii, E. Fratini, & P. Baglioni. Twin-chain polymer networks: how the semi-interpenetrating polymer chain length affects the cryogels structure. In preparation.

Paper IV: M. Baglioni, T. Guaragnone, R. Mastrangelo, F. Hidetomo Sekine, T. Ogura, & P. Baglioni (2020). NONIONIC SURFACTANTS FOR THE CLEANING OF WORKS OF ART: INSIGHTS ON ACRYLIC POLYMER FILMS DEWETTING AND ARTIFICIAL SOIL REMOVAL. ACS Applied Materials & Interfaces 12 (23), 26704-26716.
DOI: 10.1021/acsami.0c06425.

Paper V: P. Tempesti, M. Baglioni, R. Mastrangelo, & P. Baglioni. Chemo-Physical Properties of PVA and Semi-interpenetrated PVA/PVA Cryogels loaded with Nanostructured Fluids Studied by Ultra-Small-Angle X-ray Scattering. In preparation.

Paper VI: L. Pensabene Buemi, M. L. Petruzzellis, D. Chelazzi, M. Baglioni, R. Mastrangelo, R. Giorgi, & P. Baglioni (2020). Twin-chain polymer networks loaded with nanostructured fluids for the selective removal of a non-

original varnish from Picasso's "L'Atelier" at the Peggy Guggenheim Collection, Venice. *Heritage Science*, 8(1), 1-16.

DOI: 10.1186/s40494-020-00420-0.

Other Publications

T. Guaragnone, M. Rossi, D. Chelazzi, R. Mastrangelo, M. Severi, E. Fratini, & P. Baglioni. pHEMA/PAA and pHEMA/PVP semi-IPNs: effect of pH and loading with tetraethylenepentamine for the removal of bronze corrosion products.

Submitted to *ACS Applied Materials & Interfaces*.

M. Mamusa, R. Mastrangelo, T. Glen, S. Murgia, G. Palazzo, J. Smets & P. Baglioni. Rational design of sustainable liquid microcapsules for spontaneous fragrance encapsulation. Submitted to *Angewandte Chemie*.

D. Chelazzi, E. Fratini, R. Giorgi, R. Mastrangelo, M. Rossi, & P. Baglioni (2018). Gels for the Cleaning of Works of Art, Gels and Other Soft Amorphous Solids. *ACS Symposium Series 1296*.

DOI: 10.1021/bk-2018-1296.ch015.

Previous Publications:

R. Mastrangelo, C. Montis, N. Bonelli, P. Tempesti, & P. Baglioni (2017). Surface cleaning of artworks: Structure and dynamics of nanostructured fluids confined in polymeric hydrogel networks. *Physical Chemistry Chemical Physics*, 19(35), 23762-23772. DOI: 10.1039/c7cp02662e .

PAPER I

PVA-based Cryogels for the cleaning of Modern and Contemporary Art: delving into the role of semi-interpenetrating polymers

*Rosangela Mastrangelo, Claudio Resta, Emiliano Carretti, Emiliano Fratini and Ptero Baglioni**

CSGI and University of Florence, via della Lastruccia 3, 50019 Sesto Fiorentino (FI)

KEYWORDS. PVA, cryogels, semi-interpenetrating polymers, freeze-thawing, phase separation, gelation mechanism

ABSTRACT

The cleaning of Modern and Contemporary paintings requires particular care: traditional methods are too invasive and risky for their clotted, water-sensitive surfaces, where any mechanical action and spreading of free solvent should be avoided. For these reasons, highly adaptable and retentive gels, based on poly(vinyl alcohol), were formulated. The addition of semi-interpenetrating polymers allowed to obtain macroporous and cohesive networks, which showed unprecedented cleaning performances on masterpieces from Pollock¹ and Picasso². In this contribution, the effects of two semi-interpenetrating polymers on the morphology, the nanostructure and the gelation mechanism of cryogels made of a highly hydrolyzed PVA (H-PVA) were investigated. Both the semi-interpenetrating polymers, a PVA with lower hydrolysis degree and molecular weight (L-

PVA), and a high molecular weight poly(vinyl pyrrolidone), PVP, have been already used to obtain cryogels for the cleaning of paintings. The very different structure of the semi-interpenetrating chains led to different phase behaviors in the pre-gel solutions. In H-PVA – L-PVA and H-PVA – PVP mixtures, liquid-liquid demixing occurred, modifying H-PVA chains self-interaction and ability to crystallize. Overall, despite the different chemical structure of L-PVA and PVP, both polymers were proven to behave as porogens and structuring agents for the main H-PVA network.

INTRODUCTION

The aesthetic appearance of a painting changes over time: dirt accumulates on the surface, due to environmental exposure, wrong handling, or simply neglect³; concurrently, degradation of the original materials and yellowing of varnishes occur. Such factors determine both visual and physical alterations, affecting the artwork readability and disguising the artist's original message.

When possible, the layers of unwanted or aged materials can be removed. The cleaning of a painting is a delicate process, especially when it comes to the rough, clotted and often solvent-sensitive surfaces of Modern and Contemporary Art. The confinement of solvents or nanostructured fluids in gels⁴⁻⁸ grants high controllability and selectivity during the cleaning process, limiting the capillary penetration and the swelling of the paint layers, and avoiding leaching and deterioration of the artwork materials⁹⁻¹¹. However, when dealing with 3D, textured surfaces, particular care must also be taken in reaching all the nooks and crannies created by the thick brushstrokes and, at the same time, limiting any direct mechanical action.¹²

Poly(vinyl alcohol) (PVA)-based cryogels designed by our group^{1,2,13,14} were proven to be non-risky, effective tools for the cleaning of rough, water-sensitive substrates. High adaptability,

interconnected porosity, high free water content and water retentiveness are some of the key-features which granted cryogels unprecedented cleaning performances.

PVA cryogels are formed when a PVA aqueous solution undergoes a freeze-thawing (FT) process.^{15,16} They are known to be strong physical gels, obtained by the combination of the spinodal decomposition and the polymer crystallization occurring during the freezing of PVA solutions.¹⁷⁻¹⁹ The resulting networks are highly elastic and resilient, to the point of being considered good candidates to design artificial human tissues²⁰.

Rheological properties, crystallinity and porosity of cryogels are known to depend on the polymer molecular weight, concentration in solution, as well as number and conditions of freeze-thaw (FT) cycles applied.^{19,21,22}

The present work is aimed at deepening and analyzing PVA-based cryogels physico-chemical properties, deemed to be crucial for the cleaning action. Namely, the effects of the inclusion of linear semi-interpenetrating polymers, i.e. a partially hydrolyzed PVA (L-PVA) and poly(vinyl pyrrolidone), PVP, in the main PVA networks were explored. L-PVA and PVP chains alter crystallinity, gel fraction and rheological properties of the network, influencing the gelation mechanism; pores shape and dimension were proven to depend on the H-PVA/semi-interpenetrating polymer ratio and polymers behavior in aqueous solution. Concurrently, L-PVA and PVP influenced the gels structure at the nanoscale and the gelation mechanism.

MATERIALS AND METHODS

Chemicals. High-molecular weight polyvinyl alcohol, H-PVA (hydrolysis degree, HD, 98% and M_w 160 kDa), low-molecular weight polyvinyl alcohol, L-PVA (HD 88% and M_w 100 kDa) and

polyvinyl pyrrolidone, PVP (M_w 1300 kDa) for the hydrogel preparation were purchased from Sigma-Aldrich.

Water for the hydrogels preparation was purified through a Millipore system (resistivity > 18 M Ω cm).

The following fluorescent dyes were used in Confocal Imaging or Fluorescence Correlation Spectroscopy calibration/measurements: Fluorescein isothiocyanate isomer I (purity \geq 90%, FITC, Sigma-Aldrich); Rhodamine B isothiocyanate (mixed isomers, RBITC, Sigma-Aldrich); Rhodamine 110 chloride (purity \geq 99%, Sigma-Aldrich); Alexa Fluor 568 (Thermo Fisher Scientific).

Triethylamine (purity > 99%); DMSO (anhydrous, purity > 99.9%) were purchased from Sigma-Aldrich and used in the polymer-labeling reactions. All the chemicals were used as received, without further purification.

Cryogel preparation. Polymer mixtures were dissolved in purified water, in a rounded-bottom flask equipped with a condenser to prevent water evaporation. Temperature was set at 98°C and the mixture maintained under continuous stirring for 2 hours. After complete dissolution, pre-gel solutions were cooled down to room temperature, poured into polystyrene molds (14 x 7 x 0.2 cm³) and then frozen for 16 hours at -18 °C. Thawing step, at room temperature, lasted for 3-5 hours.

Different cryogels were obtained by varying H-PVA concentration (X, in % w/v).

Gels made of H-PVA only are coded as Pure Networks (PN_X), while gels containing L-PVA or PVP are identified as semi-Interpenetrating networks and coded as i-PVA_X and i-PVP_X,

respectively. i-PVA_X and i-PVP_X contain a constant quantity of semi-interpenetrating polymer (3% w/v).

To sum up, cryogels series are coded as follows:

- PN_X, with X = 3, 5, 7, 9, 12, 15 % w/v, are cryogels containing increasing concentrations of H-PVA (X);
- i-PVA_X, with X = 3, 5, 7, 9, 12, 15 % w/v, are cryogels containing 3% w/v of L-PVA and increasing concentrations of H-PVA (X);
- i-PVP_X, with X = 3, 5, 7, 9, 12, 15 % w/v, are cryogels containing 3% w/v of PVP and increasing concentrations of H-PVA (X);

To investigate the effect of increasing amounts of semi-interpenetrating polymers on a 9% w/v H-PVA network, the following samples were prepared (see Rheology and NMR experiments):

- i(Y)-PVA, with Y = 0.5, 1, 2, 3, 4, 5 % w/v, are semi-IPNs containing 9% w/v of H-PVA and increasing concentrations of L-PVA (Y);
- i(Y)-PVP, with Y = 0.5, 1, 2, 3, 4, 5 % w/v, are semi-IPNs containing 9% w/v of H-PVA and increasing concentrations of PVP (Y);

The same name, when specified, was used also to describe the pre-gel solution.

Most of the measurements were performed on gels right after thawing.

Then, selected samples of PN_X, i_PVA_X and i_PVP_X series were washed for seven days in demineralized water: each sheet was stored in ca. 1.5 L of water to extract the soluble components, and water was changed daily.

Polymers' labeling. H-PVA and L-PVA were labeled with FITC and RBITC, respectively. Details on the labeling reaction are reported elsewhere.¹ PVP was labeled with RBITC, following the same procedure used for L-PVA. In this case, the unavoidable presence of -NH₂ or -OH bearing defects on the backbone was exploited. Rhodamine labeled PVP was purified by means of several dissolution/precipitation cycles (respectively in water and ethanol) and subsequent dialysis against water. The effectiveness of covalent labeling was proved by fluorescence correlation spectroscopy experiments on labeled PVP water solutions, which showed a diffusion coefficient completely consistent with a chemically bound probe.

Confocal Laser Scanning Microscopy (CLSM) Imaging. CLSM experiments were performed on a Leica TCS SP8 confocal microscope (Leica Microsystems GmbH, Wetzlar, Germany), equipped with a 63X water immersion objective. The dyes Rhodamine 110 (used to acquire images of the washed gels) and FITC (for H-PVA labeling) were excited with a 488 nm laser line (Ar laser) and the fluorescence emitted was collected by a PMT in the 498-540 nm range. RBITC (for L-PVA and PVP labeling) was excited with a 561 nm laser (DPSS 561) and the fluorescence was collected by a PMT in the 571-630 nm range.

Crystallinity degree (X_c). The degree of crystallinity of the cryogels was evaluated through Differential Scanning Calorimetry (DSC) measurements, and specifically by integrating the melting peaks observed for the freeze-dried samples. X_c was calculated as the ratio between the specific enthalpies of fusion of the gel sample and a fully crystalline PVA (161 J/g)²³, respectively. The DSC temperature ramp was set from 25°C to 250 °C, at a heating rate of 5 °C/min. The reported X_c values, for both thawed and washed gels, are averages of 3 measurements.

Gel Fraction (G%). The fraction of polymer chains taking part to the gel structure can be evaluated gravimetrically. Namely, the percentage gel fraction was obtained as follows:

$$G\% = W_{wa}/W_0 \times 100 \quad (1)$$

W_0 is the initial gel sample's polymer content, while W_{wa} is the polymer content of the same sample after washing. W_{wa} was obtained by oven drying washed gel samples at 100 °C, to a constant weight. Values reported are averages of at least three measurements.

Equilibrium Volume Swelling Ratio (q_v). The swelling degree was evaluated on washed gels sheets. The swelling capacity was calculated by measuring the variation of the width by means of a caliper rule (resolution 0.02 mm) according to²⁴:

$$q_v = \left(L/L_0\right)^3 \quad (2)$$

where L_0 is the side length after preparation (i.e. the mold's side), and L is the side length after washing (at swelling equilibrium).

Small-angle X-ray scattering (SAXS). A HECUS S3-MICRO SWAXS-camera (Hecus XRS, Graz, Austria), equipped with a Kratky collimation system and a position-sensitive detector (PSD 50M), with 1024 channels (width = 54 μm). A Cu anode provided Cu $K\alpha$ radiation ($\lambda = 0.1542$ nm), by using a 50W microfocus source with customized FOX-3D single-bounce multilayer point focusing optics (Xenocs, Grenoble, France). The voltage is generated by the GeniX system (Xenocs). The sample-to-detector distance was 281 mm as calibrated by silver behenate ($d = 58.38$ Å)²⁵. The volume between the sample and the detector was kept under vacuum during the measurements to minimize scattering from the air. Scattering curves were obtained in the Q-range between 0.009-0.54 Å⁻¹. Temperature was kept at $25 \pm 0.1^\circ\text{C}$ by a Peltier element. Gel samples

were cut in thin slices and put in the appropriate sample holder, i.e. a demountable sealed cell for solids, with Kapton as a window material (optical path =1 mm). Standard measurement conditions were 50 kV, 1 mA. The acquisition time was from 1 to 2 hours depending on the sample. Scattering curves were corrected for the empty cell/water contribution.

The fitting of the SAXS curves was implemented through the software SASView²⁶. The scattered intensity, $I(q)$, was modeled as follows^{27,28}:

$$I(q) = I_L(0) \frac{1}{\left[1 + \frac{D+1}{3}(q^2\xi^2)\right]^{D/2}} + I_G(0)\exp(-q^2R^2/3) + B \quad (3)$$

The two terms describe the scattering due to polymer chains in a liquid-like environment, and the scattering of solid-like objects (physical polymer junctions), respectively.

$I_L(0)$ and $I_G(0)$ are called Lorentzian and Guinier parameters, and define the relative weight of the two terms in the equation; D is the fractal exponent, ξ is the correlation length of non-crystalline polymer chains and R is the radius of gyration of solid-like objects (polymer crystallites).

Fluorescence Correlation Spectroscopy (FCS). A Leica TCS SP8 confocal microscope (Leica Microsystems GmbH, Wetzlar, Germany) equipped with a 63X water immersion objective, was used to perform FCS measurements. The diffusion of FITC-labeled H-PVA in dilute solution ($[FITC] = 50$ nM) was measured by exciting FITC with the Ar laser line (488 nm) and collecting the fluorescence signal with a Hybrid SMD detector (498-540 nm). The diffusion of RBITC-labeled L-PVA and PVP in dilute solution ($[RBITC] = 50$ nM), instead, was measured by exciting RBITC with the DPSS 561 laser line (561 nm) and collecting the fluorescence signal with a Hybrid SMD detector (571–630 nm). Aqueous solutions of Alexa Fluor 568 (25 nM) and Rhodamine 110 (10 nM) were used for FCS calibration²⁹. The fitting model assumes that the three-dimensional

Brownian diffusion of labeled molecules across a 3D-ellipsoidal Gaussian volume is the only contribution to the observed decay time. FCS curves were analyzed considering either a one-component decay:

$$G(\tau) = \frac{1}{N} \left[\left(1 + \frac{\tau}{\tau_D}\right)^{-1} \left(1 + \frac{\tau}{S^2\tau_D}\right)^{-1/2} \right] \quad (4)$$

or a two-components decay:

$$G(\tau) = \frac{1}{N} \left[f_1 \left(1 + \frac{\tau}{\tau_{D1}}\right)^{-1} \left(1 + \frac{\tau}{S^2\tau_{D1}}\right)^{-1/2} + (1 - f_1) \left(1 + \frac{\tau}{\tau_{D2}}\right)^{-1} \left(1 + \frac{\tau}{S^2\tau_{D2}}\right)^{-1/2} \right] \quad (5)$$

where N is the average number of fluorescent molecules detected inside the confocal volume ($N = CV$, with $V = \pi^{3/2}w_0^3S$ and C the concentration), f_1 is the percentage of the contribution of $\tau_{D,1}$ to the total decay time, $\tau_{D,i}$ are the decay times, and $S = z_0/w_0$ is the ratio between the axial and the lateral dimensions of the confocal volume, determined through the calibration procedure with Alexa 568. The diffusion coefficients D_i of the labeled species can be determined by:

$$\tau_{D,i} = \frac{w_0^2}{4D_i} \quad (6)$$

The hydrodynamic radii of labeled H-PVA, L-PVA and PVP were calculated through the Stokes-Einstein equation.

Rheology. Rheology measurements were performed by using a Discovery HR-3 rheometer from TA Instruments (40 mm diameter parallel plate geometry), equipped with a Peltier temperature control system. Amplitude and frequency sweeps were performed on 40 mm diameter gel disks (thickness of 2 mm ca.), while flow curves were acquired on pre-gel solutions, at constant temperature (25°C). The Linear Viscoelastic Range was identified through amplitude sweep tests,

performed at 1 Hz of frequency, with oscillation strain ranging between 0.01 and 50%. The linear viscoelastic range, identified in the amplitude sweeps, lies between strains of 0.01-10 % for the cryogels. Frequency sweeps curves were thus recorded within this range, at constant oscillation strain (1 %), by increasing the oscillation frequency (0.1-100 Hz). Data of the storage moduli, G' , at 1 Hz, are plotted against the effective polymer concentration in the network (obtained either by the fraction of “reacted bonds” of percolation theory, or by $G\%$ data) in the *Gelation Mechanism* Section. G' values are averages of three-five measurements.

Nuclear Magnetic Resonance (NMR). NMR experiments were performed on a Bruker Avance Spectrometer operating at the frequency of 400 MHz for ^1H in $\text{DMSO-}d_6$. The signal due to residual proton of the solvent was used as internal reference. The amount of semi-interpenetrated polymer after washing and storage in water (2 months) was calculated for i(2)-PVA, i(3)-PVA, i(4)-PVA and i(5)-PVA samples by comparing the signals due to residual esters moieties of L-PVA with alcohols' $-\text{CH}-$ of L-PVA and H-PVA, according to the following equation:

$$\frac{L - PVA (wt)}{H - PVA (wt)} = \frac{\left(\frac{I_{1.9-2.1}}{3 \times (1 - HD_{L-PVA})} \times MW_{L-PVA} \right)}{\left[\left(\frac{I_{1-1.7}}{2} - \frac{I_{1.9-2.1}}{3 \times (1 - HD_{L-PVA})} \right) \times MW_{H-PVA} \right]} \quad (7)$$

where $I_{1.9-2.1}$ and $I_{1-1.7}$ indicate the peaks areas due to the 3 acetate's hydrogens (present in L-PVA only) and the 2 vinyl hydrogens (present in both H-PVA and L-PVA), respectively; HD is the hydrolysis degree of L-PVA; MW_{L-PVA} MW_{H-PVA} are the average molecular weights of H-PVA and L-PVA monomers, respectively. Assessment of residual PVP in i(2)-PVP, i(3)-PVP, i(4)-PVP and i(5)-PVP gels was attempted following a similar procedure and, though a trend can be identified, exact quantification was not possible because of its very low amount (less than 6 wt% with respect to H-PVA).

RESULTS AND DISCUSSION

L-PVA and PVP as porogens: the morphology of cryogels. Freezing a PVA solution leads to a water-polymer phase separation, allowing the formation of polymer crystals in the polymer-dense areas and ice in the water-rich areas; ice crystals will serve as porogens, while polymer crystals are the network physical crosslinks.³⁰ Therefore, the porosity of PVA cryogels is linked to the shape of ice crystals, and it can be influenced by the presence of semi-interpenetrating polymers¹. Confocal images of PN_X, i-PVA_X and i-PVP_X gels (H-PVA concentration, X = 5-12 % w/v), swollen in an aqueous Rhodamine 110 solution, are shown in fig. 1. PN samples are strongly anisotropic: the elongated, needle-shaped porosity of the PN series can be ascribed to the crystallization of ice in aligned needles, on surfaces perpendicular to the direction of freezing.^{1,31-33} This results in a linear ordering of the gel structure, where straight gels strands are interspersed with elongated pores. Directionality involves larger areas of the gels as X increases. In i-PVA series, gel walls still show a preferential orientation for X = 5 and X = 7, while for higher X values the network changes into a sponge-like structure: pores become almost spherical. i-PVP_X gels, for X = 5 and X = 7, do not show a high degree of local order: pores have random shapes and a wide size distribution, while the gel walls are thicker.

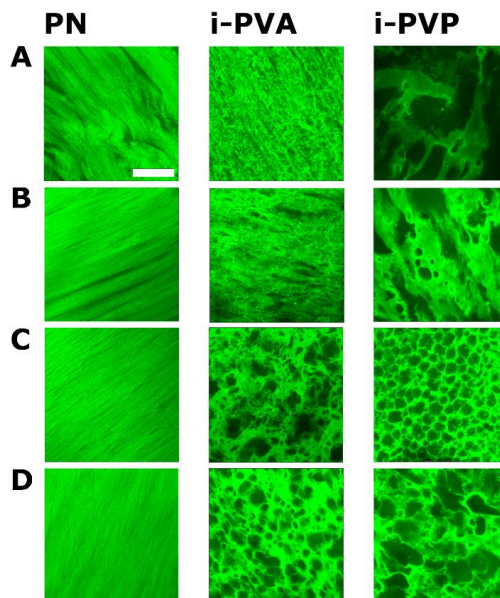


Figure 1. Confocal images of PN, i-PVA and i-PVP gels for different H-PVA concentrations: (A) X = 5; (B) X = 7; (C) X = 9; (D) X = 12. Gels were soaked in a Rhodamine 110 solution. Scalebar: 50 μm .

Overall, these gels are strongly inhomogeneous and completely different from all the others. For higher values of X, also in this case, pores become more spherical. In both i-PVA and i-PVP series, porosity drastically changes in passing from X = 7 to X = 9. However, pores in i-PVP₉ appear as not interconnected, in contrast with the sponge-like morphology of i-PVA₉.

More generally, fig. 1 suggests that, in i-PVA_X and i-PVP_X series, ice pockets formed during freezing have different shapes with respect to PN gels. As a matter of fact, pore shape and dimension are also a result of the morphology of the pre-gel solutions. In a recent work¹ we found that the structural changes in H-PVA cryogels, induced by the addition of L-PVA, can be traced

back to a polymer-polymer segregation occurring in aqueous solution, before freezing. In that case, L-PVA concentrated in spherical blobs, which acted as porogens during cryostructuring. Confocal images of i-PVP gels suggest that a similar phase behavior might occur also in i-PVP pre-gel solutions. To confirm these hypotheses, morphologies of i-PVA and i-PVP pre-gel solutions were investigated through confocal imaging. Pre-gel solutions of i-PVA and i-PVP series, for $X = 5 - 12$, were prepared using RBITC-labeled L-PVA and PVP: confocal images acquired at room temperature are shown in fig. 2.

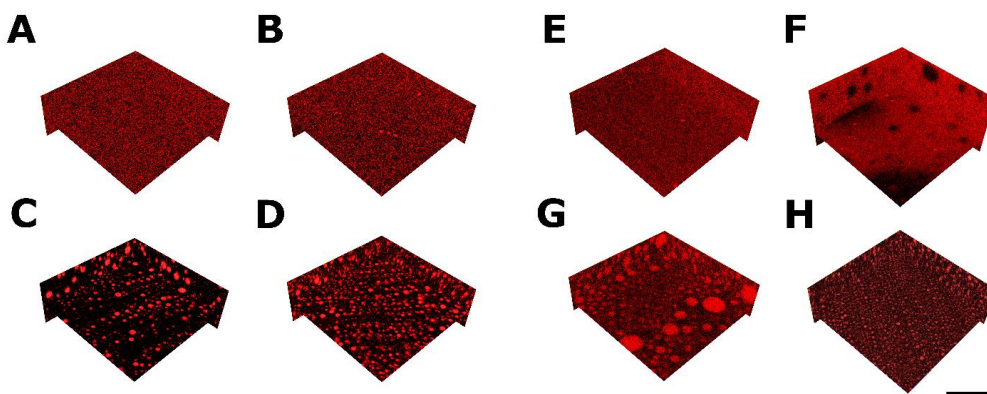


Figure 2. Confocal images of RBITC-labeled i-PVA₅₋₁₂ (A-D) and i-PVP₅₋₁₂ (E-H) pre-gel solutions. Scalebar: 50 μm .

Phase-separation is visible in both i-PVA and i-PVP series. In i-PVA series, it is incipient for $X = 7$ (fig. 2 B), while blobs form in i-PVA₉ and i-PVA₁₂ samples (fig. 2 C and D, respectively). In i-PVP series, phase separation is evident for all values of X : in i-PVP₅ and i-PVP₇ (fig. 2 E and F, respectively) there are H-PVA-rich areas and PVP-rich areas, while, also in this case, blobs form for i-PVP₉ and i-PVP₁₂ (fig. 2 G and H, respectively).

Polymer blobs are expected to affect the shape and dimension of pores, once the solution is freeze-thawed and the gel is obtained. Confocal images of gels after thawing, containing red-labeled L-PVA and PVP, are shown in fig. S1. As expected, during freezing, the blobs of L-PVA and PVP deformed and enlarged, due to the stress impressed by the freezing of water. After thawing, they have the same shapes and dimensions of the pores observed in fig. 1. Therefore, it can be inferred that both L-PVA and PVP acted as porogens during cryostructuration.

Fig. 2 and fig. S1 prove that, in both H-PVA – L-PVA and H-PVA – PVP aqueous solutions, phase segregation occurs; therefore, some degree of incompatibility should exist among the two polymer pairs.

PVAs with hydrolysis degree (HD) > 80 % are known to be water-soluble polymers^{34,35}. When we investigated the phase behavior of solutions containing both H-PVA and L-PVA, we found incompatibility for concentrations of polymers (H-PVA/L-PVA ratio of 3:1) equal or higher than 12% w/w, in the range from 5 to 100 °C: spherical blobs of L-PVA formed in the continuous H-PVA phase. Blobs were detectable also for concentrations of 9 and 7 % w/w, but only above 60°C and 70°C¹.

Polymer-polymer incompatibility can be influenced by the conformation of polymer chains in solution. Lewandowska *et al.*³⁶ reported about the thermodynamic and hydrodynamic interactions among polymer chains of PVA with higher (98-99%) and lower (85-87%) HD in aqueous solution. They demonstrated that, even though water is a good solvent for both polymers (Flory parameters for the polymer-water interaction are reported to be 0.465 for highly-hydrolyzed PVA and 0.485 for partially-hydrolyzed PVA), PVA with high HD tends to self-associate in aqueous solution. Thus, concentrated solutions of highly hydrolyzed PVAs are not stable: they form physical

networks, because of the tendency of this type of PVA to crystallize. On the other hand, aqueous solutions of partially hydrolyzed PVAs are more stable, due to the presence of acetates and the subsequent lower tendency to self-associate. The hydrodynamic radii of the labeled H-PVA and L-PVA, in dilute solutions, were calculated from FCS data (fig. S2 and Table S1): H-PVA radius is slightly larger, being 12 nm ca., while L-PVA radius is 9 nm ca. In light of the previous arguments, H-PVA – L-PVA segregation could be due to L-PVA collapsed conformation and to H-PVA preferential self-interaction.

The inter- and intra-molecular H-bonds³⁴ forming between H-PVA chains result in a pronounced shear thinning behavior, which is enhanced when the solutions are subjected to steady shear³⁷ or when the polymer concentration increases³⁸. Both i-PVA and i-PVP concentrated pre-gel solutions showed shear-thinning behavior (see fig. S3), that increases with H-PVA (X) concentration. H-PVA chains preferential orientation can also be deduced from the PN series in fig.1 and from fig. 2 D, H, where L-PVA and PVP blobs are placed in linear arrays.

However, it is worth noting that i-PVA_15 pre-gel solution is more viscous and displays a more evident shear thinning than i-PVP_15 pre-gel solution (fig. S3): this suggests that PVP is a better plasticizer than L-PVA.

PVP is a water-soluble polymer, as well. H-PVA – PVP interactions should be favored (negative values of $\chi_{PVP-PVA}$ are reported in the literature^{39,40}). In fact, PVA – PVP blends are usually described as homogeneous mixtures with a single glass transition temperature, and the two polymers are considered as compatible.^{41–46} However, their mutual miscibility decreases as the HD of PVA increases.⁴¹

PVP chains, as opposed to those of L-PVA, are not collapsed in aqueous solution (the reported Flory parameter for the water-polymer interaction is 0.5 – 0.6 at room temperature, for low- and medium-molecular weight PVPs^{47,48}). The hydrodynamic radius of a single PVP chain at room temperature, obtained by FCS data (fig. S2 and Table S1), is 25 nm ca.

The phase-behavior of H-PVA – PVP mixtures was also investigated (fig. S4): polymer-polymer demixing is slower with respect to the H-PVA – L-PVA case. Only low temperatures (5 °C) induce a faster demixing. However, 1 day-aged solutions showed PVP spherical blobs, for sufficiently high X (H-PVA conc.) values. The blob-phase in i-PVP mixtures is unstable: within few weeks at room temperature, a poorly viscous, PVP-rich phase floats on a H-PVA, gelled phase, suggesting that water is preferentially located in the PVP phase. Conversely, i-PVA mixtures remain stable for months, even if blobs enlarge either for Oswald ripening or because L-PVA is further expelled from the continuous phase. This is probably due to L-PVA blobs exposing -OH groups to the H-PVA continuous phase.

To sum up, both H-PVA – L-PVA and H-PVA – PVP phase separations are driven by the tendency of H-PVA chains to interact with themselves. However, in i-PVA solutions, the collapsed conformation of L-PVA chains also plays an important role in determining the polymer-polymer segregation. On the other hand, when the highly hydrophilic PVP is expelled from the H-PVA continuous phase, it brings with it a significant amount of water: this further concentrates the H-PVA phase, until a mild physical gelation is achieved when the mixture completely separates in two phases.

Physico-chemical properties and structure at the nanoscale. In PVA cryogels, the gelation process is driven by the water-polymer phase separation: the concentration of crystallizable

polymer chains (i.e., preferentially H-PVA chains¹) in restricted areas of the samples facilitates the formation of polymer crystals. Therefore, a higher H-PVA concentration (X) in the pre-gel solution usually leads to a higher crystallinity.⁴⁹

The presence of semi-interpenetrating polymer chains is expected to influence the cryostructure process at the nanoscale, as it could alter PVA chains ordering and ability to crystallize. As a result, gel would be more loosely structured and a higher quantity of non-structural polymer chains would be extracted during washing in water.

Crystallinity degrees of the investigated cryogels are listed in Table 1. Crystallinity of gels after thawing, X_c AT, increases with X for all the series. In presence of L-PVA or PVP, X_c AT decreases. Specifically, X_c AT is lower for i-PVA_3-7 and for i-PVP_3-9, while it approximates PN series values for higher X.

X_c AT values indicate that the presence of a semi-interpenetrating polymer hinders H-PVA crystallization during the freezing step, and this effect is maximized for low concentrations of H-PVA. PVP has a stronger impact than L-PVA on H-PVA ability to crystallize.

When thawed gels are swollen and stored in water, non-trapped polymer chains are extracted and a “second crystallization” may occur⁵⁰. The effects of the second crystallization are stronger in both i-PVA and i-PVP series: the chains of the semi-interpenetrated polymers are expected to be preferentially extracted during washing. Consequently, the chains actively involved in the network (mainly H-PVA chains) stretch and interact more with each other, to form new crystallites. In general, the crystallinity of the washed gels, X_c AW, shows the same trend of X_c AT: it is higher for PN and i-PVA with respect to i-PVP series.

Table 1. Crystallinity degree right after thawing (X_c AT) and after washing (X_c AW), Swelling Ratio (q_v) and Gel Fraction (G%) of PN, i-PVA and i-PVP cryogels. Values and relative standard deviations are listed.

X	PN_X				i-PVA_X				i-PVP_X			
	X_c AT	X_c AW	q_v	G%	X_c AT	X_c AW	q_v	G%	X_c AT **	X_c AW	q_v	G%
3	21 ± 3	--	--	--	14 ± 1	--	--	18 ± 1	N.A.	--	--	--
5	26 ± 1	34 ± 1	--	27 ± 1	17 ± 2	35 ± 1	--	21 ± 1	9 ± 3	19 ± 2	2.51	59 ± 1
7	32 ± 2	35 ± 2	1.40	29 ± 1	22 ± 1	36 ± 1	2.40	18 ± 7	11 ± 3	26 ± 6	1.40	38 ± 1
9	30 ± 1	35 ± 1	1.77	29 ± 8	27 ± 1	38 ± 1	2.15	27 ± 1	15 ± 2	26 ± 6	1.37	41 ± 2
12	33 ± 1	41 ± 5	1.90	30 ± 4	26 ± 1	39 ± 3	2.04	28 ± 1	30 ± 1	33 ± 1	1.48	41 ± 1
15	36 ± 1	--	--	38 ± 3	30 ± 1	--	--	35 ± 1	31 ± 1	--	--	--

**Data for i-PVP series before washing are indicative.

Active chains in a network can be quantified by calculating the gel fraction (G%), i.e. the fraction of polymer that is not extracted after washing. They play a major role in determining gel elasticity and the swelling ability (quantified through the equilibrium volume swelling ratio, q_v). G% and q_v for the washed samples are reported in Table 1. G% increases with X in all the series. The gel fraction of i-PVP samples is the highest. On the other hand, L-PVA destabilizes i-PVA_5 and i-PVA_7 samples, while it does not affect the G% of higher X gels.

The values of q_v show that L-PVA facilitates gels swelling for all X values. PVP, conversely, increases gels elasticity (see i-PVP_9 and i-PVP_12 in Table 1).

To sum up, L-PVA impacts the crystallinity of thawed gels, and facilitates swelling; after washing, crystallinity values are not significantly different from those of PN series. PVP, on the other hand, strongly influence the crystallinity of both thawed and washed gels. i-PVP gels contain more active polymer chains: this results in a higher elasticity of the final network and in a lower q_v for $X > 5$.

Overall, gels physico-chemical properties suggest that i-PVP gels are more rigid (higher G% and lower swelling ability q_v), even though their degree of crystallinity, X_c , is lower than those of i-PVA and PN networks with the same H-PVA concentration. Therefore, crystallization is not the only significant contribution to the i-PVP gels structuration.

Further information on gels crystallinity and polymer chains organization were obtained through Small Angle X-ray Scattering (SAXS). SAXS curves of the thawed gels PN_5-12, i-PVA_5-12, i-PVP_5-12 (fig. 3) were fitted according to Eq. 3; fitting parameters are listed in Table 2.

The correlation length, ξ , is a characteristic length describing polymer chains in the liquid-like portions of the networks; ξ values decrease linearly along PN and i-PVA series, suggesting that the gel walls become more crowded by increasing H-PVA concentration. However, ξ values of i-PVA gels are generally lower with respect to PN gels, as L-PVA chains are probably causing local crowding. An abrupt change in ξ (from 4.7 to 3.4 nm) occurs in passing from i-PVA_7 to i_PVA_9, as if chains crowding increased suddenly: this probably results from the increase of H-PVA concentration in the continuous phase, when L-PVA blobs form.

ξ values of i-PVP series are close to those of i-PVA_9,12 gels and do not show significant variations with X. This suggest that, as for i-PVA gels, H-PVA chains are crowded in the gel walls;

however, chains conformations are not influenced by higher concentrations of H-PVA, probably because a limiting value for the system was reached. Such low values of ξ have been previously obtained for cryogels that underwent 3 FT cycles, i.e., for very high local polymer concentrations.¹

The values of crystallites radius, R , increase with X for PN and i-PVA series. In fact, higher H-PVA concentration implies that polymer crystallites are more likely to form. In i-PVA series, the abrupt change between i-PVA_7 and i-PVA_9 is again clearly visible: crystallites radius becomes almost 1 nm larger, confirming that polymer crowding abruptly increases from $X = 7$ to $X = 9$.

Concerning i-PVP series, R follows the opposite trend: it decreases when X increases; these data look in contrast with the values of the $G\%$ and the increased rigidity of the i-PVP gels observed by increasing X . As stated above, H-PVA crystallization is not the only contribution to the structuration of i-PVP gels. SAXS results further suggest that H-PVA crystallites are smaller when H-PVA concentration in solution increases. In this light, we suggest that the structuration of i-PVP gels is only partially due to freezing. In fact, when the pre-gel solutions are stored at -18°C , the H-PVA – PVP phase separation is enhanced: the PVP phase contains a significant amount of water, due to the polymer hydrophilicity, while the H-PVA phase further expels water, as H-PVA self-interactions increase. As a result, H-PVA concentration in the continuous phase increases to the point that the physical gelation (i.e. formation of polymer crystals and glassy areas) starts before the effects of freezing become significant. When ice crystals finally form, they consolidate the preformed structure, causing the formation of some additional H-PVA crystallites whose dimensions decreases as H-PVA concentration increases.

In conclusion, i-PVP gels are less crystalline than their i-PVA counterparts, but more rigid, as they result from two different mechanisms, occurring at low temperatures, that subtract water to the H-

PVA phase: the polymer-polymer phase separation, that forms water-rich PVP blobs; and the water-polymer phase separation, which causes the H-PVA phase to expel water, in order to allow the H-PVA crystallization.

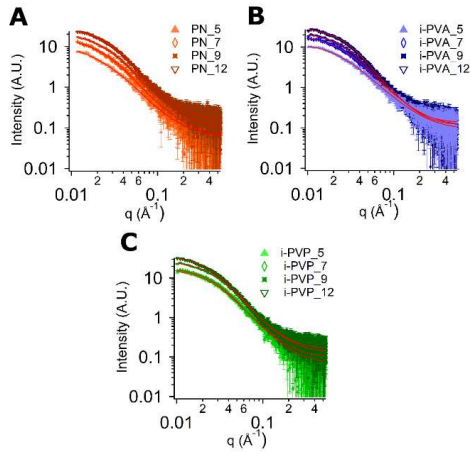


Figure 3. SAXS curves of PN (A), i-PVA (B) and i-PVP (C) thawed gels.

Further proofs are provided by $I_G(0)/I_L(0)$ ratio, i.e. an indication of the extension of crystalline portions in a sample. The ratio confirms that the number of crystallites increases with H-PVA concentration in PN and i-PVA gels, while, in i-PVP series, it increases from i-PVP_5 to i-PVP_7, but then stabilizes to a limiting value for i-PVP_7-12.

Table 2. SAXS fitting parameters obtained for PN_5-12, i-PVA_5-12 and i-PVP_5-12 cryogels.

Sample	Guinier Scale $I_G(0)$	Lorentz Scale $I_L(0)$	$I_G(0)/I_L(0)$	Correlation Length (nm)	Fractal Dimension (D)	Crystallites Radius R (nm)	Background (B)
PN_5	0.3	5.5	0.05	5.7 ± 0.8	2.1 ± 0.1	3.9 ± 0.2	0.06

PN_7	0.9	6.9	0.13	5.4 ± 0.8	2.2 ± 0.1	5.0 ± 0.1	0.06
PN_9	2.6	11	0.24	5.2 ± 0.8	2.1 ± 0.1	5.1 ± 0.1	0.09
PN_12	4.1	14	0.29	4.9 ± 0.4	2.2 ± 0.1	5.2 ± 0.1	0.14
i-PVA_5	0.4	8.1	0.05	4.7 ± 0.1	2.1 ± 0.1	5.3 ± 0.4	0.09
i-PVA_7	2.2	14	0.16	4.6 ± 0.1	2.2 ± 0.1	5.1 ± 0.2	0.11
i-PVA_9	2.0	12	0.17	3.4 ± 0.1	2.6 ± 0.1	6.2 ± 0.2	0.13
i-PVA_12	4.8	15	0.32	3.3 ± 0.1	2.7 ± 0.1	5.9 ± 0.2	0.12
i-PVP_5	1.4	11	0.13	3.6 ± 0.1	2.5 ± 0.1	5.8 ± 0.2	0.10
i-PVP_7	3.1	13	0.24	3.7 ± 0.1	2.4 ± 0.1	5.4 ± 0.1	0.07
i-PVP_9	3.3	14	0.24	3.7 ± 0.1	2.5 ± 0.1	5.2 ± 0.1	0.13
i-PVP_12	3.2	18	0.18	4.3 ± 0.1	2.5 ± 0.1	4.8 ± 0.1	0.16

The fractal dimension, D , of PN_5-12 and i-PVA_5,7 is similar to the fractal dimension of a polymer solution in semi-dilute regime. In fact, when D is about 2, the first term of the fitting equation takes the form of the Ornstein-Zernicke equation. Higher D values (2.7 – 2.9), instead, characterize systems containing a significant number of H-bonds.⁵² This is the case of i-PVA_9 and i-PVA_12 samples.

L-PVA and PVP as structuring agents. The enhanced H-PVA self-interaction induced by polymer-polymer demixing in i-PVA series, and the higher G% and network rigidity in i-PVP series, suggest that the two semi-interpenetrating polymers have a structuring role. Therefore, the

influence of increasing concentrations of L-PVA or PVP in gels prepared at a constant H-PVA concentration ($X = 9\%$ w/v) were investigated.

The G' (1 Hz) data for i(Y)-PVA and i(Y)-PVP thawed gels are reported in fig. 4, in log-log scale, as a function of the concentration of the semi-interpenetrating polymer added. The first point in each series represents the G' value in absence of L-PVA or PVP (i.e., PN_9 sample).

Both L-PVA (fig. 4 A) and PVP (fig.4 B) cause an increase in the storage modulus of H-PVA gels, until a 3% w/v concentration is reached. However, the structuring effect of L-PVA is lower: G' reaches a plateau value when L-PVA concentration is 1% w/v. In presence of PVP, instead, G' increases continuously, up to a PVP concentration of 3% w/v. For higher concentrations, both polymers act as plasticizers, and G' drops.

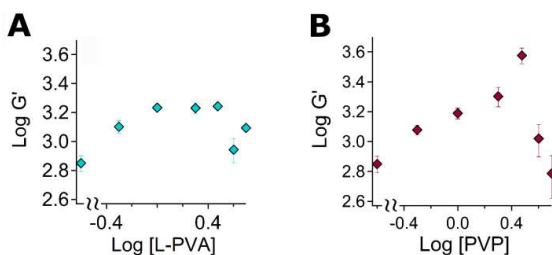


Figure 4. Log-log plots of the storage modulus, G' (1 Hz), versus the semi-interpenetrating polymer concentrations in i(Y)-PVA and i(Y)-PVP gels. A) Effect of increasing concentrations of L-PVA ($Y = 0.5, 1, 2, 3, 4, 5\%$ w/v) on a 9% w/v H-PVA solution. B) Effect of increasing concentrations of PVP ($Y = 0.5, 1, 2, 3, 4, 5\%$ w/v) on a 9% w/v H-PVA solution. The first point in both series represents a pure H-PVA gel (i.e., it is the G' of PN_9 sample).

The point of gelation of H-PVA in i-PVA and i-PVP mixtures, evaluated for L-PVA and PVP concentrations of 3% w/v (see fig S5), further confirms that PVP hinders H-PVA crystallization: while H-PVA alone forms a gel at 1.4 % w/v, i-PVP solutions become gels for a H-PVA

concentration of 2% w/v. i-PVA solutions form a gel when H-PVA concentration is at least 1%, confirming that L-PVA favors H-PVA self-interaction; nonetheless, some L-PVA chains could take part to the cryostructuration process, when present in such excess (H-PVA = 1% w/v, L-PVA = 3% w/v).

The persistence of L-PVA chains in i(3)-PVA gel, after storage in water, was already proven¹ through Confocal Microscopy. However, NMR data (see fig. S6 A) suggest that the amount of L-PVA permanently embedded in i(Y)-PVA networks is almost independent on the concentration of L-PVA in the pre-gel solution: for a given and sufficiently high concentration of H-PVA, residual L-PVA tends to a constant quantity. Such quantity could be related to the H-PVA - L-PVA interactions in the pre-gel solutions. Conversely, NMR analysis of i(Y)-PVP samples (fig. S6 B) revealed that a negligible amount of PVP is retained during washing, and only a minor trend in its concentration can be identified in good correlation with rheological data. These data support the hypothesis of PVP having only an “indirect” structuring effect, mainly due to its ability to subtract water from the H-PVA phase, before cryostructuration takes place.

Gelation mechanism. The impact of a semi-interpenetrating agent on the cryogel structuration can be quantified through rheology measurements, and specifically by observing the dependence of the storage modulus, G' , on the concentration of polymer constituting the network. G' represents the material elastic response to a certain stress applied and, according to the theory of rubber elasticity, it is proportional to the number of “active chains” in the network, i.e. the polymer chains whose ends are blocked in tie-points⁵³.

The gelation process can often be described through the percolation model.⁵⁴ According to percolation, G' is related to the fraction of reacted bonds, p , through: $G' \propto (p - p_c/p_c)^n$, where p_c is the critical value of p to obtain an infinite cluster (i.e., the gelation threshold).

For gels well beyond the gelation threshold and swollen in good solvents, the system can be considered a semi-dilute solution of polymer chains, and both G' and the osmotic pressure scale as: $G' \propto C^n$, where C is the polymer concentration and $n = 2.25$ ⁵⁴. However, the 2.25 exponent is generally more accurate to describe osmotic pressure, rather than rheology results, owing to the difficulties in preparing series of gels with negligible defects⁵⁵.

Experimental values of n usually range from 1.9 to 3.5^{56,57}. For PVA cryogels, $n = 2.4-3.8$ have been reported.⁵⁸⁻⁶⁰

PN, i-PVA and i-PVP gels were rheologically tested right after thawing and after washing (fig. 5), to verify the changes caused by the second crystallization process. G' data are reported as a function of $\frac{C_{H-PVA}}{C_g} - 1$. Values of the exponent n are reported in Table 3. Effective polymer concentrations in the washed gels were also calculated, considering the gel fraction, $G\%$, of each sample after washing (see Table 1).

In the PN series (fig. 5 A), only G' of PN_5 changed significantly after washing (structural defects caused massive loss of polymer chains). The fitting of the points describing the thawed gels is in agreement with a percolation mechanism (see Table 3).

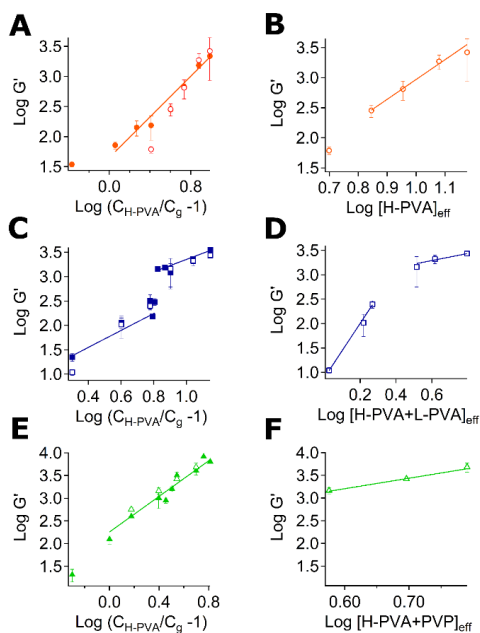


Figure 5. Log-log plots of the storage modulus (G' , 1 Hz) versus the effective concentration of polymer for the three series. A), C) and E) show the trend of G' for PN, i-PVA and i-PVP gels right after thawing (full markers) and after washing (empty markers), versus the effective H-PVA concentration, obtained from the gelation threshold. B), D) and F) show the trend of G' of some gel samples of each series after washing versus the effective polymer fraction constituting the networks, calculated using $G\%$ values.

When the gels are washed, and the effective polymer concentration is considered (fig. 5 B), the curve slope drastically increases; this is probably due to the fact that networks containing lower amounts of H-PVA have more structural defects (like dangling chains or instable polymer crystallites), thus washing causes their G' to decrease more.

The slope of i-PVP thawed gels (fig. 5 D) is also in accordance with a percolation mechanism, suggesting that the presence of PVP does not significantly alter H-PVA gelation mechanism (the

point with the lowest X was not considered in the fitting because of its very weak gel state). The slope describing the washed i-PVP series (fig. 5 E), instead, is in agreement with that of gels swollen in good solvent, $n = 2.25$.⁵⁴ This suggests that i-PVP gels are more stable (i.e. the structural defects are not significantly affecting the rheological response).

Table 3. Values of the exponent n obtained for the gels after thawing, AT (see fig. 5 A, C, E), considering the gelation point, and the gels after washing, AW (see fig. 5 B, D, F), considering the effective concentration of polymer constituting the network.

Series	n (AT)	n (AW)	n (JM model)	
PN	1.69 ± 0.06	3.3 ± 0.5	-	-
i-PVA	1.7 ± 0.1	5.6 ± 0.4	2.2 ± 0.2	1.1
	1.3 ± 0.1	0.7 ± 0.4	1.4 ± 0.1	0.9
i-PVP	1.96 ± 0.02	2.3 ± 0.5	-	-

The G' VS $\frac{c_{H-PVA}}{c_g} - 1$ trend drastically changes when networks containing a constant concentration of L-PVA are considered (fig. 5 C, D). The curves describing both thawed and washed gels of i-PVA series are characterized by two regimes.

Gelation occurring in two different regimes was already observed⁶¹, and can be justified on the basis of the Jones-Marques (JM) theory. Guenet⁶² adapted this model to the physical gelation processes characterizing fibrillar gels. He described fibrillar gels as thermoreversible networks, obtained by the connection of straight fibrils (cross-section of 2-20 nm), with micron-sized pores. PVA chains do not form fibrils in solution, that associate to build a network. However, a PVA cryogel can be described as an array of rigid objects connecting at junctions, due to the high

directionality given by both the self-association of H-PVA chains in solution and the freezing step; in fact, cryogels have already been defined fibrillar networks.^{60,63,64} Clearly, the morphology of these gels is complex and the fibrillar description is not exhaustive, but it can be used as a starting point to shed light on the gels formation mechanism.

The presence of two regimes in the G' VS [H-PVA] data for i-PVA series (see fig. S7 and Table 3) can be explained considering then presence of dangling polymer chains at lower H-PVA concentrations, which are gradually incorporated in the network when polymer concentration increases. More specifically, a transition from enthalpic elasticity, due to rigid tie-points, to entropic elasticity, due to “freely-hinged” junctions (i.e., some rotational freedom is retained after crosslinks formation) occurs. According to JM theory, the exponent n can be related to a longitudinal fractal dimension (D_F), i.e. the fractal dimension of objects at junctions: $n = (3 + D_F) / (3 - D_F)$ for enthalpic elasticity, while $n = 3 / (3 - D_F)$ for entropic networks. The values of calculated for i-PVA series are reported in Table 3. Both values are ~ 1 , indicating the presence of straight elements. D_F decreases when H-PVA concentration increases, suggesting that gel strands contain more defects for $D_F = 1.1$ (low X values), which smooth as H-PVA concentration increases and dangling chains are included in the network.

Evidences to support this hypothesis can be obtained by observing the morphology and shape of gel strands in the gel series at two different H-PVA concentration, through SEM.

Fig. 6 shows the SEM images obtained for two illustrative samples of each series ($X = 5$ and $X = 12$), after curing in water. For i-PVA series, defined linear strands are clearly visible in i-PVA_12 (fig. 6 D), while i-PVA_5 is characterized by more irregular objects (fig. 6 C): linear strands are still visible, but they present high surface roughness. These findings are in agreement with the

fractal dimensions obtained through Jones-Marques theory: $D_F \sim 1$ for i-PVA_12 and $D_F > 1$ for i-PVA_5 describe straight and smooth strands in the first case, and linear strands with some surface irregularity in the latter.

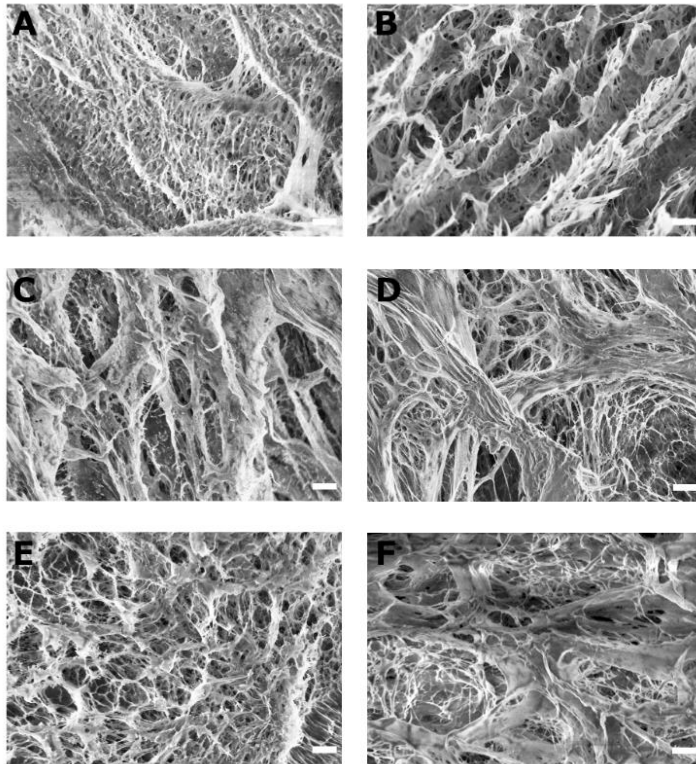


Figure 6. SEM images obtained for: (A) PN_5, (B) PN_12, (C) i-PVA_5, (D) i-PVA_12, (E) i-PVP_5, (F) i-PVP_12 samples. Scale bar is 1 μm .

In PN (fig. 6 A, B) and i-PVP series (fig. 6 E, F) gel defects are almost absent, even if some structure refinement occurs when H-PVA concentration increases.

CONCLUSIONS

In this paper, the role of L-PVA and PVP as semi-interpenetrating agents in PVA-based cryogels was investigated. Confocal micrographs revealed that the gels morphology and the pores shapes and dimensions are caused by a polymer-polymer demixing, occurring in H-PVA – L-PVA and H-PVA – PVP pre-gel solutions; L-PVA and PVP concentrate in specific areas of the solutions, acting as porogens during cryostructuration. The phase separation also concentrates H-PVA in the continuous phase: this results in higher crystallinity and structuration for gels containing L-PVA. Conversely, PVP alters the cryostructuration of H-PVA: being highly hydrophilic, it favors water expulsion from the H-PVA continuous phase at low temperature; this results in the formation of a highly concentrated H-PVA phase, which forms a physical gel that is only consolidated by the FT process. The resulting networks have higher G% and stiffness, but lower crystallinity. As regards the gelation process, gels containing H-PVA or H-PVA and PVP seem to form according to a percolation mechanism. H-PVA – L-PVA gels, instead, showed two different regimes and can possibly be described as fibrillar networks, according to the Jones-Marques theory. Overall, semi-interpenetrating agents impact the gels structure, porosity and physico-chemical properties, acting both as porogens and structuring agents. A better understanding of polymer-polymer interaction in the pre-gel solutions of different polymer pairs could allow us to predict the final gel properties, making possible the tailoring of gels for specific cleaning tasks.

References

- (1) Mastrangelo, R.; Chelazzi, D.; Poggi, G.; Fratini, E.; Buemi, L. P.; Petruzzellis, M. L.; Baglioni, P. Twin-Chain Polymer Hydrogels Based on Poly(Vinyl Alcohol) as New Advanced Tool for the Cleaning of Modern and Contemporary Art. *Proc. Natl. Acad. Sci.* **2020**. <https://doi.org/10.1073/pnas.1911811117>.
- (2) Baglioni, M.; Guaragnone, T.; Mastrangelo, R.; Sekine, F. H.; Ogura, T.; Baglioni, P. Nonionic Surfactants for the Cleaning of Works of Art: Insights on Acrylic Polymer Films Dewetting and Artificial Soil Removal. *ACS Appl. Mater. Interfaces* **2020**, *12* (23), 26704–26716. <https://doi.org/10.1021/acsami.0c06425>.
- (3) Baglioni, P.; Chelazzi, D. *Nanoscience for the Conservation of Works of Art*; Royal Society of Chemistry, 2015.
- (4) Baglioni, P.; Dei, L.; Carretti, E.; Giorgi, R. Gels for the Conservation of Cultural Heritage. *Langmuir* **2009**, *25* (15), 8373–8374. <https://doi.org/10.1021/la900961k>.
- (5) Domingues, J. A. L.; Bonelli, N.; Giorgi, R.; Fratini, E.; Gorel, F.; Baglioni, P. Innovative Hydrogels Based on Semi-Interpenetrating p(HEMA)/PVP Networks for the Cleaning of Water-Sensitive Cultural Heritage Artifacts. *Langmuir* **2013**, *29* (8), 2746–2755. <https://doi.org/10.1021/la3048664>.
- (6) D, C.; R, G.; P, B. Microemulsions, Micelles, and Functional Gels: How Colloids and Soft Matter Preserve Works of Art. *Angew. Chem. Int. Ed Engl.* **2018**, *57* (25), 7296–7303. <https://doi.org/10.1002/anie.201710711>.
- (7) Baglioni, M.; Domingues, J. A. L.; Carretti, E.; Fratini, E.; Chelazzi, D.; Giorgi, R.; Baglioni, P. Complex Fluids Confined into Semi-Interpenetrated Chemical Hydrogels for the Cleaning of Classic Art: A Rheological and SAXS Study. *ACS Appl. Mater. Interfaces* **2018**, *10* (22), 19162–19172. <https://doi.org/10.1021/acsami.8b01841>.
- (8) Bonelli, N.; Montis, C.; Mirabile, A.; Berti, D.; Baglioni, P. Restoration of Paper Artworks with Microemulsions Confined in Hydrogels for Safe and Efficient Removal of Adhesive Tapes. *Proc. Natl. Acad. Sci.* **2018**, *115* (23), 5932–5937. <https://doi.org/10.1073/pnas.1801962115>.
- (9) Ormsby, B.; Learner, T. The Effects of Wet Surface Cleaning Treatments on Acrylic Emulsion Artists' Paints – a Review of Recent Scientific Research. *Stud. Conserv.* **2009**, *54* (sup1), 29–41. <https://doi.org/10.1179/sic.2009.54.Supplement-1.29>.
- (10) Blumenroth, D.; Zumbühl, S.; Scherrer, N. C.; Müller, W. Sensitivity of Modern Oil Paints to Solvents. Effects on Synthetic Organic Pigments. In *Issues in Contemporary Oil Paint*; van den Berg, K. J., Burnstock, A., de Keijzer, M., Krueger, J., Learner, T., Tagle, de, Alberto, Heydenreich, G., Eds.; Springer International Publishing: Cham, 2014; pp 351–362. https://doi.org/10.1007/978-3-319-10100-2_23.
- (11) Murray, A.; Berenfeld, C. C. de; Chang, S. Y. S.; Jablonski, E.; Klein, T.; Riggs, M. C.; Robertson, E. C.; Tse, W. M. A. The Condition and Cleaning of Acrylic Emulsion Paintings. *MRS Online Proc. Libr. Arch.* **2002**, *712*. <https://doi.org/10.1557/PROC-712-III.4>.
- (12) Aut, L. M. J. author. Spongy Hydrogels Clean Rough Paintings. **2020**. <https://doi.org/10.1063/PT.6.1.20200326a>.
- (13) Bonelli, N.; Poggi, G.; Chelazzi, D.; Giorgi, R.; Baglioni, P. Poly(Vinyl Alcohol)/Poly(Vinyl Pyrrolidone) Hydrogels for the Cleaning of Art. *J. Colloid Interface Sci.* **2019**, *536*, 339–348. <https://doi.org/10.1016/j.jcis.2018.10.025>.

- (14) Mastrangelo, R.; Montis, C.; Bonelli, N.; Tempesti, P.; Baglioni, P. Surface Cleaning of Artworks: Structure and Dynamics of Nanostructured Fluids Confined in Polymeric Hydrogel Networks. *Phys Chem Chem Phys* **2017**. <https://doi.org/10.1039/C7CP02662E>.
- (15) Peppas, N. A.; Stauffer, S. R. Reinforced Uncrosslinked Poly (Vinyl Alcohol) Gels Produced by Cyclic Freezing-Thawing Processes: A Short Review. *J. Controlled Release* **1991**, *16* (3), 305–310. [https://doi.org/10.1016/0168-3659\(91\)90007-Z](https://doi.org/10.1016/0168-3659(91)90007-Z).
- (16) Stauffer, S. R.; Peppas, N. A. Poly(Vinyl Alcohol) Hydrogels Prepared by Freezing-Thawing Cyclic Processing. *Polymer* **1992**, *33* (18), 3932–3936. [https://doi.org/10.1016/0032-3861\(92\)90385-A](https://doi.org/10.1016/0032-3861(92)90385-A).
- (17) Pines, E.; Prins, W. Structure-Property Relations of Thermoreversible Macromolecular Hydrogels. *Macromolecules* **1973**, *6* (6), 888–895. <https://doi.org/10.1021/ma60036a020>.
- (18) Komatsu, M.; Inoue, T.; Miyasaka, K. Light-scattering studies on the sol-gel transition in aqueous solutions of poly(vinyl alcohol). *J. Polym. Sci. Part B Polym. Phys.* **1986**, *24* (2), 303–311. <https://doi.org/10.1002/polb.1986.090240207>.
- (19) Okay, O. *Polymeric Cryogels: Macroporous Gels with Remarkable Properties*; Springer, 2014.
- (20) Baker, M. I.; Walsh, S. P.; Schwartz, Z.; Boyan, B. D. A Review of Polyvinyl Alcohol and Its Uses in Cartilage and Orthopedic Applications. *J. Biomed. Mater. Res. B Appl. Biomater.* **2012**, *100B* (5), 1451–1457. <https://doi.org/10.1002/jbm.b.32694>.
- (21) Lozinsky, V. I.; Damshkaln, L. G.; Shaskol'skii, B. L.; Babushkina, T. A.; Kurochkin, I. N.; Kurochkin, I. I. Study of Cryostructuring of Polymer Systems: 27. Physicochemical Properties of Poly(Vinyl Alcohol) Cryogels and Specific Features of Their Macroporous Morphology. *Colloid J.* **2007**, *69* (6), 747–764. <https://doi.org/10.1134/S1061933X07060117>.
- (22) Hassan, C.; Peppas, N. Structure and Applications of Poly (Vinyl Alcohol) Hydrogels Produced by Conventional Crosslinking or by Freezing/Thawing Methods. *Biopolym. PVA Hydrogels Anionic Polym. Nanocomposites* **2000**, 37–65.
- (23) Wunderlich, B. *Thermal Analysis of Polymeric Materials*; Springer Science & Business Media, 2005.
- (24) Yazici, I.; Okay, O. Spatial Inhomogeneity in Poly(Acrylic Acid) Hydrogels. *Polymer* **2005**, *46* (8), 2595–2602. <https://doi.org/10.1016/j.polymer.2005.01.079>.
- (25) Blanton, T. N.; Rajeswaran, M.; Stephens, P. W.; Whitcomb, D. R.; Mixture, S. T.; Kaduk, J. A. Crystal Structure Determination of the Silver Carboxylate Dimer [Ag(O₂C₂H₄)₂]₂, Silver Behenate, Using Powder X-Ray Diffraction Methods. *Powder Diffr.* **2011**, *26* (4), 313–320. <https://doi.org/10.1154/1.3661981>.
- (26) Doucet, M.; Cho, J. H.; Alina, G.; Bakker, J.; Bouwman, W.; Butler, P.; Campbell, K.; Gonzales, M.; Heenan, R.; Jackson, A.; Juhas, P.; King, S.; Kienzle, P.; Krzywon, J.; Markvardsen, A.; Nielsen, T.; O'Driscoll, L.; Potrzebowski, W.; Ferraz Leal, R.; Richter, T.; Rozycko, P.; Snow, T.; Washington, A. *SasView Version 4.1.2*; Zenodo, 2017. <https://doi.org/10.5281/zenodo.825675>.
- (27) Mallam, S.; Horkay, F.; Hecht, A. M.; Rennie, A. R.; Geissler, E. Microscopic and macroscopic thermodynamic observations in swollen poly(dimethylsiloxane) networks <https://pubs.acs.org/doi/pdf/10.1021/ma00002a031> (accessed Apr 27, 2020). <https://doi.org/10.1021/ma00002a031>.

- (28) Shibayama, M.; Tanaka, T.; Han, C. C. Small Angle Neutron Scattering Study on Poly(N-isopropyl Acrylamide) Gels near Their Volume-phase Transition Temperature. *J. Chem. Phys.* **1992**, *97* (9), 6829–6841. <https://doi.org/10.1063/1.463636>.
- (29) Montis, C.; Maiolo, D.; Alessandri, I.; Bergese, P.; Berti, D. Interaction of Nanoparticles with Lipid Membranes: A Multiscale Perspective. *Nanoscale* **2014**, *6* (12), 6452–6457. <https://doi.org/10.1039/C4NR00838C>.
- (30) Hassan, C. M.; Peppas, N. A. Structure and Applications of Poly(Vinyl Alcohol) Hydrogels Produced by Conventional Crosslinking or by Freezing/Thawing Methods. In *Biopolymers · PVA Hydrogels, Anionic Polymerisation Nanocomposites*; Advances in Polymer Science; Springer: Berlin, Heidelberg, 2000; pp 37–65. https://doi.org/10.1007/3-540-46414-X_2.
- (31) Mattiasson, B.; Kumar, A.; Galeev, I. Y. *Macroporous Polymers: Production Properties and Biotechnological/Biomedical Applications*; CRC Press, 2009.
- (32) Zhang, L.; Zhao, J.; Zhu, J.; He, C.; Wang, H. Anisotropic Tough Poly(Vinyl Alcohol) Hydrogels. *Soft Matter* **2012**, *8* (40), 10439–10447. <https://doi.org/10.1039/C2SM26102B>.
- (33) Gutiérrez, M. C.; García-Carvajal, Z. Y.; Jobbágy, M.; Rubio, F.; Yuste, L.; Rojo, F.; Ferrer, M. L.; del Monte, F. Poly(Vinyl Alcohol) Scaffolds with Tailored Morphologies for Drug Delivery and Controlled Release. *Adv. Funct. Mater.* **2007**, *17* (17), 3505–3513. <https://doi.org/10.1002/adfm.200700093>.
- (34) Briscoe, B.; Luckham, P.; Zhu, S. The Effects of Hydrogen Bonding upon the Viscosity of Aqueous Poly(Vinyl Alcohol) Solutions. *Polymer* **2000**, *41* (10), 3851–3860. [https://doi.org/10.1016/S0032-3861\(99\)00550-9](https://doi.org/10.1016/S0032-3861(99)00550-9).
- (35) Marin, E.; Rojas, J.; Ciro, Y. A Review of Polyvinyl Alcohol Derivatives: Promising Materials for Pharmaceutical and Biomedical Applications. *Afr. J. Pharm. Pharmacol.* **2014**. <https://doi.org/10.5897/AJPP2013.3906>.
- (36) Lewandowska, K.; Staszewska, D. U.; Bohdanecký, M. The Huggins Viscosity Coefficient of Aqueous Solution of Poly(Vinyl Alcohol). *Eur. Polym. J.* **2001**, *37* (1), 25–32. [https://doi.org/10.1016/S0014-3057\(00\)00074-4](https://doi.org/10.1016/S0014-3057(00)00074-4).
- (37) Gao, H.; He, J.; Yang, R.; Yang, L. Characteristic Rheological Features of High Concentration PVA Solutions in Water with Different Degrees of Polymerization. *J. Appl. Polym. Sci.* **2010**, *116* (5), 2734–2741. <https://doi.org/10.1002/app.31900>.
- (38) Gao, H.-W.; Yang, R.-J.; He, J.-Y.; Yang, L. Rheological Behaviors of PVA/H₂O Solutions of High-Polymer Concentration. *J. Appl. Polym. Sci.* **2010**, *116* (3), 1459–1466. <https://doi.org/10.1002/app.31677>.
- (39) Nishio, Y.; Haratani, T.; Takahashi, T. Miscibility and Orientation Behavior of Poly(Vinyl Alcohol) / Poly(Vinyl Pyrrolidone) Blends. *J. Polym. Sci. Part B Polym. Phys.* **1990**, *28* (3), 355–376. <https://doi.org/10.1002/polb.1990.090280308>.
- (40) Ping, Z.-H.; Nguyen, Q. T.; Néel, J. Investigations of Poly(Vinyl Alcohol)/Poly(N-Vinyl-2-Pyrrolidone) Blends, 2. Influence of the Molecular Weights of the Polymer Components on Crystallization. *Makromol. Chem.* **1990**, *191* (1), 185–198. <https://doi.org/10.1002/macp.1990.021910115>.
- (41) Lewandowska, K. The Miscibility of Poly(Vinyl Alcohol)/Poly(N-Vinylpyrrolidone) Blends Investigated in Dilute Solutions and Solids. *Eur. Polym. J.* **2005**, *41* (1), 55–64. <https://doi.org/10.1016/j.eurpolymj.2004.08.016>.
- (42) Abou Taleb, M. H. Thermal and Spectroscopic Studies of Poly(N-Vinyl Pyrrolidone)/Poly(Vinyl Alcohol) Blend Films. *J. Appl. Polym. Sci.* **2009**, *114* (2), 1202–1207. <https://doi.org/10.1002/app.30082>.

- (43) Bernal, A.; Kuritka, I.; Saha, P. Preparation and Characterization of Poly(Vinyl Alcohol)-Poly(Vinyl Pyrrolidone) Blend: A Biomaterial with Latent Medical Applications. *J. Appl. Polym. Sci.* **2013**, *127* (5), 3560–3568. <https://doi.org/10.1002/app.37723>.
- (44) Bercea, M.; Morariu, S.; Teodorescu, M. Rheological Investigation of Poly(Vinyl Alcohol)/Poly(N-Vinyl Pyrrolidone) Mixtures in Aqueous Solution and Hydrogel State. *J. Polym. Res.* **2016**, *23* (7), 142. <https://doi.org/10.1007/s10965-016-1040-3>.
- (45) Teodorescu, M.; Bercea, M.; Morariu, S. Miscibility Study on Polymer Mixtures in Dilute Solution. *Colloids Surf. Physicochem. Eng. Asp.* **2018**, *559*, 325–333. <https://doi.org/10.1016/j.colsurfa.2018.09.062>.
- (46) Boonsuk, P.; Kaewtatip, K.; Chantarak, S.; Kelarakis, A.; Chaibundit, C. Super-Tough Biodegradable Poly(Vinyl Alcohol)/Poly(Vinyl Pyrrolidone) Blends Plasticized by Glycerol and Sorbitol. *J. Appl. Polym. Sci.* **2018**, *135* (26), 46406. <https://doi.org/10.1002/app.46406>.
- (47) Zaslavsky, B. Y. *Aqueous Two-Phase Partitioning: Physical Chemistry and Bioanalytical Applications*; CRC Press, 1994.
- (48) Guettari, M.; Belaidi, A.; Abel, S.; Tajouri, T. Polyvinylpyrrolidone Behavior in Water/Ethanol Mixed Solvents: Comparison of Modeling Predictions with Experimental Results. *J. Solut. Chem.* **2017**, *46* (7), 1404–1417. <https://doi.org/10.1007/s10953-017-0649-0>.
- (49) Hassan, C. M.; Peppas, N. A. Structure and Morphology of Freeze/Thawed PVA Hydrogels. *Macromolecules* **2000**, *33* (7), 2472–2479. <https://doi.org/10.1021/ma9907587>.
- (50) *Biopolymers · PVA Hydrogels Anionic Polymerisation Nanocomposites*; Springer, 2003.
- (51) Lozinsky, V. I.; Solodova, E. V.; Zubov, A. L.; Simenel, I. A. Study of Cryostructuration of Polymer Systems. XI. The Formation of PVA Cryogels by Freezing–Thawing the Polymer Aqueous Solutions Containing Additives of Some Polyols. *J. Appl. Polym. Sci.* **1995**, *58* (1), 171–177. <https://doi.org/10.1002/app.1995.070580119>.
- (52) Shibayama, M.; Kurokawa, H.; Nomura, S.; Muthukumar, M.; Stein, R. S.; Roy, S. Small-Angle Neutron Scattering from Poly(Vinyl Alcohol)-Borate Gels. *Polymer* **1992**, *33* (14), 2883–2890. [https://doi.org/10.1016/0032-3861\(92\)90072-5](https://doi.org/10.1016/0032-3861(92)90072-5).
- (53) Larson, R. G.; Larson, R. G. *The Structure and Rheology of Complex Fluids*; OUP USA, 1999.
- (54) Gennes, P.-G. *Scaling Concepts in Polymer Physics*; Cornell University Press: Ithaca, NY, 1979.
- (55) Candau, S.; Bastide, J.; Delsanti, M. Structural, Elastic, and Dynamic Properties of Swollen Polymer Networks. In *Polymer Networks*; Dušek, K., Ed.; Advances in Polymer Science; Springer: Berlin, Heidelberg, 1982; pp 27–71. https://doi.org/10.1007/3-540-11471-8_2.
- (56) Li, L.; Aoki, Y. Rheological Images of Poly(Vinyl Chloride) Gels. 3. Elasticity Evolution and the Scaling Law beyond the Sol–Gel Transition. *Macromolecules* **1998**, *31* (3), 740–745. <https://doi.org/10.1021/ma971449o>.
- (57) Sakai, T. Sol-Gel Transition. In *Physics of Polymer Gels*; John Wiley & Sons, Ltd, 2020; pp 161–171. <https://doi.org/10.1002/9783527346547.ch8>.
- (58) Takigawa, T.; Kasihara, H.; Urayama, K.; Masuda, T. Critical Behavior of Modulus of Poly(Vinylalcohol) Gels near the Gelation Point. *J. Phys. Soc. Jpn.* **1990**, *59* (7), 2598–2599. <https://doi.org/10.1143/JPSJ.59.2598>.
- (59) Takigawa, T.; Takahashi, M.; Urayama, K.; Masuda, T. Comparison of Model Prediction with Experiment for Concentration-Dependent Modulus of Poly(Vinyl Alcohol) (PVA)

- Gels near the Gelation Point. *Chem. Phys. Lett.* **1992**, *195* (5), 509–512. [https://doi.org/10.1016/0009-2614\(92\)85553-M](https://doi.org/10.1016/0009-2614(92)85553-M).
- (60) Hernández, R.; Sarafian, A.; López, D.; Mijangos, C. Viscoelastic Properties of Poly(Vinyl Alcohol) Hydrogels and Ferrogels Obtained through Freezing–Thawing Cycles. *Polymer* **2004**, *45* (16), 5543–5549. <https://doi.org/10.1016/j.polymer.2004.05.061>.
- (61) Ramzi, M.; Rochas, C.; Guenet, J.-M. Structure–Properties Relation for Agarose Thermoreversible Gels in Binary Solvents. *Macromolecules* **1998**, *31* (18), 6106–6111. <https://doi.org/10.1021/ma9801220>.
- (62) Guenet, J.-M. Structure versus Rheological Properties in Fibrillar Thermoreversible Gels from Polymers and Biopolymers. *J. Rheol.* **2000**, *44* (4), 947–960. <https://doi.org/10.1122/1.551121>.
- (63) Artyukhov, A. A.; Shtilman, M. I.; Kuskov, A. N.; Pashkova, L. I.; Tsatsakis, A. M.; Rizos, A. K. Polyvinyl Alcohol Cross-Linked Macroporous Polymeric Hydrogels: Structure Formation and Regularity Investigation. *J. Non-Cryst. Solids* **2011**, *357* (2), 700–706. <https://doi.org/10.1016/j.jnoncrysol.2010.06.038>.
- (64) Hernandez, R.; Lopez, D.; Mijangos, C.; Guenet, J.-M. A Reappraisal of the ‘Thermoreversible’ Gelation of Aqueous Poly(Vinyl Alcohol) Solutions through Freezing–Thawing Cycles. *Polymer* **2002**, *43* (21), 5661–5663. [https://doi.org/10.1016/S0032-3861\(02\)00470-6](https://doi.org/10.1016/S0032-3861(02)00470-6).

PAPER II



Twin-chain polymer hydrogels based on poly(vinyl alcohol) as new advanced tool for the cleaning of modern and contemporary art

Rosangela Mastrangelo^{a,b}, David Chelazzi^{a,b}, Giovanna Poggi^{a,b}, Emiliano Fratini^{a,b}, Luciano Pensabene Buemi^c, Maria Laura Petruzzellis^c, and Piero Baglioni^{a,b,1}

^aDepartment of Chemistry, University of Florence, I-50019 Florence, Italy; ^bConsorzio Interuniversitario per lo Sviluppo dei Sistemi a Grande Interfase (Center for Colloid and Surface Science), University of Florence, I-50019 Florence, Italy; and ^cConservation Department, Peggy Guggenheim Collection, Dorsoduro 701, I-30123 Venice, Italy

Edited by Michael L. Klein, Temple University, Philadelphia, PA, and approved December 28, 2019 (received for review July 10, 2019)

Conservation of our cultural heritage is fundamental for conveying to future generations our culture, traditions, and ways of thinking and behaving. Cleaning art, in particular modern/contemporary paintings, with traditional tools could be risky and impractical, particularly on large collections of important works to be transferred to future generations. We report on advanced cleaning systems, based on twin-chain polymer networks made of poly(vinyl alcohol) (PVA) chains, semiinterpenetrated (semi-IPN) with PVA of lower molecular weight (L-PVA). Interpenetrating L-PVA causes a change from gels with oriented channels to sponge-like semi-IPNs with disordered interconnected pores, conferring different gel (and solvent) dynamics. These features grant residue-free, time efficient cleaning capacity and effective dirt capture, defeating risks for the artifact, making possible a safer treatment of important collections, unconceivable with conventional methods. We report as an example the conservation of Jackson Pollock's masterpieces, cleaned in a controlled way, safety and selectivity with unprecedented performance.

poly(vinyl alcohol) hydrogel | semiinterpenetrated gels networks | cultural heritage conservation | modern art | contemporary art

The challenge in the conservation of cultural heritage is to preserve and maintain accessible a vast number of objects (e.g., up to million artifacts for a single museum) against degradation caused by environmental factors, pollution, wrong conservation practice, and microorganisms. Heritage conservation and accessibility are both an economic amplifier and an invaluable instrument that drives social inclusion and equality, improving quality of life (1–3). The most recurrent issue in the preservation of modern and contemporary art involves the removal of soil from painted surfaces. This is often problematic owing to the fact that industrial paints contain additives (4, 5) with a marked sensitiveness to solvents and cleaning fluids (6, 7) that can possibly leach and deteriorate the painting. Since most contemporary paintings are unvarnished, soil accumulates directly on the painted layers, and cleaning solvents work in contact with sensitive pigments, dyes, binders, and additives. Moreover, especially from the 1940s on, paintings display high surface roughness, which makes homogeneous cleaning with traditional tools even more difficult and risky for the artifacts. In particular, the use of solvents is uncontrolled and nonselective, i.e., sensitive original components of the artifacts can be swollen, solubilized, or leached along with undesired layers. Besides, free solvents typically used in the restoration practice pose health risks to conservators. Traditionally employed solvent thickeners, such as polyacrylic acid and cellulose derivatives, or physical gels (e.g., agar), can either be scarcely retentive or exhibit poor mechanical properties, leaving polymer residues whose removal requires invasive rinsing steps (8, 9).

In past years, we have developed a different approach based on the use of colloidal systems (10–17). The latest advancement is represented by the confinement of cleaning fluids in gels (18–20) specifically tailored to treat water- and solvent-sensitive works of art. In a previous contribution to PNAS (21), we reported on the

use of semiinterpenetrated networks (SIPNs) of poly(2-hydroxyethyl methacrylate) and poly(vinylpyrrolidone) (pHEMA/PVP) to confine oil-in-water microemulsions and gradually release them on sensitive surfaces. This allows the safe removal of detrimental pressure-sensitive tapes and adhesives from paper artworks. However, while the pHEMA/PVP SIPNs are highly retentive and effective on flat surfaces, they are not able to adapt to rough, clotted, and three-dimensional (3D) textured surfaces, such as those of modern and contemporary paints by Van Gogh, Picasso, Pollock, and others. For this reason, we designed a class of gels, based on poly(vinyl alcohol) (PVA). Freeze–thaw (FT) PVA gels can be feasibly formulated to exhibit excellent strength and elasticity, with no need of toxic cross-linkers, as largely reported in the literature (22, 23). A significant advantage with respect to the aforementioned pHEMA chemical networks is that physical networks of PVA are highly viscoelastic, meaning that gel sheets can be made flexible while retaining optimal elongability and resistance to mechanical stress. Besides, PVA is biocompatible and nontoxic. The challenge is to design PVA networks with cohesive structure, adaptability to rough surfaces, high and interconnected porosity, and high water content and retentiveness. These are key features to boost the removal of dirt from artistic surfaces and can be more easily achieved when two different types of PVA are combined in a network. Interpenetrating

Significance

From the earliest cave paintings of mankind, to Renaissance frescos and modern art masterpieces, the preservation of surfaces against soiling and degradation is fundamental to transfer such a vast heritage to future generations. However, traditional cleaning methods are often invasive and risky. We overcame these limitations by designing a cleaning system in the framework of colloid and materials science. We formulated twin-chain hydrogels with ideal mechanical properties, retentiveness, and interconnected porosity, allowing adhesion to rough and textured paint layers, and controlled wetting of surfaces, granting safe removal of soil. The gels were used to clean two Jackson Pollock masterpieces, recovering their visual aspect, marking a turning point in the field of conservation of important collections worldwide.

Author contributions: P.B. designed research; R.M., D.C., L.P.B., M.L.P., and P.B. performed research; R.M., D.C., G.P., and E.F. analyzed data; and R.M., D.C., G.P., E.F., and P.B. wrote the paper.

The authors declare no competing interest.

This article is a PNAS Direct Submission.

This open access article is distributed under [Creative Commons Attribution-NonCommercial-NoDerivatives License 4.0 \(CC BY-NC-ND\)](https://creativecommons.org/licenses/by-nc-nd/4.0/).

¹To whom correspondence may be addressed. Email: piero.baglioni@unifi.it.

This article contains supporting information online at <https://www.pnas.org/lookup/suppl/doi:10.1073/pnas.191181117/-DCSupplemental>.

the network of a higher molecular weight PVA (H-PVA) with PVA of lower molecular weight (L-PVA) is expected to impact the pores size and structure and the mechanical properties of the gels. Namely, we hypothesized that L-PVA could remain at least partially entangled in the H-PVA network, interposing between H-PVA chains, possibly altering the formation of walls and pores and changing the rheological properties of the network. Controlling the pore size distribution and the rheological behavior of the gels would allow to optimize the adhesion of the gel to the surface or the capture and transport of matter through the gel matrix.

We report a detailed picture of the formation mechanism of these twin-chain polymer network hydrogels (TC-PNs) and of the PVA dynamics in the final network. We demonstrated that the addition of L-PVA changes the gel porosity from a packed structure of elongated channels into a nonordered pattern of interconnected and larger pores similar to a sponge. The morphological changes and the presence of L-PVA likely make the TC-PNs more mechanically compliant. These combined features grant higher cleaning efficacy than pure PVA networks and overcome the limitations of rigid gel sheets (e.g., gellan) and previously developed SIPNs (chemically cross-linked networks).

The advanced TC-PNs were used for the cleaning and conservation of two Pollock masterpieces from the Peggy Guggenheim Collection of Venice (Solomon R. Guggenheim Foundation, New York). The gels allowed safe removal of soil without uncontrolled spreading and excessive wetting of the painted layers. The gels do not leave residues and can be applied to vertical surfaces and then completely removed even from cracked and morphologically complex areas, reducing the risk of mechanical stresses. This is a dramatic improvement over the traditional cleaning approach with nonconfined solvents, which can require a long process under the microscope.

Results and Discussion

The Structure of PVA-Based Cryogels. In this contribution, PVA-based FT hydrogels were cryoformed: pure PVA hydrogels were

prepared using H-PVA, and TC-PNs were obtained by mixing H-PVA and L-PVA. The terms TC-PNs and PVA/PVA gels will be used hereafter interchangeably. Hydrogels were either prepared with one (FT1) or three (FT3) FT cycles. The physical gelation of PVA solutions is driven by the freezing steps, which cause a water–polymer phase separation (22). PVA chains accumulate in the polymer-rich phase, while ice crystals form in the water-rich phase; owing to the pressure exerted by freezing water, polymer crystallites form and act as tie points in the gel structure, while ice crystals act as porogens. More details about the preparation are reported in *SI Appendix*. Confocal microscopy and scanning electron microscopy (SEM) were used to characterize the hydrogels. The freezing of H-PVA solutions leads to a more homogeneous structure with smaller pores than the TC-PNs (Fig. 1A). The pores are arranged into a pseudo-hexagonal packed structure (see detail of the β -plane section in Fig. 1A). The formation of the PVA gel walls follows the dendritic growth of ice during crystallization: there is a central branch from which new ice strands originate and arrange perpendicular to each other (Fig. 1A, α -plane section). As a consequence, pores have an elongated shape and exhibit an elliptical section, as if ice grew in aligned needles along axes that are slightly tilted with respect to the plane of the gel sheet's main surface (Fig. 1A). Instead, in the TC-PNs, pores are not aligned along axes and show a nonordered pattern similar to what is expected for a sponge-like network (Fig. 1B). The dimensions and distribution of the pores in the TC-PNs (3 to 30 μm) suggest the presence of obstacles that prevent the growth of ice, resulting in an interconnected porosity across the gel network. We hypothesized that this feature might favor the capture and retaining of dirt by the TC-PN gels: when the gel is applied on a soiled surface, the soil migrates inside the porosity, all through the gel volume; evaporation at the gel upper surface is expected to recall water from the bulk through the interconnected porosity, favoring dirt pick-up. Dirt capture should also be favored by the larger pore dimensions in the TC-PNs.

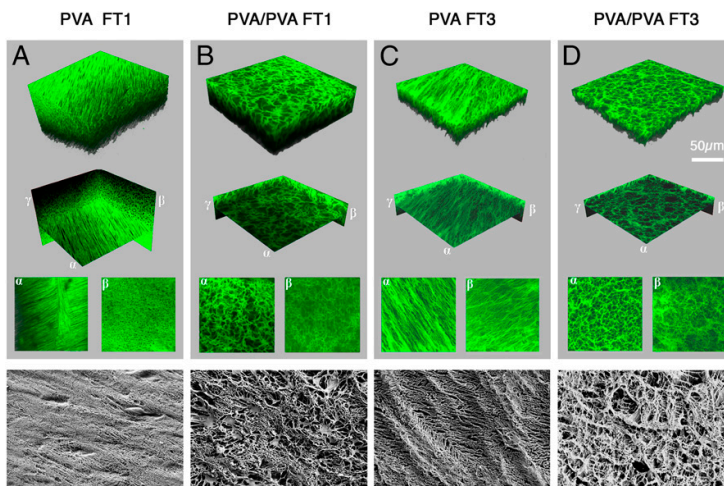


Fig. 1. The structure of PVA cryogels at the micron scale. Confocal-microscopy images of the FT PVA gels, loaded with an aqueous solution of the green dye rhodamine 110, which preferentially interacts with the gel's walls. A–D also include images of horizontal (α) and vertical (β and γ) sections of the imaged volumes. (A) PVA FT1 gel. The pores are cylindrical and arranged into a hexagonally packed structure (see detail of the β -plane section), with central branches from which new strands originate and arrange perpendicular to each other (see detail of the α -plane section). (B) TC-PN FT1 gel. The presence of L-PVA as semiinterpenetrated polymer leads to the formation of larger and nonoriented pores; the pore distribution resembles that of a sponge-like network (see sections along the α and β planes) (C) PVA FT3 gel. (D) TC-PN FT3 gel. In both FT3 hydrogels, the pores walls are thicker, as repeated FT cycles cause further phase separation, increasing local polymer concentration. The bottom row in A–D shows SEM images of xerogels obtained from the PVA-based gels, highlighting the presence of a wide range of pores' diameters in TC-PNs (B and D), including pores $< 1 \mu\text{m}$. Bar dimension is 20 μm .

The strong directional growth of the pores in the pure PVA network is also evident when the number of FT cycles is higher, and the pores' section is larger, owing to the ice expansion during the second and third freezing steps (24) (Fig. 1C). Some of the pores merge together, resulting in a less orderly packed structure (24) than FT1 (Fig. 1C, α and β sections). For what concerns the TC-PNs, the FT3 network exhibits a similar disordered sponge-like pattern, suggesting that the TC-PN conserves its structure after the first cycle (Fig. 1D).

In both FT3 hydrogels the pores walls are thicker, because repeated cycles cause further phase separation, squeezing water out of the liquid-like portions of the gels' walls and increasing local polymer concentration (22). This is in agreement with the higher gel fraction (G%) reported in *SI Appendix, Table S1*. Small-angle X-ray scattering (SAXS) analysis shows that with increasing FT cycles, gel walls become denser also at the nanoscale, as evidenced by the decrease of the correlation lengths, and by the higher number of PVA crystallites, as shown by changes in the ratio between the Guinier scale (I_G) and the Lorentz scale (I_L) (*SI Appendix, Table S2* and Fig. S1).

The SEM images of xerogels confirm that the pure PVA gels have an ordered pore structure (Fig. 1A and C), while PVA/PVA xerogels show the same disordered, sponge-like porosity observed for the hydrogels in confocal images (see Fig. 3B and C); the SEM images highlighted the presence of a wide range of pores' diameters in TC-PNs, including pores smaller than 1 μm .

A quantitative characterization of the confocal images was obtained performing chord-length distribution analysis (Fig. 2 and *SI Appendix, Fig. S2*). This method was firstly introduced by Tchoubar and Levitz (25, 26) and allows to extract stringent structural descriptors for biphasic media. Chords are defined as the segments that form when a set of randomly oriented lines cross phase boundaries. Fig. 2A and B show the averaged frequency of chords with given length ($f(R)$) for both pores and gel-phases of the four confocal stacks (PVA and PVA/PVA, FT1, FT3). The distributions always show a peak and an exponential tail (27), from which a characteristic persistence length (λ) of the structure was obtained for each type of gel (*SI Appendix, Table S3*).

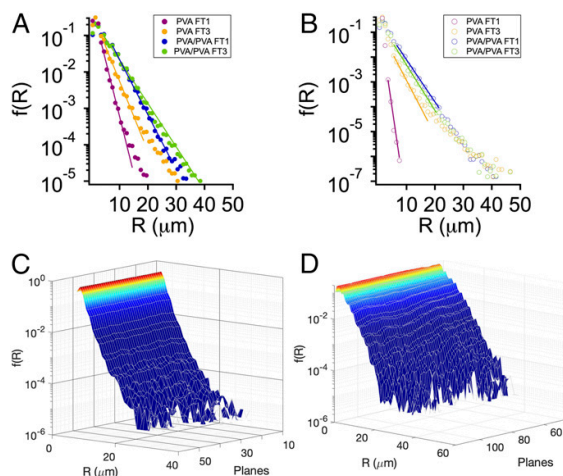


Fig. 2. Chord-length analysis of PVA cryogels. (A and B) Averaged chord-length distributions for the pore phase (A) and the gel phase (B) of PVA cryogels. The lines are the fitting of the data to exponential decays (*SI Appendix*). (C and D) The variance of chord distributions of pores with the depth of confocal stacks for PVA FT1 (C) and PVA/PVA FT1 (D).

The chord distributions of pores (Fig. 24) show that λ increases with the number of FT cycles. In PVA/PVA samples, both the persistence length and the maximum pores' size are higher than the PVA gels, suggesting that L-PVA acts as a porogen in the final structure. The gels' walls thickness increases passing from PVA FT1 to PVA FT3 (Fig. 2B and *SI Appendix, Table S3*), and some further increase occurs passing from pure to PVA/PVA gels. It must be noticed that the higher thickness of walls in PVA/PVA FT3 as compared to PVA/PVA FT1, observed with SEM, could not be appreciated with chord analysis as the difference probably falls beyond the resolution of confocal images.

Fig. 2C and D shows how the pore chord distribution varies along the depth of the stacks: all samples show a faster decay for confocal planes closer to the gel surface (see also *SI Appendix, Fig. S3*). This is probably due to the stronger effect of freezing on the exposed surfaces of the samples, which causes the formation of more elongated pores, while the inner planes are characterized by pores with larger cross-sections and polydispersity (*SI Appendix, Fig. S2*).

Gelation Mechanism of TC-PNs. The gelation mechanism of TC-PN FT1 was further studied with confocal microscopy, using labeled polymers to explain the difference in the hydrogel porosity with respect to the pure network. L-PVA was red-labeled with rhodamine B isothiocyanate (RBITC), while H-PVA was green-labeled with fluorescein isothiocyanate (FITC) (*SI Appendix, section S1.3*). Confocal images of the H-PVA/L-PVA pregel solution show the presence of 2- to 20- μm blobs, mainly composed of L-PVA (Fig. 3A). In the H-PVA solution, no such aggregates are detectable.

The phase separation in the H-PVA/L-PVA solution is an intriguing behavior that needs further comments.

In principle, the solubility of PVAs strongly depends on their hydrolysis degree, molecular weight, and crystallinity (28). According to the literature, both PVAs with a high (>95%) and low (87 to 89%) degree of hydrolysis are soluble in water at the conditions that we used for the preparation of the pregel solution (i.e., mixing at 98 $^{\circ}\text{C}$ and then cooling down to room temperature; *SI Appendix, section S1.1*) (29–31). Therefore, we do not ascribe the phase separation to poor solubility of either H-PVA or L-PVA in water. Phase separation was observed even using higher dissolution temperature (125 $^{\circ}\text{C}$, close to the boiling temperature of the mixture). More information was gained from the phase diagrams reported in *SI Appendix, Fig. S4*. H-PVA does not show phase separation in the considered temperature and concentration ranges (5 to 100 $^{\circ}\text{C}$ and 3 to 15% wt/wt), while L-PVA, being less hydrolyzed, shows, according to the literature (32, 33), a lower critical solution temperature. The H-PVA/L-PVA mixtures, which are used to realize the gels presented in this paper, show a different behavior than the single-polymer solutions (*SI Appendix, Fig. S4C*). The confocal analysis of the mixtures is in agreement with a liquid-liquid polymer demixing that could be explained considering that, in the concentrated regime, H-PVA chains preferentially interact with each other, as a result of the polymer conformation in solution and of the high number of hydroxyl groups. According to Crowther et al. (34), the solvation of PVA after decoiling ($T > 20$ $^{\circ}\text{C}$) appears to be hydrophilic in character with further increasing temperature. Budhlall et al. (35) confirmed via NMR that the interaction of R-OHs with water is temperature-dependent, while methyl protons associated with the acetate groups are more hydrophobic. Thus, in the pregel PVA solution, the highly hydrolyzed H-PVA is expected to be in the form of decoiled and solvated chains. Instead, partially hydrolyzed PVAs (such as L-PVA) adopt in solution different conformations, depending on the polymer blockiness, i.e., whether acetate blocks are long (“blocky”) or randomly distributed (“less blocky”). Namely, blocky PVAs adopt a pseudomicelle conformation (with the acetate groups in a tight core and the

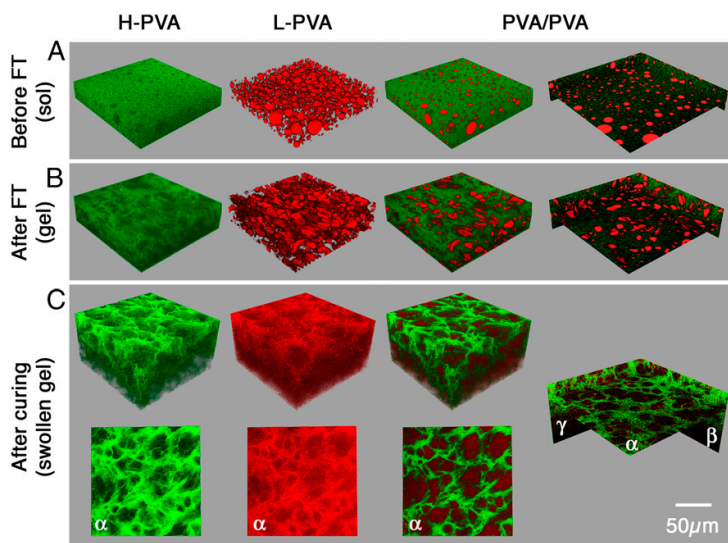


Fig. 3. Confocal-microscopy images of the PVA/PVA system. H-PVA is labeled in green with FITC and L-PVA in red with RBITC. Thus, the first column shows the FITC-PVA, the second column shows the RBITC-PVA, and the third and fourth columns show the sum of both components. (A) The PVA/PVA solution before the FT process. (B) The PVA/PVA gel network obtained after the FT process (1 cycle). The formation of ice crystals along preferential axes leads to the deformation of the blobs, which are distorted from spherical to elongated shapes; some of the smaller blobs coalesced together. (C) The PVA/PVA network after the first cycle of the FT process and 1 wk of curing in water. The 2D view of the top horizontal planes (α) highlights that L-PVA is preferentially localized on the gel's walls, interacting with the green-labeled H-PVA. L-PVA is also present inside the pores, throughout the gel volume.

highly solvated vinyl alcohol chains dangling in water), while less blocky polymers collapse on themselves in a denser conformation (35). Comparing the data obtained by Budhlall et al. with the hydrodynamic radius of L-PVA chains in extremely dilute solutions ($R_H = 10.2$ nm, obtained through the Stokes–Einstein equation using the diffusion coefficient [D] obtained by fluorescence correlation spectroscopy [FCS] measurements; $D = 24 \mu\text{m}^2/\text{s}$; *SI Appendix, Table S4*), we deduced that in our case L-PVA chains fall in the second type of behavior (collapsed structures). H-PVA–L-PVA interaction is probably not favored in the PVA/PVA pre-gel solution: decoiled H-PVA chains preferentially interact with each other through intermolecular H bonding, while L-PVA chains are collapsed and intramolecular hydrophobic interactions prevail. Therefore, L-PVA is expelled by the continuous phase of H-PVA and forms spherical droplets. As a matter of fact, the diffusion coefficient obtained by fluorescence recovery after photobleaching (FRAP) measurements in the blobs is significantly higher than that measured in the continuous phase (*SI Appendix, Table S4*), suggesting that the blob phase is less viscous, i.e., chains or aggregates in this phase are not strongly interacting with each other.

As previously mentioned, the physical crosslinking of PVA chains is driven by the freezing steps, applied to a PVA solution, which cause water–polymer phase separation and the formation of PVA crystallites that act as tie points in the structure. Ice crystals act as porogens in the process; therefore, ice formation plays a key role along with the H-PVA/L-PVA phase separation in the formation of the final network. In fact, the confocal images in Fig. 3 show that the L-PVA spherical blobs act as templates during the cryoformation of the TC-PN structure. Because L-PVA is more water soluble than H-PVA, it does not undergo further phase separation in the freezing step, thus remaining confined in the water pockets during freezing and after thawing. The formation of ice crystals along preferential axes leads to the deformation of the blobs from spherical to elongated shapes (36) (red features in Fig. 3B).

Typically, IPNs undergo both nucleation and growth and spinodal decomposition kinetics of phase separation (37). As a general rule, the most probable mechanism of phase separation is nucleation and growth for sequential IPNs, and spinodal decomposition for networks created by simultaneous formation from “monomers” or, in our case, preformed polymers (38). This, along with the role of ice as a porogen, would point in the direction of having nucleation and growth as the main mechanism for pore formation in the case of the FT TC-PNs. Indeed, nucleation and growth tend to produce spheres of the second phase in the matrix of the first phase, similarly to the structures observed with confocal microscopy, while spinodal decomposition produces interconnected cylinders of the second phase in the first phase matrix, even if coarsening and coalescence can cause significant structural changes at later stages (the final structure will be determined by the time at which the system loses its mobility). It must be also considered that, when phase separation occurs before gelation (as clearly shown in our case by confocal images), the phase domains will tend to be large, as gelation will tend to keep the domains apart (37); this is in good agreement with the large pore size observed for the FT TC-PNs. However, we cannot fully rule out that the gels can be described through an arrested spinodal decomposition driven by demixing of the two different polymers (39).

Washing the gels in water causes partial removal of L-PVA, leading the disordered and interconnected porous structure of the TC-PNs. However, confocal microscopy showed that the RBITC-labeled L-PVA is still observable in the swollen gel, either confined in the pores or included in the walls (Fig. 3C). The TC-PN FT3 shows a more intense red fluorescence than FT1 (*SI Appendix, Fig. S5*), suggesting that the amount of L-PVA that remains in the TC-PN after washing increases with the number of FT cycles. This suggests that the ice crystals that form during freezing push the L-PVA droplets onto the continuous H-PVA gel, producing a “force-coating” of the initially microphase separated gel with L-PVA and originating a quasibigel (27).

Overall, passing from pregel solutions to swollen FT gels causes the formation of inhomogeneities also at the nanoscale; this, along with the swelling of PVA chains in water, leads to an increase of the correlation lengths, as evidenced by SAXS (*SI Appendix, Table S2*).

The lower value of the correlation length of TC-PN FT1 as opposed to the PVA FT1 suggested that the spontaneous H-PVA/L-PVA phase separation produces a higher concentration of H-PVA in the continuous phase, which eventually led to the formation of denser gel walls than in the single-polymer network. In fact, the crystallinity of TC-PN gels is higher than the pure PVA network (*SI Appendix, Table S1 and Fig. S6*). In the pure PVA networks, crystallinity increases with increasing FT cycles, as expected (24, 40, 41), while, in the PVA/PVA systems, it stabilizes, confirming that the TC-PN conserves its structure after the first cycle, as discussed under *The Structure of PVA-Based Cryogels*.

The Diffusion of PVA Chains in the Pregel Solutions and Gels.

FCS and FRAP were employed to study the mobility of the polymer chains in the PVA and PVA/PVA pregel solutions and gel networks. The two techniques allow measuring different ranges of the diffusion coefficient, ideally $D > 1 \mu\text{m}^2/\text{s}$ for FCS and $0.01 \mu\text{m}^2/\text{s} < D < 50 \mu\text{m}^2/\text{s}$ for FRAP (*SI Appendix, section S2.4*).

As expected, the diffusion of the H-PVA chains in the walls of the cryogels is too slow to be detected by FRAP (*SI Appendix, Fig. S7*). While other techniques could be employed to study such slow diffusion rates, e.g., single-particle tracking (42), image correlation spectroscopy (43), or NMR diffusometry (44), for the scopes of this work, it was important to observe that the polymer chains are essentially blocked in the gels' walls, providing an upper limit ($0.01 \mu\text{m}^2/\text{s}$) for their diffusion coefficients. A qualitative comparison of the FRAP curves (*SI Appendix, Fig. S7D*) shows that in the PVA FT1 network, H-PVA is less strongly blocked than in the TC-PN FT1, indicating that the latter has a more crowded gel structure. When the number of FT cycles increases, the differences between PVA and PVA/PVA level off.

In the PVA/PVA pregel solutions, the chains of H-PVA are less mobile (lower values of D ; *SI Appendix, Fig. S7 and Table S4*) than in the single-polymer pregels, in agreement with the gelation process illustrated with confocal microscopy, where the phase separation in the PVA/PVA system causes a concentration increase of H-PVA outside the blobs of L-PVA (Fig. 3).

The most striking observation concerns the mobility of L-PVA in the formed TC-PNs, after curing in water. Inside the gels' pores, the polymer shows two diffusional behaviors, with a predominant component of free polymer (as in diluted solution) and a minor component of slower diffusing chains (Fig. 4 A–C and *SI Appendix, Table S4*). We reasonably hypothesized that the slow-diffusing components are constituted by L-PVA chains that are not included in the TC-PNs, but interact with them through hydrogen bonds, or are chains partially protruding out of the walls. Instead, the L-PVA chains on the walls of the TC-PNs are strongly blocked and do not show a diffusional behavior as evidenced by FRAP (Fig. 4D and *SI Appendix, Table S4*). Both the inclusion of L-PVA and its protrusion from the gel walls could also be explained considering the possibility that some “force-coating” of the walls with L-PVA occurs through the FT process, as mentioned above. Overall, we concluded that L-PVA contributes to the structure of the TC-PNs, and this is expected to produce significant changes in the mechanical properties of the PVA/PVA gels as opposed to the single-polymer networks.

Rheological Properties of PVA Gels. Rheological measurements clearly demonstrate the influence of composition and FT cycles on the mechanical properties of the gels. The rheological data were related to the structural characterization reported in the previous sections.

Amplitude sweep curves show that the cross-over between the storage modulus (G') and loss modulus (G'') can be found at lower oscillation strains for the FT3 hydrogels (arrows in Fig. 5A). The peak that appears in the G'' curves, the “weak strain overshoot” (45), is shifted to lower strains with increasing FT cycles; this behavior can be explained considering that a higher number of cycles

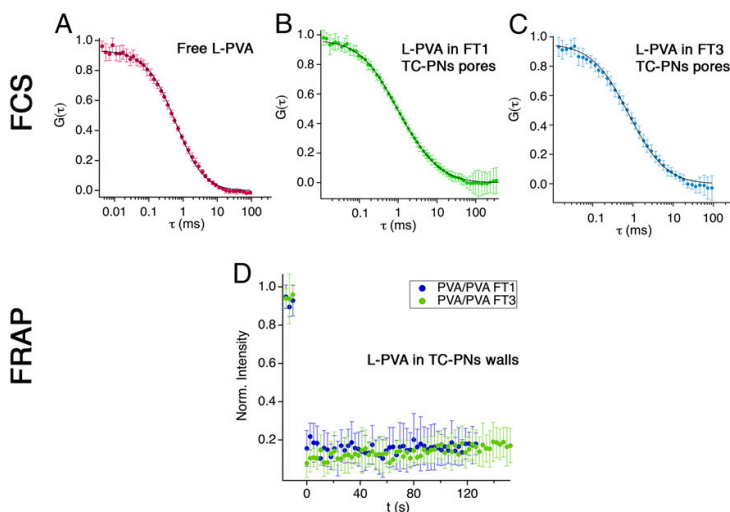


Fig. 4. The diffusion of L-PVA in the TC-PN gels. (Top) FCS autocorrelation curves (marks) and fitting functions (solid lines) for a diluted solution of L-PVA in water (*SI Appendix*) (A), L-PVA in the pores of TC-PN FT1 gel (B), and L-PVA in the pores of TC-PN FT3 gel (C). The results of the fittings (values of the diffusion coefficient, D) are reported in *SI Appendix, Table S4*. (D) FRAP recovery profiles of L-PVA on the walls of TC-PN FT1 (blue markers) and FT3 (green markers) gels; the curves are flat, without recovery in the fluorescence intensity, which indicates that no diffusion of the polymer chains is detectable (*SI Appendix, section S2.3*).

leads to stiffer and less mobile networks that are less capable of relaxing mechanical stresses. For the same number of FT cycles, TC-PNs show G'' peaks at higher strain. It can be thus hypothesized that the presence of L-PVA chains included in the gel walls make the final structure more compliant. However, it must be considered that the observed changes in rheological properties could also be due to the morphological differences (e.g., larger and less-oriented pores) induced by templating from L-PVA droplets during gelation.

After one cycle, the TC-PN has a higher G' than the single-polymer network, as shown in the frequency sweep curves reported in Fig. 5B. This seems in contrast to the lower gel fraction, $G\%$, reported in *SI Appendix*, Table S1, as G' is known to depend on the polymer concentration (46). However, as previously discussed, denser gel walls are formed during gelation of the TC-PN due to the spontaneous H-PVA/L-PVA phase separation in the pregel solution (Fig. 3). This can explain the increase in the storage modulus.

FT3 gels have all similar G' , significantly higher than the FT1 systems, highlighting that polymer accumulate on gel walls during the freezing steps; in the case of TC-PNs, this could be possibly due also to the “force-coating” of the gel walls with L-PVA through repeated FT cycles. Fig. 5C shows visually the increase in the rigidity of the systems with increasing number of cycles. It must be noticed that systems with excessively high storage moduli are not able to adapt to surface irregularities typical of painted artifacts (i.e., ≥ 1 mm) (20). This is further visualized in *SI Appendix*, Fig. S8, where FT1 PVA gels are compared to a pHEMA/PVP SIPN we previously formulated for the cleaning of artifacts (19, 21) and to a gellan sheet similar to those traditionally employed in

the restoration practice (47). The pHEMA/PVP gels have G' values of 4 to 5×10^3 Pa (17), roughly half the modulus of a typical gellan sheet (48). In turn, the newly formulated PVA gels have G' moduli 4 to 5 times lower than those of pHEMA/PVP and still exhibit very good resistance to handling and elongation. Both the pure and TC-PN FT1 PVA gels are able to adapt to the rough painted surface, covering irregularities and insinuating into cavities (*SI Appendix*, Fig. S8 D and E), whereas the pHEMA/PVP SIPN and gellan sheet are too rigid to cover the surface homogeneously (*SI Appendix*, Fig. S8 B and C). This is expected to boost the cleaning efficacy of the PVA gels. Being more compliant than the pure PVA network, the H-PVA/L-PVA gel might adhere better to the painted surface, producing a more homogeneous cleaning. Moreover, given that L-PVA is hydrolyzed to a lesser degree than H-PVA, a coating of L-PVA on the surfaces of the pores could result in a material that more efficiently adsorbs hydrophobic particles, enhancing particle uptake.

Removing Dirt from Pollock's Masterpieces. As reported in *SI Appendix*, Table S1, all of the PVA-based gels contain high percentages of water ($>90\%$), which behaves almost completely as free water and is responsible for effective cleaning action. In fact, water is a good solvent for the surface dirt commonly found on artifacts, and its cleaning power is easily enhanced when solutions of chelants or surfactants are used. Besides, as reported in *SI Appendix*, Table S1, the water release of the PVA-based formulations reported here is in the range of 21 to 24 mg/cm² (over 30 min, on Whatman paper) for FT1 gels and 17 to 19 mg/cm² for FT3 gels. These values are comparable with those of pHEMA/PVP gels used

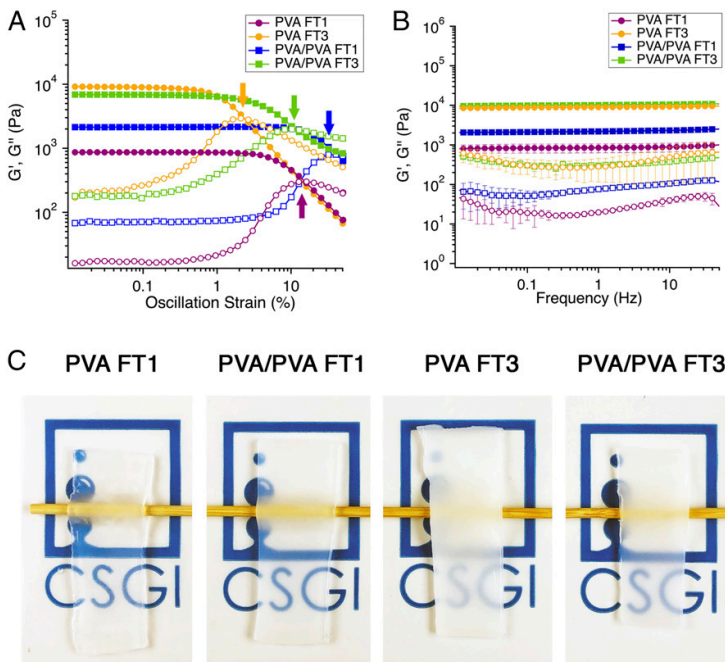


Fig. 5. Rheological measurements and visual aspect of cryogels. (A) Amplitude sweep curves of cryogels; the arrows indicate the cross-over of G' and G'' in different systems. Solid and empty markers indicate G' and G'' , respectively. The oscillation strains at the cross-over follow the trend: PVA FT3 $<$ PVA/PVA FT3 \sim PVA FT1 $<$ PVA/PVA FT1. Error bars are not included to facilitate the readability of the image (*SI Appendix*); errors do not affect cross-over trend. (B) Frequency sweeps of cryogels. Solid and empty markers indicate G' and G'' , respectively. Error bars show the SDs; when not visible, they are smaller than the markers' size. (C) Cryogels on wooden sticks and colored logos. The increase in the number of cycles leads to opaquer and more rigid systems. CSGI, Consorzio Interuniversitario per lo Sviluppo dei Sistemi a Grande Interfase (Center for Colloid and Surface Science).

for restoration, i.e., 15 to 16 mg/cm² (49), and both formulations are more retentive than traditional agar or gellan (30–33 mg/cm²; ref. 49), which proved too risky to water-sensitive dyes (19). These features, combined with the ability to adapt to rough surfaces, indicate PVA gels as good candidates for the cleaning of sensitive painted layers, based on the background we acquired on the application of gels to the cleaning of artifacts (19, 20, 50). The gels were practically assessed on soiled glass slides (*SI Appendix, Fig. S9*) and on representative mockups that mimic modern/contemporary paintings (*SI Appendix, Fig. S10*) and were compared with conventional cleaning tools such as gellan sheets and swabs (Figs. 6 and 7). The soil was efficiently removed from glass slides and from the rough painted surface using the TC-PN (Fig. 6E and *SI Appendix, Fig. S9*), while only partial cleaning was achieved using the pure PVA gel (Fig. 6D and *SI Appendix, Fig. S9*). Scarce soil removal was obtained using the gellan sheet (Fig. 6F), as expected considering the poor adhesion of the rigid sheet to the clotted painted surface.

Fig. 7 shows that, when the swabs (soaked with the same cleaning solution as gels) are used, repeated mechanical action and scarce water retentiveness inevitably causes pigment loss. Instead, the application of TC-PNs leads to the safe removal of the soil; softened soil residues are easily removed via gentle mechanical action with an “eraser gum”-shaped TC-PN without detaching the pigment from the surface (Fig. 7A).

Two-dimensional (2D) Fourier-transform infrared spectroscopy (FTIR) imaging allowed assessment of the gel-cleaning effectiveness down to the micron scale. The spectra of the cleaned sample are comparable to those of the pristine mockup (Fig. 7B), mainly showing the peaks of oil paintings (51). The bands of kaolin in the 3,725 to 3,592 cm⁻¹ region (3,665 cm⁻¹, Al–OH stretching; 3,625 cm⁻¹, OH stretching, crystalline hydroxyl) (52) are intense in the spectra of the soiled mockup and absent in those of the pristine and cleaned samples, indicating effective soil removal. Previously,

we had shown that conventional rigid gels have poor adhesion to such rough surfaces, resulting in scarce removal of soil (20).

Besides, mapping the absorbance intensity in the PVA OH stretching region (3,440 to 3,180 cm⁻¹) showed no significant differences between the pristine and cleaned samples; no absorption bands ascribable to PVA could be detected (Fig. 7C), i.e., no residues of PVA were left on the surface (up to the detection limit of ca. 0.02 pg/μm²; *SI Appendix, Fig. S11* and section S2.5). This was deemed as a fundamental feature, as opposed to traditional thickeners (e.g., polyacrylic acid, cellulose ethers); the latter are known to leave residues after cleaning and require detrimental rinsing steps (9, 53, 54).

The TC-PN FT1 hydrogels were then used to clean two Jackson Pollock masterpieces at the Peggy Guggenheim Collection (Venice), namely “Eyes in the Heat” (1946 to 1947) and “Two” (1943 to 1945), jeopardized by surface dirt accumulated over the last decades (Fig. 8). These artifacts are particularly important in the Pollock oeuvre, showing the transition from a relatively traditional language, to the revolutionary dripping technique that produces textured 3D surfaces. Moreover, “Two” is made using only oil paints, while “Eyes in the Heat” represents the artist’s transition from oil paints to the application of both oils and alkyd colors. In both cases, the painted surface is highly solvent sensitive. These combined features make the removal of dirt particularly challenging and risky with conventional cleaning tools.

The removal of soil using the gels is appreciated as the paints’ hue is brought back (Fig. 8A and D). The gels’ mechanical properties and retention/release rate allowed feasible dirt removal without unwanted effects, whereas swabs were shown to remove pigments along with dirt and were thus avoided. Because dirt removal takes place through controlled wetting and dirt detachment at the gel–paint interface, rather than via traditional solution chemistry, the systems reported here allow safe cleaning. Therefore, the length of the cleaning intervention was optimized as opposed to

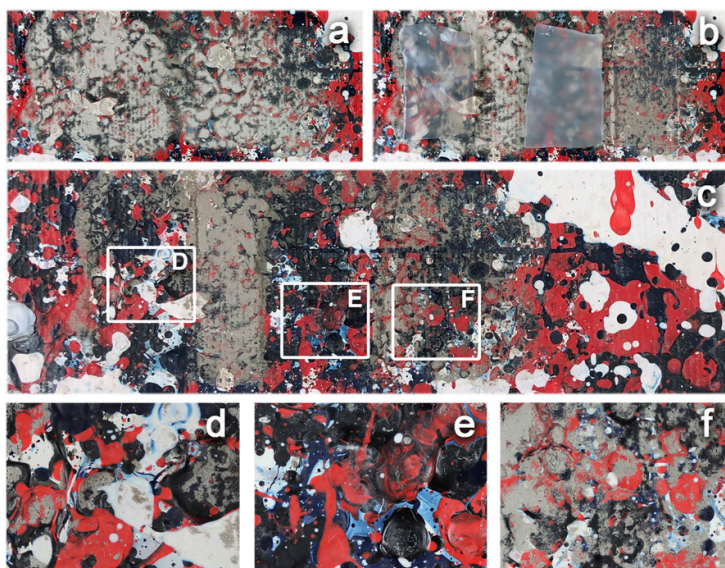


Fig. 6. Cleaning tests on mockups: assessment of PVA and traditional gels. (A) Clotted painting mockup that mimics Pollock’s alkyd paintings, artificially soiled. (B) Application of a pure PVA FT1 gel (Left), a PVA/PVA FT1 TC-PN (Center), and a gellan gel sheet similar to those used in the traditional restoration practice (Right). (C) Soil removal after the application of the gels (8 min each); no additional mechanical action was carried out after the removal of the gels. D–F detail the removal efficacy of each type of gel: the soil was efficiently removed using the TC-PN (E), while partial cleaning was achieved using the pure PVA gel (D). Scarce soil removal was obtained using the gellan sheet (F), as expected considering the poor adhesion of the rigid sheet to the clotted painted surface. A and B represent areas of 9.5 × 4.1 cm². C has a magnification of 1.25×. D–F have magnification of 3.4× with respect to A and B, and are magnifications of Insets (D–F) in C.

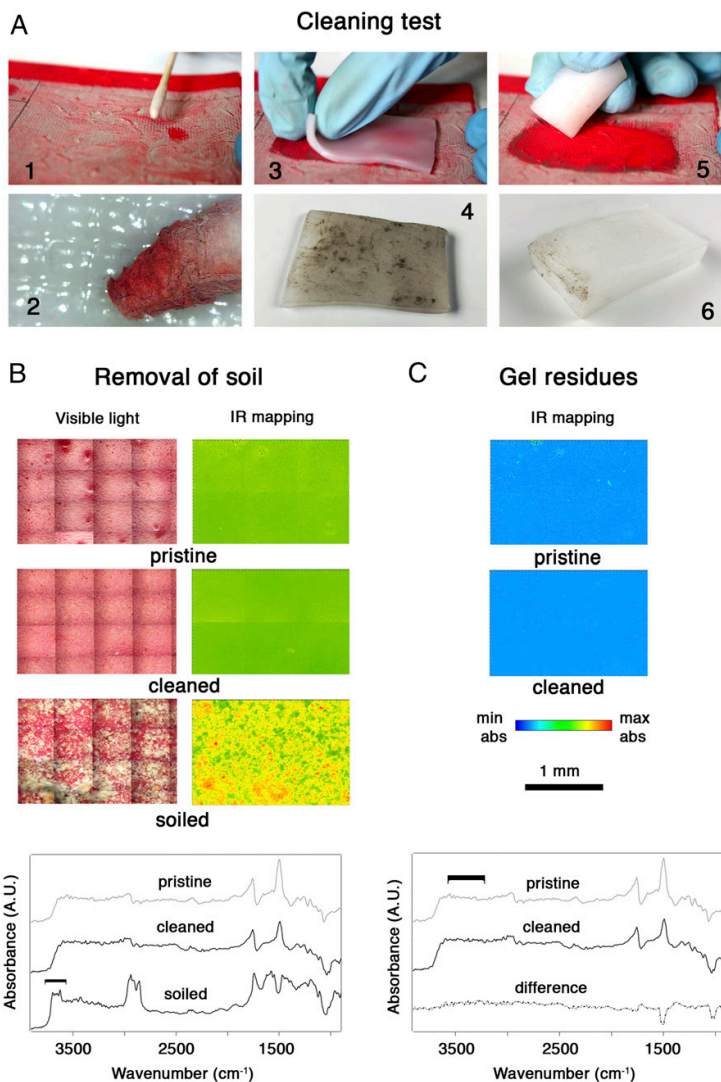


Fig. 7. Cleaning tests on mockups: assessment of the cleaning using FTIR 2D Imaging. (A) Removal of artificial soil from an oil painting mockup (water sensitive cadmium red color) that mimics Pollock paintings (1, 2). Removal of some red pigment along with the soil (3, 4). Application of the TC-PN FT1 hydrogel sheet on the soiled surface (i.e., approach proposed in this contribution); 4 shows that only soil, and no red pigment, adheres to the gel sheet following the application (5, 6). The cleaning is completed using the TC-PN FT1 hydrogel shaped as an eraser gum; gentle mechanical action with the gel leads to the complete removal of the soil. The detail in 6 shows that no red pigment adheres to the eraser gum. (B) Assessment of the cleaning effectiveness of the TC-PNs hydrogel using FTIR 2D Imaging. The IR maps show the imaging of the bands of kaolin (present in the artificial soil mixture) in the $3,725$ to $3,592$ cm^{-1} region. (Top) Pristine painted surface. (Center) Painted surface that was soiled and then cleaned using the TC-PN gel. (Bottom) Soiled painted surface. Representative spectra of the pristine, cleaned, and soiled surfaces are shown below the maps. (C) Assessment of the absence of gel residues. The IR maps (acquired on the same areas as panel b) show the imaging of the $3,440$ to $3,180$ cm^{-1} region, where characteristic bands of PVA would be found in case of gel residues after cleaning. (Top) Pristine painted surface. (Bottom) Painted surface that was soiled and then cleaned using the TC-PN gel. Representative spectra of the pristine and cleaned surface are shown below the maps, along with the difference between the two spectra, showing no absorptions ascribable to PVA. abs, absorbance; max, maximum; min, minimum.

the traditional approach that sometimes involves working with nonconfined solvents under the microscope. Thanks to their mechanical properties and effective solvent confinement, these gels are promising tools in order to obtain a safe and noninvasive action, reducing the actual risks for the painted surface, i.e., swelling, solubilization, leaching, and unwanted removal of fatty acids, plasticizers, and metal soaps.

Conclusions

FT gels entirely based on PVA were specifically designed to address the challenge of dirt removal from solvent-sensitive artistic surfaces. At the micron scale, pure PVA networks show an ordered pore structure, with elongated and oriented pores. Instead, TC-PNs exhibit a sponge-like disordered and interconnected macroporosity, with larger pores and increased surface roughness,

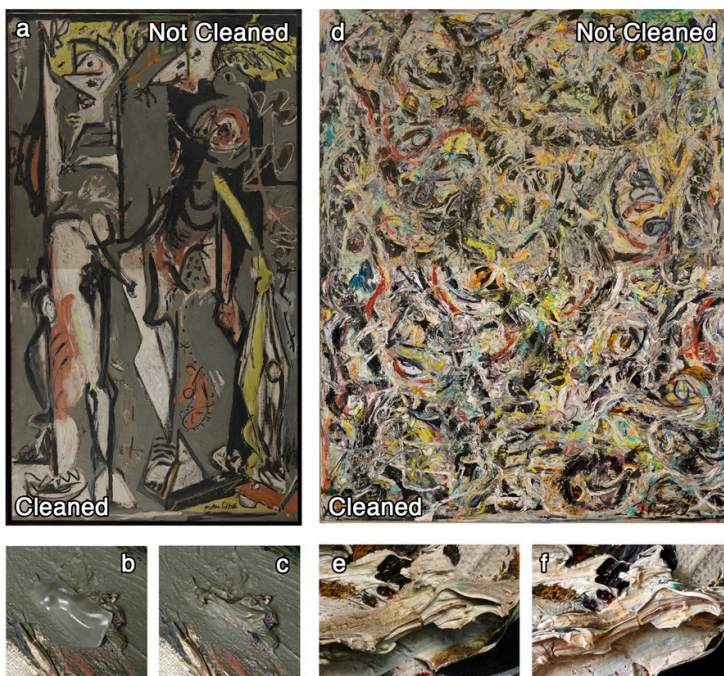


Fig. 8. Cleaning of Pollock's masterpieces. (Left) *Two* by Jackson Pollock, © Pollock-Krasner Foundation/Artists Rights Society (ARS), New York. (Right) *Eyes in the Heat* by Jackson Pollock, © Pollock-Krasner Foundation/Artists Rights Society (ARS), New York. (A and D) Collages showing the paintings before and after the cleaning intervention, where the soil was removed using the TC-PN FT1 hydrogels. The collages allow to better appreciate the removal of soil as the paints' hue and brightness were brought back. The whole paintings were cleaned during the cleaning intervention. (B and C) A detail showing the gel adhering to the painting and the same area after cleaning. (E and F) A detail of the painting before and after cleaning with the TC-PN gels. B and C have a magnification of 13x with respect to A. E and F have a magnification of 20x with respect to D.

which were shown to enhance the capture of dirt at the gel–paint interface and its inclusion in the gels.

The TC-PNs exhibit higher storage modulus but better relief of mechanical stress than the pure PVA networks, possibly as a result of the plasticizing action of L-PVA or of the morphological changes induced by templating from L-PVA droplets during gelation. Remarkably, these gels behave mechanically as chemical networks, despite being held by noncovalent bonds.

TC-PNs were used to safely remove dirt from the surface of Jackson Pollock's masterpieces, “Two” and “Eyes in the Heat.” Thanks to their adhesion to the textured surface, to the controlled release of cleaning fluids at the gel–paint interface, and to the enhanced removal of dirt, the TC-PNs allowed the cleaning of the artifacts without undesired effects on sensitive painted layers, overall optimizing the cleaning process. TC-PNs offer innovative solutions to several needs in cleaning of modern and contemporary paintings in terms of dirt removal, cleaning selectivity, decreased impact on the painted surface, and accuracy of the intervention.

The results presented here are an important step forward in the field of conservation of cultural heritage, opening to feasible treatment of important sets of artifacts, granting their transfer to future generations, with a vast potential socioeconomic impact.

Materials and Methods

Hydrogel Preparation. PVA-based cryogels were prepared through one or three FT cycles starting from PVA solutions. After the last thawing step, gel samples were stored in demineralized water for 1 wk.

Hydrogel Characterization. Hydrogel structure was characterized with confocal laser scanning microscopy, SEM, and SAXS. The mechanical properties were studied with rheological measurements (amplitude and frequency sweeps). Crystallinity degree, equilibrium water content, and free water index were measured using derivative thermogravimetry and differential scanning calorimetry. FCS and FRAP were used to study the dynamics of the PVA chains in the hydrogels' network.

Painting Mockups. Painting mockups were prepared using a commercial primed canvas, oil (Windsor & Newton), and alkyd colors (Ferrario). After about 1 y from the preparation, an artificial dirt mixture in ligroin was applied by means of a brush over the paint layer.

Cleaning Trials. The hydrogels were applied on the surface of soiled mockups for 1 min. The cleaning was completed by gentle mechanical action using an “eraser gum”-shaped hydrogel. The cleaning effectiveness and the absence of PVA residues on the treated surfaces were checked using 2D FTIR imaging with a focal-plane array detector. The same cleaning protocol was adopted for the removal of soil from “Two” and “Eyes in the Heat” by Jackson Pollock. Full methods and materials are available in [SI Appendix](#).

Data and Materials Availability. All data are available in the main text or [SI Appendix](#).

ACKNOWLEDGMENTS. The Italian Consorzio Interuniversitario per lo Sviluppo dei Sistemi a Grande Interfase (Center for Colloid and Surface Science) and the European Union Horizon 2020 projects NANORESTART (Nanomaterials for the Restoration of Works of Art) and APACHE (Active & Intelligent Packaging Materials and Display Cases as a Tool for Preventive Conservation of Cultural Heritage), under Horizon 2020 Research and Innovation Programme Grant Agreements 646063 and 814496, respectively, are gratefully acknowledged for financial support.

- C. Dümcke, M. Gnedovsky, "The social and economic value of cultural heritage: Literature review" (European Expert Network on Culture Paper, Interarts Foundation, 2013).
- N. Stanley-Price, "The thread of continuity: Cultural heritage in post-war recovery" in *Cultural Heritage in Postwar Recovery: Papers from the ICCROM FORUM Held on October 4–6, 2005* (International Center for the Study of the Preservation and Restoration of Cultural Property, 2007), pp. 1–16.
- C. Holtorf, The changing contribution of cultural heritage to society. *Mus. Int.* **63**, 8–16 (2011).
- T. J. S. Learner, "The chemistry of modern paints" in *Analysis of Modern Paints* (Getty Conservation Institute, 2004), pp. 12–13.
- F. C. Izzo, K. J. van den Berg, H. van Keulen, B. Ferriani, E. Zendri, "Modern oil paints—Formulations, organic additives and degradation: Some case studies" in *Issues in Contemporary Oil Paint*, K. J. Van der Berg et al., Eds. (Springer International Publishing, 2014), pp. 75–104.
- A. Burnstock, K. J. van der Berg, S. de Groot, L. Wijnberg, "An investigation of water-sensitive oil paints in 20th century paintings" in *Modern Paints Uncovered: Proceedings from the Modern Paints Uncovered Symposium*, T. J. S. Learner, P. Smithen, J. Krueger, M. R. Shilling, Eds. (The Getty Conservation Institute, 2007), pp. 177–188.
- B. Ormsby, T. Learner, The effects of wet surface cleaning treatments on acrylic emulsion artists' paints—A review of recent scientific research. *Stud. Conserv.* **54**, 29–41 (2009).
- E. Carretti, R. Giorgi, "Cleaning IV: Applications and case studies" in *Nanoscience for the Conservation of Works of Art*, P. Baglioni, D. Chelazzi, Eds. (Royal Society of Chemistry, 2013), pp. 287–288.
- A. Casoli, Z. Di Diego, C. Isca, Cleaning painted surfaces: Evaluation of leaching phenomenon induced by solvents applied for the removal of gel residues. *Environ. Sci. Pollut. Res. Int.* **21**, 13252–13263 (2014).
- P. Baglioni, E. Carretti, D. Chelazzi, Nanomaterials in art conservation. *Nano-technol.* **10**, 287–290 (2015).
- P. Baglioni, D. Chelazzi, R. Giorgi, G. Poggi, Colloid and materials science for the conservation of cultural heritage: Cleaning, consolidation, and deacidification. *Langmuir* **29**, 5110–5122 (2013).
- D. Chelazzi, R. Giorgi, P. Baglioni, Microemulsions, micelles, and functional gels: How colloids and soft matter preserve works of art. *Angew. Chem. Int. Ed. Engl.* **57**, 7296–7303 (2018).
- E. Carretti, L. Dei, C. Miliani, P. Baglioni, "Oil-in-water microemulsions to solubilize acrylic copolymers: Application in cultural heritage conservation" in *Progress in Colloid and Polymer Science*, P. Koutsoouk, Ed. (Springer, 2001), pp. 63–67.
- M. Baglioni, D. Berti, J. Teixeira, R. Giorgi, P. Baglioni, Nanostructured surfactant-based systems for the removal of polymers from wall paintings: A small-angle neutron scattering study. *Langmuir* **28**, 15193–15202 (2012).
- M. Baglioni et al., Polymer film dewetting by water/surfactant/good-solvent mixtures: A mechanistic insight and its implications for the conservation of cultural heritage. *Angew. Chem. Int. Ed. Engl.* **57**, 7355–7359 (2018).
- M. Baglioni et al., Nanomaterials for the cleaning and pH adjustment of vegetable-tanned leather. *Appl. Phys. A Mater. Sci. Process.* **122**, 114 (2016).
- M. Baglioni et al., Complex fluids confined into semi-interpenetrated chemical hydrogels for the cleaning of classic art: A rheological and SAXS study. *ACS Appl. Mater. Interfaces* **10**, 19162–19172 (2018).
- R. Mastrangelo, C. Montis, N. Bonelli, P. Tempesti, P. Baglioni, Surface cleaning of artworks: Structure and dynamics of nanostructured fluids confined in polymeric hydrogel networks. *Phys. Chem. Chem. Phys.* **19**, 23762–23772 (2017).
- J. A. L. Domingues et al., Innovative hydrogels based on semi-interpenetrating p-(HEMA)/PVP networks for the cleaning of water-sensitive cultural heritage artifacts. *Langmuir* **29**, 2746–2755 (2013).
- N. Bonelli, G. Poggi, D. Chelazzi, R. Giorgi, P. Baglioni, Poly(vinyl alcohol)/poly(vinyl pyrrolidone) hydrogels for the cleaning of art. *J. Colloid Interface Sci.* **536**, 339–348 (2019).
- N. Bonelli, C. Montis, A. Mirabile, D. Berti, P. Baglioni, Restoration of paper artworks with microemulsions confined in hydrogels for safe and efficient removal of adhesive tapes. *Proc. Natl. Acad. Sci. U.S.A.* **115**, 5932–5937 (2018).
- N. A. Peppas, S. R. Stauffer, Reinforced uncrosslinked poly(vinyl alcohol) gels produced by cyclic freezing-thawing processes: A short review. *J. Control. Release* **16**, 305–310 (1991).
- N. A. Peppas, D. Tennenhouse, Semicrystalline poly(vinyl alcohol) films and their blends with poly(acrylic acid) and poly(ethylene glycol) for drug delivery applications. *J. Drug Deliv. Sci. Technol.* **14**, 291–297 (2004).
- V. I. Lozinsky, L. G. Damshkaln, I. N. Kurochkin, I. I. Kurochkin, Study of cryostructuring of polymer systems: 28. Physicochemical properties and morphology of poly(vinyl alcohol) cryogels formed by multiple freezing-thawing. *Colloid J.* **70**, 189–198 (2008).
- P. Levitz, D. Tchoubar, Disordered porous solids: From chord distributions to small angle scattering. *J. Phys. I*, **2**, 771–790 (1992).
- P. Levitz, Toolbox for 3D imaging and modeling of porous media: Relationship with transport properties. *Cement Concr. Res.* **37**, 351–359 (2007).
- L. Di Michele et al., Multistep kinetic self-assembly of DNA-coated colloids. *Nat. Commun.* **4**, 2007 (2013).
- N. Limpan, T. Prodpran, S. Benjakul, S. Prasarnpran, Influences of degree of hydrolysis and molecular weight of poly(vinyl alcohol) (PVA) on properties of fish myofibrillar protein/PVA blend films. *Food Hydrocol.* **29**, 226–233 (2012).
- C. M. Hassan, J. E. Stewart, N. A. Peppas, Diffusional characteristics of freeze/thawed poly(vinyl alcohol) hydrogels: Applications to protein controlled release from multilaminate devices. *Eur. J. Pharm. Biopharm.* **49**, 161–165 (2000).
- V. I. Lozinsky, L. G. Damshkaln, Study of cryostructuring of polymer systems. XVII. Poly(vinyl alcohol) cryogels: Dynamics of the cryotropic gel formation. *J. Appl. Polym. Sci.* **77**, 2017–2023 (2000).
- K. Pal, A. K. Banthia, D. K. Majumdar, Poly(vinyl alcohol)–gelatin patches of salicylic acid: Preparation, characterization and drug release studies. *J. Biomater. Appl.* **21**, 75–91 (2006).
- B. J. Pae et al., Phase behavior in PVA/water solution: The coexistence of UCST and LCST. *Korea Polym. J.* **5**, 126–130 (1997).
- H.-G. Elias, "Solution thermodynamics" in *Macromolecules* (Springer, 1977), p. 233.
- N. J. Crowther, D. Eagland, The volumetric behaviour of poly(vinyl alcohol) in aqueous solution. *J. Chem. Soc. Faraday Trans. 1* **82**, 2791–2799 (1986).
- B. M. Budhllal et al., Characterization of partially hydrolyzed poly(vinyl alcohol). Effect of poly(vinyl alcohol) molecular architecture on aqueous phase conformation. *Macromolecules* **36**, 9477–9484 (2003).
- V. I. Lozinsky et al., Study of cryostructuring of polymer systems VII. Structure formation under freezing of poly(vinyl alcohol) aqueous solutions. *Colloid Polym. Sci.* **264**, 19–24 (1986).
- L. H. Sperling, "Interpenetrating polymer networks: An overview" in *Interpenetrating Polymer Networks*, D. Klemperer, L. H. Sperling, L. A. Utracki, Eds. (American Chemical Society Advances in Chemistry, 1994), pp. 3–38.
- Y. S. Lipatov, T. T. Alekseeva, "Thermodynamics and phase separation in IPNs" in *Phase-Separated Interpenetrating Polymer Networks* (Advances in Polymer Science, Springer, 2007), vol. 208, p. 47.
- L. Di Michele et al., Aggregation dynamics, structure, and mechanical properties of bigels. *Soft Matter* **10**, 3633–3648 (2014).
- F. Yokoyama, I. Masada, K. Shimamura, T. Ikawa, K. Monobe, Morphology and structure of highly elastic poly(vinyl alcohol) hydrogel prepared by repeated freezing-and-melting. *Colloid Polym. Sci.* **264**, 595–601 (1986).
- R. Ricciardi, C. Gallet, G. Ducouret, F. Lafuma, F. Lauprêtre, Investigation of the relationships between the chain organization and rheological properties of atactic poly(vinyl alcohol) hydrogels. *Polymer* **44**, 3375–3380 (2003).
- Y. Chen, B. C. Lagerholm, B. Yang, K. Jacobson, Methods to measure the lateral diffusion of membrane lipids and proteins. *Methods* **39**, 147–153 (2006).
- M. J. Saxton, K. Jacobson, Single-particle tracking: Applications to membrane dynamics. *Annu. Rev. Biophys. Biomol. Struct.* **26**, 373–399 (1997).
- E. Fischer, R. Kimmich, U. Beginn, M. Möller, N. Fatkullin, Segment diffusion in polymers confined in nanopores: A fringe-field NMR diffusometry study. *Phys. Rev. E* **59**, 4079–4084 (1999).
- K. Hyun et al., A review of nonlinear oscillatory shear tests: Analysis and application of large amplitude oscillatory shear (LAOS). *Prog. Polym. Sci.* **36**, 1697–1753 (2011).
- A.-L. Kjøniksen, B. Nyström, Effects of polymer concentration and cross-linking density on rheology of chemically cross-linked poly(vinyl alcohol) near the gelation threshold. *Macromolecules* **29**, 5215–5222 (1996).
- C. Mazzuca et al., Gellan hydrogel as a powerful tool in paper cleaning process: A detailed study. *J. Colloid Interface Sci.* **416**, 205–211 (2014).
- C. Mazzuca et al., Cleaning of paper artworks: Development of an efficient gel-based material able to remove starch paste. *ACS Appl. Mater. Interfaces* **6**, 16519–16528 (2014).
- J. Domingues, N. Bonelli, R. Giorgi, P. Baglioni, Chemical semi-IPN hydrogels for the removal of adhesives from canvas paintings. *Appl. Phys. A* **114**, 705–710 (2013).
- P. Baglioni, D. Chelazzi, R. Giorgi, "Cleaning of easel paintings" in *Nanotechnologies in the Conservation of Cultural Heritage: A Compendium of Materials and Techniques* (Springer, 2015), pp. 83–116.
- C. Duce et al., FTIR study of ageing of fast drying oil colour (FDOC) alkyd paint replicas. *Spectrochim. Acta A Mol. Biomol. Spectrosc.* **130**, 214–221 (2014).
- B. J. Saikia, G. Parthasarathy, Fourier transform infrared spectroscopic characterization of kaolinite from Assam and Meghalaya, Northeastern India. *J. Mod. Phys.* **01**, 206–210 (2010).
- A. Burnstock, R. White, "A preliminary assessment of the aging/degradation of Ethomeen C-12 residues from solvent gel formulations and their potential for inducing changes in resinous paint media" in *Tradition and Innovation: Advances in Conservation: Contributions to the Melbourne Congress, 10–14 October 2000*, A. Roy, P. Smith, Eds. (International Institute for Conservation of Historic and Artistic Work, 2000), pp. 34–38.
- D. Stulik et al., *Solvent Gels for the Cleaning of Works of Art: The Residue Question*, D. Stulik, V. Dorge, Eds. (The Getty Conservation Institute, J. Paul Getty Trust, 2004).

PAPER IV

Nonionic Surfactants for the Cleaning of Works of Art: Insights on Acrylic Polymer Films Dewetting and Artificial Soil Removal

Michele Baglioni, Teresa Guaragnone, Rosangela Mastrangelo, Felipe Hidetomo Sekine, Taku Ogura, and Piero Baglioni*



Cite This: *ACS Appl. Mater. Interfaces* 2020, 12, 26704–26716



Read Online

ACCESS |



Metrics & More



Article Recommendations



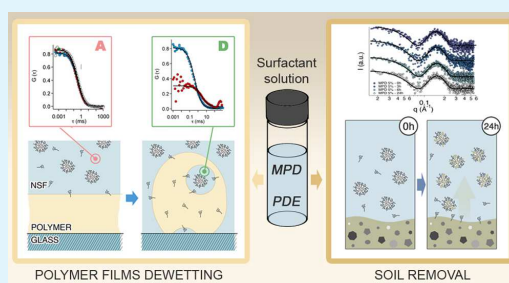
Supporting Information

ABSTRACT: The use of nanostructured fluids (NSFs), that is, micellar solutions and microemulsions, in art conservation is often associated with cleaning purposes as the removal of polymeric coatings and/or soil from artistic surfaces. In both cases, the use of NSFs grants significant improvements over the use of traditional cleaning techniques that employ neat unconfined organic solvents, water, or aqueous solutions. The study of the nature and properties of surfactants present in NSF formulations is important to boost the effectiveness of these systems in applicative contexts and in the search of innovative and highly performing amphiphiles. This work reports on the methoxy-pentadeca(oxyethylene) dodecanoate (MPD) surfactant in two different NSFs, whose utilization in conservation of cultural heritage is new. Its effectiveness is compared to the conventional nonionic amphiphiles used in conservation practice, as pentadeca(oxyethylene) dodecyl ether, for the cleaning of poly(ethyl methacrylate/methyl acrylate) 70:30, p(EMA/MA), and artificially soiled surfaces. The mechanism, through which NSFs interact with polymeric coatings or soiled surfaces, was investigated by confocal laser scanning microscopy, fluorescence correlation spectroscopy, photographic observation, contact angle, surface tension measurements, and small-angle X-ray scattering. The results highlighted the superior MPD's performance, both in inducing polymer removal and in detaching the soil from coated surfaces. At the microscale, the cleaning involves dewetting-like processes, where the polymer or the soil oily phase is detached from the surface and coalesce into separated droplets. This can be accounted by considering the different surface tensions and the different adsorption mechanisms of MPD with respect to ordinary nonionic surfactants (likely due to the methyl capping of the polar head chain and to the presence of the ester group between the hydrophilic and hydrophobic parts of the MPD surfactant molecule), showing how a tiny change in the surfactant architecture can lead to important differences in the cleaning capacity. Overall, this paper provides a detailed description of the mechanism and the kinetics involved in the NSFs cleaning process, opening new perspectives on simple formulations that are able to target at a specific substance to be removed. This is of utmost importance in the conservation of irreplaceable works of art.

KEYWORDS: methoxy-pentadeca(oxyethylene) dodecanoate, pentadeca(oxyethylene) dodecyl ether, microemulsions, cleaning, conservation of cultural heritage, confocal laser scanning microscopy, fluorescence correlation spectroscopy, small-angle X-ray scattering

1. INTRODUCTION

Nanostructured fluids (NSFs), such as micellar solutions and microemulsions, have been proposed as innovative cleaning systems in the field of conservation of cultural heritage, see Chelazzi et al.,¹ Baglioni et al.,² and references there in. Nowadays, they are an important part of the palette of the methodologies commonly used by conservators for the cleaning of works of art.^{1–8} NSFs used in art conservation are mostly related to two main cleaning issues: the removal of polymeric coatings^{9–11} (protective and consolidating agents, fixatives, adhesives, aged or fresh varnishes, graffiti, overpaintings, etc.) and the removal of soil^{1,2,12–14} (dust, particulate matter, grime, oily substances, sebum, wax stains, etc.). This last represents the most common of the



interventions on artworks. In both cases, the use of NSFs grants significant improvements over the use of traditional cleaning methods, that is, the use of neat unconfined organic solvents, water, or aqueous solutions. The synergistic action of organic solvents and surfactants allows excellent cleaning performances, combined with a safe and controlled application. In fact, in a generic NSF, the organic solvent is confined in the

Received: April 7, 2020

Accepted: May 12, 2020

Published: May 12, 2020



water continuous phase and its amount is reduced to a few percentages, drastically lowering both the environmental impact of the methodology and the health risk for operators. Moreover, compared to unconfined organic solvents, NSF s are particularly effective for the removal of (hydrophobic) polymeric coatings. Different from organic solvents, which are chosen to dissolve a given polymer, NSF s are usually selected to be non-solvents for the polymer, in order to swell the film and detach it from the substrate surface through, depending on the polymer nature, a dewetting process.^{15–18} Dewetting is a well-known physical phenomenon defined as the spontaneous withdrawal of a film of fluid (i.e., from low viscosity liquids to highly viscous swollen polymers) from a surface and subsequent rearrangement in the form of separated droplets.^{19–24} The dewetting process of polymeric coatings from artistic surfaces induced by NSF s grants that polymer macromolecules are not spread into the work of art, as it would happen with neat unconfined organic solvents, resulting in an effective and controlled cleaning action. The nature of the organic solvents included in the NSF has a major role in the dewetting of polymers from solid surfaces, as they are selected to increase the mobility of polymer chains by swelling the film. Moreover, the surfactant nature is crucial to kinetically favor this process. In fact, the surfactant, lowering the polymer/solid interfacial tension, energetically favors the detachment of the film from the solid surface, and it was shown that a partial detachment of the polymer from the surface represents the first step of dewetting processes.^{16–18} Thus, amphiphile-based systems having low interfacial tension may be particularly effective as dewetting agents. Most recently, it was also observed that surfactants too have a role in increasing polymer chains mobility, making them the key components in NSF s for polymer removal.^{17,18}

In many cases, works of art do not present polymeric coatings, but their visual aspect is compromised by the presence of soil/grime at the surface. Soil is composed of a variety of usually low molecular weight substances that accumulate on the surface of works of art as a result of ageing, unsuitable storage, or detrimental practices, from previous conservations, and so forth. A wide choice of cleaning methodologies is employed for soil removal, according to the specific needs of the given conservation case, spanning from the use of mechanical methods, to pure water, to the use of aqueous solutions of pH buffers, chelating agents, or surfactants, which may be applied by means of brushes, cotton swabs, poultices, thickeners, physical gels,^{25–28} or technologically more advanced solutions, such as highly retentive semi-interpenetrated or twin-chain polymer chemical gels, which grant the safest and most controllable cleaning action.^{10,29,30} Among the chemicals used for soil removal, surfactants certainly play a major role, and in particular when they are formulated as micellar solutions or microemulsions constitute the most effective tools available to conservators. Thus, nature and properties of surfactants are important to boost the effectiveness of NSF s in applicative contexts, and the search for innovative and highly performing amphiphiles is one of the main goals in the field of conservation of Cultural Heritage and in many practical applications in cosmetics, detergency, and so forth.

This work reports on the use of a relatively innovative surfactant, a methoxy-pentadeca(oxyethylene) dodecanoate (MPD),^{31–35} which is sometimes present in commercial detergents,^{36–38} but its cleaning mechanism is poorly under-

stood and its utilization in conservation of cultural heritage is completely new, to the best of our knowledge. In particular, the effectiveness of MPD-based NSF s was studied and compared to the commonly employed PDE (C₁₂EO₁₅, pentadeca(oxyethylene) dodecyl ether)-based NSF s. In order to quantify the mechanism of action and the effectiveness of the cleaning systems, the MPD- and PDE-based NSF s were formulated to solve two conservative challenges: (i) polymer coatings removal and (ii) soil removal. In the first case, the removal of poly(ethyl methacrylate/methyl acrylate) 70:30, p(EMA/MA), commercially known as Paraloid B72, was studied on model systems as polymer-coated glass slides. The interaction mechanism between the polymer film and the cleaning fluid was investigated by means of confocal laser scanning microscopy (CLSM), fluorescence correlation spectroscopy (FCS), dynamic light scattering (DLS), and small-angle X-ray scattering (SAXS). Paraloid B72 is one of the most used polymers in conservation of cultural heritage,^{39–42} and it was widely used for a variety of different purposes and on different substrates. MPD- and PDE-based NSF s have been tested for soil removal from glass and polystyrene substrates coated with an artificial soil, prepared following standard procedures available in the literature,⁴³ and characterized by means of visual and photographic observation, CLSM investigation, contact angle, surface tension measurements, and SAXS. Overall, MPD-NSF s were found to be superior over NSF s based on conventional nonionic surfactants.

2. MATERIALS AND METHODS

2.1. Chemicals. C₁₁(C=O)EO₁₅-CH₃, MPD (Nikko Chemicals, assay 99%), C₁₂EO₁₅, PDE (Nikko Chemicals, assay +99%), dodecyl dimethyl amine oxide (DDAO, Sigma-Aldrich, 30% aqueous solution), sodium dodecyl sulfate (SDS, Sigma-Aldrich, assay 99%), propylene carbonate (PC, Sigma-Aldrich, assay 99%), 2-butanone (MEK, Sigma-Aldrich, purity 99%), 2-butanol (BuOH, Sigma-Aldrich, assay >99%), ethyl acetate (EtAc, Sigma-Aldrich, ACS Reagents, assay ≥99.5%), and the fluorescent probes used for CLSM experiments, i.e., rhodamine 110 chloride, Nile red, coumarin 6 (Sigma-Aldrich, purity >98–99%), and Bodipy 558/568 C12 (4,4-difluoro-5-(2-thienyl)-4-bora-3a,4a-diaza-s-indacene-3-dodecanoic acid) (Thermo Fisher) were used without further purification. Water was purified with a Millipore Milli-Q gradient system (resistivity >18 MΩ cm). Carbon black, iron oxide (ochre), silica, kaolin, gelatin powder, Japanese paper (9.6 g/m²), poly(ethyl methacrylate/methyl acrylate) [p(EMA/MA)], Paraloid B72, pellets, and cellulose powder (Arbocel BC200, J. Rettenmaier & Sohne, GmbH) were purchased from Zecchi, Florence. Soluble starch, cement, olive oil, mineral oil, and white spirit were commercially available and thus purchased in non-specialized stores.

2.2. Nanostructured fluids. The experiments reported in this study involved different NSF s. In particular, for the experiments on polymer (Paraloid B72) removal, four different formulations were selected, by combining the two surfactants MPD and PDE with two different organic solvents, PC and MEK, both partly miscible with water, and used as reference solvents in previous studies^{16,17} (see Tables S1 and S2). Besides MPD and PDE, an anionic (SDS) and a zwitterionic/cationic (DDAO) surfactant were used as reference amphiphiles.⁴⁴ For soil removal experiments, micellar solutions of MPD and PDE were used, at two different surfactant concentrations, that is, 1 and 5% w/w.

2.3. Artificial Soil. The artificial soil mixture was prepared according to the standard formulation available in the literature⁴³ and detailed in Supporting Information Table S3.

2.4. Sample Preparation. **2.4.1. CLSM Investigation on Polymer/NSF Interaction.** For CLSM experiments on Paraloid B72/NSF s interaction, polymer films of about 2 μm thickness were prepared by spin-coating about 200 μL of a 10% w/w p(EMA/MA)

solution in EtAc on coverglasses (2000 rpm, 120 s). The polymer films were stained with coumarin 6, co-dissolved with the polymer solution.

2.4.2. Polymer Removal Tests on Glass Slides. Weighed $5 \times 5 \text{ cm}^2$ frosted glass slides were coated by drop-casting a 10% w/w p(EMA/MA), Paraloid B72, solution in EtAc, which was let drying until constant weight was reached. The average final amount of p(EMA/MA) on each glass slide was about 80 mg.

2.4.3. CLSM Investigation on Soil/NSF Interaction. For CLSM experiments on soil/NSF interaction, glass slides were coated by drop-casting 150 μL of the artificial soil dispersion stained with Nile red 10^{-6} M , previously dissolved in white spirit. The samples were let completely drying for at least a week and then used for the experiments.

2.4.4. Soil Removal Tests on Glass and Polystyrene Slides. Weighed $5 \times 5 \text{ cm}^2$ frosted glass and polystyrene slides were coated by drop-casting 1 mL of the artificial soil dispersion. The samples were let drying until constant weight was reached, and the final "dry" weight of the soil coating was about 2–3 mg/cm^2 , on average.

2.4.5. FCS Investigation on Polymer/NSF Interaction. Paraloid B72 films were labeled by dissolving the hydrophobic dye coumarin 6 in the 10% w/w p(EMA/MA) solution in EtAc, to a final concentration of 1 mM ca. 2 μm thick films were prepared on glass slides through the same spin-coating procedure reported for CLSM experiments. FCS allows the tracking of fluorescent-labeled species diffusing in solution. Thus, the microemulsion droplets in solution were labeled by dissolving Bodipy in the NSF to a final concentration of 10 nM. Bodipy is an amphiphilic dye with absorption and emission spectra well separated from the ones of coumarin 6.

2.5. Paraloid B72 Removal on Glass Slides. The study of the polymer removal was performed on frosted glass slides, prepared as reported in Section 2.4.2, using cellulose pulp poultices imbibed with the NSFs, and placing a sheet of Japanese paper between the poultices and the polymer film. The poultices were left interacting for 1.5 h, removed, and then the surface was gently rinsed with water to remove possible surfactant residues. After complete drying of the samples, the treated glass slides were weighed to obtain the % of removed polymer.

2.6. Soil Removal Tests on Glass and Polystyrene Slides. Soiled glass and polystyrene slides were immersed for 24 h in 40 mL of the following aqueous micellar solutions: MPD 1%, MPD 5%, PDE 1%, PDE 5% (w/w). During the experiments, the samples were not subjected to any mechanical action. At $t = 0, 3, 6,$ and 24 h, the immersed samples were photographed and the cleaning fluid in contact with the soil layer was sampled by taking small amounts of liquid, which was subsequently investigated by SAXS measurements, in order to follow the possible NSF structural evolution during the interaction with soil. After 24 h, samples were taken out from the NSFs and tilted with care, in order to check for the residual adhesion of the soil coating to the glass/polystyrene surface.

2.7. Confocal Laser Scanning Microscopy. Confocal Microscopy experiments were performed on a Leica TCS SP8 confocal microscope (Leica Microsystems GmbH, Wetzlar, Germany) equipped with a 63 \times water immersion objective. Rhodamine 110 chloride and coumarin 6 were excited with the 488 nm laser line of an argon laser, while Nile red was excited with a DPSS solid state laser at 561 nm. The emission of the dyes was acquired with two PMTs in the range 498–530 and 571–630 nm, respectively. CLSM experiments were performed to monitor the interaction of the polymer films or soil with different NSFs, as detailed in Section 2.2.

2.7.1. Paraloid B72/NSF Interaction. Unlabeled liquid phase (200 μL) were left in contact with the coumarin 6-stained Paraloid B72-coated coverglass, and the morphological variations of the polymeric film were monitored over time, up to 20 min.

2.7.2. Soil/NSFs Interaction. Liquid phase (200 μL) labeled with rhodamine 110 chloride were left in contact with the Nile red-stained soiled coverglass, and the morphological variations of the soil coating were monitored over time, up to 10 min.

2.8. Contact Angle Measurements. Surfactant adsorption was indirectly evaluated by measuring the contact angle of 5 μL of Milli-Q water droplets on soiled glass slides with a Rame-Hart model 190 CA

Goniometer. Three samples were analyzed, that is, pristine soil-coated glass slide and two soil-coated glass slides immersed for 1 min in a 1% w/w MPD and PDE solution, respectively. The equilibrium contact angle was measured in at least five different areas, and the average value and standard deviation were evaluated.

2.9. Surface Tension Measurements. Surface tension values of MPD and PDE aqueous solutions were determined with a K100 Tensiometer (Krüss, GmbH, Hamburg, Germany). The surface tension was measured at different concentrations by adding a concentrated stock solution of surfactant in water to a known volume of water (40 mL). Surface tension measurements were carried out with a platinum plate, and for each concentration, the average of ten readings was taken after attaining the equilibrium.

2.10. Small-Angle X-ray Scattering. SAXS measurements were performed with a HECUS S3-MICRO SWAXS-camera, equipped with a Hecus System 3 2D-point collimator (min divergence $0.4 \times 0.9 \text{ mrad}^2$), and two position sensitive detectors (PSD-50M) consisting of 1024 channels with a width of 54 μm . The K_α radiation ($\lambda = 1.542 \text{ \AA}$) emitted by a Cu anode from the Oxford 50 W microfocus source with customized FOX-3D single-bounce multilayer point focusing optics (Xenocs, Grenoble) was used, while the K_β line was removed using a multilayer filter. The voltage was generated by the GeniX system (Xenocs, Grenoble). The sample-to-detector distance was 26.9 cm. The volume between the sample and the detector was kept under vacuum during the measurements to minimize the scattering from the atmosphere. The camera was calibrated in the small-angle region using silver behenate ($d = 58.38 \text{ \AA}$). Scattering curves were obtained in the q -range between 0.008 and 0.5 \AA^{-1} . The temperature control was set to 25 $^\circ\text{C}$. Samples were contained in 2 mm thick quartz capillary tubes sealed with hot-melting glue. Scattering curves were corrected for the empty capillary contribution considering the relative transmission factors. Desmearing of the SAXS curves was not necessary thanks to the focusing system. The fitting model adopted is described in detail in the Supporting Information file.

2.11. Fluorescence Correlation Spectroscopy. FCS measurements were performed with a Leica TCS SP8 confocal microscope (Leica Microsystems GmbH, Wetzlar, Germany) equipped with a PicoQuant FCS modulus (PicoQuant, Berlin, Germany). A water immersion objective 63 \times /1.2 W (Zeiss) was used. The evolution of the structure of the fluorescent-labeled film during the interaction with the NSFs was followed by confocal imaging, exciting the green dye coumarin 6 with the 488 nm laser line, and collecting the emitted signal with a PMT in the range 498–530 nm, as reported in the Confocal Laser Scanning Microscopy section. Once the polymer film structure was stabilized (i.e., no fast rearrangements were occurring) the diffusion of Bodipy, located at the microemulsion droplet interfaces, was monitored through FCS. The dye was excited with the DPSS 561 laser (561 nm), while the fluorescence intensity was acquired using a hybrid SMD detector in the 571–630 nm range. Freshly-prepared samples (water/solvents, water/surfactants and the four NSFs labeled with 10 nM Bodipy) were, at first, analyzed before the interaction with the polymer film by pouring the solutions in the appropriate sample-holder (Lab-Tek Chambered #1.0 Borosilicate Coverglass System, Nalge Nunc International, Rochester, NY, USA). Then, 200 μL of the labeled solutions were poured on the polymer-coated glass slides. During the liquid–polymer interaction, different areas were probed through FCS measurements. Depending on the sample, the diffusion of Bodipy was measured either in the liquid-filled cavities formed at the polymer/glass interface (for MEK-based NSFs), or in the cavities found inside the dewetted polymer (for PC-based NSFs), and in the bulk liquid on the top of the polymer film, after 20 min of interaction (for all the systems). Measurements were performed at 25 $^\circ\text{C}$. More details on the data analysis are reported in the Supporting Information file (FCS data analysis).

2.12. Dynamic Light Scattering. DLS measurements were performed on a Brookhaven Instruments apparatus (BI 9000AT correlator and BI 200 SM goniometer) equipped with a EMI 9863B/350 photomultiplier. The 633 nm He-Ne laser was used to avoid light absorption by the Bodipy labeled systems. Measurements on the simple water-surfactant systems and on the NSFs were carried out at

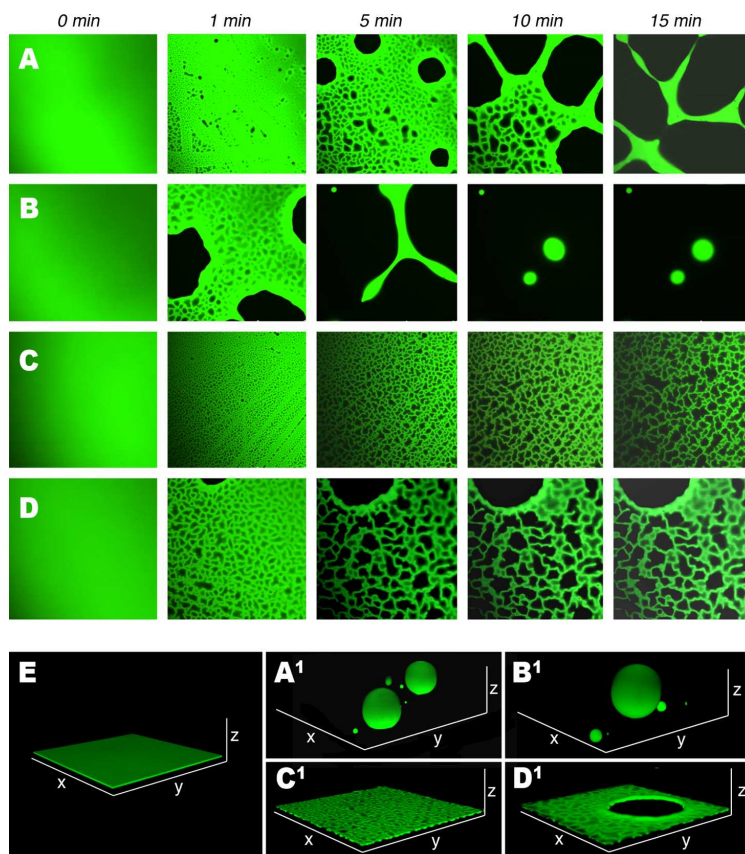


Figure 1. CLSM results on p(EMA/MA) interacting with (A) H₂O/PC/PDE, (B) H₂O/PC/MPD, (C) H₂O/MEK/PDE, and (D) H₂O/MEK/MPD. (E) 3D reconstruction of the polymer film before the interaction with NSFs, (A¹–D¹) 3D reconstructions of the polymer after 20 min of interaction with (A¹) H₂O/PC/PDE, (B¹) H₂O/PC/MPD, (C¹) H₂O/MEK/PDE, and (D¹) H₂O/MEK/MPD, which clarify the morphology of the film at the end of the experiments. The bottom side of each CLSM frame is 150 μ m long.

90 and 25 °C. The signal was collected performing 8 min measurements, and the diffusion coefficients were obtained either from a second-order cumulant analysis or by the weighted average of the values obtained by the CONTIN algorithm.⁴⁵ In the second case, the values of diffusion coefficients were obtained as weighted average of the most recurrent components (components accounting for less than 8% of the population were not considered). All data shown are the average of three repetitions, with relative standard deviations.

3. RESULTS AND DISCUSSION

This study focuses on the mechanism and kinetics of MPD cleaning and detergent properties in the context of cultural heritage conservation. As reported above, two main conservative issues are the scope of this study, that is, polymer removal and soil removal. Besides testing the efficacy of proposed NSFs based on MPD surfactant, our aim was to understand the interaction between this surfactant and the materials to be removed because in art conservation the value of the works of art impose very specific, controlled, and performing cleaning, without any possible damage to the original works. To this aim, all the experiments on MPD behavior and performances were compared to those obtained

replacing MPD surfactant with its alcohol ethoxylate homologue, PDE.

Recently, a thorough study by Sato et al.⁴⁶ showed that the physico-chemical behaviors of MPD and PDE are significantly different, despite their similar molecular architecture. In particular, phase behavior in water and the polar head hydration are different for the two surfactants. This leads to a different excluded volume for the micelles and different effective micellar volume fraction for the two systems. These findings partly explain the experimental evidence that MPD possesses better cleaning efficiency than PDE, especially in low mechanical conditions, that is, when micellar solutions are kept in contact with soiling materials without stirring. In particular, the removal of oleic acid from fabrics by PDE and MPD micellar solutions was studied by means of several techniques, and it was found that at the equilibrium state both surfactants have almost the same emulsification and solubilization power toward oleic acid, while, before the system is equilibrated, PDE is preferentially adsorbed onto oleic acid coatings in the form of lamellar structures. On the contrary, MPD is less efficiently

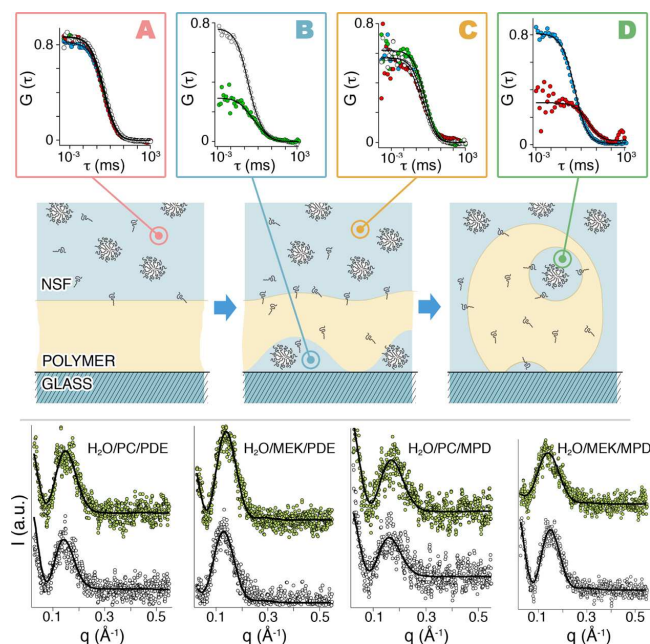


Figure 2. Cartoon illustrates the behavior of the NSF droplets. After the local detachment of the polymer from the glass surface, the complex fluid droplets penetrate through the polymer and reach liquid-filled cavities. The top boxes report the FCS curves taken at $t = 0$ min (A), at time $t = 5$ – 15 min (B,D) and after 20 min of incubation (C) of the polymer with the four different NSFs; H₂O/PC/PDE (blue circles), H₂O/PC/MPD (red circles), H₂O/MEK/PDE (white circles), and H₂O/MEK/MPD (green circles). The best fittings are shown as solid black lines. (Bottom) SAXS profiles of the four NSFs before (white circles) and after (green circles) 20 min of incubation of interaction with the polymer. The best fittings are shown as solid black lines. The curves have been arbitrarily offset for sake of clarity.

adsorbed onto the soil surface and tends to solubilize the oil in the hydrophobic core of micelles.⁴⁷

3.1. Polymer Film Removal. As already stated, polymer film removal with NSFs usually involves dewetting. From a thermodynamic point of view, the tendency of a film to dewet from a surface is described by the spreading coefficient, S , which accounts for the energetic balance of the system. In the case of a polymer film laid on a glass surface and immersed in a liquid, S is expressed as follows⁴⁸

$$S = \gamma_{LG} - \gamma_{PG} - \gamma_{PL}$$

where γ_{LG} is the interfacial tension between the glass and the liquid, γ_{PG} is the interfacial tension between the glass and the polymer, and γ_{PL} is the interfacial tension between the polymer and the liquid. In total wetting regime ($S > 0$), films are always stable and dewetting does not occur. On the other hand, when a fluid (or a polymer, considered as a fluid in this context) is only partly wetting ($S < 0$), films are unstable or metastable and dewetting is thermodynamically favored below a critical thickness h_c , which for most substances is in the range of millimeters. Even in these last conditions, dewetting does not necessarily take place. In fact, it can be inhibited by a kinetic factor, that is, an energy barrier has to be overcome in order to induce the process. For thin films (thickness, $h < 100$ nm), this energy barrier is usually low and the film is unstable. This instability generates capillary waves through the film, and when their fluctuation exceeds the film thickness h , the film itself spontaneously breaks down into separated droplets according

to a mechanism termed spinodal dewetting.¹⁹ Thick films ($h > 100$ nm), on the other hand, are metastable. A $2 \mu\text{m}$ -thick hydrophobic polymer film laid on a hydrophilic surface, such as glass, as in the case of the experiments here reported, is a good example of metastable system, where dewetting would be thermodynamically favored but kinetically inhibited because of the low mobility of entangled macromolecular chains in the film. Whenever this mobility is enhanced, the film becomes unstable and dewetting occurs. Enhanced chain mobility can be induced essentially in two distinct ways: (i) the film is heated at a temperature higher than its glass transition temperature, T_g ⁴⁹ and (ii) the film is exposed to some organic solvents, which swell the polymer, lowering its T_g below room temperature.^{22,50} The experiments shown in Figure 1 belong to this latter case. The figure reports the results of CLSM investigation on the interaction of $2 \mu\text{m}$ thick p(EMA/MA) films, deposited on glass slides, with four different NSFs based on two different organic solvents, PC and MEK, and the two surfactants object of this study, MPD and PDE. PC and MEK were selected as the NSF organic solvents because it was recently found that they show a different behavior in inducing p(EMA/MA) dewetting, and, in particular, PC is more efficient than MEK.^{16,17}

The interaction process was monitored at the polymer/glass interface. Figure 1 shows the morphological evolution of continuous polymeric films (visible in green). Upon interacting with the NSFs, some dark areas appear in the confocal plane, meaning that the polymer is no longer present in those areas.

The observation of the film along the z-axis (here not reported) shows that the dark areas are not holes that go through the whole film thickness; instead, they are liquid-filled cavities that form as the polymer is locally detached and lifted from the solid surface. The rims of polymer remaining onto the glass surface draw a characteristic shape termed Voronoi pattern or tessellation.¹⁹ As the cavities grow and coalesce, they become weaker and the film eventually breaks with the nucleation of holes, according to a well-known and described mechanism for the dewetting of thick films,¹⁹ and as the glass is exposed to the bulk liquid phase, the polymer withdraws from the surface in the form of thick rims, which again describe a Voronoi pattern but on a larger scale. Complete dewetting is reached when polymer rims are also disrupted and swollen polymer globular droplets form.

It was found that the two PC-based NSF s are able to completely dewet the polymer from the glass, while in the case of MEK-based NSF s, no complete dewetting was observed after 20 min of interaction (see Figure 1). Interestingly, considering the time for the dewetting onsets for NSF s based on the same solvent (compare the series of Figure 1A,B), MPD is more efficient than PDE in inducing polymer dewetting. After only 5 min, the polymer interacting with the H₂O/PC/MPD system is almost completely dewetted, while at the same time, the film interacting with the H₂O/PC/PDE system showed just a few 20–30 μm large holes in an otherwise continuous polymer film. The same trend could be observed in the MEK-based systems. Figure 1C,D clearly shows that the interaction process is boosted by the presence of MPD. The difference in the dewetting process can be explained in view of the mechanism through which dewetting takes place in its early stages. When the polymer is locally detached from the solid surface, a portion of the polymer/glass interface is “destroyed”, while new interfacial regions are formed between the polymer/liquid and the glass/liquid phases, with an overall increase of the total interfacial area of the system. It was found that the main role of surfactants in this process is reducing the energy costs related to the formation of this intermediate state, by lowering the interfacial tension.¹⁷ Therefore, the interfacial tension of both surfactants was measured over a wide concentration range, from well above the cmc of the surfactants to more than 100 times lower (see Figure S5). It was found that the surface tension of the MPD micellar solution, $\gamma_{MPD} \approx 34.5$ N/m, is lower than that of PDE, $\gamma_{PDE} \approx 37.5$ N/m, which is in agreement with a kinetically boosted dewetting process for this surfactant. In addition, it can be hypothesized that the presence of the methyl capping at the end of the polyoxyethylene chain of MPD confers to this surfactant an increased hydrophobicity and thus a higher capability of penetrating into the p(EMA/MA) film, with a consequent enhancement of polymer chains mobility. Overall, these factors account for the better performances of MPD over PDE.

In order to get a detailed picture of the polymer dewetting process, induced by MPD- and PDE-based NSF s, the diffusion and the evolution of the droplets during the film/liquid interaction were investigated by means of FCS and SAXS measurements. The main results of these experiments are reported in Figure 2.

For confocal experiments, micellar solutions (H₂O/PDE 5% and H₂O/MPD 5%) were labeled with Bodipy, as described in the Materials and Methods section. In order to determine if the Bodipy dye addition affects the micelles, the diffusion of

micellar species in labeled and unlabeled systems was measured through DLS. The results show that micelles' diameter does not significantly change after labeling (the *D* values obtained by the cumulant analysis are reported in Table 1).

Table 1. Average Diffusion Coefficients, *D* (μm²/s), Obtained by DLS Analysis

system	<i>D</i> (μm ² /s) for unlabeled sample	<i>D</i> (μm ² /s) for Bodipy-labeled sample
H ₂ O/PDE	85 ± 3 ^a	81 ± 2 ^a
H ₂ O/MPD	88 ± 6 ^a	86 ± 3 ^a
H ₂ O/MEK/PDE	85 ± 11 ^b	87 ± 10 ^b
H ₂ O/PC/PDE	72 ± 5 ^b	75 ± 15 ^b
H ₂ O/MEK/MPD	73 ± 5 ^a	87 ± 6 ^b
H ₂ O/PC/MPD	77 ± 2 ^a	78 ± 2 ^b

^aValues and standard deviations obtained by cumulant analysis. ^bWeighed averages of the most recurrent *D* values obtained by CONTIN algorithm, with standard deviation.

PC or MEK addition to the unlabeled or labeled micellar systems produces small changes of the micellar diffusion coefficients, indicating that micelle size is only slightly affected. The diffusion coefficients reported in Table 1 were obtained as weighed average of the most recurrent *D* values obtained from the CONTIN analysis.

The analysis of the light scattering data by the CONTIN algorithm on labeled and unlabeled systems returns an average diffusion coefficient of 80 μm²/s that was used as “guess value” for the FCS data analysis. SAXS measurements performed on the four NSF s before and after 20 min of interaction with the polymer were also used as an input for FCS analyses. Figure 2 (bottom) shows the fitted scattering profiles of all the investigated samples, while Table 2 reports the main fitting

Table 2. SAXS Fitting Parameters for the NSF s, Measured before and after the Interaction with the p(EMA/MA) Film^a

system	fitting parameter	before interaction	after 20 min interaction
H ₂ O/MEK/MPD	<i>r_c</i> (Å)	16.2 ± 0.1	15.2 ± 1.6
	<i>t</i> (Å)	15.3 ± 0.4	15.6 ± 3.4
	PDI	0.12 ± 0.01	0.15 ± 0.01
H ₂ O/PC/MPD	<i>r_c</i> (Å)	11.5 ± 0.2	12.0 ± 3.6
	<i>t</i> (Å)	19.7 ± 0.7	17.0 ± 6.5
	PDI	0.15 ± 0.01	0.15 ± 0.01
H ₂ O/MEK/PDE	<i>r_c</i> (Å)	17.3 ± 0.1	16.8 ± 0.8
	<i>t</i> (Å)	16.0 ± 0.5	16.2 ± 1.6
	PDI	0.14 ± 0.01	0.12 ± 0.01
H ₂ O/PC/PDE	<i>r_c</i> (Å)	13.2 ± 0.1	13.8 ± 2.5
	<i>t</i> (Å)	22.1 ± 0.6	18.7 ± 4.7
	PDI	0.15 ± 0.01	0.15 ± 0.01

^aPDI is the polydispersity index; *r_c* is the average core radius; *t* is the shell thickness.

parameters. SAXS analysis shows that the size, shape, and polydispersity are poorly affected by the interaction of MPD and PDE-based NSF s with the Paraloid B72 film, suggesting that up to 20 min of application, the NSF s do not solubilize the p(EMA/MA) polymer film.

The confocal analysis of the cleaning process indicated that dewetting was, as expected, the main process for the polymer

Table 3. Diffusion Coefficient Values ($\mu\text{m}^2/\text{s}$) and Percentage of D_1 Component in the Total Decay, Obtained Through the Fitting of FCS Curves of MEK-Based NSF^a

NSF	D_{bulk} ($t = 0$ min)	D_{cav} ($t = 5$ min)	D_{cav} ($t = 12$ min)	D_{bulk} ($t = 20$ min)
H ₂ O/MEK/PDE	$D_1 = 80$ (40%)	$D_1 = 80$ (80%)	$D_1 = 80$ (80%)	$D_1 = 80$ (40%)
	$D_2 = 17 \pm 2$	$D_2 = 0.4 \pm 0.2$	$D_2 = 6 \pm 2$	$D_2 = 16 \pm 5$
H ₂ O/MEK/MPD	$D_1 = 80$ (50%)	$D_1 = 80$ (70%)	$D_1 = 80$ (60%)	$D_1 = 80$ (50%)
	$D_2 = 17 \pm 3$	$D_2 = 7 \pm 3$	$D_2 = 6 \pm 3$	$D_2 = 6 \pm 2$

^aFCS was performed into liquid-filled cavities trapped inside the dewetted polymer (Cav) and in the solution on the top of the film D_{bulk} . Error for D_1 component is about 10%.

removal. FCS was used to shed light on the cleaning mechanism in the “dewetting-like” polymer removal. The autocorrelation functions, $G(t)$, obtained by FCS measurements have been analyzed considering two-components decays (see Supporting Information, FCS data analysis) and using as initial guess the parameters obtained from DLS and SAXS data analysis. The diffusion of the Bodipy-labeled NSFs was measured through FCS, before and during the interaction with the polymer film, in different sample regions, as shown in Figure 2. Data on the diffusion of the droplets forming the NSFs disperse phase were collected both inside the liquid-filled cavities that form in the swollen polymer (i.e., at the polymer/glass interface for MEK-based systems, inside the dewetted polymer droplets for PC-based systems), and in the bulk liquid on top of the film, after 20 min of interaction.

The results are shown in Figure 2A–D, and the calculated diffusion coefficient, D , are reported in Tables 3 and 4.

Table 4. Diffusion Coefficient Values ($\mu\text{m}^2/\text{s}$) and Percentage of D_1 Component in the Total Decay, Obtained through Fitting of FCS Curves of PC-Based NSF^a

NSFs with PC	D_{bulk} ($t = 0$ min)	D_{cav} ($t = 10$ min)	D_{bulk} ($t = 20$ min)
H ₂ O/PC/PDE	$D_1 = 80$ (50%)	$D_1 = 33 \pm 2$ (99%)	$D_1 = 80$ (50%)
	$D_2 = 19 \pm 4$	$D_2 = 0.01$	$D_2 = 13 \pm 4$
H ₂ O/PC/MPD	$D_1 = 80$ (60%)	$D_1 = 5 \pm 2$ (90%)	$D_1 = 64 \pm 40$ (40%)
	$D_2 = 18 \pm 4$	$D_2 = 0.1$	$D_2 = 4$

^aFCS was performed into liquid-filled cavities trapped inside the dewetted polymer (Cav) and in the solution on the top of the film D_{bulk} . Error for D_1 component is about 10%.

The composition and aggregates' size in the bulk MEK-based NSFs remains almost the same before and after the interaction with the polymer film, except for the slow component $D_{2\text{-bulk}}$ in the H₂O/MEK/MPD system, which decreases after the interaction. However, the most remarkable features of these systems lie in the description of the diffusive behavior of labeled species in the NSF confined into the polymer cavities that form at the polymer/glass interface. The main result is that according to measured diffusion coefficients, NSF droplets are able to penetrate inside these cavities (see $D_{1\text{-cav}}$ values in Table 3). Thus, the swollen film is somehow permeable to the passage of either micellized or monomeric surfactant. In fact, data show that the polymer film is more easily penetrated by the smaller droplets, diffusing at $80 \mu\text{m}^2/\text{s}$.

The values of $D_{2\text{-cav}}$ for both MEK- and PC-based NSFs suggest the presence of micelles/microemulsion droplets–polymer interactions inside the cavities formed at the polymer/glass interface. This can be explained either as diffusion coefficient of NSF droplets being slowed down by the

interaction with the polymer walls of the cavity or as droplet growth due to the solubilization of low-molecular weight polymer chains extracted from the swollen polymer. Apart from this similarity, the two surfactants show a different behavior.

In the case of the H₂O/MEK/PDE system, the NSF inside the confined cavities never reaches the diffusion coefficient of bulk NSF on top of the polymer film (i.e., $D_{2\text{-cav}} \neq D_{2\text{-bulk}}$), suggesting that the interaction with the NSF only slightly alters the polymer film permeability, and the polymer film acts as a sort of “molecular sieve”, where only smaller aggregates, probably swollen surfactant micelles, are able to reach the liquid-filled cavities at the polymer/glass interface.

On the other hand, the H₂O/MEK/MPD NSF shows an evolution with time, that is, the NSF confined into the cavities at the polymer/glass interface eventually reaches the diffusion coefficient of bulk NSF located above the polymer film. The decrease of D_2 values at $t = 20$ min seems to be mainly ascribable to the extraction and solubilization of low-molecular weight polymer chains into micelles/microemulsion droplets.

The analysis of PC-based NSFs was more complicated in view of the fact that the polymer is completely and relatively quickly dewetted from the glass surface. It was not possible to perform any FCS measurements into the cavities that form at the polymer/glass interface, as they evolved too fast. Conversely, it was possible to measure the diffusion of labeled species inside the liquid-filled cavities that were found trapped into the large droplets of swollen polymer (see the right image of the cartoon in Figure 2), which remain onto the glass surface at the end of the dewetting process.

The H₂O/PC/PDE NSF composition before and after the interaction is almost the same. The diffusive species detected inside the cavities are, in part, strongly interacting with the polymer walls ($D_{2\text{-cav}} = 0.01$), while the $D_{1\text{-cav}}$ value is probably an average of faster and slower diffusing species. In fact, before the rearrangement of the polymer in the form of large droplets, the NSF penetrates the film and is confined in the cavities at the glass/polymer interface, see panel D in Figure 2.

On the other side, the H₂O/PC/MPD NSF significantly changes during the interaction with the polymer. Slow-diffusing species can be found both in the cavities confined into dewetted polymer droplets and in the liquid on top of the film. These data confirm that, as in the case of H₂O/MEK/MPD, micelles/microemulsion droplets are probably able to extract and dissolve some low-molecular polymer chains present inside the polymer film, and this effect is boosted by the co-presence of both the most effective solvent, PC, and surfactant, MPD.

In conclusion, the different NSFs show different mechanisms that depend both on the organic solvent and surfactant forming the NSF. Considering the obtained results, we challenged the NSFs to the removal of Paraloid B72 polymer

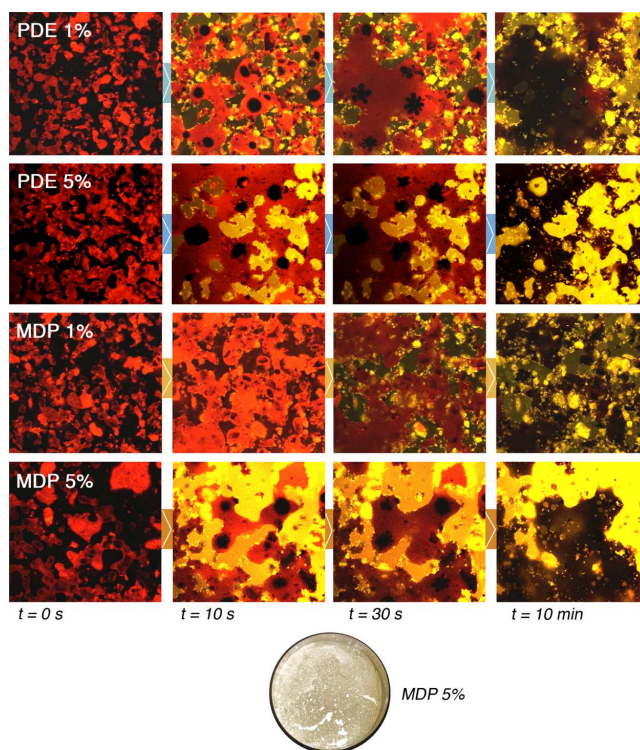


Figure 3. CLSM experiments on soil/NSF interaction. The round picture below the confocal images sequences represents the appearance of the glass incubated for 10 min with the MPD 5% micellar solution. Nile red fluorescence is seen as red; rhodamine 110 chloride fluorescence is seen as green; yellow areas indicate the co-presence of both fluorescent dyes. The bottom side of each CLSM frame is 150 μm long. In the bottom picture, cracks and holes are clearly visible as the result of the MPD 5% NSF action on the soil coating.

films to real cases, that is, thickness of several μm . We compared and quantify the performances of four different NSFs having the same composition (see Table S2, in Supporting Information) but different surfactant. Besides MPD and PDE, two additional surfactants (SDS, DDAO) were selected and used as reference.

Figure S6 in Supporting Information reports the outcome of the cleaning tests with the % of polymer removal obtained via gravimetric measurements. All the selected NSFs resulted highly effective for Paraloid B72 removal from glass slides, yielding an average removal of about 75% of the polymer after a single application of 1.5 h. Some slight differences could be spotted among different NSFs, for example, DDAO is the less effective of the tested surfactants, with a removal of $69 \pm 3\%$, and MPD, with a removal of $78 \pm 1\%$, was the most effective.

3.2. Soil Removal. Soil removal is a very complex subject because of the number of variables mainly linked to the heterogeneous composition of soil. The chemical nature of soiling materials and artworks constituents, the micro-morphology of the surface, and possible surface/soil interactions are only some of the factors that might change from one case to another.

In the present study, glass and polystyrene slides were used as specimen for the experiments. They were coated with very thick layers ($\sim 10\text{--}20 \mu\text{m}$) of artificial soil; this amount of soil is not easily encountered on real artworks surfaces, where the

soil layer is usually less than 1–2 μm thick. Therefore, these experimental conditions have been chosen to amplify possible differences in the behavior of different NSFs involved with the cleaning process. Furthermore, the composition of the artificial soil used in the present work (see Table S3) is very complex, including different materials, ranging from oils (i.e., mixtures of more or less hydrophobic molecules, such as alkanes, fatty acids, fatty acid esters and triglycerides) to more hydrophilic polymeric materials (i.e., gelatin and starch) and to an inert mineral fraction composed of carbon black, iron oxide, kaolin, and silica. This makes the understanding of the interaction process between the NSFs and the soil coating more complex. Most likely, a synergistic combination of concomitant physical phenomena occurs; however, this system is closer to real cases.

Several studies dealing with artificial or real soil removal in the context of conservation of cultural heritage are reported in the literature.^{14,51–56} However, to the best of our knowledge, this paper reports for the first time an insight on the interaction mechanism occurring when a surfactant-based NSF is in contact with a soiled surface.

In order to follow the evolution of sample morphology at the glass/soil interface, as reported for CLSM experiments on soil/NSFs interactions (see Section 2.7.2), both the liquid aqueous phase and the soil layer were stained with fluorescent dyes. Figure 3 summarizes the result of an extensive CLSM investigation on several soiled glasses. In the false-colors

images, soil is labeled with Nile red, whose fluorescence is seen as red, while rhodamine 110 chloride fluorescence is seen as green. The yellow areas indicate the co-presence of both fluorescent dyes and label the interaction of surfactant solution with soil. Because of the heterogeneous composition of the soil, the images reported in Figure 3 show patches with different colors, which evolve with time during the cleaning process. Four different 1 and 5% MPD and PDE solutions have been studied. As shown in Figure 3, the interaction of the surfactants with the soil is very fast in the first 30 s to 1 min. After this initial interaction, the soil morphology continues to evolve at slower rate. The appearance of the soil layer at the glass interface at $t = 0$ s shows the presence of several non-contact areas (dark zones), meaning that the adhesion (or wetting) of the soil to glass is not particularly favored, that is, the soil has a poor affinity for the glass slides surface, and in a few seconds, the oily phase present in the soil coalesces and rearranges itself in large droplets, recalling a dewetting-like process. This appears dark in the confocal images at z coordinates close to the glass slides surface. For both 5% MPD and PDE solutions, because of the presence of the dissolved rhodamine 110, the aqueous phase is initially seen as green, and turns to bright yellow when the Nile red, present in the soil layer, interacts (within 10 min of incubation) with rhodamine. At longer time of incubation, the oily phase of the soil is dark brownish because of the depletion in the fluorescent dye, which was initially dispersed in the coating. At the end of the cleaning process, the bright yellow spots unevenly distributed are related to starch and gelatin particles that remain adherent on the glass.

Even if the interpretation of the collected images is not straightforward, it is evident that surfactant concentration plays a major role in determining a displacement of the soil coating, by detaching it from the glass surface. As observed for polymer/NSF interactions, soil detachment from the surface may be regarded as the first key step of the removal process. The process observed for MPD 5% and PDE 5% is similar; however, on average, larger and more continuous soil detachment areas were evidenced in samples incubated with 5% MPD.

The effectiveness of MPD-based NSFs was also compared to PDE-based NSFs on macroscopic soil removal experiments performed on both frosted glass and polystyrene slides. Four NSFs (40 mL) used in CLSM experiments were left for 24 h in contact with the samples. The samples were monitored at 0, 3, 6, and 24 h. Figure 4-top shows that the majority of samples are unaffected by the action of the NSFs having PDE and MPD concentration below 5%. For 5% concentration, the dewetting-like process evidenced in CLSM experiments was clearly observable with the formation of cracks and holes in the originally coherent soil layer. The soil coating on polystyrene slides was adherent to the surface, and only in the case of the sample treated with PDE 5%, a significant (about 40%—see Figure 4-bottom) soil removal was observed. Figure 4-bottom shows that soil removal is proportional to surfactant concentration and that the MPD surfactant is the most efficient removing almost 100% for 5% MPD surfactant concentration in the absence of any mechanical action, see Figure 4-middle. This feature is very important in the conservation field in view of soil removal from the delicate and fragile surface of works of art.

To better clarify the MPD and PDE performances, the contact angle for pure water on soil was measured. The contact

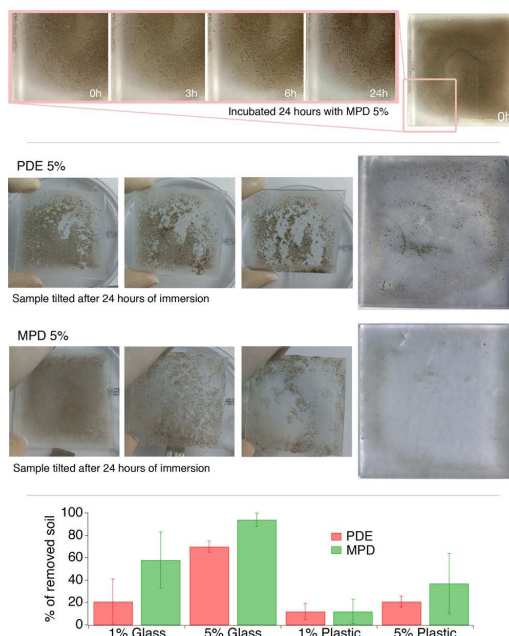


Figure 4. Soil removal experiments on glass slides. (Top) Sequence of zoomed picture taken during the 24 h of immersion of a soiled glass slide in the MPD 5% micellar solution. The dewetting-like process, with the formation of cracks and holes, is clearly visible. (Middle) Glass slides incubated respectively with PDE 5% and MPD 5% micellar solutions were tilted, in order to check for residual soil adhesion to the glass surface. The soil was partially (PDE) or completely (MPD) detached from the glass; the final appearance of treated glass slides is reported. (Bottom) The histogram shows the % of soil removal achieved with the different NSFs on the two different substrates, that is, glass and polystyrene. It is evident that soil removal from polystyrene is incomplete.

angle at the water/soil interface was $52 \pm 8^\circ$. After the artificial soil immersion for 1 min in the two 1% surfactant solutions, the contact angle was 29 ± 1 and $<10^\circ$ for soil incubated with MPD and PDE, respectively. This, contrarily to what can be expected, results in a lower effectiveness of MPD surfactant, when a solubilization process is involved in the cleaning mechanism. SAXS measurements performed on the cleaning fluids samples at 0, 3, 6, and 24 h on glass and polystyrene slides, shed light on the different cleaning mechanism for the two surfactants.

Figure 5 reports the scattering curves of 5% MPD and PDE solutions in contact with soiled glass slides for 24 h. The main fitting results are listed in Table 5, where the volume fraction and the micelles core radius and shell thickness are reported (the description of the fitting model is reported in Supporting Information). According to published data on the effective volume fraction of these two surfactants in water,⁴⁶ it was assumed that the volume fraction of both MPD and PDE 5% w/w (at $t = 0$ h) is 0.2 with a 10% uncertainty on this value.

The geometrical parameters obtained from the fitting are in good agreement with previously published SAXS data on these surfactants, where a model-free Fourier-transform approach was used.⁴⁶ It is worth noting that the shell thickness is

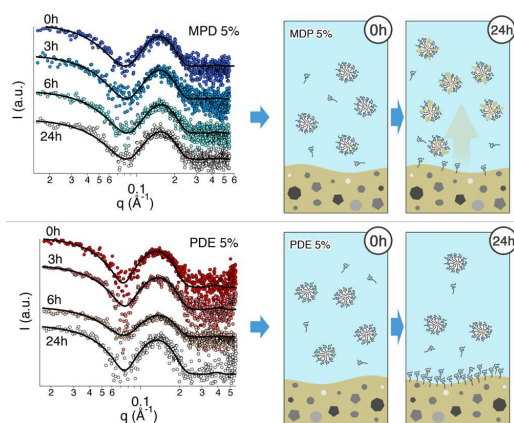


Figure 5. SAXS curves of the MPD 5% and PDE 5% systems, interacting with soiled glass slides. The measurements were performed on samples taken at different times, that is, 0, 3, 6, and 24 h. Solid black lines represent the best fitting curves for experimental data. The curves have been offset for sake of clarity.

significantly high for both surfactants, having MPD micelles a smaller shell, in agreement with literature data,⁴⁶ that report a lower hydration number for the polar head of MPD because of the methyl capping at the end of the polyoxyethylene chain. The results obtained for MPD and PDE micellar solutions in contact with the soil layer show a different behavior for the two surfactants. For both surfactants, micelles' size is almost constant, while the volume fraction significantly changes. For the 5% MPD solution, the volume fraction of scattering particles starts to increase after 6 h of interaction with the soil layer, and after 24 h, it is about 80% larger than its original value. SAXS data show that micelles do not grow indicating that the solubilization into the micelles of hydrophobic components from the soil layer occurs with a subsequent reorganization of the micellar structure. In other words, the solubilization of soil leads to a higher number of micelles with oil molecules replacing the surfactant, with the resulting effect of the presence of aggregates with similar size of the original micelles but with a different number (see the top cartoon in Figure 5).

Considering the composition of the artificial soil, see Table S3, it can be assumed that main soil components solubilized in the micelles come from mineral oil and olive oil. The mineral oil present in the artificial soil is mainly composed of saturated linear C₁₅–C₅₀ hydrocarbons, while the main component of olive oil is glyceryl trioleate⁵⁷ or triolein, a bulky and high molecular weight triglyceride. Several studies in the literature, about the solubilization of hydrophobic substances by nonionic surfactants' micelles,^{57–61} are consistent with the interaction mechanism between MPD micelles and the soil. In particular, Kralchevsky et al. proposed a mechanism for the solubilization of triolein into nonionic micelles, where a direct interaction of the surfactant micelles with the interface, accompanied by an uptake of oil, occurs.⁶¹ Interestingly, they found that after triolein solubilization, the rod-like micelles did not swell but rather they split into several smaller micelles, undergoing a structural reorganization,⁶¹ similarly to the SAXS results of the present study. Interestingly, 5% PDE solution shows the opposite trend for the volume fraction of scattering objects. In fact, after an initial slight size increase, the volume fraction decreases and after 24 h is about 25% less than its original value. Therefore, at the end of the process, a number of micelles had disappeared because of surfactant depletion from the aqueous phase as a consequence of significant PDE adsorption on the soil surface (see the bottom cartoon in Figure 5). These results clearly account for the higher effectiveness of MPD in removing the soil from glass surfaces, even in the absence of any mechanical action.

SAXS from 5% MPD and PDE aqueous solutions interacting with soil layers on polystyrene slides shows a different behavior with respect to glass slides, which is mainly due to the different hydrophilic character of the two materials. Figure 6 reports the SAXS curves, together with their best fitting. The main results are listed in the second half of Table 5. Micelles' size is almost unaltered after the surfactant interaction with soil, and the volume fraction decreases for both surfactants, similarly to PDE interacting with the soiled glass slide. This is related to the higher affinity between polystyrene and the soil layer that inhibits the solubilization of its oily fraction into the micellar core. Thus, because of the adsorption of surfactant at the soil surface, a fraction of micelles is disrupted, with a subsequent decrease in the volume fraction of scattering objects. Figure 7 shows the trend of the volume fraction in the different cases,

Table 5. SAXS Fitting Results^a

	system	fitting parameter	sampling time			
			0 h	3 h	6 h	24 h
soiled glass	MPD 5%	ϕ	0.20 ± 0.02	0.20 ± 0.02	0.33 ± 0.03	0.36 ± 0.02
		r_c (Å)	14.6 ± 1.2	14.5 ± 0.1	13.9 ± 0.9	13.9 ± 0.9
		t (Å)	19.0 ± 1.7	19.0 ± 0.3	19.0 ± 1.6	19.2 ± 1.6
	PDE 5%	ϕ	0.20 ± 0.02	0.25 ± 0.03	0.17 ± 0.02	0.15 ± 0.01
		r_c (Å)	15.6 ± 0.1	15.1 ± 0.1	15.2 ± 0.1	15.3 ± 0.2
		t (Å)	23.5 ± 0.2	22.4 ± 0.2	21.7 ± 0.2	23.4 ± 0.3
soiled polystyrene	MPD 5%	Φ	0.20 ± 0.02	0.13 ± 0.02	0.15 ± 0.02	0.14 ± 0.01
		r_c (Å)	14.6 ± 1.2	15.7 ± 0.1	15.7 ± 0.1	14.7 ± 0.5
		t (Å)	19.0 ± 1.7	22.0 ± 1.4	22.0 ± 0.3	20.0 ± 1.2
	PDE 5%	ϕ	0.20 ± 0.02	0.17 ± 0.01	0.14 ± 0.01	0.13 ± 0.01
		r_c (Å)	15.6 ± 0.1	15.3 ± 0.2	15.5 ± 0.4	15.7 ± 0.7
		t (Å)	23.5 ± 0.2	22.0 ± 0.3	23.0 ± 0.2	23.0 ± 1.1

^a ϕ is the volume fraction of the scattering objects, with respect to the whole volume system; r_c is the average core radius; t is the shell thickness.

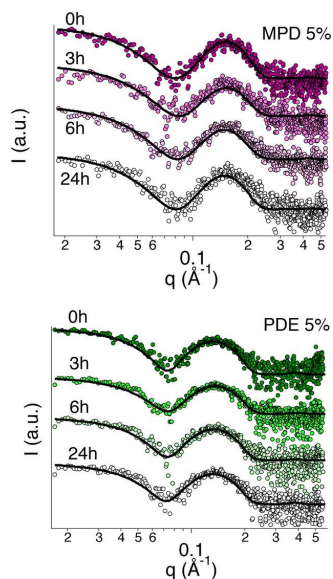


Figure 6. SAXS curves of the MPD 5% and PDE 5% systems, interacting with soiled polystyrene slides. The measurements were performed on samples taken at different times, that is, 0, 3, 6, and 24 h. Solid black lines represent the best fitting curves for experimental data. The curves have been arbitrarily stacked for sake of clarity.

highlighting that the oil solubilization occurs only in the case of MPD 5% interacting with soiled glass.

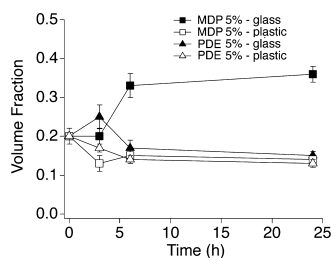


Figure 7. Trend of the volume fraction of the scattering objects for the 5% surfactant systems interacting with glass and polystyrene slides for 24 h, as obtained by the analysis of SAXS data.

The above results report a detailed picture on the surfactant interactions with two different “coatings” commonly found in classic and contemporary/modern art. Overall, it is shown that a tiny change in the molecular structure of the PDE leads to consistent changes in the mechanisms of action, the kinetics, and the cleaning efficacy of the surfactant.

4. CONCLUSIONS

Complex systems composed by MPD have been investigated, and its effectiveness was compared to PDE, a conventional nonionic amphiphile, for the cleaning of two common materials disfiguring the aesthetical aspects of works of art. In particular, MPD- and PDE-NSFs were challenged for the removal of poly(ethyl methacrylate/methyl acrylate) 70:30,

p(EMA/MA), commercially known as Paraloid B72 from glass and polystyrene surfaces, while aqueous micellar solutions of the two surfactants were used for the cleaning of artificially soiled surfaces. The overall results highlighted the better performance of MPD both for the polymer and the soil removal from coated surfaces. The interaction mechanism of NSF for the removal of p(EMA/MA) polymer, observed at the micro-scale through CLSM imaging, involves a dewetting-like process. The polymer is detached from the surface and coalesces into separated droplets as the liquid phase/solid surface interfacial area increases. The PDE- and MPD-NSFs exhibit different mechanisms that depend both on the organic solvent and surfactant because of the different surface tensions and to the different adsorption/penetration of MPD onto/into the polymer film, with respect to PDE. This is likely due to the methyl capping of the surfactant polar head and to the presence of the ester group between the hydrophilic and hydrophobic moiety of the surfactant molecule (PDE). FCS provided a more detailed picture of the cleaning process showing that the surfactants present in the NSF are able to penetrate through the Paraloid B72 film, that acts as a sort of “sieve”, and reach the polymer/solid surface interface, where liquid-filled cavities are formed. Moreover, CLSM experiments highlighted better performances of MPD, if compared to PDE, also in soil removal. The mechanism involves a dewetting-like process, where the oily phase is detached from the glass or polystyrene substrates and coalesces into large droplets. Surfactant concentration was found to be crucial to boost the interaction with the heterogeneous soil. 1% surfactant solutions are less effective than 5%, even if micelles are present in both cases. Differently to PDE that adsorb on the soil layer surface it was found, for both glass and polystyrene substrates, that MPD micellar solutions solubilize soil. Both surfactants allow the removal of soil and grime with different efficacy, no mechanical action, and with different times. The time necessary to perform the cleaning and the mechanical action in conservation are of uppermost importance because long application times and mechanical action should be avoided particularly in the case of fragile and delicate surfaces as those of works of art, which hardly tolerate mechanical stresses during the cleaning operations. Overall, the results reported in the present work open up to new formulations for better-performing and safer cleaning systems to be used by restorers for the conservation of cultural heritage or in other applications as detergency, cosmetics, and so forth.

■ ASSOCIATED CONTENT

Supporting Information

The Supporting Information is available free of charge at <https://pubs.acs.org/doi/10.1021/acsami.0c06425>.

Details on materials and methods and additional figures of all FCS curves, cleaning tests, and surface tension measurements (PDF)

■ AUTHOR INFORMATION

Corresponding Author

Piero Baglioni – Department of Chemistry and CSGI, University of Florence, 50019 Sesto Fiorentino, Florence, Italy; orcid.org/0000-0003-1312-8700; Email: baglioni@csgi.unifi.it

Authors

Michele Baglioni – Department of Chemistry and CSGI, University of Florence, 50019 Sesto Fiorentino, Florence, Italy

Teresa Guaragnone – Department of Chemistry and CSGI, University of Florence, 50019 Sesto Fiorentino, Florence, Italy; orcid.org/0000-0002-7226-0958

Rosangela Mastrangelo – Department of Chemistry and CSGI, University of Florence, 50019 Sesto Fiorentino, Florence, Italy; orcid.org/0000-0003-0420-947X

Felipe Hidetomo Sekine – NIKKOL GROUP Nikko Chemicals Co., Ltd., 103-0002 Tokyo, Japan

Taku Ogura – NIKKOL GROUP Nikko Chemicals Co., Ltd., 103-0002 Tokyo, Japan; NIKKOL GROUP Cosmos Technical Center Co., Ltd., 174-0046 Tokyo, Japan; Research Institute for Science & Technology, Tokyo University of Science, Chiba 278-8510, Japan; orcid.org/0000-0003-4205-2477

Complete contact information is available at: <https://pubs.acs.org/10.1021/acsami.0c06425>

Funding

This work was partly supported by the European Union (CORDIS)—Project NANORESTART (H2020-NMP-21-2014/646063). MIUR Project PRIN-2017249YEF and CSGI “progetti competitivi” are also acknowledged for financial support.

Notes

The authors declare no competing financial interest. Michele Baglioni and Piero Baglioni are not related.

ACKNOWLEDGMENTS

NIKKOL GROUP Cosmos Technical Center (Tokyo, Japan) is gratefully acknowledged for providing the MPD and PDE surfactants.

REFERENCES

- Chelazzi, D.; Bordes, R.; Giorgi, R.; Holmberg, K.; Baglioni, P. The Use Of Surfactants In The Cleaning Of Works Of Art. *Curr. Opin. Colloid Interface Sci.* **2020**, *45*, 108–123.
- Baglioni, P.; Carretti, E.; Chelazzi, D. Nanomaterials In Art Conservation. *Nat. Nanotechnol.* **2015**, *10*, 287–290.
- Baglioni, M.; Rengstl, D.; Berti, D.; Bonini, M.; Giorgi, R.; Baglioni, P. Removal of Acrylic Coatings from Works of Art by Means of Nanofluids: Understanding the Mechanism at the Nanoscale. *Nanoscale* **2010**, *2*, 1723.
- Giorgi, R.; Baglioni, M.; Berti, D.; Baglioni, P. New Methodologies for the Conservation of Cultural Heritage: Micellar Solutions, Microemulsions, and Hydroxide Nanoparticles. *Acc. Chem. Res.* **2010**, *43*, 695–704.
- Baglioni, M.; Giorgi, R.; Berti, D.; Baglioni, P. Smart Cleaning of Cultural Heritage: A New Challenge for Soft Nanoscience. *Nanoscale* **2012**, *4*, 42–53.
- Baglioni, M.; Jaidar Benavides, Y.; Berti, D.; Giorgi, R.; Keiderling, U.; Baglioni, P. An Amine-Oxide Surfactant-Based Microemulsion for the Cleaning of Works of Art. *J. Colloid Interface Sci.* **2015**, *440*, 204–210.
- Baglioni, M.; Berti, D.; Teixeira, J.; Giorgi, R.; Baglioni, P. Nanostructured Surfactant-Based Systems for the Removal of Polymers from Wall Paintings: A Small-Angle Neutron Scattering Study. *Langmuir* **2012**, *28*, 15193–15202.
- Baglioni, M.; Raudino, M.; Berti, D.; Keiderling, U.; Bordes, R.; Holmberg, K.; Baglioni, P. Nanostructured Fluids from Degradable Nonionic Surfactants for the Cleaning of Works of Art from Polymer Contaminants. *Soft Matter* **2014**, *10*, 6798–6809.
- Baglioni, P.; Chelazzi, D.; Giorgi, R.; Poggi, G. Colloid and Materials Science for the Conservation of Cultural Heritage: Cleaning, Consolidation, and Deacidification. *Langmuir* **2013**, *29*, 5110–5122.
- Baglioni, M.; Domingues, J. A. L.; Carretti, E.; Fratini, E.; Chelazzi, D.; Giorgi, R.; Baglioni, P. Complex Fluids Confined into Semi-Interpenetrated Chemical Hydrogels for the Cleaning of Classic Art: A Rheological and SAXS Study. *ACS Appl. Mater. Interfaces* **2018**, *10*, 19162.
- Giorgi, R.; Baglioni, M.; Baglioni, P. Nanofluids and Chemical Highly Retentive Hydrogels for Controlled and Selective Removal of Overpaintings and Undesired Graffiti from Street Art. *Anal. Bioanal. Chem.* **2017**, *409*, 3707.
- Baglioni, M.; Poggi, G.; Ciolli, G.; Fratini, E.; Giorgi, R.; Baglioni, P. A Triton X-100-Based Microemulsion for the Removal of Hydrophobic Materials from Works of Art: SAXS Characterization and Application. *Materials* **2018**, *11*, 1144.
- Mastrangelo, R.; Montis, C.; Bonelli, N.; Tempesti, P.; Baglioni, P. Surface Cleaning of Artworks: Structure and Dynamics of Nanostructured Fluids Confined in Polymeric Hydrogel Networks. *Phys. Chem. Chem. Phys.* **2017**, *19*, 23762–23772.
- Ormsby, B.; Keefe, M.; Phenix, A.; von Aderkas, E.; Learner, T.; Tucker, C.; Kozak, C. Mineral Spirits-Based Microemulsions: A Novel Cleaning System for Painted Surfaces. *J. Am. Inst. Conserv.* **2016**, *55*, 12–31.
- Raudino, M.; Selvolini, G.; Montis, C.; Baglioni, M.; Bonini, M.; Berti, D.; Baglioni, P. Polymer Films Removed from Solid Surfaces by Nanostructured Fluids: Microscopic Mechanism and Implications for the Conservation of Cultural Heritage. *ACS Appl. Mater. Interfaces* **2015**, *7*, 6244–6253.
- Baglioni, M.; Montis, C.; Brandi, F.; Guaragnone, T.; Meazzini, I.; Baglioni, P.; Berti, D. Dewetting Acrylic Polymer Films with Water/Propylene Carbonate/Surfactant Mixtures – Implications for Cultural Heritage Conservation. *Phys. Chem. Chem. Phys.* **2017**, *19*, 23723–23732.
- Baglioni, M.; Montis, C.; Chelazzi, D.; Giorgi, R.; Berti, D.; Baglioni, P. Polymer Film Dewetting by Water/Surfactant/Good-Solvent Mixtures: A Mechanistic Insight and Its Implications for the Conservation of Cultural Heritage. *Angew. Chem., Int. Ed.* **2018**, *57*, 7355–7359.
- Montis, C.; Koynov, K.; Best, A.; Baglioni, M.; Butt, H.-J.; Berti, D.; Baglioni, P. Surfactants Mediate the Dewetting of Acrylic Polymer Films Commonly Applied to Works of Art. *ACS Appl. Mater. Interfaces* **2019**, *11*, 27288–27296.
- Gentili, D.; Foschi, G.; Valle, F.; Cavallini, M.; Biscarini, F. Applications of Dewetting in Micro and Nanotechnology. *Chem. Soc. Rev.* **2012**, *41*, 4430–4443.
- Reiter, G. Unstable Thin Polymer Films: Rupture and Dewetting Processes. *Langmuir* **1993**, *9*, 1344–1351.
- Reiter, G. n.; Khanna, R.; Sharma, A. Self-Destruction and Dewetting of Thin Polymer Films: The Role of Interfacial Tensions. *J. Phys. Condens. Matter* **2003**, *15*, S331.
- Xu, L.; Sharma, A.; Joo, S. W. Dewetting of Stable Thin Polymer Films Induced by a Poor Solvent: Role of Polar Interactions. *Macromolecules* **2012**, *45*, 6628–6633.
- Xu, L.; Shi, T.; An, L. Nonsolvent-Induced Dewetting of Thin Polymer Films. *Langmuir* **2007**, *23*, 9282–9286.
- Tomasetti, E.; Rouxhet, P. G.; Legras, R. Viscoelastic Behavior of Polymer Surface during Wetting and Dewetting Processes. *Langmuir* **1998**, *14*, 3435–3439.
- Khandekar, N. A Survey of the Conservation Literature Relating to the Development of Aqueous Gel Cleaning on Painted and Varnished Surfaces. *Stud. Conserv.* **2000**, *45*, 10–20.
- Stulik, D.; Miller, D.; Khandekar, N.; Wolbers, R.; Carlson, J.; Petersen, W. C. *Solvent Gels for the Cleaning of Works of Art: The Residue Question*; Getty Publications: Los Angeles, 2004.
- Angelova, L. V.; Ormsby, B.; Townsend, J.; Wolbers, R. *Gels in the Conservation of Art*; Archetype Publications, 2017.
- Carretti, E.; Dei, L. Gels as Cleaning Agents in Cultural Heritage Conservation. In *Molecular Gels*; Weiss, R. G., Terech, P., Eds.; Springer: Netherlands, 2006; pp 929–938.

- (29) Mastrangelo, R.; Chelazzi, D.; Poggi, G.; Fratini, E.; Pensabene Buemi, L.; Petruzzellis, M. L.; Baglioni, P. Twin-Chain Polymer Hydrogels Based On Poly(Vinylalcohol) As New Advanced Tool For The Cleaning Of Modern And Contemporary Art. *Proc. Natl. Acad. Sci. U.S.A.* **2020**, *117*, 7011–7020.
- (30) Bonelli, N.; Poggi, G.; Chelazzi, D.; Giorgi, R.; Baglioni, P. Poly(Vinyl Alcohol)/Poly(Vinyl Pyrrolidone) Hydrogels for the Cleaning of Art. *J. Colloid Interface Sci.* **2019**, *536*, 339–348.
- (31) Hama, I.; Okamoto, T.; Nakamura, H. Preparation and Properties of Ethoxylated Fatty Methyl Ester Nonionics. *J. Am. Oil Chem. Soc.* **1995**, *72*, 781–784.
- (32) Hama, I.; Sasamoto, H.; Okamoto, T. Influence of Catalyst Structure on Direct Ethoxylation of Fatty Methyl Esters over Al-Mg Composite Oxide Catalyst. *J. Am. Oil Chem. Soc.* **1997**, *74*, 817–822.
- (33) Hama, I.; Sakaki, M.; Sasamoto, H. Effects of Ethoxylate Structure on Surfactant Properties of Ethoxylated Fatty Methyl Esters. *J. Am. Oil Chem. Soc.* **1997**, *74*, 823–827.
- (34) Hama, I.; Sakaki, M.; Sasamoto, H. Nonionic Surfactant Properties of Methoxypolyoxyethylene Dodecanoate Compared with Polyoxyethylene Dodecylether. *J. Am. Oil Chem. Soc.* **1997**, *74*, 829–835.
- (35) Cox, M. F.; Weerasooriya, U. Impact of Molecular Structure on the Performance of Methyl Ester Ethoxylates. *J. Surfactants Deterg.* **1998**, *1*, 11–22.
- (36) Nagai, Y.; Togawa, N.; Tagawa, Y.; Gotoh, K. Comparison of Cleaning Power Between Alcohol Ethoxylates or Methyl Ester Ethoxylates Having Different EO Chain Lengths and a Common Anionic Surfactant. *Tenside Surfactants Deterg.* **2014**, *51*, 113–118.
- (37) Renkin, M.; Fleurackers, S.; Szwach, I.; Hreczuch, W. Rapeseed Methyl Ester Ethoxylates: A New Class of Surfactants of Environmental and Commercial Interest. *Tenside Surfactants Deterg.* **2005**, *42*, 280–287.
- (38) Yu, Y.; Zhao, J.; Bayly, A. E. Development of Surfactants and Builders in Detergent Formulations. *Chin. J. Chem. Eng.* **2008**, *16*, 517–527.
- (39) Chiantore, O.; Lazzari, M. Photo-Oxidative Stability of Paraloid Acrylic Protective Polymers. *Polymer* **2001**, *42*, 17–27.
- (40) Bracci, S.; Melo, M. J. Correlating Natural Ageing and Xenon Irradiation of Paraloid B72 Applied on Stone. *Polym. Degrad. Stab.* **2003**, *80*, 533–541.
- (41) Borgia, G. C.; Bortolotti, V.; Camaiti, M.; Cerri, F.; Fantazzini, P.; Piacenti, F. Performance Evolution of Hydrophobic Treatments for Stone Conservation Investigated by MRI. *Magn. Reson. Imag.* **2001**, *19*, 513–516.
- (42) Crisci, G. M.; La Russa, M. F.; Malagodi, M.; Ruffolo, S. A. Consolidating Properties of Regalrez 1126 and Paraloid B72 Applied to Wood. *J. Cult. Herit.* **2010**, *11*, 304–308.
- (43) Ormsby, B.; Keefe, M.; Phenix, A.; Learner, T. *A Summary of Recent Developments in Wet Surface Cleaning Systems: Unvarnished Modern and Contemporary Painted Surfaces*; Archetype Publications, 2015.
- (44) Baglioni, M.; Poggi, G.; Jaidar Benavides, Y.; Martínez Camacho, F.; Giorgi, R.; Baglioni, P. Nanostructured Fluids for the Removal of Graffiti – A Survey on 17 Commercial Spray-Can Paints. *J. Cult. Herit.* **2018**, *34*, 218.
- (45) Provencher, S. W. CONTIN: A General Purpose Constrained Regularization Program for Inverting Noisy Linear Algebraic and Integral Equations. *Comput. Phys. Commun.* **1982**, *27*, 229–242.
- (46) Sato, T.; Akahane, T.; Amano, K.; Hyodo, R.; Yanase, K.; Ogura, T. Scattering and Spectroscopic Study on the Hydration and Phase Behavior of Aqueous Alcohol Ethoxylate and Methyl Ester Ethoxylate: Effects of Terminal Groups in Hydrophilic Chains. *J. Phys. Chem. B* **2016**, *120*, 5444–5454.
- (47) Ogura, T.; Kaneko, Y.; Suekuni, T.; Tabori, N.; Glatter, O. *Dynamics of Spontaneously-Generated Solubilization of Oleic Acid by the Plant-Based Ingredient MEE (Methyl Ester Ethoxylate)*, 2012.
- (48) Butt, H.-J.; Graf, K.; Kappel, M. Contact Angle Phenomena and Wetting. In *Physics and Chemistry of Interfaces*; Wiley-VCH Verlag GmbH & Co. KGaA, 2003; pp 118–144.
- (49) Castro, L. B. R.; Almeida, A. T.; Petri, D. F. S. The Effect of Water or Salt Solution on Thin Hydrophobic Films. *Langmuir* **2004**, *20*, 7610–7615.
- (50) Verma, A.; Sharma, A. Submicrometer Pattern Fabrication by Intensification of Instability in Ultrathin Polymer Films under a Water–Solvent Mix. *Macromolecules* **2011**, *44*, 4928–4935.
- (51) Wolbers, R. *Cleaning Painted Surfaces: Aqueous Methods*; Archetype Publications, 2000.
- (52) Phenix, A.; Burnstock, A. *The Deposition of Dirt: A Review of the Literature with Scanning Electron Microscope Studies of Dirt on Selected Paintings*; UKIC, 1990.
- (53) Murray, A.; Berenfeld, C. C. d.; Chang, S. Y. S.; Jablonski, E.; Klein, T.; Riggs, M. C.; Robertson, E. C.; Tse, W. M. A. The Condition and Cleaning of Acrylic Emulsion Paintings. *MRS Online Proc. Libr.* **2002**, *712*, 1–8.
- (54) Morrison, R.; Bagley-Young, A.; Burnstock, A.; van den Berg, K. J.; van Keulen, H. An Investigation of Parameters for the Use of Citrate Solutions for Surface Cleaning Unvarnished Paintings. *Stud. Conserv.* **2007**, *52*, 255–270.
- (55) Phenix, A.; Burnstock, A. The Removal of Surface Dirt on Paintings with Chelating Agents. *The Conservator* **1992**, *16*, 28–38.
- (56) Stulik, D. *Solvent Gels for the Cleaning of Works of Art: The Residue Question*; Getty Publications, 2004.
- (57) Tongcumpou, C.; Acosta, E. J.; Scamehorn, J. F.; Sabatini, D. A.; Yanumet, N.; Chavadej, S. Enhanced Triolein Removal Using Microemulsions Formulated with Mixed Surfactants. *J. Surfactants Deterg.* **2006**, *9*, 181–189.
- (58) Chen, B.-H.; Miller, C. A.; Garrett, P. R. Rates of Solubilization of Triolein into Nonionic Surfactant Solutions. *Colloids Surf., A* **1997**, *128*, 129–143.
- (59) Cox, M. F.; Weerasooriya, U. Methyl Ester Ethoxylates. *J. Am. Oil Chem. Soc.* **1997**, *74*, 847–859.
- (60) Christov, N. C.; Denkov, N. D.; Kralchevsky, P. A.; Broze, G.; Mehreteab, A. Kinetics of Triglyceride Solubilization by Micellar Solutions of Nonionic Surfactant and Triblock Copolymer. 1. Empty and Swollen Micelles. *Langmuir* **2002**, *18*, 7880–7886.
- (61) Kralchevsky, P. A.; Denkov, N. D.; Todorov, P. D.; Marinov, G. S.; Broze, G.; Mehreteab, A. Kinetics of Triglyceride Solubilization by Micellar Solutions of Nonionic Surfactant and Triblock Copolymer. 2. Theoretical Model. *Langmuir* **2002**, *18*, 7887–7895.


PAPER VI

RESEARCH ARTICLE

Open Access



Twin-chain polymer networks loaded with nanostructured fluids for the selective removal of a non-original varnish from Picasso's "L'Atelier" at the Peggy Guggenheim Collection, Venice

Luciano Pensabene Buemi^{1*}, Maria Laura Petruzzellis¹, David Chelazzi², Michele Baglioni², Rosangela Mastrangelo², Rodorico Giorgi² and Piero Baglioni^{2*} 

Abstract

This paper reports on the evaluation of a polyvinyl alcohol (PVA) "twin-chain" polymer network (TC-PN) combined with an oil-in-water nanostructured fluid (NSF) for the removal of a polyvinyl acetate (PVAc) varnish. Small Angle X-ray Scattering, Confocal Laser Scanning Microscopy, and Fluorescence Correlation Spectroscopy showed that the structure of the gel and the NSF are only minimally altered by loading the fluid into the gel. The NSF is partially free to diffuse through the network, but also interacts with the gel walls. During the cleaning, the dynamics of the fluid at the gel-substrate interface are controlled by the osmotic balance taking place among the interconnected pores. These features grant effective and controlled cleaning performances. The case study identified for this research is Pablo Picasso's *The Studio (L'Atelier, 1928)*, one of the masterpieces in the Peggy Guggenheim Collection, Venice (PGC). In 1969 the oil painting, originally unprotected, was wax-lined and then varnished using a PVAc varnish. Over the years, the white shades of the painting have been compromised by the yellowing of the varnish and soiling of deposits. On painting mock-ups, the NSF-loaded hydrogels allowed the swelling and softening of PVAc varnish and wax layers, which were then removed with gentle mechanical action. Effective varnish and wax removal at the micron scale, and the absence of residues from the cleaning system (gel and NSF), were confirmed by Fourier Transform Infrared Spectroscopy (FTIR) 2D imaging. The effective and safe removal of the aged PVAc varnish and wax layer from the surface of the painting was then carried out using the same cleaning protocol successfully tested on the mock-ups, setting the NSF-loaded PVA TC-PNs as robust and reliable tools for the cleaning of sensitive works of art.

Introduction

Over the last three decades, research increased our knowledge of the chemical, physical and mechanical properties of modern paints, and of their behavior and

ageing over time. However, their conservation is still an open issue. The Peggy Guggenheim Collection, Venice, (PGC) took part in the Nanorestart project funded by the European Union to evaluate novel nanostructured complex fluids and gel systems for cleaning the sensitive surfaces of modern and contemporary paintings. The research focused on the removal of grime and dirt from unvarnished and complex surfaces, and the removal of non-original coatings from modern oil paints. Some issues have been identified as the occasion for ethical,

*Correspondence: lpensabene@guggenheim-venice.it; piero.baglioni@unifi.it

¹ Conservation Department, Peggy Guggenheim Collection, Venice, Italy

² Consorzio Interuniversitario per lo Sviluppo dei Sistemi a Grande Interfase (Center for Colloid and Surface Science), CSGI, and Chemistry Department, University of Florence, Via della Lastruccia 3, Sesto Fiorentino, 50019 Florence, Italy

theoretical, scientific and practical in-depth study. The 3-year project involved selected case studies from the collection of the PGC: Jackson Pollock, *Two* (1943–45), and *Eyes in the Heat* (1946–47); Pablo Picasso, *The Studio* (1928); Giorgio de Chirico, *The Gentle Afternoon* (1916). These served as exemplary studies of the many conservation issues addressed by research, given the specific needs of each work of art. *Two* and *The Gentle Afternoon* are made using only oil paints, while *Eyes in the Heat* represents the transition of Pollock from oil paints to the application of both oils and alkyd colors [1]. *The Studio* is made of oil paints and black crayon on canvas.

The teamwork by conservators and scientists and their careful assessment allowed the validation of PVA-based hydrogels, made of polymer chains combined with PVA of lower molecular weight, which were developed at the Consorzio Interuniversitario per lo Sviluppo dei Sistemi a Grande Interfase (CSGI). Because the two polymers that make up the gel network are in fact the same polymer (PVA), differing by the hydrolysis degree and molecular weight, these gels were named “twin-chain” polymer networks (TC-PNs). This represents a new approach as opposed to the semi-interpenetrated networks (semi-IPNs) previously developed at CSGI, which used two different types of polymers. It was shown that the addition of the lower molecular weight PVA changes the porosity and mechanical properties of these gels as compared to single-PVA gels, and the cleaning efficacy is improved [1]. These TC-PNs proved to be advantageous systems for the cleaning of paintings, owing to their mechanical properties, retentiveness, ability to remove soil, and the controlled cleaning process. The TC-PNs were used for the first time to confine aqueous solutions and remove dust and dirt from the two aforementioned works by Pollock [1], as part of a conservation program on the eleven works by Pollock at the PGC (for overview of the program <https://www.guggenheim-venice.it/en/art/conservation/case-studies/pollock/>). The TC-PN used on the Pollock paintings had a tailored formulation in order to adapt to the specific requirements of those works, but served as a prototype for a series of multipurpose gels, which were formulated to target typical cleaning cases and named Nanorestore Peggy Gels[®] and Nanorestore Peggy Gums[®], after the PGC.

This paper reports on the evaluation of a PVA TC-PN formulated to be combined with an oil-in-water (o/w) nanostructured fluid (NSF), and specifically targeted to the removal of a polyvinyl acetate (PVAc) non-original varnish from the oil painting *The Studio* by Picasso. Despite the diffusion of a large amount of pigment binders, oil remains one of the most favored media by artists, thanks to its desirable properties and optical qualities. Indeed, oil-based paintings are the most common in the

holdings of the PGC. The composition of modern oil paints has changed significantly over time. They contain additives such as dryers, fillers, stabilizers, and dispersion agents to stabilize the paint in the tubes whilst controlling the rheology as well as the drying time of the paint [2]. The incorporation of dryers, fillers, dispersion agents, and stabilizers increased during the twentieth century, and over time it has impaired the stability and resistance of the oil paints. The quality of the paint and binder can significantly affect the characteristics of the final paint-film and its subsequent reaction to ageing and treatments [2, 3]. In addition, previous conservation treatments may have caused major changes in the chemical or physical characteristics of the paintings, determining their response to ageing and successive treatments. This is the case, for instance, with wax-resin lining, which can cause the alteration of the paintings surface texture and appearance, as occurred with *The Studio*.

The removal of non-original materials from painted surfaces still remains one of the most frequently executed tasks in the conservation of modern and contemporary art, and it requires conservators to make complex decisions. Cleaning is an irreversible and delicate operation, where conservators are required to minimize the risk of interaction between paints and cleaning agents, and the diffusion of solubilized dirt or coatings through the paint layer. This is often problematic, as the additives in modern paints may increase the sensitivity to cleaning fluids, which could leach and deteriorate the paints. In many cases, the painted layers have a low binder content, which causes pigments to be poorly protected and more solvent-sensitive; moreover, specific colors can show a higher sensibility to water and to solvents employed in conservation treatments. In addition, the roughness of the painted surface, which is typical of modern works of art, makes homogeneous cleaning with traditional tools even more difficult and risky. Indeed, water in cleaning solutions may act both as a reaction medium and as a high polarity solvent, with deep penetration into the micro-porosities of paint layers, and organic solvents can interact with paint components driving leaching and swelling phenomena [2, 3].

In the last decades efforts have focused on the development of gelled-systems that are capable of retaining liquids and reducing their uncontrolled spreading and vertical diffusion. Cellulose ethers, carboxymethyl cellulose, and polyacrylic acid neutralized with strong bases have been extensively used as thickening agents in order to avoid the use of free cleaning fluids. The intrinsic limit of these thickeners is that they may leave polymer residues on the surface after cleaning, due to the weak interactions between the polymer molecules, and to the poor control of the solvent diffusion. Invasive rinsing steps

are thus needed to remove such residues [4–7]. Besides thickening agents, conservators employ a variety of ‘traditional rigid’ physical gels (e.g. agar, gellan), as well as rigid chemical gels such as semi-IPNs of poly(2-hydroxyethyl methacrylate) and poly(vinylpyrrolidone) (pHEMA/PVP) [4]. However, rigid gels are not able to adapt to textured surfaces, such as those of modern and contemporary paintings by Picasso, Pollock, Van Gogh, and others, characterized by both the presence of high brush strokes and the usage of sensitive paints, sometimes squeezed directly from the tubes to the canvas [1].

In view of the above issues, one of the main goals in the cleaning of modern and contemporary paintings is the development of novel classes of gels, that are able to adhere to textured surfaces and to minimize the interaction between cleaning fluids and the paint surface thanks to: (1) effective confinement of solvents, i.e. controlled amount of the solvent that is in direct contact with the surface and its limited penetration in the paint layers; (2) absence of residues on the paint surface; (3) selective interaction of the complex fluid with the material to be removed.

Based on such requirements, the study group investigated and tested for the first time a combined system where an o/w NSF, specifically targeted at the removal of the non-original varnish used on *The Studio*, was confined into a TC-PN hydrogel. In the last decades, NSFs have proved to be highly efficient in the swelling and removal of hydrophobic coatings [8–16], as they work through a removal mechanism that, for high molecular weight substances such as polymers, is based on dewetting and detachment, thus allowing a more controlled surface cleaning with respect to traditional solvent chemistry [17–21]. As mentioned, the use of aqueous fluids on modern oil paints requires special attention, and an optimal strategy is thus to confine cleaning fluids in retentive gel matrices, minimizing the risks to the artifacts [22–30].

The physicochemical characterization of the combined gel-NSF cleaning system included the interaction of the NSF with the gel and its diffusion inside the gel network, which were investigated using Confocal Laser Scanning Microscopy (CLSM) and Fluorescence Correlation Spectroscopy (FCS). The structure of the combined NSF and gel was analyzed with Small Angle X-ray Scattering (SAXS) in order to check the effects of the confinement on both components.

Preliminary cleaning tests were performed on mock-up samples (made using the original recipes and protocols employed during the 1969 restoration of the work), and monitored through 2D Fourier Transform Infrared Spectroscopy (FTIR) imaging to verify the efficacy of the cleaning as well as the absence of residues; this allowed

to define the ideal procedure to be used on the original artwork. The TC-PN gels, loaded with the NSF, were then tested on the painting itself, *The Studio*.

The case study

Picasso completed *The Studio* in 1928 in his studio in Paris. The following year he gave it to his dealer, Daniel-Henry Kahnweiler, and 5 years later he asked the painting to be returned in an unusual exchange for five other paintings, thus demonstrating the importance he attributed to the work. The painting was lent to the Museum of Modern Art in New York for two exhibitions in 1939–40 and in 1941, and then remained in the United States most likely by decision of the artist. Peggy Guggenheim acquired it for her collection in 1942. In the words of Robert Motherwell: “That painting was perhaps the most important influence on my life in those first ten years in New York. That incredible white [...], surely one of the most austere and powerful works since the height of Cubism [...] unquestionably one of the masterpieces of the 20th century”. In 1948, Guggenheim brought the painting to Venice, exhibited it at the Biennale, and then installed it in her home. Since her death in 1979, it has been part of the PGC, the Italian branch of the Solomon R. Guggenheim Foundation, New York.

The painting is an oil and black crayon on canvas; it presents the vivid colors of Synthetic Cubism, but is dominated by a vast expanse of white, with figures defined by geometric, wire-like contours in the manner of Picasso’s wire sculptures of the same period. Shortly after completion Picasso returned to the painting and substantially reworked it by overpainting large areas with white and reducing the variety of the palette and the complexity of the composition. The colors underneath the expanse of white paint can be detected with a microscope or even with the naked eye. The black crayon lines were traced on the upper level of white preparation. After the sketching of principal figures Picasso painted around the crayon lines with abundant oil paints brush strokes, which creates the illusion of a mural incision.

Previous documentation was studied in depth to understand materials and methods used by conservators. In 1969, Margaret Watherston examined the oil painting at the Metropolitan Museum of Art, but she did not identify the earlier version painted by the artist. Her materials, notes, recipes, and photos from her professional career are collected in a series of files [31]. The files that pertain to *The Studio* include the recipes for the wax-resin and the varnish employed in the lining of the work. These materials were confirmed by subsequent studies carried out on the painting. In the condition report Watherston wrote: “Surface of painting is extremely dirty, with numerous pressure and age cracks. Thickness

of paint varies considerably, and texture of canvas is exposed in many places. Painting should be given water-chemical treatment on the vacuum table to minimize cracks, then be lined and mounted, if this seems necessary, on a honeycomb panel with linen counter-mount on the reverse side." At the time, it was thought that to prevent dangerous cracking and flaking one should protect paintings by working on the verso. Therefore, *The Studio* was lined with wax-resin adhesive and mounted on a honeycomb panel, and its recto sprayed with a synthetic final varnish (a PVAc, commercially named AYAC). This ignored the original, unvarnished state of the painting and eliminated visual effects that were previously visible. The lining treatment caused cracks and flattening of the complex surface morphology: the rough brush strokes were originally more evident on the entire painting except for the area delimited by the yellow lines. The difference between the yellow-limited area and the rest of the painting suggests the idea of a mirror. Over the years the varnish yellowed and affected the areas painted in white. Probably some of the wax migrated up through the outer layer of the paint, partly mixing with the varnish and favoring the embedding of environmental particulates that led to darkening of the surface. In fact, both wax and AYAC (which has a glass transition temperature of 18–33 °C depending on its purity) are quite sensitive to temperature fluctuations, and this explains their capacity to embed solid particulates. Over time the delicate tonal contrast of white on white was compromised by the deposits of dust and grime, by the appearance of wax through the cracks, and by the flattening effect of the yellowed varnish that was applied in the late sixties. Therefore, we decided to remove the non-original varnish in order to minimize the amount of deposits on the surface and to recover the readability of the paintings, especially of the white shades that had been altered by yellowing varnish.

Materials and methods

Chemicals

Polyvinyl alcohol polymers, PVA, (hydrolysis degree = 88%, M_w 100 kDa, and hydrolysis degree 98%, M_w 160 kDa) were purchased from Sigma-Aldrich for the hydrogel preparation. $C_{9-11}E_{5,5}$ alcohol ethoxylate (Berol 266[®], AkzoNobel), sodium dodecylsulfate (SDS, Sigma-Aldrich, purity \geq 99%), 2-butanol (BuOH, Sigma-Aldrich, purity 99%), butanone (methyl ethyl ketone, MEK, Sigma-Aldrich, purity 99%), and Bodipy[®] 558/568 C12 ((4,4-difluoro-5-(2-thienyl)-4-bora-3a,4a-diaza-s-indacene-3-dodecanoic acid), ThermoFisher) were used as received without further purification, for the NSF preparation and for CLSM experiments, respectively.

Water was purified with a Millipore Milli-Q gradient system (resistance > 18 M Ω cm).

NSF preparation

The selected NSF is composed as follows (w/w): H₂O, 65.9%; $C_{9-11}E_{5,5}$, 3.3%; SDS, 0.2%; BuOH, 9.7%; MEK, 20.9%. The system was prepared by mixing water and the two surfactants at room temperature until a clear solution was obtained. Then the two solvents were added in the formulation and the system was stirred until all the solvent was dissolved either in the continuous aqueous phase or in the micelles. BuOH and MEK are partly water-miscible [32].

A labeled NSF was prepared for Fluorescence Correlation Spectroscopy experiments by adding the amphiphilic dye Bodipy to the formulation (10 nM).

Hydrogel preparation

PVA "twin-chain" polymer networks (TC-PNs) hydrogels were prepared through a synthetic process, which has been described elsewhere [1]. For the TC-PN used in this study, we selected a 3:1 ratio between the high molecular weight PVA and the low molecular weight PVA, and a single freezing/thawing cycle. Prior to use, gel sheets (e.g. 10 × 20 cm²) were immersed in the NSF (at least for 24 h) to upload the cleaning fluid.

Painting mock-up preparation and cleaning procedure

Painting mock-up samples were made by using Windsor&Newton oil paints (zinc white, cadmium orange, raw Siena, ivory back) brushed on commercially prepared canvas. After 1 year, some of the mock-up samples were lined, using a wax-resin adhesive based on Watherston's original recipe [31]: "5 lb Beeswax; 5 lb Multiwax (white synthetic wax); 6 lb Dammar resin crystals; 2 Pounds of Venice Turpentine." In addition to mock-up samples, several oil paintings and fragments from warehouses and flea markets were used as naturally aged mock-ups in order to provide a further comparison.

All the mock-up samples, either lined or not, were varnished by spraying with commercial PVAc (AYAC, Union Carbide, Dow Chemical, USA) dissolved (20% w/w) in toluene or methyl alcohol (Sigma-Aldrich), as reported in Watherston's documents. Then, the mock-ups were aged in a light box at 11,000 lux for 1 month.

Prior to the application, gel sheets uploaded with the NSF were gently squeezed with blotting paper to remove the excess fluid from their surface. Correct drying of the gel is important for the cleaning process in order to avoid the presence of non-confined solvent on the painting surface.

During application, the contact time of the gel with the paint layer varied from few seconds to 2 min. The

application caused the varnish and wax layer to swell and soften. Gentle mechanical action with a dry cotton swab allowed the removal of the swollen/softened varnish and wax. Finally, a water-loaded gel was shortly applied on the same spot to remove possible residues of the NSF.

Small-angle X-ray scattering (SAXS)

Small-angle X-ray Scattering (SAXS) measurements were performed with a HECUS S3-MICRO SWAXS-camera, equipped with a Hecus System 3 2D-point collimator (min divergence 0.4×0.9 mrad²) and two position sensitive detectors (PSD-50 M), consisting of 1024 channels with a width of 54 μm . During the experiments, the K_{α} radiation ($\lambda = 1.542$ Å) emitted by a Cu anode from the Oxford 50 W microfocus source with customized FOX-3D single-bounce multilayer point focusing optics (Xenocs, Grenoble) was used, while the K_{β} line was removed by a multilayer filter. The voltage was generated by the GeniX system (Xenocs, Grenoble). The sample-to-

Bodipy with a DPSS solid state laser at 561 nm and collecting its fluorescence at 571–630 nm. FCS experiments were performed by probing the NSF diffusion inside the hydrogel: the fluorescent signal of Bodipy was collected, in this case, by using a hybrid detector (HyD) in the 571–630 nm range.

FCS curves were normalized and averaged (6–10 repetitions per sample). A 10 nM (nanomolar) aqueous solution of Alexa Fluor 568 was used for FCS calibration [33].

The autocorrelation curves were analyzed according to a model that considers the three-dimensional Brownian diffusion of fluorescent species across a 3D-ellipsoidal Gaussian volume as the only phenomenon influencing the decay. The curves were analyzed considering either a one-component decay [34]:

$$G(\tau) = \frac{1}{N} \left[\left(1 + \frac{\tau}{\tau_D} \right)^{-1} \left(1 + \frac{\tau}{S^2 \tau_D} \right)^{-\frac{1}{2}} \right]$$

or a two-components decay [35]:

$$G(\tau) = \frac{1}{N} \left[f_1 \left(1 + \frac{\tau}{\tau_{D1}} \right)^{-1} \left(1 + \frac{\tau}{S^2 \tau_{D1}} \right)^{-\frac{1}{2}} + (1 - f_1) \left(1 + \frac{\tau}{\tau_{D2}} \right)^{-1} \left(1 + \frac{\tau}{S^2 \tau_{D2}} \right)^{-\frac{1}{2}} \right]$$

detector distance was 26.9 cm. The volume between the sample and the detector was kept under vacuum during the measurements to minimize the scattering from the atmosphere. The camera was calibrated in the small-angle region using silver behenate ($d = 58.38$ Å). Scattering curves were obtained in the q -range between 0.01 and 0.6 Å⁻¹. The temperature control was set to 25 °C. Liquid samples (i.e. the NSF and neat water, used as a reference) were contained in 2 mm thick quartz capillary tubes sealed with hot-melting glue. The gel and NSF-loaded gel samples were contained in a sample holder for solids, with Kapton windows. Desmearing of the SAXS curves was not necessary thanks to the focusing system.

Confocal laser scanning microscopy (CLSM)-fluorescence correlation spectroscopy (FCS)

CLSM-FCS experiments were performed on a Leica TCS SP8 confocal microscope (Leica Microsystems GmbH, Wetzlar, Germany) equipped with a 63X water immersion objective. A fluorescent PVA hydrogel was obtained by labeling high molecular weight PVA with Fluoresceine Isothiocyanate (FITC), as previously reported [1], while NSF was labeled with Bodipy, as described above. Imaging of the labeled gel was performed by exciting FITC with the 488 nm laser line (Ar laser) and collecting its fluorescence with a PMT (498–530 nm). The labeled NSF was also observed by imaging, exciting

where N is the average number of fluorescent molecules detected inside the confocal volume ($N = CV$, with $V = \pi^{\frac{3}{2}} w_0^3 S$ and C the concentration), f_1 is the percentage of the contribution of $\tau_{D,1}$ to the total decay time, $\tau_{D,i}$ are the decay times, and $S = \frac{z_0}{w_0}$ is the ratio between the axial and the lateral dimensions of the confocal volume, determined through the calibration procedure with Alexa 568. The diffusion coefficients D_i of the labeled species can be determined by:

$$\tau_{D,i} = \frac{w_0^2}{4D_i}$$

2D-imaging fourier-transform infrared spectroscopy (FTIR)

The 2D imaging-FTIR analysis on painting mock-ups was carried out using a Cary 620–670 FTIR microscope, equipped with an FPA 128 × 128 detector (Agilent Technologies). This set up allows the highest spatial resolution currently available to FTIR microscopes. The spectra were recorded directly on the surface of the samples (or of the Au background) in reflectance mode, with open aperture and a spectral resolution of 8 cm⁻¹, acquiring 128 scans for each spectrum. A “single-tile” analysis results in a map of 700 × 700 μm^2 (128 × 128 pixels), and the spatial resolution of each imaging map is 5.5 μm

(i.e. each pixel has dimensions of $5.5 \times 5.5 \mu\text{m}^2$). Multiple tiles can be combined in mosaics. In each 2D map, the intensity of characteristic bands of the varnish, or of the gel, was imaged. The chromatic scale of the maps shows increasing absorbance of the bands as follows: blue < green < yellow < red.

Results and discussion

The constant dialogue between conservators and scientists allowed to define the main requirements that novel materials and systems must fulfill to overcome the limitations of traditional cleaning methods. Besides the ability to effectively remove the aged PVAc varnish from the painting's surface, such requirements include: (1) Reduction of the toxicity of cleaning materials to decrease risks to operators and the environment; this was tackled by adopting non-toxic gel components and an aqueous nanostructured fluid (NSF) with reduced amount of organic solvents; (2) The use of a thermodynamically stable cleaning fluid with low surfactant content, which was addressed by selecting the NSF used in this study; (3) Complete avoidance of free, non-confined cleaning fluids (including rinsing steps), which was addressed by confining the NSF in the hydrogel; (4) The use of highly retentive gels, to control the amount of fluid in direct contact with the varnish and to maintain the fluid at the varnish-paint interface without excessive penetration; this grants control of the cleaning action in response to subtle differences in paint sensitivity and varnish/soiling behavior, and maximizes the cleaning efficacy, reducing the need of mechanical action; (5) Optimal mechanical properties of the gels, i.e. high viscoelasticity and flexibility, which grant the capacity to adapt to complex and textured paint surfaces, the easy handling of the gels, and the absence of gel residues left on the surface after cleaning.

The TC-PNs hydrogels were synthesized and optimized to meet these requirements, and an extensive characterization of the type of structure, rheological properties, and PVA dynamics in the gel network, has been recently provided for the formulation used on the paintings by Pollock, *Two and Eyes in the Heat* [1]. The TC-PN used in this study has similar characteristics, but a slightly different formulation and some structural differences (detailed in the following paragraphs) owing to the presence of the o/w nanostructured fluid.

The TC-PNs gels are opalescent and offer optimal mechanical properties and solvent retention. They are flexible and elastic, and their controlled release of uploaded fluids grants the possibility of varying the fluids

contact time with the paint surface, controlling the interaction between solvents and paint layers. These features have already established the TC-PNs as suitable tools for the cleaning of modern and contemporary art in previous case studies [1, 36, 37], which proved that their synthetic process can be feasibly tuned and changed in order to vary the gels' characteristics and to adapt them to specific needs.

The loading of the gel with the NSF was obtained simply by immersing a piece of gel in an excess of NSF for at least 24 h, according to our previous experiments with these systems. Previous studies demonstrated that similar gels exhibit a structure and porosity that allows aqueous NSFs to be loaded in the gel without disrupting the structure of the gel and the fluid, thus demonstrating that the cleaning properties of the combined system are not altered [25, 29]. However, in view of the application of the system in the cleaning of a Picasso masterpiece, SAXS and FCS measurements were carried out also in this case, in order to study the interaction of the gel with the NSF. SAXS analyses were performed on the sole hydrogel and NSF, and on the combined NSF-loaded hydrogel. Figure 1 shows the resulting scattering profiles together with their best fitting curves, while Tables 1, 2 report the main fitting parameters obtained by the analysis of the curves. A cleaning system similar to the NSF here reported was recently investigated by means of SANS analyses [20], and was found to be constituted of elongated ellipsoidal micelles dispersed in a water/BuOH/MEK continuous phase. The shape and size of supramolecular aggregates was attributed to the proximity of the system to the nonionic surfactant's cloud point at room temperature. In this study, a close NSF formulation was used, but with a substantial variation, i.e. a small amount of SDS (0.2% w/w) was included in the system in order to optimize the cleaning capacity by increasing the surfactant cloud point. Moreover, having a cloud point significantly higher than room temperature can be crucial in practical applications, and the addition of even very low concentrations of ionic surfactants to nonionic surfactants-based systems is well known to drastically increase the clouding temperature [37–41]. This is due to the increase of surface charge of the disperse phase droplets, which confers a slight repulsion between the aggregates [38, 39]. The overall effect is the stabilization of the system even at temperatures at which the nonionic surfactant alone would have phase-separated. For this main reason, the nonionic/ionic mixed micelles, in this case, could be fitted only using a spherical model, differently from the cited paper, where the aggregates were elongated.

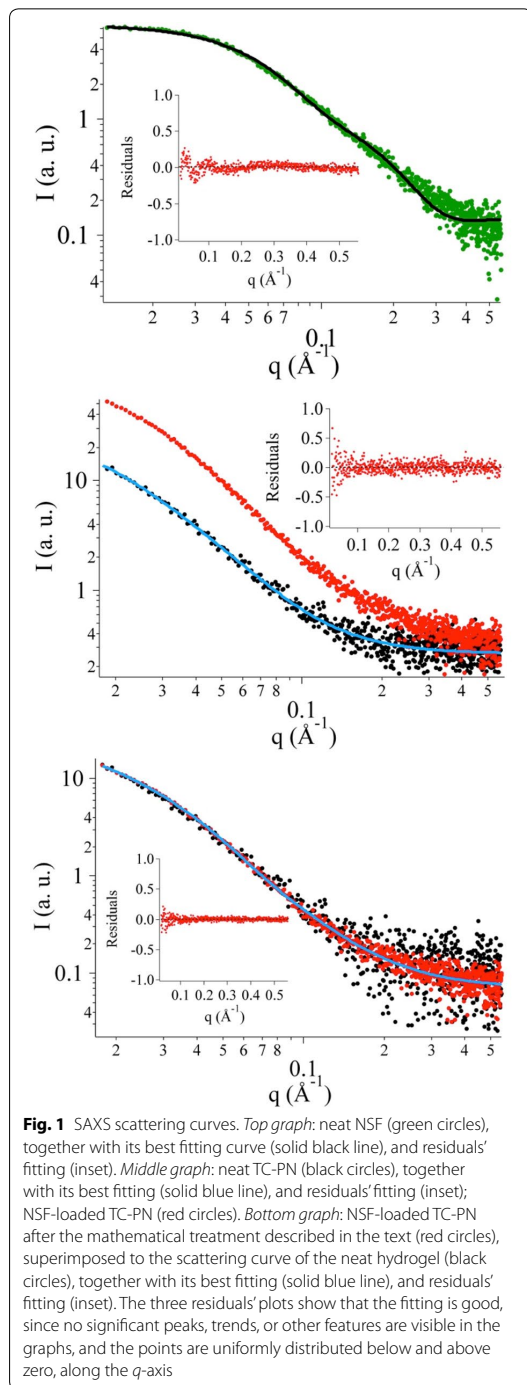


Table 1 SAXS fitting parameters obtained by the analysis of the NSF scattering profile

Fitting parameter	Best value
Core radius, r (Å)	10.1 ± 0.1
Shell thickness, t (Å)	15.2 ± 0.1
Core polydispersity index (PDI)	0.58 ± 0.01
SLD_{core} (10^{-6} \AA^{-2})	7.8
SLD_{shell} (10^{-6} \AA^{-2})	9.5
SLD_{bulk} (10^{-6} \AA^{-2})	8.8

Table 2 SAXS fitting parameters obtained by the analysis of the hydrogel and the NSF-loaded TC-PN scattering profiles

Fitting parameter	TC-PN	NSF-loaded TC-PN
$I_L(0)$ (cm^{-1})	31 ± 2	25 ± 4
$I_G(0)$ (cm^{-1})	0.3 ± 0.1	2.7 ± 1.0
D	2.5 ± 0.1	2.5 ± 0.2
ξ (nm)	5.1 ± 0.5	5.1 ± 1.0
R (nm)	3.2 ± 0.8	4.9 ± 0.4

In more detail, after several attempts using a range of possible different models, the best fitting was obtained by considering the NSF micelles as non-interacting poly-disperse core-shell spheres, defined by two contrasts, i.e. bulk/shell and shell/core. The scattering length density (SLD) of bulk, shell and core, i.e. ρ_{bulk} , ρ_{shell} and ρ_{core} respectively, were calculated according to the SLD of each chemical included in the formulations. For globular micelles of homogeneous scattering length density, the total scattered intensity $I(q)$ (cm^{-1}) is given by [42, 43]:

$$I(q) = N_p V_p^2 \Delta \rho^2 P(q) S(q) + b k g_{inc}$$

where N_p is the number density of the scattering particles (cm^{-3}), V_p is the volume (cm^3), $\Delta \rho$ is the contrast term (cm^{-2}), $P(q)$ is the form factor and $S(q)$ is the structure factor. In this case $S(q) = 1$, as the particles were considered to be non-interacting due to the very low concentration of the anionic surfactant. In the case of spherical core-shell aggregates, the particle scattering intensity is expressed as follows [44]:

$$I(q) = \frac{\phi}{V_p} \left[(\rho_{\text{core}} - \rho_{\text{shell}}) \frac{3V_c j(qr_c)}{qr_c} + (\rho_{\text{shell}} - \rho_{\text{bulk}}) \frac{3V_p j(qr_s)}{qr_s} \right]^2$$

where $j(x)$ is expressed as:

$$j(x) = \frac{(\sin x - x \cos x)}{x^2}$$

and where ϕ is the volume fraction of the micellar phase, V_c is the core volume, r_c is the core radius, $r_s = r_c + t$ (t is the shell thickness). Since this model takes into account a polydisperse core, which follows the Schultz distribution, the form factor is normalized by the average particle volume:

$$\langle V \rangle = \frac{4\pi}{3} \langle r_c^3 \rangle$$

where:

$$\langle r_c^3 \rangle = \frac{(z+2)(z+3)}{(z+1)^2} \langle r_c \rangle$$

and z is the width parameter of the Schultz distribution [45]:

$$z = \frac{1}{\left(\frac{\sigma}{\langle r_c \rangle}\right)^2} - 1$$

being σ^2 the variance of the distribution. The polydispersity index (PDI), reported in Table 1 is defined as $\sigma/\langle r_c \rangle$ and its value is comprised between 0 and 1.

Figure 1 reports the best fitting obtained using the core-shell model. An average core radius, r , of 10 Å was obtained by the fitting, which is reasonably in agreement with the 14 Å theoretical length for an average 10 carbon atoms aliphatic chain, as calculated using the Tanford's formula [46]. The core polydispersity is quite high, but this value likely reflects the fact that the nonionic surfactant itself actually is a mixture of different chemical species having a distribution both for the aliphatic chain length (9–11 carbon atoms) and for the polyethoxylate polar head chain (5.5 CH₂CH₂O-units, in average).

Moreover, a system composed by mixed micelles of nonionic/ionic surfactants in the presence of two water-miscible solvents, which are partitioned between the aqueous and the micellar phase, is structurally more complex than classically-defined o/w microemulsions composed of water/oil/surfactant and whose PDI usually does not exceed 0.2–0.4 [47, 48]. The shell thickness is quite high, as usually is for systems based on alcohol ethoxylates with medium/long polar head chains, but in agreement with the data obtained on previous systems based on the same or similar surfactants [18, 19, 49, 50]. Finally, the SLD of the continuous phase is consistent with the almost complete solubilization of both BuOH and MEK in the ethoxylates groups/water, with little penetration of the organic solvents in the micelles' hydrophobic core. For instance, for similar NSF formulations,

it was previously found that about 10% of the total MEK content is found associated with micelles [17, 49], which is why these systems are referred to as NSF rather than classic oil-in-water microemulsions. It is important to recall that the presence of a good solvent and of the alcohol ethoxylate surfactant (in the form of micelles) is key for the removal of polymer films. While the solvent mobilizes the polymer chains, the crucial role of the surfactant from a kinetic standpoint is in reducing the activation energy necessary to induce dewetting of the polymer film; the surface activity of a surfactant is related to the reduction of surface tension at a defined concentration, which explained the higher efficiency of the surfactant above its critical micellar concentration (cmc) in promoting dewetting with respect to the same systems below the cmc [17–19, 21]. Besides, the presence of MEK induces a decrease in the aggregation number and size of the surfactant micelles, thus an increase in the total surface area of the micelles, which boosts their surface activity [49].

The fitting model for the neat TC-PN was chosen, according to published papers on similar systems [1, 51, 52], as the sum of two superimposed contributions to the scattered intensity, due to fixed polymer junctions (i.e. the solid-like tie points of the network) and to the polymer chains the gel water-rich environment, respectively. The scattered intensity, $I(q)$, is then modeled as follows:

$$I(q) = I_L(0) \frac{1}{\left[1 + \frac{D+1}{3}(q^2\xi^2)\right]^{\frac{D}{2}}} + I_G(0) \exp\left(-q^2 \frac{R^2}{3}\right) + B$$

where $I_L(0)$ and $I_G(0)$ are the Lorentzian and the Guinier parameters, D is the fractal exponent, ξ is a correlation length, R is the radius of gyration of solid-like scattering objects, and B is an incoherent background scattering. Table 2 reports the fitting parameters obtained by the analysis of the experimental scattering curves.

Considering previous studies on PVA-based hydrogels [53], R was assumed to be the radius of gyration of PVA crystallites in the solid-like portions of the gel, while ξ can be seen as a characteristic length of the polymeric network in the water-rich gel regions, where polymer chains are less constrained. This dimension depends on the local concentration of polymer, and it is strongly dependent on synthetic pathway.

The fitting values obtained for the neat hydrogels are in perfect agreement with the ones obtained in a previous study, which included the same formulation used here, among other PVA-based gels [1]. In particular, the fractal exponent, D , of 2.5 (PVA gels usually show fractal exponents in the 2–4 range), a correlation length, ξ , of about 5 nm, and PVA crystallites of about 3 nm (R) are also in agreement with previous observations on PVA hydrogels [54]. Finally, the quite high value of the $I_L(0)/I_G(0)$ ratio

indicates that the number of solid-like scattering objects (crystallites) is limited [1].

The analysis of the scattering curve of the NSF-loaded TC-PN was not straightforward. Figure 1 (middle graph) shows that the scattering profiles of the NSF-loaded TC-PN (red circles) and of the neat hydrogel (black circles) look similar, apart from a multiplicative factor. Actually, the NSF-loaded TC-PN curve also includes scattering signals coming from the NSF, which are not easily isolable from the curve, because the NSF scattering curve does not present particular features, such as peaks or bumps. The adopted fitting strategy based on the assumption that the NSF structure inside the gel was not significantly altered, as actually found in a previous study on the loading of NSFs into different hydrogels [25]. Therefore, it should be possible to separate the contributions of both the NSF and the sole hydrogel to the total scattering intensity. The experimental scattering curves of these two samples (i.e., the NSF and the TC-PN) were linearly combined, and it was found that:

$$0.2 \times \text{“NSF”} + 4 \times \text{“TC - PN”} \\ = \text{“NSF - loaded TC - PN”}$$

In other words, when the opportunely scaled NSF scattering curve was subtracted from the NSF-loaded TC-PN curve, the resulting curve, divided by a factor 4 (red circles), could be superimposed almost perfectly to the sole hydrogel curve (black circles), as shown in Fig. 1 (bottom graph). This curve was fitted using the model described above and, as predictable, the fitting parameters obtained did not significantly differ from the ones of the neat TC-PN (compare second and third column in Table 2). The factor 4 between the TC-PN curve and the “subtracted curve” is actually easily explainable in view of the different SLD of the solvent in the gel, when water was replaced by the continuous phase of the NSF where significant amounts of BuOH and MEK were dissolved. Looking at the other parameters, a slight increase in the size of the solid-like domains in the gel (4.9 nm vs. the initial 3.2 nm size) and a decrease of the $I_L(0)/I_G(0)$ ratio are observed, which can be ascribed possibly to the interaction of the polymer network with the organic solvents and surfactants included in the NSF. The slight increase of R might be due to the lower affinity of PVA towards water/BuOH/MEK with respect to water alone. In the peripheral regions of crystallites, PVA chains are normally more hydrated and less tightly packed than in the crystallites core; in the presence of a worse solvent than water, the looser chains start to interact more tightly and collapse, leading overall to an increase of the crystallites core. Since the structure becomes more crowded, this could also explain the decrease of the $I_L(0)/I_G(0)$ ratio. No stiffening of the gel was noted after loading with the

NSF. Apart from these changes, both the NSF and the TC-PN have shown to preserve their nanostructure and, subsequently, their cleaning properties are expected to be maintained in view of a potential application.

According to the literature [55], PVA, even when highly hydrolyzed, interacts with both anionic and nonionic surfactants through hydrophobic interactions between the polymer carbon-chain skeleton and the hydrophobic tails of the surfactants. Therefore, the hydrophilicity of the polymer increases, especially in the case of polymer-anionic surfactant interactions: in this case, the network becomes a polyelectrolyte hydrogel [56].

CLSM imaging of the labeled gel and NSF confirms that an interaction occurs when the NSF is loaded in the gel (see Fig. 2a, b): the pattern of the gel porosity (green, Fig. 2a) is closely traced by the fluorescent signal of labeled micelles (red, Fig. 2b), as also highlighted by the overlay image in Fig. 2c, suggesting that micelles are able to stick on the gel walls. At the surfactant concentration used in the study, there is an equilibrium between micellar species and monomeric surfactants; the equilibrium is shifted towards the micellar state. Therefore, the majority of the Bodipy interacting with PVA is included in the micelles, even if we can detect a small signal from probe interacting with PVA. Overall, the macroporosity of the gel was not significantly altered by loading with the NSF.

The diffusion of the NSF in the TC-PN's pores was investigated through FCS and compared to the diffusion of the free NSF. The free NSF decay curve can be described by a single diffusion coefficient (see Table 3 and Fig. 2c). The hydrodynamic diameter of the micelles ($d_H = 5.0 \pm 0.4$ nm) evaluated through the Stokes–Einstein equation, using the diffusion coefficient obtained by FCS fitting and assuming the viscosity of the NSF to be the same as water at 25 °C, is in agreement with the micelle dimension obtained through the fitting of SAXS (ca. 5 nm, see Table 1). Regarding the diffusion of the NSF inside the gel, FCS curves could be described only considering a two-component decay. The diffusion coefficient characterizing the free NSF can still be detected inside the gel pores after loading, and accounts for the 60% ca. of the total decay. However, a slower component was detected as well, probably due to the micelle-gel interaction (see Table 3). CLSM and FCS demonstrate that micelles are able to diffuse through the gel matrix, but also interact with the gel walls. Overall, the combination of the SAXS and CLSM/FCS results suggests that such interaction probably takes place in the more external and less crowded regions of the gel walls, rather than in the crystallites.

The ability of the microemulsion droplets to move freely in the porous gel structure, as shown by FCS

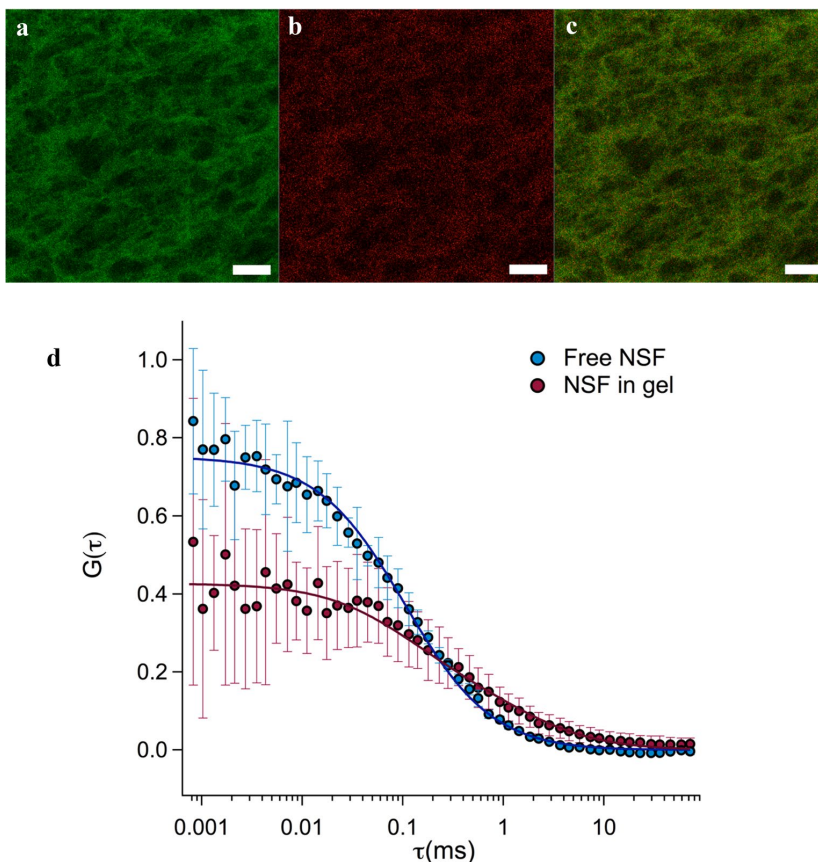


Fig. 2 CLSM images of the TC-PN after the loading with NSF: **a** the fluorescence of FITC-labeled PVA (green) shows the gel structure; **b** the fluorescence of Bodipy-labeled NSF (red) seems to trace the gel porosity, suggesting that some micelles are interacting with the gel walls. Scale bar is 20 μm long. **c** Overlay of the images in (a, b). **d** FCS autocorrelation curves describing the diffusion of the NSF before (blue markers) and after (purple markers) loading inside the TC-PN

measurements either on the PVA TC-PNs studied here or on single-PVA gels [29], suggests that the replacement of water in the gel with the NSF occurs effectively after loading overnight.

Table 3 NSF diffusion coefficients (D , $\mu\text{m}^2/\text{s}$) and their contribution to the total FCS decay (f , %), before (free NSF) and after (NSF in the TC-PN) loading inside the hydrogel

	Free NSF	NSF in the TC-PN
D_1 ($\mu\text{m}^2/\text{s}$)	100 ± 6	100
f_1 (%)	100	60 ± 16
D_2 ($\mu\text{m}^2/\text{s}$)	–	7 ± 4

When the system is in contact with a substrate, the cleaning process is accomplished by the osmotic equilibrium inside the network: while the NSF freely diffusing in the outer pores interacts with the painted surface, fresh NSF is recalled at the gel-paint interface due to the interconnected porosity and the free/bound micelles equilibrium.

In other words, the diffusion dynamics of the micelles are altered after the NSF confinement in TC-PNs. At the same time, the uncontrolled spreading of the cleaning fluid is avoided. Therefore, a time- and space-controlled cleaning action results, not achievable when non-confined fluids are used.

Cleaning tests on mock-up samples showed that it was possible to remove the wax lining residues along with the PVAc varnish. Reduced application times (5–10 s) produced lesser softening of the PVAc layer, keeping the cleaning action more superficial. The softening of the varnish increases with longer contact times. After ca. 40–60 s PVAc became streaky, but still well separated from the paint layer. The short contact times and controlled fluid release from the gel allowed avoiding uncontrolled penetration of varnish

and damages to the paint layer. Rinsing steps with gels simply loaded with water (applied to the painting surface for 1–2 s) made the usage of free liquids on the surface unnecessary. Mock-up samples, lined or not, showed similar positive response to the cleaning methodology. After the cleaning tests, observation under microscope and UV lamp showed the cleaning efficacy of the method. A more detailed assessment was obtained through FTIR 2D imaging. Figure 3 shows the visible light microscope images and FTIR 2D

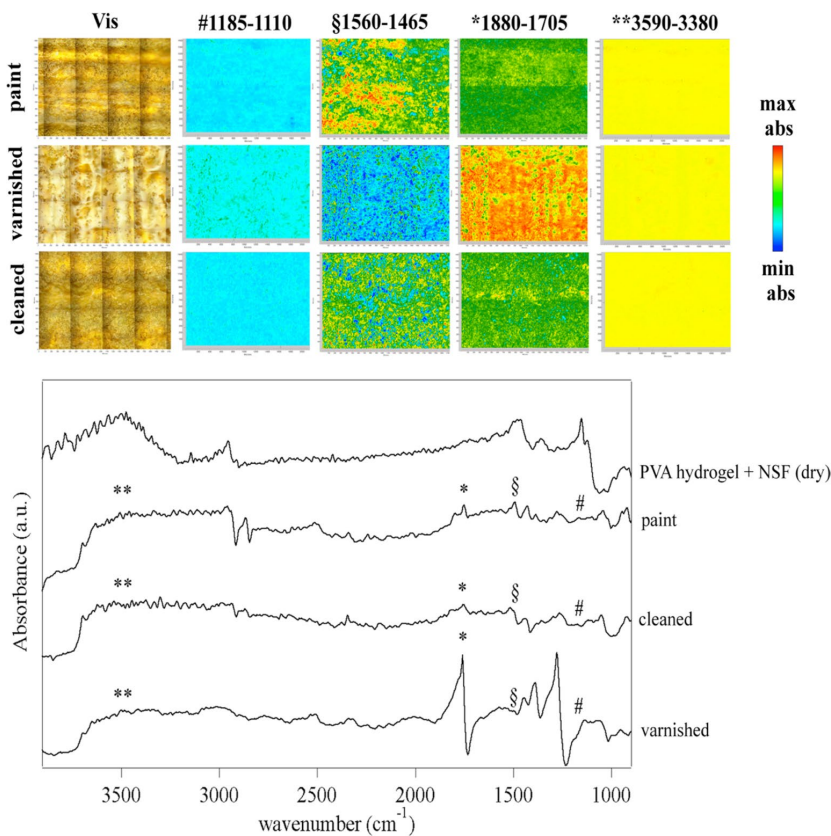


Fig. 3 FTIR 2D imaging of paintings' mock-up samples. Top panel: visible light and 2D FTIR maps of mock-ups that were unvarnished ("paint", top row), varnished (center row), or varnished and then cleaned with the PVA hydrogels loaded with the NSF ("cleaned", bottom row). The tests were carried out in the wax-lined regions. For each sample, the images beside the visible map show the corresponding 2D FTIR maps, where the intensities of the following peaks were imaged: 1185–1110 cm^{-1} (where the C–O stretching band of the $\text{C}_{9-11}\text{E}_{55}$ surfactant would be found in case of NSF residues after cleaning), 1560–1465 cm^{-1} (CH_2 bending, wax used in the lining), 1880–1705 cm^{-1} (C=O stretching, polyvinyl acetate-based varnish), and 3590–3380 cm^{-1} (where the characteristic OH stretching band of PVA would be found in case of gel residues after cleaning). All maps have dimensions of $2100 \times 1400 \mu\text{m}^2$, each axis tick being 50 μm . The FTIR Reflectance spectra are shown in the bottom panel, each spectrum relating to a single pixel ($5.5 \times 5.5 \mu\text{m}^2$) of the corresponding 2D imaging map. The maps show the removal of the varnish and surface removal of wax spots, while no absorptions ascribable to PVA or surfactants from the NSF could be detected. The spectrum of a PVA hydrogel (loaded with the NSF and then let dry before acquiring the spectra) is also showed as a reference

imaging of mock-ups that mimic the lined painting by Picasso. The application of the NSF-loaded hydrogel on the surface of the mock-ups led to the removal of the PVAc-based varnish, as observed under visible light and by the disappearance of the characteristic bands of PVAc (e.g. C=O stretching in the 1880–1705 cm^{-1} region) from the spectra recorded on the samples' surface. The application of the gel also allowed the surface removal of wax spots (due to the lining intervention), as shown by the decrease of the characteristic band of wax around 1475 cm^{-1} (CH_2 bending); in the varnished mock-up, the band is not observable, as the wax spots are likely covered by the poly(vinyl acetate) layer. The 3590–3380 cm^{-1} region of the spectra was also imaged, where the most intense absorption of PVA (OH stretching) should be observed in case of detectable gel residues left on the surface after the cleaning intervention. No difference in the absorbance intensity was observed in the spectra of the samples treated with the gels with respect to pristine samples; therefore, it was concluded that no detectable gel residues were left by the treatment. The absence of gel residues was expected, considering that the PVA TC-PN hydrogels exhibit a mechanical behavior typical of chemical gels, despite

being physical networks (i.e. held by secondary bonds) [1].

No relevant bands ascribable to the surfactants used in the NSF were observed. Alcohol ethoxylate surfactants, such as $\text{C}_{9-11}\text{E}_{5,5}$, have a characteristic FTIR band around 1120 cm^{-1} (C-O stretching), while SDS has a characteristic peak centered at 1220 cm^{-1} (asymmetric stretching of OSO_3); no significant bands at those wavelengths were observed in the spectra of the cleaned painting mock-ups, as compared to pristine samples. Besides, the application of a water-loaded gel after cleaning leads to the absorption of possible surfactant residues.

It must be noticed that the detection limit of an FPA detector has been reported to be significantly lower than that of conventional mercury cadmium telluride (MCT) detectors, when trace amounts of materials are considered; in fact, in that case the heterogeneous distribution of the analyte can result in small areas with high localized concentration, which can be detected thanks to the spatial resolution of the FPA detector [57]. In a previous work, a detection limit of ca. 1 $\mu\text{g}/\text{cm}^2$ for the detection of PVA was found, using the same FPA detector and instrumental setup [1]. Overall, we concluded that the cleaning procedure led to the removal of the varnish and

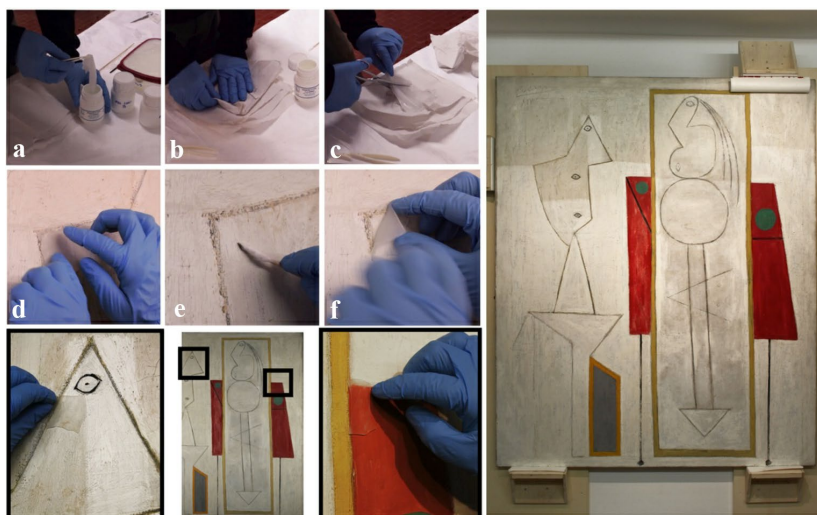


Fig. 4 The cleaning of Pablo Picasso, *The Studio*, 1928, oil and black crayon on canvas, 161.6 × 129.9 cm, Peggy Guggenheim Collection, Venice (The Solomon R. Guggenheim Foundation, New York). **a** The TC-PN hydrogel is loaded with the o/w NSF (24 h immersion). **b** Gel sheets loaded with the NSF are gently squeezed with blotting paper to remove the fluid excess from their surface, and **(c)** cut to desired shape and size. **d** The gel is applied onto the painted surface. **e** Gentle mechanical action with a dry cotton swab allows the removal of the swollen/softened varnish and wax. **f** Rinsing step: a water-loaded gel is shortly applied on the same spot to remove possible residues of the NSF. At bottom, center panel and related black boxed details show the cleaning of white and red areas. On the right, the painting during the cleaning: the cleaned lighter areas can be easily distinguished from the darker uncleaned areas at the top. ©Succession Picasso, by SIAE 2020

wax contaminants, without leaving detectable residues of the gel or of the NSF. Because these alcohol ethoxylate surfactants are readily biodegradable, non-detectable residues (below the FPA detection limit) are expected to degrade into fatty alcohols and polyethylene glycols (PEG), which are further degraded one glycol unit at a

time from the terminus of the PEG, and/or via an oxidative hydrolysis [58, 59].

Following the tests on the mock-up samples, the NSF-loaded hydrogels were used for the cleaning of Picasso's *The Studio*. The tests (see Fig. 4) confirmed that the PVAc-based varnish was swollen after ca. 5 s of contact with the gel, and then the swollen varnish was gently and easily peeled off with a dry cotton swab just like a second

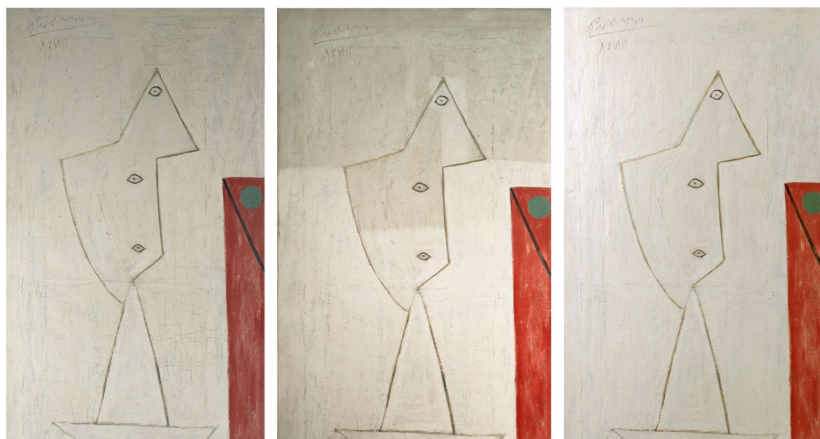


Fig. 5 Pablo Picasso, *The Studio*, 1928, Peggy Guggenheim Collection, Venice (The Solomon R. Guggenheim Foundation, New York), before (left), during (center), and after (right) the cleaning carried out with TC-PN hydrogels loaded with the o/w NSF. ©Succession Picasso, by SIAE 2020

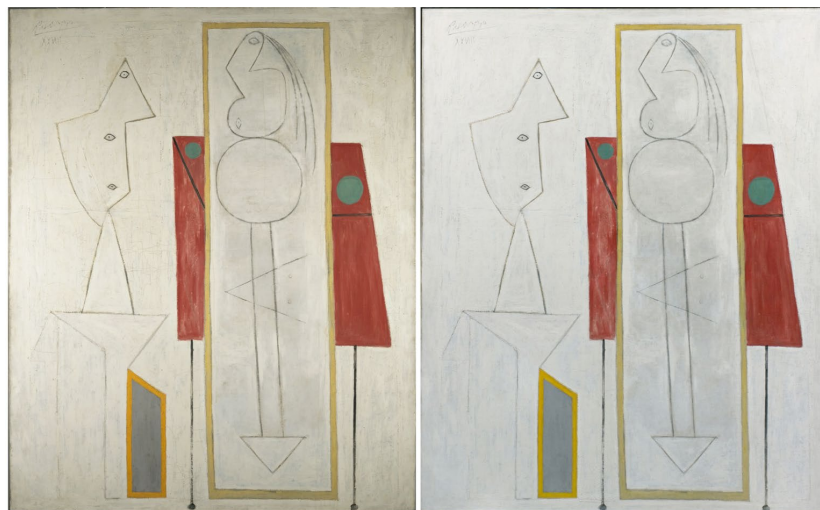


Fig. 6 Pablo Picasso, *The Studio*, 1928, Peggy Guggenheim Collection, Venice (The Solomon R. Guggenheim Foundation, New York), before (left) and after (right) the cleaning carried out with TC-PN hydrogels loaded with the o/w NSF. ©Succession Picasso, by SIAE 2020

skin, with no alteration of the color layers. Figures 5, 6 show the painting before, during, and after the cleaning intervention.

Because the black crayon lines are at a deeper level than the white color background (simulating the effect of an incision), they are hardly accessible; therefore, it was decided to carefully and accurately remove the varnish around the lines, without affecting them. Such delicate intervention was possible thanks to the capability of the gels (that can be cut and shaped to desired size) to confine the NSF and wet only the surface in direct contact with the gels, with superior control of the cleaning action.

Conclusions

Polyvinyl alcohol (PVA) “twin-chain” polymer networks (TC-PNs) hydrogels were combined with a nanostructured fluid (NSF), and the resulting complex system was used to safely remove the aged varnish and wax layer from the surface of Pablo Picasso, *The Studio* (1928). The NSF loading within the TC-PNs was associated to interactions between the NSF and the TC-PN that take place in the more external and less crowded regions of the gel walls, rather than in the internal crystallites, without significant alteration of the system's components. The diffusion of the complex fluid in the gel matrix and at the gel-painting interface, during cleaning, is granted by the osmotic balance in the network. Overall, these factors guarantee the effective and controlled cleaning action of the gel + NSF system.

Cleaning tests on painting mock-ups showed that the NSF-loaded TC-PNs allow the swelling and softening of varnish and wax layers, which can then be removed with gentle mechanical action using dry cotton swabs, without added mechanical stress to the painted layers. FTIR 2D imaging confirmed the removal of varnish and wax at the micron scale, with no observable residues of the gel or of the NSF (down to the detection limit of the FPA detector, ca. $0.02 \text{ pg}/\mu\text{m}^2$). Residues of the alcohol ethoxylate surfactant (below the FPA detection limit) are expected to be readily biodegradable.

The removal of the aged PVAc varnish and wax layer from the surface of the painting was then carried out by using the same cleaning protocol successfully tested on the mock-ups. The use of the combined gel + NSF system allowed a highly effective and safe cleaning action thanks to the controlled wetting and swelling of the painting surface, and the easy mechanical removal of the swollen PVAc layer, with no evident color alteration. It is worth mentioning that TC-PNs gels with the confined NSFs allow to choose the most appropriate NSFs contact time with the painting surface for the cleaning operation. In the present case the chosen contact time

was of about 5 s, which was enough to obtain a perfect swelling of the layer to be removed, without interacting with the original pictorial layer. These results set NSF-loaded PVA TC-PNs as a robust and reliable tool for the cleaning of sensitive paintings, opening new perspectives in the conservation of works of art.

Acknowledgements

The Italian Consorzio Interuniversitario per lo Sviluppo dei Sistemi a Grande Interfase, CSGI (Center for Colloid and Surface Science), MUR PRIN-2017249YEF, and the European Union Horizon 2020 projects NANORESTART (Nanomaterials for the Restoration of Works of Art) and APACHE (Active & Intelligent Packaging Materials and Display Cases as a Tool for Preventive Conservation of Cultural Heritage), under the Horizon 2020 Research and Innovation Programme Grant Agreements 646063 and 814496, respectively, are gratefully acknowledged for the financial support. The authors also acknowledge Chiara Barbieri, Director of Publications and Special Projects, Peggy Guggenheim Collection.

Abbreviations: All acronyms and abbreviations are written in full letter when they first appear

Authors' contributions

LPB and MLP (PGC) researched the appearance and the art historical context of the painting, and defined the specific and broader aims of the cleaning treatment. MLP and LPB documented the evaluation of cleaning materials, managed the acquired data for the evaluation phase and treatment, and the technical and conservation images and documentation. MLP prepared the mock-up samples and performed the cleaning tests on all mock-ups. LPB performed the cleaning tests on the painting, and carried out the full conservation treatment and the technical examination of the painting. PB (CSGI) conceptualized the PVA TC-PN gel series and their application to Cultural Heritage conservation; MB, RM and DC carried out the physico-chemical characterization of the gel and NSF, and the 2D FTIR assessment of the cleaning treatment on mock-ups. PB, MB, RM, DC and RG analyzed the data. All authors read and approved the final manuscript.

Authors' information

LPB (PGC) designed, led and managed the Peggy Guggenheim Collection contribution to the NANORESTART project, and was the PGC NANORESTART conservator for this case study (2017–2018). MLP was the PGC NANORESTART conservation researcher (2017–2019). The NANORESTART project was led by PB (CSGI); DC and RG (CSGI) were project coordinator contacts. MB (CSGI) was a post-doctoral researcher during the project, and RM a PhD student at CSGI and the Department of Chemistry, University of Florence. Piero Baglioni and Michele Baglioni are not related.

Funding

This research has received funding from the European Union NANORESTART (Nanomaterials for the Restoration of Works of Art), APACHE (Active & Intelligent Packaging Materials and Display Cases as a Tool for Preventive Conservation of Cultural Heritage), under the Horizon 2020 Research and Innovation Programme Grant Agreements 646063 and 814496 respectively, and CSGI (Center for Colloid and Surface Science, Progetti Competitivi), MUR PRIN-2017249YEF.

Availability of data and materials

All the available data have been included in the article.

Ethics approval and consent to participate

Not applicable.

Competing interests

The authors declare no conflict of interest.

Received: 12 May 2020 Accepted: 20 July 2020
Published online: 05 August 2020

References

1. Mastrangelo R, Chelazzi D, Poggi G, Fratini E, Pensabene Buemi L, Petruzzezzis ML, et al. Twin-chain polymer hydrogels based on poly(vinyl alcohol) as new advanced tool for the cleaning of modern and contemporary art. *Proc Natl Acad Sci USA*. 2020;117:7011–20.
2. Learner T. Modern paints: uncovering the choices. In: Learner T, Smithen P, Krueger J, Schilling MR, editors. *Mod Paints uncovered proc mod paints uncovered Symp*. Los Angeles: Getty Conservation Institute; 2007.
3. Burnstock A, van den Berg KJ. Twentieth Century Oil Paint The Interface Between Science and Conservation and the Challenges for Modern Oil Paint Research. In: van den Alberto Tagle, de Berg KJ, Burnstock A, de Keijzer M, Krueger J, Learner T, et al., editors. *Issues Contemp Oil Paint*. Cham: Springer International Publishing; 2014. p. 1–19.
4. Domingues JAL, Bonelli N, Giorgi R, Fratini E, Gorel F, Baglioni P. Innovative hydrogels based on semi-interpenetrating p(HEMA)/PVP networks for the cleaning of water-sensitive cultural heritage artifacts. *Langmuir*. 2013;29:2746–55.
5. Casoli A, Cremonesi P, Isca C, Groppetti R, Pini S, Senin N. Evaluation of the effect of cleaning on the morphological properties of ancient paper surface. *Cellulose*. 2013;20:2027–43.
6. Volk A, Berg KJ van den. Agar—a new tool for the surface cleaning of water sensitive oil paint? In: Berg KJ van den, Burnstock A, Keijzer M de, Krueger J, Learner T, de AT, et al., editors. *Issues Contemp Oil Paint*. Cham: Springer International Publishing; 2014. p. 389–406.
7. Burnstock A, White R. A preliminary assessment of the aging/degredation of Ethomeen c-12 residues from solvent gel formulations and their potential for inducing changes in resinous paint media. *Stud Conserv*. 2000;45:34–8.
8. Giorgi R, Baglioni M, Berti D, Baglioni P. New methodologies for the conservation of cultural heritage: micellar solutions, microemulsions, and hydroxide nanoparticles. *Acc Chem Res*. 2010;43:695–704.
9. Baglioni M, Rengstl D, Berti D, Bonini M, Giorgi R, Baglioni P. Removal of acrylic coatings from works of art by means of nanofluids: understanding the mechanism at the nanoscale. *Nanoscale*. 2010;2:1723.
10. Baglioni M, Giorgi R, Berti D, Baglioni P. Smart cleaning of cultural heritage: a new challenge for soft nanoscience. *Nanoscale*. 2012;4:42.
11. Baglioni M, Berti D, Teixeira J, Giorgi R, Baglioni P. Nanostructured surfactant-based systems for the removal of polymers from wall paintings: a small-angle neutron scattering study. *Langmuir*. 2012;28:15193–202.
12. Baglioni M, Jáidar Benavides Y, Berti D, Giorgi R, Keiderling U, Baglioni P. An amine-oxide surfactant-based microemulsion for the cleaning of works of art. *J Colloid Interface Sci*. 2015;440:204–10.
13. Baglioni M, Jáidar Benavides Y, Desprat-Drapela A, Giorgi R. Amphiphile-based nanofluids for the removal of styrene/acrylate coatings: cleaning of stucco decoration in the Uaxactun archeological site (Guatemala). *J Cult Herit*. 2015;16:862–8.
14. Baglioni M, Poggi G, Jáidar Benavides Y, Martínez Camacho F, Giorgi R, Baglioni P. Nanostructured fluids for the removal of graffiti—a survey on 17 commercial spray-can paints. *J Cult Herit*. 2018;34:218–26.
15. Chelazzi D, Giorgi R, Baglioni P. Microemulsions, micelles, and functional gels: how colloids and soft matter preserve works of art. *Angew Chem Int Ed Engl*. 2018;57:7296–303.
16. Chelazzi D, Bordes R, Giorgi R, Holmberg K, Baglioni P. The use of surfactants in the cleaning of works of art. *Curr Opin Colloid Interface Sci*. 2020;45:108–23.
17. Raudino M, Selvolini G, Montis C, Baglioni M, Bonini M, Berti D, et al. Polymer Films removed from solid surfaces by nanostructured fluids: microscopic mechanism and implications for the conservation of cultural heritage. *ACS Appl Mater Interfaces*. 2015;7:6244–53.
18. Baglioni M, Montis C, Brandi F, Guaragnone T, Meazzini I, Baglioni P, et al. Dewatering acrylic polymer films with water/propylene carbonate/surfactant mixtures—implications for cultural heritage conservation. *Phys Chem Chem Phys*. 2017;19:23723–32.
19. Baglioni M, Montis C, Chelazzi D, Giorgi R, Berti D, Baglioni P. Polymer film dewatering by water/surfactant/good-solvent mixtures: a mechanistic insight and its implications for the conservation of cultural heritage. *Angew Chem Int Ed*. 2018;57:7355–9.
20. Baglioni M, Alterini M, Chelazzi D, Giorgi R, Baglioni P. Removing polymeric coatings with nanostructured fluids: influence of substrate, nature of the film, and application methodology. *Front Mater*. 2019;6:311. <https://doi.org/10.3389/fmats.2019.00311>.
21. Montis C, Koynov K, Best A, Baglioni M, Butt H-J, Berti D, et al. Surfactants mediate the dewatering of acrylic polymer films commonly applied to works of art. *ACS Appl Mater Interfaces*. 2019;11:27288–96.
22. Baglioni M, Bartoletti A, Bozec L, Chelazzi D, Giorgi R, Odlyha M, et al. Nanomaterials for the cleaning and pH adjustment of vegetable-tanned leather. *Appl Phys A*. 2016;122:114.
23. Bonelli N, Poggi G, Chelazzi D, Giorgi R, Baglioni P. Poly(vinyl alcohol)/poly(vinyl pyrrolidone) hydrogels for the cleaning of art. *J Colloid Interface Sci*. 2019;536:339–48.
24. Bonelli N, Chelazzi D, Baglioni M, Giorgi R, Baglioni P. Confined aqueous media for the cleaning of cultural heritage: innovative gels and amphiphile-based nanofluids. In: Dillmann P, Bellot-Gurlet L, Nenner I, editors. *Nanosci Cult Herit*. Atlantis Press; 2016. p. 283–311.
25. Baglioni M, Domingues JAL, Carretti E, Fratini E, Chelazzi D, Giorgi R, et al. Complex fluids confined into semi-interpenetrated chemical hydrogels for the cleaning of classic art: a rheological and SAXS study. *ACS Appl Mater Interfaces*. 2018;10:19162–72.
26. Baglioni P, Berti D, Bonini M, Carretti E, Del Carmen Casas Perez M, Chelazzi D, et al. Gels for the conservation of cultural heritage. *MRS Online Proc Libr*. 2012;1418:17–26.
27. Baglioni P, Carretti E, Chelazzi D. Nanomaterials in art conservation. *Nat Nanotechnol*. 2015;10:287–90.
28. Bonelli N, Montis C, Mirabile A, Berti D, Baglioni P. Restoration of paper artworks with microemulsions confined in hydrogels for safe and efficient removal of adhesive tapes. *Proc Natl Acad Sci*. 2018;115:5932–7.
29. Mastrangelo R, Montis C, Bonelli N, Tempesti P, Baglioni P. Surface cleaning of artworks: structure and dynamics of nanostructured fluids confined in polymeric hydrogel networks. *Phys Chem Chem Phys*. 2017;19:23762–72.
30. Giorgi R, Baglioni M, Baglioni P. Nanofluids and chemical highly retentive hydrogels for controlled and selective removal of overpaintings and undesired graffiti from street art. *Anal Bioanal Chem*. 2017;409:1–6.
31. Watherston M. Conservation paper stored at The Winterthur Library, Winterthur, Delaware, USA. http://findingaid.winterthur.org/html/HTML_finding_Aids/col0935.htm.
32. Verschuere K. *Handbook of environmental data on organic chemicals*. Hoboken: Wiley; 2001.
33. Montis C, Maiolo D, Alessandri I, Bergese P, Berti D. Interaction of nanoparticles with lipid membranes: a multiscale perspective. *Nanoscale*. 2014;6:6452–7.
34. Ries J, Schwille P. Fluorescence correlation spectroscopy. *BioEssays*. 2012;34:361–8.
35. Milani S, Baldelli Bombelli F, Pitek AS, Dawson KA, Rädler J. Reversible versus irreversible binding of transferrin to polystyrene nanoparticles: soft and hard corona. *ACS Nano*. 2012;6:2532–41.
36. Bartoletti A, Barker R, Chelazzi D, Bonelli N, Baglioni P, Lee J, et al. Reviving WHAAM! a comparative evaluation of cleaning systems for the conservation treatment of Roy Lichtenstein's iconic painting. *Herit Sci*. 2020;8:9.
37. Bartoletti A, Maor T, Chelazzi D, Bonelli N, Baglioni P, Angelova LV, et al. Facilitating the conservation treatment of Eva Hesse's Addendum through practice-based research, including a comparative evaluation of novel cleaning systems. *Herit Sci*. 2020;8:35.
38. Sadaghiana AS, Khan A. Clouding of a nonionic surfactant: the effect of added surfactants on the cloud point. *J Colloid Interface Sci*. 1991;144:191–200.
39. Nilsson PG, Lindman B. Mixed micelles of nonionic and ionic surfactants. A nuclear magnetic resonance self-diffusion and proton relaxation study. *J Phys Chem*. 1984;88:5391–7.
40. Valaulikar BS, Manohar C. The mechanism of clouding in triton X-100: the effect of additives. *J Colloid Interface Sci*. 1985;108:403–6.
41. Gu T, Qin S, Ma C. The effect of electrolytes on the cloud point of mixed solutions of ionic and nonionic surfactants. *J Colloid Interface Sci*. 1989;127:586–8.
42. Sheu EY, Chen SH. Thermodynamic analysis of polydispersity in ionic micellar systems and its effect on small-angle neutron scattering data treatment. *J Phys Chem*. 1988;92:4466–74.
43. Liu YC, Ku CY, LoNostro P, Chen SH. Ion correlations in a micellar solution studied by small-angle neutron and x-ray scattering. *Phys Rev E*. 1995;51:4598–607.
44. Kline SR. Reduction and analysis of SANS and USANS data using IGOR Pro. *J Appl Crystallogr*. 2006;39:895–900.

45. Degiorgio V, Corti M, fisica S italiana di. Physics of amphiphiles–micelles, vesicles, and microemulsions: Varenna on Lake Como, Villa Monastero, 19-29 July 1983. North-Holland; 1985.
46. Tanford C. The hydrophobic effect: formation of micelles and biological membranes. 2nd ed. New York: Wiley; 1980.
47. Watarai H. Microemulsions in separation sciences. *J Chromatogr A*. 1997;780:93–102.
48. Eriksson JC, Ljunggren S. Thermodynamic evaluation of the polydispersity of droplet microemulsions. *Langmuir*. Am Chem Soc. 1995;11:1145–53.
49. Baglioni M, Raudino M, Berti D, Keiderling U, Bordes R, Holmberg K, et al. Nanostructured fluids from degradable nonionic surfactants for the cleaning of works of art from polymer contaminants. *Soft Matter*. 2014;10:6798–809.
50. Baglioni M, Poggi G, Ciolli G, Fratini E, Giorgi R, Baglioni P. A Triton X-100-based microemulsion for the removal of hydrophobic materials from works of art: SAXS characterization and application. *Materials*. 2018;11:1144.
51. Mallam S, Horkay F, Hecht AM, Rennie AR, Geissler E. Microscopic and macroscopic thermodynamic observations in swollen poly(dimethylsiloxane) networks. *Macromolecules*. 1991;24:543–8.
52. Shibayama M, Tanaka T, Han CC. Small angle neutron scattering study on poly(N-isopropyl acrylamide) gels near their volume-phase transition temperature. *J Chem Phys*. 1992;97:6829–41.
53. Hudson SD, Hutter JL, Nieh M-P, Pencer J, Millon LE, Wan W. Characterization of anisotropic poly(vinyl alcohol) hydrogel by small- and ultra-small-angle neutron scattering. *J Chem Phys*. 2009;130:034903.
54. Shibayama M, Kurokawa H, Nomura S, Muthukumar M, Stein RS, Roy S. Small-angle neutron scattering from poly(vinyl alcohol)-borate gels. *Polymer*. 1992;33:2883–90.
55. Lozinsky VI, Damshkaln LG, Kurochkin IN, Kurochkin II. Study of Cryostructuring of Polymer Systems: 25. The influence of surfactants on the properties and structure of gas-filled (Foamed) Poly(vinyl alcohol) Cryogels. *Colloid J*. 2005;67:589–601.
56. Caykara T, Kiper S, Demirel G. Thermosensitive poly(N-isopropylacrylamide-co-acrylamide) hydrogels: synthesis, swelling and interaction with ionic surfactants. *Eur Polym J*. 2006;42:348–55.
57. Chan KLA, Kazarian SG. Detection of trace materials with Fourier transform infrared spectroscopy using a multi-channel detector. *Analyst*. 2006;131:126–31.
58. Marcomini A, Zanette M, Pojana G, Suter MJ-F. Behaviour of aliphatic alcohol polyethoxylates and their metabolites under standardized aerobic biodegradation conditions. *Environ Toxicol Chem*. 2000;19:549–54.
59. Marcomini A, Pojana G, Carrer C, Cavalli L, Cassani G, Lazzarin M. Aerobic biodegradation of monobranched aliphatic alcohol polyethoxylates. *Environ Toxicol Chem*. 2000;19:555–60.

Publisher's Note

Springer Nature remains neutral with regard to jurisdictional claims in published maps and institutional affiliations.

Submit your manuscript to a SpringerOpen[®] journal and benefit from:

- Convenient online submission
- Rigorous peer review
- Open access: articles freely available online
- High visibility within the field
- Retaining the copyright to your article

Submit your next manuscript at ► [springeropen.com](https://www.springeropen.com)